Charon
Mars SRV
Final Report
Group 25

Delft University of Technology

TU Delft

Charon
Mars SRV

Final Report
Version 2.0

by

Group 25

As the fourth and final phase of the spring DSE 2020
to obtain the degree of Bachelor of Science in Aerospace Engineering
at the Delft University of Technology,

Students:	D. Apostolidis	4653963
	M. Berger	4667921
	L. Ciunaitis	4662431
	M. Fazaeli	4654226
	J. Gaffarel	4651634
	W. Helsdingen	4547101
	A. Kadhum	4666917
	L. Landergren	4672127
	M. Lentner	4673824
	J. Neeser	4657551
	L. Trotta	4557085
Tutor:	M.C. Naeije	TU Delft
Coaches:	S. di Mascio	TU Delft
	L. Laguarda	TU Delft
Clients:	H. Cruissen	Airbus Defence and Space
	L. Meijer	Airbus Defence and Space

Version	Purpose	Date	Comment	Responsible
0.1	Technical Draft	15/06/2020	-	Group 25
1.0	Final Draft	22/06/2020	Technical draft implementation and PMSE draft	Group 25
2.0	Final Report	30/06/2020	Feedback implementation	Group 25

TU Delft

Preface

The purpose of the this document is to provide the details of the preliminary design of the Mars Reusable Vehicle, performed by Group 25 as the final part of the Design Synthesis Exercise to obtain Bachelor of Science in Aerospace Engineering. The vehicle, named Charon after the mythological ferryman on the river Styx, is intended to be a fully reusable, economical, and sustainable solution to transport crew and cargo from an orbital node around Mars to a Martian base at the surface of Mars. The report concludes 10 weeks of work by a group of 11 students for Airbus Defence & Space Netherlands, a primary stakeholder of this project.

Acknowledgements

Group 25 would like to thank Henk Cruijssen and Lex Meijer from Airbus Defence & Space Netherlands for their invaluable feedback throughout the whole period of the Design Synthesis Exercise. We would also like to thank ir. Barry Zandbergen and Dr.ir. Erwin Mooij for their feedback during the Midterm Review.

Special acknowledgement goes to teaching assistant Anique Altena, coaches Luis Laguarda and Stefano di Mascio for their great feedback and ideas on improvement troughout the DSE process. Most importantly, we would like to thank our Tutor Ir. Marc C. Naeije, whose guidance and comments have shaped this work to the most significant extent.

Nomenclature

Abbreviations

[S]	Requirement from Stakeholder
[T]	Requirement from Discovery Tree
APDS	Androgynous Peripheral Docking System
BDRC	Brinkley Dynamic Response Criterion
BER	Bit Error Rate
c.g.	Centre of Gravity
c.p.	Centre of Pressure
DR	Dynamic Response
EKF	Extended Kalman Filter
FBS	Functional Breakdown Structure
FEM	Finite Element Method
FFBD	Functional Flow Block Diagram
FTA	Fault Tree Analysis
GLOC	Gravity-induced Loss Of Consciousness
GNC	Guidance, Navigation, and Control
HTP	High Test Peroxide (H_2O_2 above 85% concentration)
ICE	Internal Combustion Engine
IRC	Injury Risk Criterion
ISS	International Space Station
IVF	Integrated Vehicle Fluids
LOC	Loss of Crew (probability)
LOM	Loss of Mission (probability)
LOV	Loss of Vehicle (probability)
MAI	Manufacturing, Assembly and Integration
MDRS	Mars Data Relay Satellite
MGA	Maximum Growth Allowance
MMOI	Mass Moment of Inertia
PEM	Proton-Exchange Membrane
PMSE	Project Management and System Engineering
RCS	Reaction Control System
RPA	Rocket Propulsion Analysis
SOFC	Solid Oxide Fuel Cell
TPS	Thermal Protection System
TWR	Thrust to Weight Ratio
VSWR	Voltage Standing Wave Ratio

Symbols

α	Angle of attack [-]
β	Bearing Angle [-]
β	Side slip angle [-]
χ	Heading angle [-]
ΔV	Change in Velocity [m/s]
δ	Latitude [-]
$\dot{m}$	Mass flow [kg/s]
η_{ant}	Antenna efficiency [-]
η_{circ}	Circle packing density [-]
$\frac{T}{W}$	Thrust-to-Weight ratio [-]
γ	Flight path angle [-]
Λ	Mass fraction: $\frac{M_{wet}}{M_{wet}-M_{prop}}$ [-]
λ	Wavelength [m]
λ_S	Space loss [dBl]
$\mathbf{f}(\cdot)$	Process nonlinear vector function [-]
$\mathbf{h}(\cdot)$	Observation nonlinear vector function [-]
$\mathbf{P}_k$	State covariance matrix [-]
$\mathbf{Q}_k$	Process noise covariance matrix [-]
$\mathbf{v}_k$	Measurement noise vector [-]
$\mathbf{w}_k$	Process noise vector [-]
$\mathbf{x}_k$	State vector [-]
$\mathbf{z}_k$	Observation vector [-]
μ	Bank angle [-]
ν	Poisson's ration [-]
Ω_t	Rotational velocity of Mars [rad/s]
ϕ	Elevation angle [-]
ψ	Yaw angle [deg]
ρ	Density [kg/m^3]
σ	Standard Deviation [-]
σ_{cc}	Crippling stress [Pa]
σ_{crit}	Critical stress [Pa]
σ_{cr}	Radar Cross-section [m^2]
σ_y	Yield stress [Pa]
τ	Longitude [-]
$\tau(z)$	Moment force distribution [Nm]
τ_w	Pulse Width [s]
θ	Pitch angle [deg]
φ	Roll angle [deg]
A	Cross-sectional area [m^2]
a	Semi-major axis [m]
a	Speed of sound [m/s]
$A(z)$	Normal force distribution [N]
A_e/A_t	Ratio of engine exit Area to throat Area [-]
A_e	Nozzle exit area [m^2]

A_s, A_r	Cross sectional area of stiffener and ring [m^2]
a_x	Axial acceleration [m/s^2]
a_y	Lateral acceleration [m/s^2]
B	Boom area [m^2]
B	Effective Bandwidth [Hz]
b	Semi-minor axis [m]
C	Buckling constant [-]
c	Speed of light [m/s]
C_D	Drag coefficient [-]
c_{eff}	Jet velocity: $9.80665 \cdot I_{sp}$ [m/s]
C_L	Lift coefficient [-]
d	Diameter of the vehicle (tanks) [m]
D_e	Engine exit diameter [mm]
E	Young's modulus [Pa]
e	Eccentricity [-]
E_b/N_o	Signal to noise ratio [-]
E_s, E_r	Modulus of elasticity of stiffener and ring [Pa]
f	Frequency [Hz]
F_D	Drag force [N]
F_L	Lift force [N]
F_{sp}	Specific fuel power [Wh/kg]
F_T	Thrust force [N]
G	Gain [-]
G_s, G_r	Shear Modulus of stiffener and ring [Pa]
I_{sp}	Specific impulse [s]
I_s, I_r	Moment of area of stiffener and ring [m^4]
I_{xx}, I_{yy}, I_{zz}	Second moment of Area in x, y, and z direction [m^4]
J_s, J_r	Torsional constant of stiffener and ring [m^4]
kd	Safety factor [-]
L	Length [m]
L	Radar Losses [-]
l_c	Engine chamber length [mm]
l_e	Engine nozzle length [mm]
L_{pr}	Pointing loss receiver [dBl]
lc	Length of the cylinder [m]
MDS	Minimum Discernible signal [-]
$MH2$	Molar mass hydrogen [g/mol]
$MO2$	Molar mass oxygen [g/mol]
N_A	Avogadro constant [-]
N_p	Number of Crew Members [-]
P	Power [s]
p	Atmospheric pressure [Pa]
p_e	Exhaust pressure [Pa]
PRF	Pulse repetition frequency [Hz]
q	Heat flux [W/m^2]
$q(z)$	Shear force distribution [N]
q_e	Electronic charge [C]
R	Distance to centre of Mars [m]
r	Radar-object range [m]
R_e	Radius of the ellipse [m]
Rc	Radius of the cylinder [m]
T	Temperature [K]
t	Thickness of the skin [mm]
T_S	System noise temperature [dBl]
t_{abort}	Maximum abort time [s]
t_b	Burn time [s]
t_d	Thickness of the dome [m]
tc	Thickness of the cylinder [m]
u_f	Free Volume [m^3]
u_p	Pressurised Volume [m^3]
V	Velocity [m/s]
v	Poisson constant [-]
v_t	Volume of the tank [m^3]
v_w	Volume of the tank walls [m^3]
V_x, V_y	Shear force in x,y direction [N]
z_{cog}	C.G. location along z-coordinate [m]
z_s, z_r	Distance from c.m. to stiffener and ring [m]
m	Mass [kg]
m	Mass of the vehicle [kg]
m	Number of buckle half waves in axial direction [-]
N	Number of Phased array nodes [-]
n	Number of buckle waves in circumferential direction [-]
s	Reference surface area [m^2]

Executive Overview

For many years humanity has dreamt about exploring space and stepping on to other worlds. Our generation is lucky enough to live in the times when such exploration is moving beyond its infancy and is starting to become possible. As such, the eyes of many have turned to Mars - the first planet outside of Earth that would receive human visitors. Multiple plans for a Martian habitat for humans have been already designed and discussed, but one topic providing heated debates is the means of transportation of colonists to the Martian surface. Airbus Defence & Space has tasked the 11 students to come up with a preliminary design of a reusable vehicle, capable of functioning on Mars for a prolonged period of time. The team has further established a Mission Need Statement and a Project Objective Statement:

Mission Need Statement - *Provide a reliable continuous transportation service vehicle for crew and cargo between a Low Mars Orbit orbiter (node) and a Mars base.*

Project Objective Statement - *Design a reliable, sustainable, and reusable vehicle to transport cargo and crew between Low Mars Orbit and a Mars base from 2040 onward, in a time frame of 10 weeks, and by 11 students.*

These statements, together with basic analysis have resulted in a list of requirements, compiled in the Baseline Report [1] and checked for compliance under each subsystem throughout this report. Furthermore, the trade-off between four concepts has been performed in the Midterm Report [2], resulting in the single stage vehicle being the most obvious choice for such mission, as opposed to a multi-stage vehicle, spaceplane and space elevator.

Ascent & Reentry

For the vehicle mission to succeed, the mission profile needs to be established. As such, an orbital node height is defined and the flight path is determined. Both ascent and reentry paths are simulated to have a better understanding of the loads experienced by the vehicle during both phases of the flight, the amount of fuel needed for propulsive landing, as well as for aerodynamic control and heating of the vehicle during the mission.

Guidance, Navigation & Control

A vital part of the system is tracking of the vehicle during flight, enabling navigation of the vehicle and its control. The vehicle is thus equipped with sensors for tracking, including cameras and radar. Control modes and techniques are also discussed, together with configuration and propellant trade-off for reaction control thrusters.

Aerothermodynamics

During the return phase of flight, the vehicle experiences extreme heating from the atmosphere, even though the Martian atmosphere is much thinner than that of Earth.Therefore, the thermal protection is discussed, coupled with aerodynamic coefficients and stability of the vehicle in flight.

Life Support

Charon is designed to support a crew of up to 6 persons. Any human-rated spacecraft needs to have life support, which includes breathable air in a pressurised environment, food and water management, as well as human waste management. For that, an oxygen tank is sized, together with water containers, food supply, and a toilet. Moreover, life support includes thermal control sizing and a radiation shield, making sure the crew is as safe and comfortable as possible during flight.

Main Engine
As any reusable rocket, much of Charon is defined by a propulsive system it utilises. Charon will use a thrust vector controlled 9 engine configuration with 2 engine-out-capability. Due to a requirement mandating manufacture of the propellant on Mars, the engines use liquid methane as fuel and liquid oxygen as oxidiser, fed to an engine in a closed expander cycle. Maximum thrust achievable by a single engine is 310 [kN]. The chapter on main engine system thus explains the design of this engine, including means of achieving such thrust and cooling the combustion chamber and nozzle.

Structures
None of the subsystem sizing and design would matter if it all was not kept together by vehicle structures. The vehicle loading and materials are discussed, mass moments of inertia are computed and the vehicle is sized. This includes sizing crew and cargo compartment, capable of bringing 6 people on board and keeping them safe during various flight modes. The same chapter discusses sizing of the docking mechanism and fuel tanks, concluding with integrating the subsystems into the vehicle.

Power
The vehicle has an updated power budget of 7.8 [kW], powered by a gas turbine using boil-off from the main propellant tanks. Simultaneously, the vehicle is equipped with PEM fuel cells, which can provide power after abort and produce drinking water for the crew. Then, the 4 Power Distribution Units, connected to the main computer, distribute the power throughout the vehicle.

Communications
Charon needs to communicate with the base and orbital node at all times during the mission. For this purpose, a system architecture is discussed later in the chapter, with 4 antennas, two sets of transmitters and receivers, as well as a set of relay satellites around Mars. Furthermore, a link budget is computed and an antenna configuration is discussed, resulting in a final communication flow diagram, describing all the components of the communication infrastructure necessary for Charon operations.

Abort System
Designing a vehicle to be as safe as possible means that astronauts need to have a way to exit the vehicle in case of an emergency. For that, an abort system is designed, analysing different modes of flight abort. Furthermore, the design analyses possible propellants used for escape from the rest of the vehicle, sizing their tanks and the engines. Lastly, deceleration methods are discussed, sizing parachutes needed to slow down and propulsive landing strategies.

Ground Operations
Lastly, the ground operations of Charon are discussed. These include the launch infrastructure and pad location, chosen to be in a Deuteronillus Mensae valley for its scientific interest and abundance of subsurface water resources. Crew and cargo discharge is discussed, making sure the vehicle is protected from dust storms and the crew is discharged safely. Most importantly, a great deal of discussion is devoted to propellant manufacturing on Mars, from water mining and carbon dioxide capture for Sabatier reaction based plant, to the reaction itself and subsequent water electrolysis for oxygen production from water. This process is very energy consuming, therefore energy production methods are discussed, with a conclusion being that solar power method is too inefficient, hence nuclear power reactor is necessary to provide roughly 20 [MW] of power continuously, excluding Martian habitat energy consumption.

Vehicle Characteristics

Charon has a dry mass of 36 tons and a wet mass of 201 tons. It is capable of lifting 6 people with personal belongings, at a total of 1200 [kg] on a mission of a 4-day duration. The vehicle design, development and testing are estimated to cost roughly 3 billion US dollars, with a subsequent 548 million dollars for production of every vehicle, assuming minimal cost reduction from the learning curve. Initial Charon operations assume a five vehicle fleet, hence bringing a total project cost to 8.2 billion dollars without accounting for ground operations. The following operations assume a presence of some infrastructure, for example, propellant manufacturing plant and a nuclear reactor, the total cost of which, together with equipment for refurbishment, would be in the range of 11-17 billion dollars. This cost, however, does not include all the infrastructure and colony necessary to be established on Mars prior to entering into operation.

Mission Profile

Charon will start and finish its missions on the base at Deuteronilus Mensae, 42.5 [degrees] latitude and 25.5 [degrees] longitude. It will then undergo a Hohmann transfer to the node, orbiting at a 609.74 [km] height above Mars at roughly 42.5 [degree] inclination. The vehicle would end its Hohmann transfer at 1000 [m] behind the node, at which point it would initialise the docking procedures. With a duration time of the mission being 4 days, the vehicle would run a quick crew and cargo insertion procedure before reentering the Martian atmosphere and landing propulsively.

Safety

Prior to this report, driving requirements were established, mostly relating to the allowable safety margins and probabilities of Loss of Mission, Loss of Vehicle and Loss of Crew. To evaluate such risks, a detailed fault tree analysis was performed, with a failure probability of each component is evaluated, bringing the total LOM value to 9.75E-3, LOV value to 1.20E-3 and LOC value to 7.90E-4, all meeting the requirements.

Life Cycle

Consideration of all parts of the life cycle of the vehicle is necessary, hence a Project Design and Development Plan is included as well, explaining in detail steps to be performed before the design is frozen and the manufacturing, assembly and integration are performed. Furthermore, the system is verified and validated before being shipped to Mars for the start of its operational cycle. Charon design puts a high emphasis on sustainability, leading to active implementation and assessment of identified sustainability parameters concerning the mission. Additionally, the End-of-Life disposal is discussed thoroughly. It is the intention to reuse Charon as a facility to train astronauts, rather than disposing of the materials altogether.

Taking everything into account, Charon is a unique vehicle with its primary objective to allow a Mars base to operate with near full autonomy, having reliability and sustainability at the forefront of the design. It is, however, a vehicle that requires some prior infrastructure on Mars, primarily due to its requirement to be fully operable on Mars without journeys to Earth. Therefore, it is assumed that this vehicle would not enter operations for the first Martian missions, but would assume a more established colony with some basic infrastructure available.

Further design should take a look into Martian colony and detailed design of ground infrastructure, mostly in terms of refurbishment and parts production. Charon designers should look at manufacturing methods for all parts to have a more detailed budget estimation and minimise risks of going over budget.

Contents

1

Introduction

Human curiosity for space exploration is ever evolving. From the first satellites around Earth, humans have increased their need to explore space. In the Apollo era, only governmental organisations, driven by political needs, controlled space exploration. Eventually, companies also started sharing this curiosity, leading to rapid commercialisation and bringing with it more opportunities.

With current exploration interests shifting towards the sustained human presence on the Moon, as seen with NASA's Artemis programme, manned missions to Mars are also into development. With the long term intentions of exploiting and colonising Mars, a Martian base would have to be established. With this in mind, a continuous supply of humans and materials is needed on a long-term basis. Next to a transportation system between Earth and Mars, a need arises for continuous, economical and sustainable transportation between the Mars surface and an orbiter, functioning as the connecting station. With only a few of such concepts in an early development phase, the opportunity of providing this transportation service arises.

The purpose of this report is to present the design feasibility of a reliable, continuous transportation service vehicle for crew and cargo between a Low Mars Orbit orbiter and a Mars base. In order to do this, a design framework was built, driven by key and stakeholder requirements. From those, the following driving requirements were identified: The vehicle shall reach the Low Mars Orbit. Furthermore, high reliability shall be achieved, resulting in a LOV, LOM and LOC of 2.5 %, 5.5 % and 0.5 %, respectively. Finally, regarding sustainability, all refurbishment components and consumables shall be produced in-situ and 50 % of the dry mass shall be recycled or reused.

From this framework, multiple design concepts were obtained, namely a Single Stage vehicle, Multi Stage vehicle, Spaceplane and Space Elevator. Taking into account safety, sustainability, cost and re-usability, a weighted trade-off was conduced, with the following six input parameters ranging from most to least important: complexity, LOV risk, propellant mass, dry mass, TRL and LOM risk. Out of this trade-off the Single Stage vehicle was identified as the winner.

Before the Single Stage vehicle could be designed, the Market is analysed in Chapter 2 to identify competitors and key design advantages. Next, the functional flow of the mission and its breakdown are defined in Chapter 3. These are needed to understand which functions the vehicle has to perform throughout its mission. With the functions set, the trajectories of the vehicle and its astrodynamic parameters, during ascent (Chapter 4) and reentry (Chapter 5) are analysed. Following this, the aerodynamic and thermal characteristics of the vehicle are examined in Chapter 6. After this, the design of the Guidance, Navigation and Control subsystem is discussed in Chapter 7, where ways of tracking and controlling the vehicle throughout its flight are designed. In Chapter 8 the life support subsystem is designed. Following this, in Chapter 9, the preliminary design of the main propulsion subsystem is discussed. Next, in Chapter 10, structural analysis of the vehicle is completed. The power distribution is then analysed in Chapter 11. Then the communication methods between the vehicle and either base or node, and the Command and Data Handling unit, are discussed in Chapter 12 and Chapter 13 respectively. The latter two precede the safety-critical abort subsystem, analysed in Chapter 14. The ground operations required for the vehicle are then discussed in Chapter 15. The final vehicle layout is presented in Chapter 16, and the vehicle's budgets described in Chapter 17. Following is Chapter 18, assessing the risk, accessibility, maintainability and safety of the vehicle. The sustainability approach and implementation are then explained in Chapter 19. Having completed all designs, requirement compliance is checked in Chapter 20 and the system sensitivity assessed in Chapter 21. Additionally, sensitivity for each subsystem is checked separately. Finally, the design development, conclusion and recommendations are given in Chapter 22 to 24.

2

Market Analysis

To gain an overview of the existing market and how Charon will fit into this market, market analysis has been performed in the baseline report [1]. Building upon it, this chapter presents Charon's place in the projected market. In addition, analyses of the key design advantages and possible competitors are performed.

2.1. Market segmentation

While the launch vehicle market on Earth is getting more and more crowded, the decision to completely ignore it and make a reusable vehicle tailor-made for Martian environments poses a few advantages. Firstly, this reduces the requirements and costs of such vehicle operation, as it is mostly independent of Earth, which reduces cost, while also satisfying conditions for most other celestial bodies, making it usable on the Moon and possibly in an asteroid belt. This market is still not established, giving a time advantage of having a developed and matured concept before the Martian colony is even founded. Simultaneously, the vehicle parameters allow for purposes as suborbital flights on Earth similar to New Sheppard, requiring some heat shield adjustment for reentry. Therefore, according to a market segmentation document from the European Commission [3], Charon falls under Manned and robotic space science, while also being a possible support vehicle for emerging space tourism.

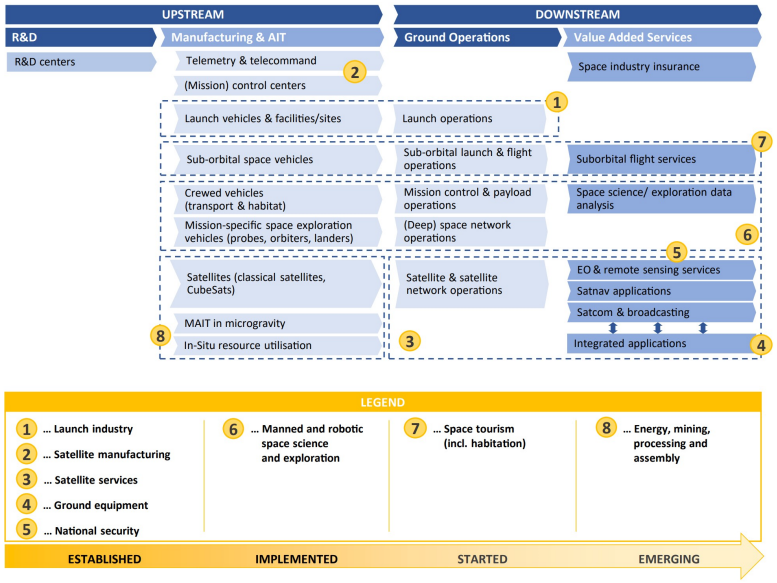

Figure 2.1: Market segments and maturity [3, p 23]

2.2. Market trends

The space industry has been growing steadily ever since its establishment, and so far shows no signs of concern that this growth would be stopped. Bryce Technologies estimate [4] the global space industry to be worth 344.5 billion US Dollars, while Morgan Stanley predicts growth 1.1 trillion US dollars in the next 20 years, with Bank of America Merill Lynch expecting it to be 2.7 trillion US dollars. An interesting note here is that the evaluated industry concerns a "Cislunar economy", not taking into account the 400 quintillion dollars value of Martian, Jupiter and the asteroid belt environment. Currently, it is too difficult to estimate the growth of the space industry around interplanetary colonies, mainly because it is yet not known when and how such colonies will be established. A fact remains that such an undertaking will create a lot of jobs, while being both scientifically and politically important, hence bringing a lot of added value. For this reason, the Martian colony is seen as a definite trend that will be realised eventually, providing a market placement for Charon. The advantage of having a

far developed concept, already before the start of this market segment, along with this definite market placement, leads to a beneficial market share of possibly being more than 50%.

2.3. Stakeholders

Stakeholders are identified in the baseline report [1]. The client is Airbus Defence and Space (ADS). European governmental organisation ESA is an important partner, just as any collaborator in work for ADS. Furthermore, the future Martian colony is an important party, significantly affecting design decisions.

Regarding competition, there is no vehicle that would be a competitor to Charon, as there is no mission happening on Mars presently. However, some concepts for vehicles to operate on Mars are present, such as NASA's Hercules or SpaceX's Starship. Therefore, it is important to note the differences and similarities with competitive designs.

- **SpaceX**: The flagship project Starship is an already in development Earth-to-Mars vehicle, with the largest payload to LEO capacity ever made. [1] Since Starship has to return to Earth, it will need a lot more fuel to be produced on Mars, at higher costs. Moreover, the vehicle has no abort system planned, which will definitely be a downside for any human flight operating organisation. That being said, the vehicle has much higher payload capacity to transport on and off Mars, which is far more suitable for initial colony building, but may prove too expensive in the later stages.
- **NASA**: NASA has already presented the Hercules vehicle concept, their idea for Martian transportation mode. [2] Being very similar to Charon design, Hercules is adaptable for Martian, Lunar and interplanetary conditions, however, their crew is only 4 people, which, while being optimal for initial Mars missions, may not be a big enough transportation mode for a larger colony size.

2.4. Market strategy

Charon is a highly reusable and efficient vehicle, being tailor-designed for Martian environment. Therefore, it would be wise for Airbus to advertise it as the cheapest possible version of a vehicle for Martian node-base transfer, albeit for a more developed colony. This was achieved by making sure the vehicle is as independent from Earth as possible, manufacturing almost all of its components in-situ, from propellant to core structural parts. The vehicle is also designed to require as little maintenance as possible, hence bringing the costs down even more. All of this makes Charon a highly competitive vehicle on the market, with no competitive design being built or tested up to date. The exact cost breakdown is presented in Section 17.3.

2.5. SWOT analysis

Finally, a SWOT analysis is considered, as seen in Figure 2.2. Multiple opportunities and strengths are arising from the client company, such as manpower, infrastructure and funding.

However, there are also downsides. Firstly, due to company risk, design development will likely be postponed until a similar mission has commenced. Furthermore, due to little experience in flight-proven manned space vehicles, a vehicle built by Airbus has to be cheaper to improve concept attractiveness to potential customers.

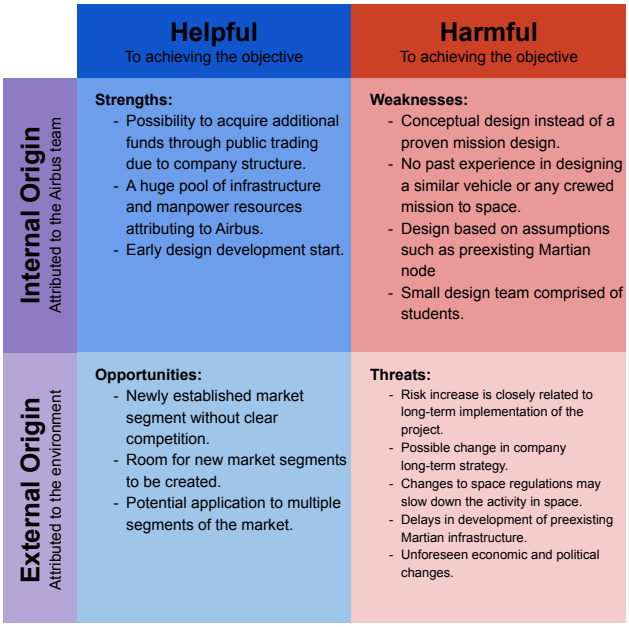

Figure 2.2: SWOT Market Analysis

[1] Starship payload capacity, https://www.popularmechanics.com/science/a32052844/spacex-starship-user-guide-payload/., accessed on the 7th of June 2020

[2] VAB Projects, https://sacd.larc.nasa.gov/vab/vab-projects/hercules/, accessed on the 7th of June 2020

3

Functional Analysis

In this chapter, the functional flow of the mission is presented through the generation of a Functional Flow Block Diagram (FFBD) and a Functional Breakdown Structure (FBS) respectively. Through these two diagrams a better understanding of the functions needed to be executed by the system is obtained. It is important to mention that no way of how this function is succeeded is presented but rather the function itself only. The use of FFBD and FBS is further explained in Section 3.1 and Section 3.2

3.1. Functional Flow Block Diagram

The FFBD shows in a clear and chronological way the functions that have to be performed during the mission as well as how those are inter-connected. It is a rather logical diagram consisting of simple functions following one another on a specific sequence such as that the mission is fulfilled. The generation of the diagram was based on similar missions to that of Charon and is presented in Figure 3.1 [5–7].

3.2. Functional Breakdown Structure

Once the FFBD was obtained, the FBS was easily generated by simply breaking the introduced functions into smaller and as a result, more easily manageable, functions that the different systems of Charon have to do. The FBS presented in the baseline report [1] was extended and updated in such a way that the Single Stage concept is presented. The updated FBS is presented in Figure 3.2. In contrast to the FFBD the FBS is a tree containing all the different functions that the higher levels consist of. No flow and no sequence is presented in it.

Similarly to the baseline report several abort strategies had to be taken into account for the different phases of the mission. Depending on the trajectory phase that the vehicle is at it has to be determined whether or not the crew will return to the surface of the Mars or to the orbital node after abort. In the ascent and descent phase the crew could be safely returned to the Mars' surface, while for the case of the orbital phases the crew will be either abort and return to the orbiter or to the colony.

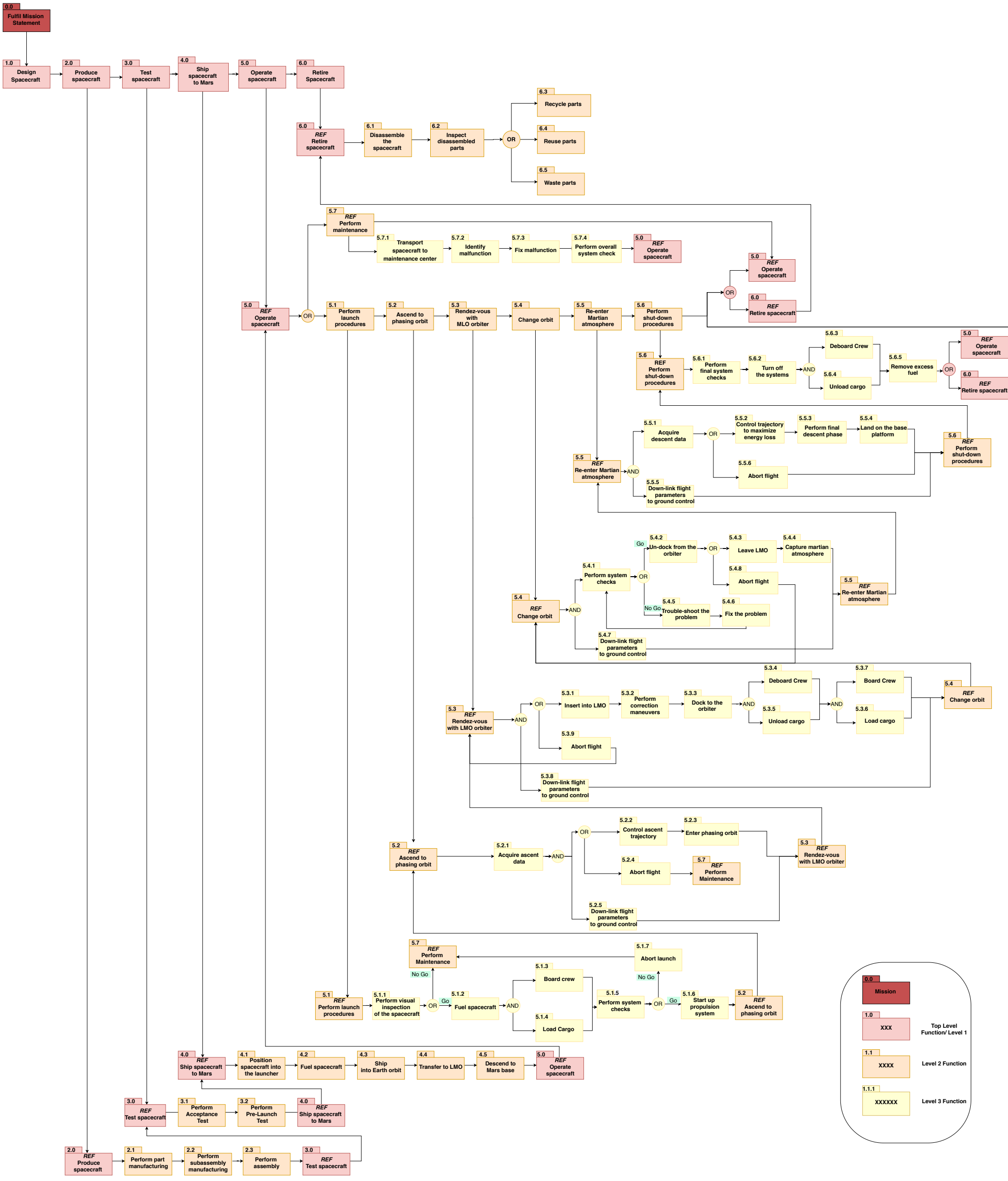

Figure 3.1: Functional Flow Block Diagram

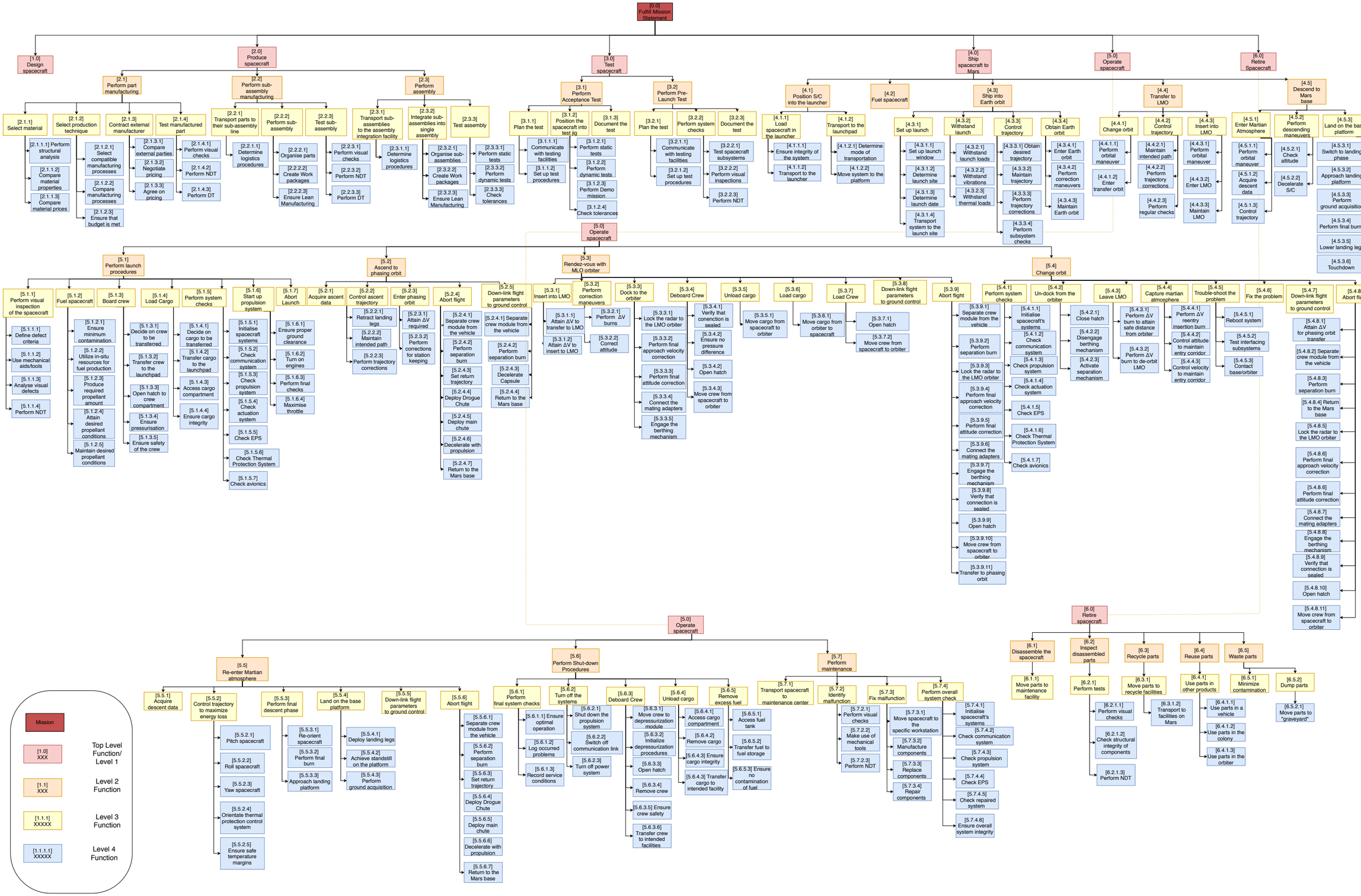

Figure 3.2: Functional Breakdown Structure

4

Ascent Simulation

The following chapter will discuss the ascent trajectory of the vehicle from the launchpad to the phasing orbit. The latter is firstly discussed in Section 4.1. The requirements that have to be met during the design of the ascent trajectory follow discussed in Section 4.2. In Section 4.3 the inputs and outputs of the ascent simulations are introduced. Followed by Section 4.4, explaining how the vehicle will ascend to orbit. This precedes Section 4.5 and Section 4.6, which describe the point-mass simulation and rigid-body simulation, respectively. Finally, the chapter is concluded with Section 4.7 by looking back to the requirements to see whether they were met, and with a discussion analysing the sensitivity of the point-mass simulation, which is the one with most used outputs.

4.1. Phasing orbit

For the vehicle to insert into the LMO, its phase with respect to the node has to be such that when the rendezvous is initialised, as explained in Subsection 7.7.3, the vehicle at the end of the Hohmann transfer is at a 1000 [m] from the node, to be able to start its proximity operations leading to docking. Therefore, the vehicle first attains a phasing orbit to initiate the Hohmann transfer at the required phase difference. Since the vehicle was designed for a maximum orbital operational time of 4 days, of which 2 days allocated from launch to docking, the phasing orbit was chosen to have a synodic period of 2 days. Using Equation 4.1, T_1 is the period of the LMO (as calculated in Subsection 15.3.1), and T_2 the required period of the phasing orbit. In the above, the altitude of the phasing orbit is chosen to be larger than the node's, since attaining such an orbit requires less ΔV. With T_2 known, the semi-major axis, a of the phasing orbit can be solved for by using Equation 4.2.

$$\frac{1}{T_{\text{syn}}} = \frac{1}{T_1} - \frac{1}{T_2} \tag{4.1}$$

$$T = 2\pi\sqrt{\frac{a^3}{\mu}} \tag{4.2}$$

Solving for a and for circular orbits using: $a = R + h$, leads an altitude of 609.74 [km]. The phasing also lies in the same orbital plane as the LMO, meaning that it also is a Mars-repeat orbit, explained in Chapter 15 for the node's orbit.

4.2. Requirements

The requirements that directly influence the design of the ascent trajectory, are:

- **SRV-CONS-TECH-2.4-B**: [T] The burn program shall limit maximum linear accelerations to 4 g during launch and reentry operations. *Originally stated as 3 g*
- **SRV-CONS-TECH-3**: [S] The vehicle shall be able to carry a payload in the range of 500 [kg] to 1000 [kg] on payload-only flights.
- **SRV-CONS-TECH-4**: [S] The vehicle shall be able to transport a crew of up to 6 persons.
- **SRV-TECH-OPER-1.2**: [T] The propulsion system shall have a minimum thrust-to-weight ratio of 1.5 relative to Martian gravitational acceleration at maximum mass.
- **SRV-CONS-TECH-2.7**: [T] The maximum g-forces experienced by the crew during nominal operations shall not exceed 4 g.

4.3. Analysis; Inputs and Outputs

All inputs required by other subsystems, in generating the ascent simulations, are presented in Table 4.1 together with their outputs needed by other subsystems.

Table 4.1: Inputs and Outputs of Ascent

Analysis	Inputs	Outputs
For point-mass simulation	Launch pad location, performance parameters, diameter, aerodynamic coefficients, mass, Martian parameters	acceleration, position, velocities, forces, propellant mass, pitch angle, pitch rate, pitch acceleration, time
For rigid-body simulation	Launch pad location, performance parameters, diameter, aerodynamic coefficients, mass, MMOI, c.g., vehicle's geometry	acceleration, position, velocities, forces, propellant mass, moments, time

The aerodynamic coefficients, from Chapter 6, are the lift coefficient C_L and drag coefficient C_D used for ascent were based on Space Shuttle data.The performance parameters needed, from Chapter 9, are: the specific impulse I_{sp}, needed to compute the exhaust velocity c_{eff}, the nozzle exit area A_e and the exhaust exit pressure p_e.The diameter d, used to compute the reference surface area of the vehicle, S (required to compute the aerodynamic forces), together with the MMOI, c.g. and general vehicle's geometry, were taken from Chapter 10. The surface area was defined as the cross-sectional area of the vehicle perpendicular to the incoming flow.

Furthermore, before the general subsystems iteration, the wet mass used was taken from the Class II mass budget [2]. Later on, the Class III mass estimation, stemming from the general subsystem iteration, was used. The latter served as input to generate the results presented in Subsection 4.5.3 and Subsection 4.6.3. Finally, the latitude, longitude and elevation of the launch pad were taken from Chapter 15. Regarding the Mars data [1], the required parameters are: the equatorial radius, the mean volumetric radius, the gravitational parameter, the J_2 scaling factor, the rotational speed about its axis, the mean molecular weight and the ratio of specific heats of its atmosphere.

4.4. Ascent strategy

The type of ascent profile greatly influences the ΔV and as a result, the propellant mass required to attain orbit. Therefore it is desirable to ascend such that the ΔV required to attain orbit is kept to a minimum. From [8], it can be seen that for orbital altitudes greater than 300 [km], a Hohmann Transfer Ascent (HTA), Figure 4.1a, leads a more efficient ascent with respect to ΔV required, if compared to a Direct Ascent (DA), Figure 4.1b.

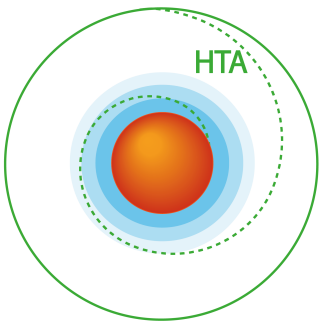

(a) Hohmann Transfer Ascent (HTA)

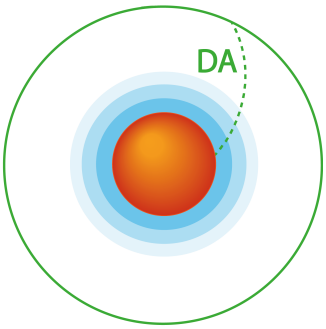

(b) Direct Ascent (DA)

Figure 4.1: Ascent methods

Albeit being more propellant efficient, the HTA requires longer flight times, a more complex control system and a more involved tracking system, which would require a world-wide network of tracking stations to be present on Mars. Since having such an elaborate network system present at Mars by 2040 is not realistic, the Direct Ascent was chosen. Also, in the case of an abort scenario during HTA, the capsule could end up stranded on the other side of the planet, meaning that complex rescue operations would be required. For the DA, a gravity turn was chosen, since this ascent manoeuvre

[1]Mars Fact Sheet, NASA, `https://nssdc.gsfc.nasa.gov/planetary/factsheet/marsfact.html`, accessed on the 7th of June 2020

makes use of the available gravity of the planet to turn the vehicle. In addition to minimising the energy used to get into orbit, during a gravity turn the vehicle will fly with zero angle of attack, hence reducing the aerodynamic forces to a minimum.

To prevent having measurement errors influencing the initial flight path angle too much, it was decided to start the gravity turn at an altitude of 100 [m] off the ground. Thus, Charon will fly the first 100 [m] vertically up, and then pitch over to follow a gravity turn directly into the phasing orbit. The gravity turn part of the trajectory was designed to limit the acceleration experienced by the crew to a maximum of 4 Martian-g's, since the crew would be accustomed to experiencing one Martian g. Subjecting the crew for a prolonged period to accelerations higher than that was deemed to put their health at unnecessary risk, given the small amount of propellant mass that could be saved, as presented in Subsection 4.5.3.

4.5. 2D point-mass simulation

A 2D point-mass simulation was developed to be able to study how given flight parameters influence the vehicle's loads and trajectory, to generate the inputs for the more detailed 3D rigid-body simulation, discussed in 4.6, and as a tool capable of quickly generating the flight data required by other subsystems during their design and to iterate the design of the vehicle together with the latter subsystems. This section will first start with a discussion on the reference frame used and the assumptions made. This is followed by Subsection 4.5.1, in which the equation used during the simulation, and the procedure used to solve them, are explained. Then Subsection 4.5.3 follows with the results of the simulation. Afterwards, in Subsection 4.5.4, the simulation is verified and validated.

4.5.1. Reference frame and assumptions

The reference and Free Body Diagram used throughout this section are shown in Figure 4.2. The reference frame is fixed on the surface of Mars, with its origin on the launch pad. It is also positioned such that it lies in the same orbital plane as the phasing orbit, with the X-axis pointing eastward in the direction of the ground track of the phasing orbit.

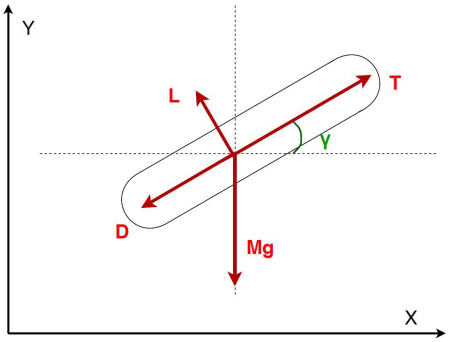

Figure 4.2: 2D point-mass Free Body Diagram

In Figure 4.2, it is assumed that Mars is flat and non-rotating, in order to simplify the problem, so to obtain better estimates of variables that influence the trajectory. Once the desired trajectory is achieved, the latter variables are input into the rigid-body simulation. As will be explained in the following subsection, the effect of Mars' rotation is taken into account in the point-mass simulation at the end of flight, where the velocity gained due to launching eastward from the rotating surface of Mars is added to the final velocity of the vehicle.

Additionally, for the vertical part of the ascent, aerodynamic forces were neglected due to the very low velocity that the vehicle has, combined with the low density of the Martian atmosphere.

4.5.2. Equations and solving procedure

Following from Figure 4.2, and Equations 4.3 and 4.4the gravity turn part of the ascent has been derived.

$$M\frac{dVx}{dt} = (F_T - F_D)\frac{Vx}{V} - F_L\frac{Vz}{V} \qquad (4.3) \qquad M\frac{dVz}{dt} = (F_T - F_D)\frac{Vz}{V} - Mg + F_L\frac{Vx}{V} \qquad (4.4)$$

The fact that for an ideal gravity turn, the angle of attack is zero, hence the flight path angle equals the pitch angle, results in : $cos(\gamma) = \frac{Vx}{V}$ and $sin(\gamma) = \frac{Vz}{V}$. The lift and drag were computed through Equation 4.5 and Equation 4.6, respectively.

$$F_L = \frac{1}{2}\rho V^2 C_L S \qquad (4.5) \qquad F_D = \frac{1}{2}\rho V^2 C_D S \qquad (4.6)$$

The simulation was initially only run for a gravity turn from the launch pad, but since the required initial tilt off of the vertical axis required is too small, the gravity turn instead has to be initiated at a to be defined altitude. Until this altitude, the vehicle will ascend vertically under a constant Thrust-to-Weight ratio. Therefore from [9] Equation 4.7 and Equation 4.8 could then be used to calculate the

conditions at the instance the gravity turn is initiated.

$$t_b = \frac{c_{eff}}{g_0 \frac{T}{W}} \ln(\Lambda) \quad (4.7) \qquad V_e = \frac{c_{eff}}{\frac{T}{W}} \ln(\Lambda)(\frac{T}{W} - 1) \quad (4.8)$$

The altitude at which the gravity turn would be initiated was chosen such that the initial tilt would be at least 0.5 [°]. The corresponding velocity at that altitude used the Falcon Heavy as reference [2]. Then, to obtain the initial conditions for the gravity turn, Equation 4.7 and Equation 4.8, were solved for the burn time t_b and the propellant mass (gotten from the mass fraction Λ). The latter was subtracted from the initial wet mass to obtain the mass at the start of the gravity turn. Next, from Equation 4.3 and Equation 4.4 the accelerations were computed, which were used to determine V_x and V_z using Forward Euler with a time step of 0.01 [s]. The latter velocities were then differentiated using a Forward Difference scheme to obtain the altitude Z and lateral distance X.

The thrust required was computed from the Thrust-to-Weight ratio profile, such that the thrust would correspond to the maximum Thrust-to-Weight ratio allowed to be achieved at that instance of flight. Achieving the highest Thrust-to-Weight ratio allowed, minimises the gravity losses (defined as gt_b), since it would lead to a lower burn time (see Equation 4.7). For that, a linear Thrust-to-Weight ratio profile was used, varying from a minimum of 1.5 to a maximum 4, which keeps the maximum thrust below its limit, see Chapter 9. For the burn time, an initial guess corresponding to a burn time with constant Thrust-to-Weight ratio of 1.5 was used, while for the initial tilt a 5 [°] tilt was used.

Once an iteration was completed, the atmospheric properties, the gravity, aerodynamic coefficients and the mass, were updated for the new achieved height. The gravity at a given altitude was computed using the gravity potential presented in Equation 5.1, accounting for the oblateness of Mars (19% higher than Earth's), to be able to account for the most dominant perturbation effect in Mars' gravity. The new mass was found by subtracting the current mass flow from the previous mass. The mass flow, $\dot{m}$, was computed by solving Equation 4.9 for the latter.

$$F_T = \dot{m} c_{eff} + A_e(p_e - p) \quad (4.9)$$

After engine cut-off, the vehicle is left coasting. The equations were solved until the orbital altitude was achieved. If the final velocity, accounting for the initial velocity due to Mars' rotation, was below the required velocity orbital velocity, the burn time was increased. Since the burn time influenced the final velocity more than the initial tilt, the latter was reduced from its initial guess, so to limit the maximum acceleration of the vehicle to 3 Martian g's. The initial tilt was chosen such that the gravity gradient of Mars could be used as much as possible to rotate the vehicle while keeping the experienced acceleration below 3 Martian g's. With the orbital velocity achieved, the burn time and initial tilt were finally tweaked to make the apoapsis of the trajectory coincide with the phasing orbit. The final flight path angle (needed to be zero to attain orbit), was then given to Chapter 7 as an attitude correction needed to be performed before the phasing orbit altitude is achieved.

4.5.3. Results

After having iterated the design, and taking the updated values of the inputs described in Section 4.3, the results can be discussed. With a total burn time of 506.39 [s] and initial tilt of 0.51 [°], the vehicle is able to attain phasing orbit with the required velocity of 3.27 [km/s] by experiencing a maximum acceleration felt by the crew of 2.83 Martian g's (or 1.45 Earth g's). The wet mass included a payload mass of 1200 [kg], together with margins for each subsystem, as seen in Table 17.1. The payload mass corresponded to either a crew-only flight of 6 people or cargo-only flight. The mass of one person was taken to be 200 [kg], to also account for the mass of the spacesuit and personal belongings.

Table 4.2: Output burn time, ΔV and propellant mass of the point-mass simulation

Parameters	Burn time [s]	ΔV [m/s]
Vertical flight	16.47	91.67
Gravity turn	489.52	4532.69
Total	**505.99**	**4624.36**

[2]Falcon Heavy Test Flight, SpaceX, `https://www.youtube.com/watch?v=wbSwFU6tY1c`, accessed on the 8th of June 2020

Figure 4.3a shows the ascent altitude profile (blue) and the velocity profile (orange) for the gravity turn, and Figure 4.3b depicts the acceleration experienced by the crew in Martian g's (red) and the thrust (green). The flight path angle that will have to be corrected by the RCS was found to be 27.5[°]. The maximum acceleration experienced by the crew was found to be 3.83 Martian-g's, or 14.2 [m/s^2] (equal to 1.45 Earth g's). While the maximum acceleration of the vehicle is 10.5 [m/s^2].

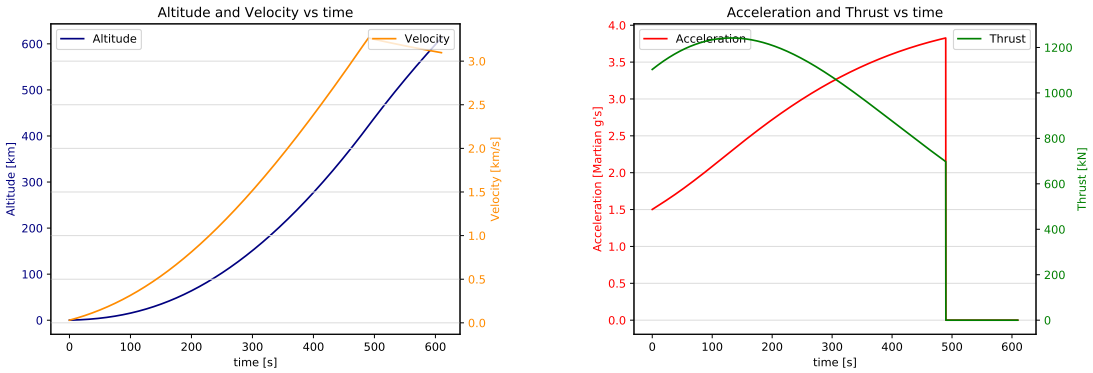

(a) Altitude and Velocity vs time

(b) Acceleration experienced by the crew, and Thrust, vs time

Figure 4.3: Variation of parameters in time

From the results generated, Figure 4.4 was created to illustrate the main flight phases during ascent.

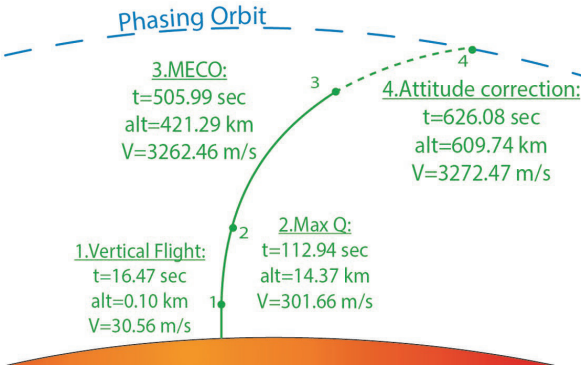

Figure 4.4: Ascent profile

To demonstrate that the propellant mass saved by achieving higher accelerations is small, the maximum Thrust-to-Weight ratio was increased to 5.2 (while still keeping a linear variation), the burn time decreased to 383 [s] and initial tilt increased to 1 [°]. Doing so leads the new values presented in Table 4.3. The maximum thrust achieved is 1528.45 [kN], which leaves 15.55 [kN] of margin to achieve the maximum allowable thrust. This leads a 3% saving in ΔV, reducing the propellant mass by 2154.65 [kg], while achieving a maximum perceived acceleration by the crew of 4.88 Martian-g's (1.84 Earth-g's). Therefore the maximum allowable thrust is more constraining than the required maximum acceleration.

Table 4.3: Output burn time, ΔV and propellant mass of the point-mass simulation, for higher maximum thrust

Parameters	**Burn time [s]**	ΔV **[m/s]**
Vertical flight	16.47	91.67
Gravity turn	383	4398.19
Total	**399.47**	**4489.86**

4.5.4. Verification and Validation

The point-mass simulation was verified by means of unit tests, where for simple inputs a function's output was compared to solutions from worked out examples in [9], [10] or [11] and integration tests.

For the latter, the code was run at each major function's addition to check that the output values made sense, and if for null inputs the program returned a null output or inf. Once the whole program was completed, it was first checked whether various plotted results looked similar to analytical solutions plotted in [9] for a gravity turn, and whether the results made sense. Then the inputs were drastically changed to see whether they would significantly change the results.

For validation, the ascent data from the Space Shuttle[3] was used, where the altitude and mass are provided as a function of time until an altitude of 44.7 [km]. To ensure that the data used already corresponded to a gravity turn, only the points with an altitude above 10 [km] were used. Moreover, the data provided only considered the trajectory pre boosters separation, hence regarded a single-stage vehicle. To this data a parabola was fitted, evaluating its parameters by means of a non-linear least square regression [4] and the standard deviation errors of the estimated parameters computed. The astrodynamic parameters of Mars were substituted with Earth's [5], and the atmospheric properties replaced by an International Standard Atmosphere calculator [6].

Before the point-mass could be validated, the missing parameters for the Space Shuttle had to be found. To account for the Shuttle having boosters, the point-mass simulation was slightly modified to be able to work with multiple propulsion systems. To compute the new mass, the mass flow was divided into the one for the solid rocket boosters and the main engine one. Once the total thrust was computed, the mass flows were found following that the boosters provide 71.4% of the total thrust at lift-off[7]. Necessary data for the Space Shuttle is shown in Table 4.4. For the Space Shuttle, a linearly varying Thrust-to-Weight ratio from 2 to 3 was used[8]. Doing so leads a 15% throttleability of the solid rocket boosters for the considered data, which is in line with the one-third total throttleability of the boosters from lift-off[7]. Due to missing data on the exhaust pressure of the boosters, they were assumed to be ideally expanded. The specific impulse of the boosters was computed with the thrust per booster and initial mass flow of a booster from Table 4.4, leading $I_{sp} = 242.1$ [s].

Table 4.4: Space Shuttle data used for Validation of point-mass simulation

Parameter	Value	Reference
Initial mass flow of a booster	5265.00 [kg/s]	[12]
Thrust of a booster (sea level)	$12.5 \cdot 10^6$ [N]	[12]
I_{sp} main engines (sea level)	395.90 [s]	[12]
Initial velocity	447.93 [m/s]	[8]
surface area	249.90 [m^2]	[13]
percent of thrust from boosters	71.4%	[7]
p_e main engines	27357.20 [Pa]	[12]
throat area main engines	0.053 [m^2]	[12]
expansion ratio main engines	77.45 [-]	[12]

The results comparing altitude and mass are shown in Figure 4.5a and Figure 4.5b respectively, where simulation results are plotted against the data (crosses). The shaded areas represent the boundaries of the parabolic fit if one standard deviation of the estimated parameters is used. Since no data could be found on the initial tilt that the Space Shuttle at around 11 [km], the latter was estimated to be 30 [°].

To compute the error in the simulation, the MAPE (Mean Absolute Percentage Error) was used, which was computed via Equation 4.10, where: n is the number of samples, A_i the data value and F_i

[3]Exploring space through ALGEBRA, Space Shuttle Ascent, https://www.nasa.gov/pdf/466767main_AL_ED_Shuttle_Ascent_5-13-08.pdf, accessed on the 7th of June 2020

[4]scipy.optimize.curve_fit, https://docs.scipy.org/doc/scipy/reference/generated/scipy.optimize.curve_fit.html, accessed on the 7th of June 2020

[5]Earth Fact Sheet, https://nssdc.gsfc.nasa.gov/planetary/factsheet/earthfact.html, accessed on the 7th of June 2020

[6]Properties Of The U.S. Standard Atmosphere 1976, http://www.pdas.com/atmos.html, accessed on the 7th of June 2020

[7]SOLID ROCKET BOOSTERS , https://science.ksc.nasa.gov/shuttle/technology/sts-newsref/srb.html, accessed on the 7th of June 2020

[8]STS-134 - The final launch of Endeavour , https://www.youtube.com/watch?v=ShRa2RG2KDI, accessed on the 7th of June 2020

the simulated value at time i. Computing it for the altitude leads $MAPE = 1.78\%$, while for the mass $MAPE = 1.55\%$, which is deemed low enough for the current preliminary design phase. The previous errors are to be considered as estimates of the real error, due to the possible variation in the required parameters (e.g. mass flow) and due to the fact that an estimate for the initial tilt was used, instead of the real value.

$$MAPE = \frac{100}{n} \sum_{i}^{n} \left| \frac{A_i - F_i}{A_i} \right| \tag{4.10}$$

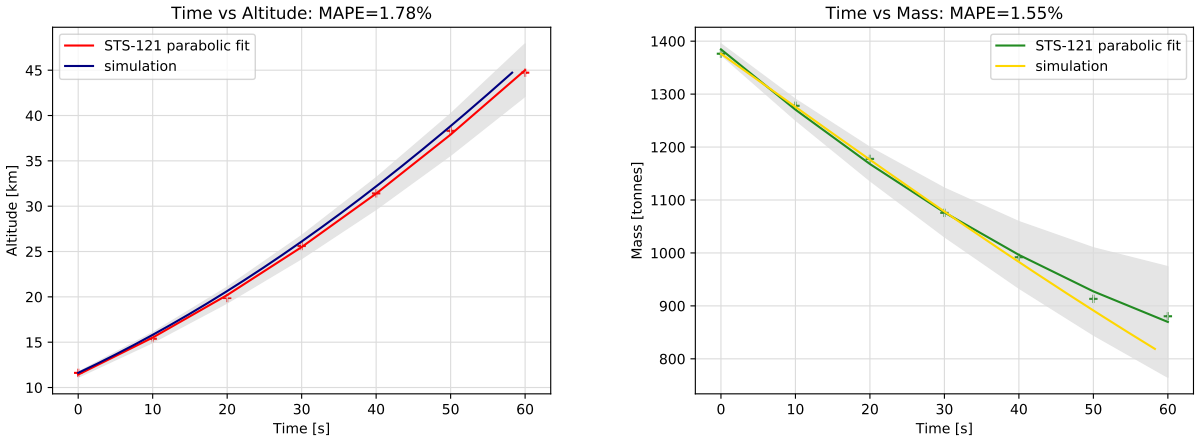

(a) Altitude vs time: point-mass model validation

(b) Mass vs time: point-mass model validation

Figure 4.5: Point-mass model validation: data vs simulation

4.6. 3D rigid-body simulation

After having solved the point-mass simulation and iterated the design with it, a 3D rigid-body simulation was created. The latter was mainly developed to investigate the stability of the vehicle during the gravity turn. The following section about the rigid-body simulation will follow the same layout as the previous section about the point-mass simulation.

4.6.1. Reference frames and assumptions

To describe the motion of the vehicle, an inertial reference frame is needed. For that, the Mars-Centred Inertial reference frame (F_I) was used. The translational equations of motion were solved with respect to F_I in the vehicle-carried normal Mars reference frame (F_E), to make use of the spherical coordinates in which the location of the Mars base, from Chapter 15 is given. The velocities were instead computed in Cartesian coordinates. Figure 4.6a shows the relationship between F_I and F_E.

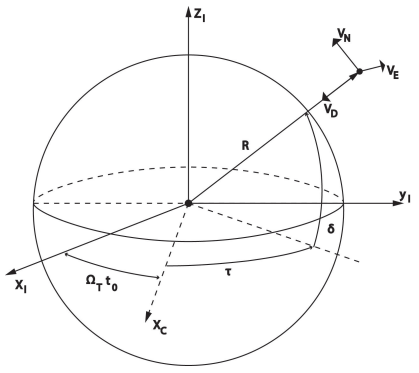

(a) Relation between F_I and F_E

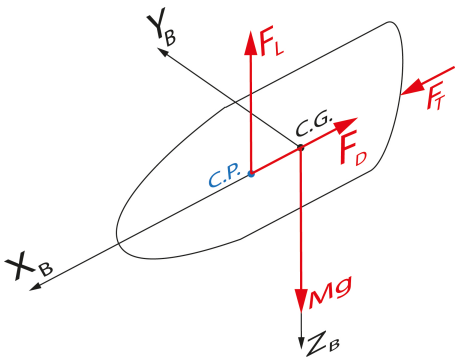

(b) Free Body Diagram in F_B

Figure 4.6: Reference frames

The forces were computed in the Body-fixed reference frame (F_B), which together with the Free-Body-Diagram is shown in Figure 4.6b, with its origin in the c.g. of the vehicle. The equations of rotational motion were computed in the Body-fixed frame with respect to the inertial frame. Which were then linked to F_E via the attitude equations. To do so, use of the Euler angles was made.

Assumptions made throughout this section were: the vehicle is infinitely stiff (no deformation of the structure), the stationary propellant in the tanks (no c.g. shift and forces induced by sloshing), no thrust misalignment (pure axial thrust) or manufacturing faults, the vehicle is symmetric and the c.p. is independent of Mach number (remains fixed during flight). Also, the Coriolis moment and relative moment due to the mass variation were neglected, since the velocity at which the c.g. shifts is much smaller than the exhaust velocity, as described in [9].

4.6.2. Equations and solving procedure

The equations of motion presented in the following subsection were derived from the Principle of Solidification, discussed in [10]. Also, the aerodynamic forces and the mass flow were computed the same way as in Subsection 4.5.2 with Equation 4.5, Equation 4.6 and Equation 4.9. The computation of the Thrust-to-Weight ratio,thrust, atmospheric and aerodynamic properties followed the same procedures described in Subsection 4.5.2. Moreover, the same steps as in Subsection 4.5.2 were used to go from accelerations to velocities and then positions. The burn time and initial tilt used, where the ones that originated from the point-mass simulation lead to Table 4.3. To rotate the vehicle from F_E to the correct F_B attitude, to point in the same way as in Subsection 4.5.1, the vehicle was rolled 90 [°] and pitched -(90-initial tilt) [°]. A step size of 0.01 [s] for the numerical methods was used. The required initial parameters were first computed. Then to compute the accelerations equations of motion, the external forces experienced by the vehicle had to be calculated.

$$\dot{V}_N = \frac{F_x^E}{M} - 2\Omega_t V_E \sin\delta - \Omega_t^2 R \sin\delta\cos\delta - \frac{V_E^2 \tan\delta - V_N V_D}{R} \tag{4.11}$$

$$\dot{V}_E = \frac{F_y^E}{M} + 2\Omega_t \left(V_D \cos\delta + V_N \sin\delta\right) + \frac{V_E}{R}\left(V_N \tan\delta + V_D\right) \tag{4.12}$$

$$\dot{V}_D = \frac{F_z^E}{m} - 2\Omega_t V_E \cos\delta - \Omega_t^2 R \cos^2\delta - \frac{V_E^2 + V_N^2}{R} \tag{4.13}$$

From Figure 4.6b, the thrust and aerodynamic forces in F_B used are: $(-F_T - F_D)\mathbf{x_B} + (-F_L)\mathbf{z_B}$. While the weight used to account for the vehicle tilting, pitching and rolling, taken from [9], is: $(-Mgsin(\theta))\mathbf{x_B} + (Mgcos(\theta)sin(\varphi))\mathbf{y_B} + (Mgcos(\theta)cos(\varphi))\mathbf{z_B}$. The forces were then transformed to F_E by using the transpose of Equation 4.14 leading $(F_x^E, F_y^E, F_z^E)^T$.

$$T_{BE} = \begin{bmatrix} 1 & 0 & 0 \\ 0 & \cos\varphi & \sin\varphi \\ 0 & -\sin\varphi & \cos\varphi \end{bmatrix} \begin{bmatrix} \cos\theta & 0 & -\sin\theta \\ 0 & 1 & 0 \\ \sin\theta & 0 & \cos\theta \end{bmatrix} \begin{bmatrix} \cos\psi & \sin\psi & 0 \\ -\sin\psi & \cos\psi & 0 \\ 0 & 0 & 1 \end{bmatrix} \tag{4.14}$$

Once the accelerations and velocities were computed, the new position was attained by using a Forward Differences scheme using the rate of change of latitude, $\dot{\delta}$, and of longitude, $\dot{\tau}$, from Equation 4.15 and Equation 4.16 respectively. The altitude was computed from: $\dot{R} = -V_D$.

$$\dot{\delta} = \frac{V_N}{R} \tag{4.15}$$

$$\dot{\tau} = \frac{V_E}{R\cos\delta} \tag{4.16}$$

A similar procedure was adopted to solve for the new angular rates of the vehicle, $\Omega_{bI}^b = (p, q, r)^T$, and Euler angles, using the equations of rotational motion Equation 4.17 and kinematic equations Equation 4.18, Equation 4.19 and Equation 4.20.

$$\dot{\Omega}_{bI}^b = I^{-1}\left(\tilde{M}_{cm}^b - \frac{\delta I}{\delta t}\Omega_{bI}^b - \Omega_{bI}^b \times I\Omega_{bI}^b\right) \tag{4.17}$$

$$\dot{\psi} = \frac{\sin\varphi}{\cos\theta}\tilde{q} + \frac{\cos\varphi}{\cos\theta}\tilde{r} \tag{4.18}$$

$$\dot{\theta} = \cos\varphi\tilde{q} - \sin\varphi\tilde{r} \tag{4.19}$$

$$\dot{\varphi} = \tilde{p} + \sin\varphi \tan\theta \tilde{q} + \cos\varphi \tan\theta \tilde{r} \tag{4.20}$$

with:

$$\tilde{p} = p + c\theta s\psi \dot{\delta} - [c\delta c\psi c\theta + s\delta s\theta](\dot{t} + \Omega_t) \tag{4.21}$$

$$\tilde{q} = q + (\mathrm{s}\psi\mathrm{s}\theta\mathrm{s}\varphi + \mathrm{c}\psi\mathrm{c}\varphi)\dot{\delta} - [\mathrm{c}\delta(\mathrm{c}\psi\mathrm{s}\theta\mathrm{s}\varphi - \mathrm{s}\psi\mathrm{c}\varphi) - \mathrm{s}\delta\mathrm{c}\theta\mathrm{s}\varphi](\dot{t} + \Omega_t) \tag{4.22}$$

$$\tilde{r} = r + (\mathrm{s}\psi\mathrm{c}\varphi\mathrm{s}\theta - \mathrm{c}\psi\mathrm{s}\varphi)\dot{\delta} - [c\delta(\mathrm{s}\psi\mathrm{s}\varphi + \mathrm{c}\psi\mathrm{s}\theta\mathrm{c}\varphi) - \mathrm{s}\delta\mathrm{c}\theta\mathrm{c}\varphi](\dot{t} + \Omega_t) \tag{4.23}$$

With c being the cosine and s the sine. In Equation 4.17, I and $\delta I \delta t$ are diagonal matrices containing the MMOI: I_x, I_y, I_z, and their derivatives, respectively. The MMOI at a given time were computed by fitting a parabolic function to the MMOI provided by Chapter 10, using the same method as previously mentioned in Subsection 4.5.4. The derivative of the MMOI was again computed with a Forward Differences scheme. To compute Equation 4.17, the external moments experienced by the vehicle had to be calculated. From Figure 4.6b the only moment that the vehicle is subjected to is the aerodynamic moment due to lift, that is: $F_L x_{c.p.}$. Although assumed fixed on the vehicle, the c.p. moves with respect to the c.g. due to the location of the latter varying throughout flight. To account for the moving c.g. from c.p., first a third-order polynomial (due to larger curvature than MMOI) was fitted to the c.g. data from Chapter 10 and the c.g. shift computed. Then, the vehicle-stationary c.p. computed through the Method of Projected Areas, discussed in [14], and the distance between c.p. and c.g. computed. For the Projected Area Method, only the capsule and the tanks with skirts were considered. The results of the MMOI and varying c.g. are depicted in Figure 4.7a. The c.g. fit slightly overshoots at the boundaries, meaning that for future iterations more data point from Chapter 10 would be required. Since the aerodynamic moment made the vehicle unstable, due to the c.p. being between 5.6 and 4.8 [m] in front of the c.g., the former was set to zero in the simulation, and its corresponding value, at every time, given to the RCS system, discussed in Chapter 7, to counteract it to make the vehicle stable.

Once the angular rates were computed, each parameter was updated, and the new mass computed the same way as in Subsection 4.5.2.

4.6.3. Results and Verification

Using as input for the pitch rate the one found in the point-mass model, due to the gravity turn, leads to Figure Figure 4.7b which shows the trajectory with respect to Mars, together with the aerodynamic moments to be counteracted by the control subsystem. The latter was found to have a maximum value of 2112.4 [Nm].

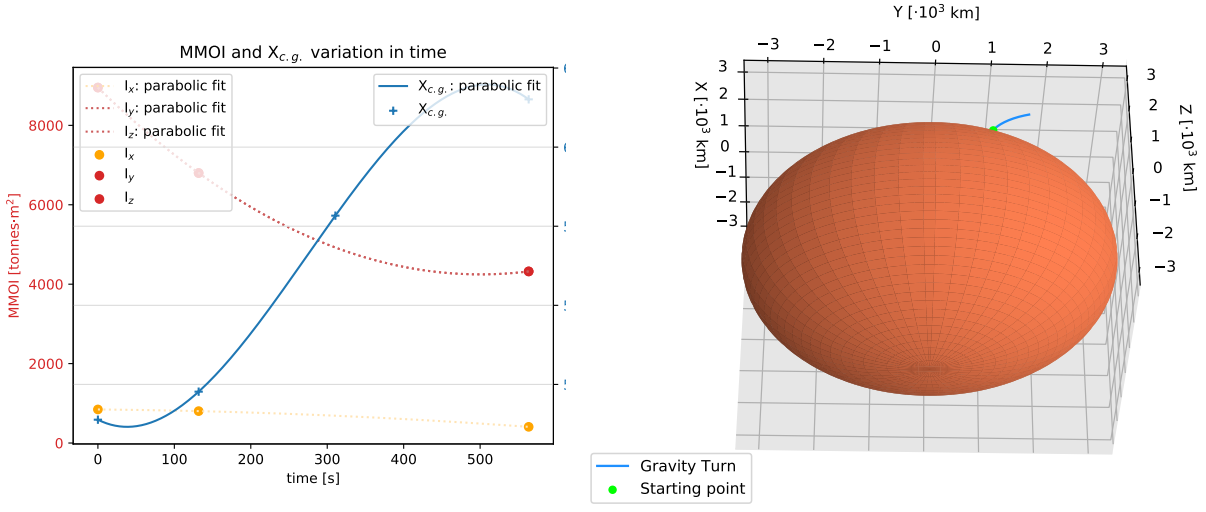

(a) MMOI and c.g. fits

(b) View of the trajectory with respect to Mars

Figure 4.7: Data fit and trajectory

The same verification procedure as in Subsection 4.5.4 was applied to the rigid-body. Then the results of the rigid-body simulation were compared to the point-mass results, to analyse their magnitude and behaviour.

4.7. Requirement Compliance and Sensitivity Analysis

With the ascent trajectory finalised, the compliance with the requirements can be assessed, which is shown in Table 4.5.

Table 4.5: Requirement compliance for Ascent

Requirement	Completion	Explanation
SRV-CONS-TECH-2.4-B	✓	max. acceleration is 1.07 Earth-g's
SRV-CONS-TECH-3	✓	Designed for 1200 kg
SRV-CONS-TECH-4	✓	Designed for 6 people+margins
SRV-TECH-OPER-1.2	✓	Designed for its low thrust-to-weight ratio
SRV-CONS-TECH-2.7	✓	max. acceleration experienced is 1.45 Earth-g's

The sensitivity analysis for the point-mass ascent trajectory simulation is used to determine the standard deviation on the propellant mass needed to reach orbit, given the uncertainty of certain initial conditions. A Monte Carlo implementation is used with 100000 runs to determine this standard deviation. Here, the relevant input parameters are assumed to be normally distributed with their respective means and standard deviations. The varied parameters are presented in Table 4.6.

Table 4.6: Initial parameters varied for Monte Carlo simulation

Parameter	Mean	Standard Deviation
Initial thrust to weight ratio	1.5	0.02
Atmospheric scale height	11015 [m]	866.13 [m]
Initial flight path angle	89.49 [°]	1.5 [arcsec]

The standard deviation on the thrust to weight ratio is obtained from [15] where test data from the RL10A engine was compared to similar empirical models that were used to design the engines for Charon in Chapter 9. From this analysis, a standard deviation on engine thrust of 1.333% was inferred. The atmospheric density used in this simulation is derived from an exponential model outlined in Chapter 5. Its standard deviation is determined from the difference in maximum and minimum atmospheric scale heights during a Martian year. Finally, the standard deviation of the flight path angle is taken as 1.5 [arcsec] from Subsection 7.3.1. From the Monte Carlo simulation, the mean of the propellant mass was found to be 143273.34 [kg], with a standard deviation of 146.40 [kg]. Meaning that in order to reach orbit, under the given uncertainties, with a confidence of 99.9%, 439.213 [kg] of additional propellant are required. This number is less than 3% of the amount of reserve propellant for the mission, meaning that the impact of this deviation is almost negligible.

As a further recommendation for the next design phase, it is advised to look into more accurate predictor-corrector single-step integration schemes (e.g. Runge-Kutta), or multi-step integration schemes (e.g. Adams-Bashforth), to obtain more accurate results, required in the next more detailed design phase. For the Forward Euler used in this Chapter, a step-size of 0.01 [s] was chosen since it kept the solution stable while achieving higher accuracy, without too large computational time. Although the global discretisation error with Forward Euler is directly proportional to the step-size, the accuracy attained with this method was deemed appropriate for the current design phase. To be able to iterate the design relatively fast, Forward Euler with a small step-size was chosen over a more accurate integration method.

5

Reentry Simulation

The simulation of the reentry trajectory dynamics of Charon has a significant impact on the design of the control and thermal subsystems. Starting from the reentry altitude and velocity determined in the midterm report [2] a three dimensional simulation of the reentry trajectory has been performed in Section 5.4, using the model in Section 5.3. The ground tracking system designed in Section 7.4 has been used in Section 5.5 to determine positional uncertainty of the initial conditions, with a Monte Carlo simulation used to determine possible impact points. In Section 5.6 these impact points are used to determine the necessary manoeuvring interval of the vehicle during the reentry phase. The model is extended to include aerodynamic heating and thrust control in Section 5.7 and 5.8.

5.1. Analysis: Inputs and Outputs

Table 5.1 presents the inputs and outputs of the reentry simulations.

Table 5.1: Inputs and outputs of the relevant simulation tools

Analysis	**Inputs**	**Outputs**
Trajectory Simulation	Initial state, Vehicle properties	Evolution of state over time
Monte Carlo	Trajectory simulation, number of runs, variances	Impact points
Control simulation	Trajectory simulation, desired kinematic angles	Required aerodynamic moments

5.2. Atmospheric and Gravitational Model

For a three dimensional simulation the perturbations of the gravitational field become relevant. Very detailed gravitational field maps have been constructed for Mars [16]. However, the most significant perturbations can be attributed to the J_2 effect, caused by the difference in equatorial and polar radius. This allows an expression for the gravitational acceleration only as a function of altitude and latitude. The gravitational potential is given by Equation 5.1, derived from [17].

$$V = \frac{\mu}{R} + \frac{J_2 \mu R_{eq}^2}{2R^3}\left[3sin(\delta) - \frac{1}{2}\right] \tag{5.1}$$

Where R is the distance to the centre of Mars, R_{eq} is the equatorial radius and δ is the latitude. The result of this perturbation is that the surface gravitational acceleration varies between 3.735 [m/s^2] at the poles and 3.71 [m/s^2] near the equator. A model for the Martian atmosphere has been selected that allows the simulation to capture seasonal variations in the atmosphere due to changing temperatures. This exponential density model, using Equation 5.2, has been chosen for the reentry simulations

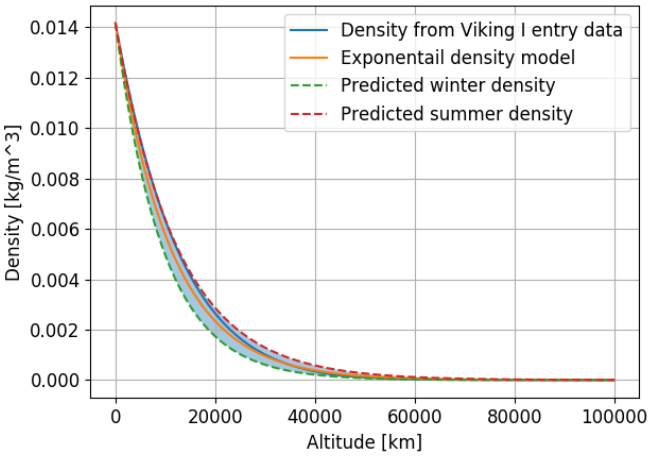

Figure 5.1: Comparison of exponential atmosphere to Viking 1 reentry data

with a scale height h_s depending on the sea-
level temperature and atmospheric composition. This model is taken from [18] and shows good conformity with data obtained from Mars reentry vehicles, as shown in Figure 5.1.

$$\rho = \rho_0 e^{-h/h_s} \tag{5.2}$$

$$h_s = \frac{kT}{\mu_{avg} g} \tag{5.3}$$

With $\rho_0 = 0.01417$ [kg/m^3], as obtained from the Viking 1 mission and h being the current altitude. For determining the scale height information about the atmospheric composition is required. The Martian atmosphere consists of 95.32% Carbon Dioxide, 2.7% Nitrogen and 1.6% Argon [1] giving an average molecular weight μ_{avg} of $7.196 \cdot 10^{-26}$ [kg]. Using Equation 5.3 the scale height can be determined for a range of observed temperatures. Here, k is the Boltzmann constant and g is the local gravitational acceleration. Using an average temperature of 213 [K], this scale height is 11015 [m]. With a minimum winter temperature of 184 [K] and a maximum summer temperature of 242 [K] observed by Viking 1[2], this scale height can vary between 9515 [m] and 12514 [m]. This variation is shown in in Figure 5.1.

5.3. Equations of Motion

This section presents the full non-linear equations of motion used to model the translation of the vehicle during atmospheric reentry. During reentry the angle of attack, angle of side slip and bank angle are kept constant, simulating active rotational control. The model then uses the kinematic attitude equations in Section 5.6 to determine the required moments to maintain these angles. The translational equations and kinematic position equations are expressed in a rotating (Mars-Centered Mars-Fixed) reference frame, with the kinematic attitude equations expressed in a body reference frame. The use of the rotating Mars centred reference frame allows for determining the vehicles impact point relative to the Martian base and allows for the integration of the trajectory into the EKF simulation performed in Section 7.4. The reference frames used are shown in Figure 5.2.

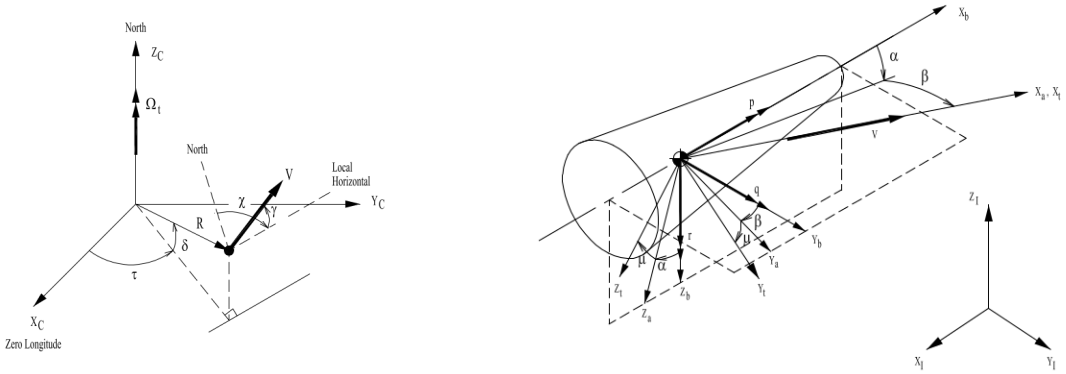

(a) Rotating reference frame obtained from [10]

(b) Body Rotating reference frame obtained from [10]

Figure 5.2: Reference frames

The translational equations of motion are given below, with the full derivation taken from [10] and [19]. The effect of the rotation of Mars is included in these equations in order to accurately capture the impact point of the vehicle relative to the Mars base.

$$\dot{V} = -\frac{D}{m} - g\sin\gamma + \Omega_t^2 R\cos\delta(\sin\gamma\cos\delta - \cos\gamma\sin\delta\cos\chi) \tag{5.4}$$

$$\begin{aligned} V\dot{\gamma} = \frac{L\cos\mu}{m} - g\cos\gamma + 2\Omega_t V\cos\delta\sin\chi + \frac{V^2}{r}\cos\gamma + \\ + \Omega_t^2 R\cos\delta(\cos\delta\cos\gamma + \sin\gamma\sin\delta\cos\chi) \end{aligned} \tag{5.5}$$

[1] https://nssdc.gsfc.nasa.gov/planetary/factsheet/marsfact.html accessed on June 9th 2020

[2] https://atmos.nmsu.edu/data_and_services/atmospheres_data/MARS/viking/pt_by_pt_footpad_temp.html, accessed on June 2nd 2020

$$V\cos\gamma\dot{\chi} = \frac{L\sin\mu}{m} + 2\Omega_t V(\sin\delta\cos\gamma - \cos\delta\sin\gamma\cos\chi) + \frac{V^2}{r}\cos^2\gamma\tan\delta\sin\chi + \\ + \Omega_t^2 r\cos\delta\sin\delta\sin\chi \tag{5.6}$$

The kinematic position equations are used to gain information about altitude, latitude and longitude of the vehicle position with respect to the centre of Mars.

$$\dot{R} = \dot{h} = V\sin\gamma \tag{5.7}$$

$$\dot{\tau} = \frac{V\sin\chi\cos\gamma}{R\cos\delta} \tag{5.8}$$

$$\dot{\delta} = \frac{V\cos\chi\cos\gamma}{R} \tag{5.9}$$

5.3.1. Initial Conditions

The reentry trajectory simulation starts from the reentry transfer orbit described in the midterm report [2]. This Kepler orbit has its apocentre at the orbital altitude of the node and its pericentre 300 [km] below the Martian surface. This orbit was found to place the vehicle into an appropriate reentry corridor. The initial flight path angle is calculated from the local tangent of the ellipse at the starting point of the simulation and the local horizon. The starting point of the simulation is taken at 80 [km] altitude. This point is somewhat arbitrary and serves primarily to reduce run time, while still including the most relevant phases of descent. The starting roll, pitch and yaw rates are set to zero, with the heading angle set to the inclination of the transfer orbit.

5.3.2. Time Discretisation

From the initial conditions until the vehicle reaches the altitude of the Martian base a Forward Euler time stepping scheme is used with a step size of 0.01 [s]. This scheme has an order of accuracy of $O(dt)$ for the cumulative error, which is deemed sufficient for this simulation. Numerical instability of the simulation is observed at time steps above 1 [s]. For the Monte Carlo implementation, the time step is increased to 0.1 [s] to avoid excessive run times. At every new timestep, each state is updated based on the previous state as shown below.

$$\mathbf{x}^{i+1} = \mathbf{x}^i + dt\cdot\begin{bmatrix}\dot{V}^i & \dot{\gamma}^i & \dot{\chi}^i & \dot{R}^i & \dot{\tau}^i & \dot{\delta}^i\end{bmatrix}^T \tag{5.10}$$

5.4. Reentry Trajectory

Using the model in Section 5.3 the flight path of the vehicle can be plotted. At each time step the lift and drag coefficients are calculated as a function of the angle of attack, Mach number and pressure after the bow shock wave. The local dynamic pressure and gravitational acceleration are also determined from the previous state. These values, as well as the previous state are used in Equation 5.4 to 5.9 to arrive at the next state. A constant angle of attack of $50°$ was selected for the nominal trajectory to give the highest possible drag while still providing sufficient lift for limiting deceleration and larger downrange distance. Other lifting body reentry vehicles follow similar angle of attack patterns [19].

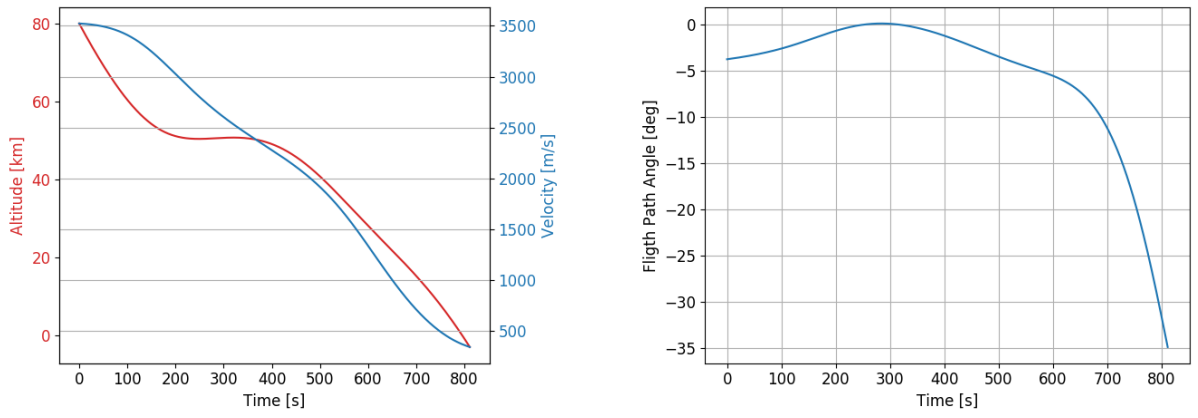

(a) Altitude and Velocity during reentry

(b) Flight path angle during reentry

Figure 5.3: Nominal entry trajectory of Charon, part 1

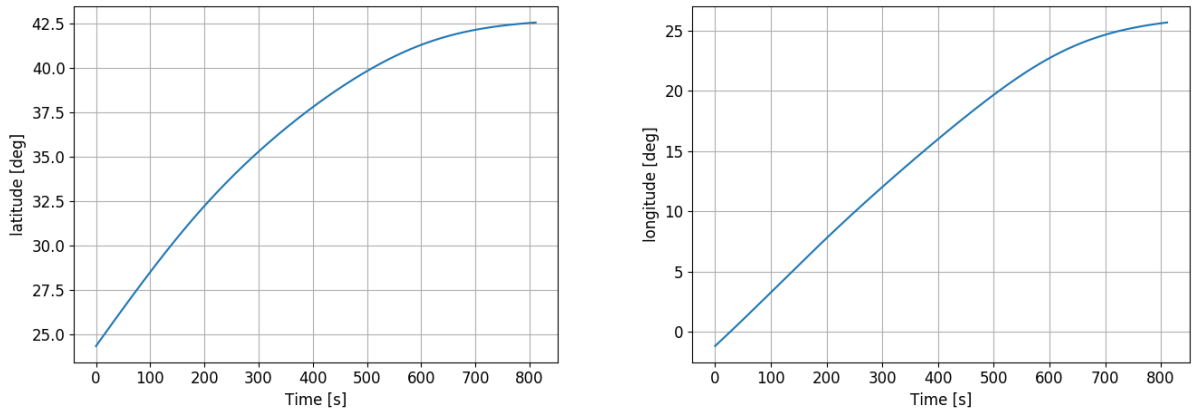

(a) Latitude changes during reentry

(b) Longitude changes during reentry

Figure 5.4: Nominal entry trajectory of Charon, part 2

The flight path followed by Charon on its reentry is similar to other lifting body designs [19]. As seen in Figure 5.3a the vehicle descends into the atmosphere along the flight path initially set by its reentry transfer orbit. As the atmospheric density increases, the vehicle generates significantly more lift, leading to the vehicle levelling off at an altitude of 50 [km]. Once velocity decreases sufficiently the flight path angle lowers again and the vehicle completes its descent. Without any additional propulsion, the vehicle would impact the ground at 338.3 [m/s]. The timing for the propulsive landing is elaborated on in Section 5.8.

5.5. Monte Carlo Simulation

In order to perform a simulation for the possible impact locations the initial conditions for the reentry simulations were assumed to follow a normal distribution with a mean at the nominal initial conditions and a certain standard deviation. This standard deviation for the initial position, velocity and altitude is taken from the EKF simulation in Section 7.4 using the trajectory of the vehicle between the orbital node and 80 [km] altitude. This flight path is shown in Figure 5.5. Table 5.2 shows the standard deviations obtained from the EKF simulations, as well as these standard deviations translated to the initial conditions of the trajectory simulations. All of these parameters are varied simultaneously in 100,000 simulations to determine the possible impact regions due to positional uncertainty.

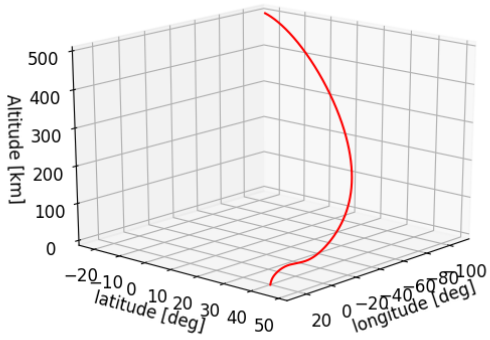

Figure 5.5: Flight path from the orbital node to the surface of Mars

Table 5.2: Variance of initial parameters for the Monte Carlo simulation

EKF Parameter	standard deviation	Initial Parameter	standard deviation
x	45.17444 [m]	latitude	7.4313e-4 [deg]
y	336.08044 [m]	longitude	5.5487e-3 [deg]
z	7.88649 [m]	altitude	7.88649 [m]
V	0.195 [m/s]	V	0.195 [m/s]

It is assumed that the heading and flight path angles are known with a standard deviation of 1.5 [arcsec] from Subsection 7.3.1. The resultant impact points are shown in Figure 5.6. Confidence ellipses of one, two and three standard deviations are also indicated in the figure.

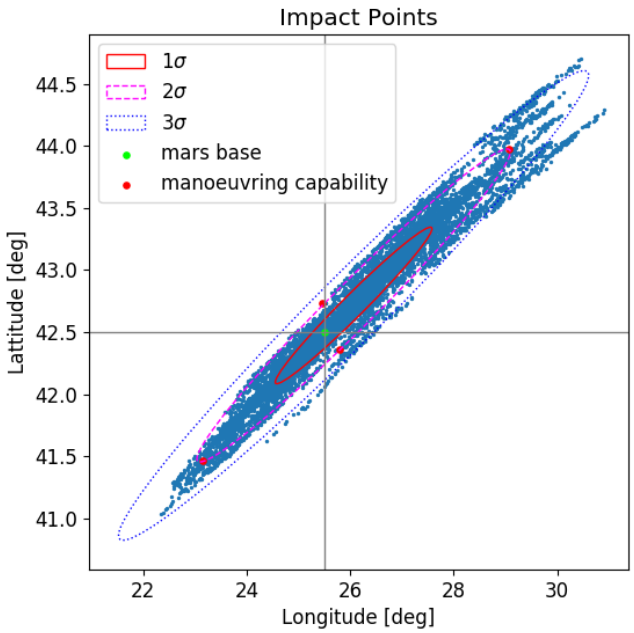

Figure 5.6: Monte Carlo simulation of 100,000 impact points

The location of the Mars base is indicated by the grey crosshairs. The deviation from the desired impact point is very large considering the low variance of the initial conditions. The downrange length of the 2σ confidence ellipse is 126.662 [km], with a cross range length of 52.712 [km]. This shows how sensitive the reentry flight path is to varying initial conditions. Figure 5.6 also highlights the need for active control of the vehicle during reentry. This impact point spread can be used to determine the required variation in pitch and roll angle to achieve a landing footprint large enough to cover the majority of these impact points. The red points in Figure 5.6 indicate the manoeuvring capability required by the vehicle to reach any point within the 2σ confidence ellipse. Here the driving flight conditions are an angle of attack of $5.1°$ above the nominal angle of attack and a bank angle of $\pm 3.4°$.

5.6. Reentry Control

In order to control the vehicle during reentry, the required pitching and rolling moments need to be determined. This required using the kinematic attitude equations in conjunction with the Euler equations of rotational motion from [10]. For these equations, it is assumed that the vehicle is rotationally symmetric and that the effect of the rotation of Mars is small on the change in pitch, yaw and bank angle. The Euler equations are given in Equation 5.11 to 5.13. The moments M_x, M_y and M_z, are determined using the distances between the centre of pressure and the aerodynamic centre.

$$\dot{p} = \frac{M_x}{I_{xx}} + \frac{I_{yy} - I_{zz}}{I_{xx}} qr \quad (5.11) \qquad \dot{q} = \frac{M_y}{I_{yy}} + \frac{I_{zz} - I_{xx}}{I_{yy}} pr \quad (5.12) \qquad \dot{r} = \frac{M_z}{I_{zz}} + \frac{I_{xx} - I_{yy}}{I_{zz}} pq \quad (5.13)$$

The required torques on the vehicle are determined by $\dot{p}$, $\dot{q}$ and $\dot{r}$ necessary to maintain a certain angle of attack, bank angle or sideslip angle. $\dot{\alpha}$, $\dot{\beta}$ and $\dot{\mu}$ are assumed to be 0 for maintaining a constant angle. The kinematic attitude equations are shown below.

$$\dot{\alpha} = q - (p\cos\alpha + r\sin\alpha)\tan\beta - \frac{L - mg\cos\gamma\cos\mu}{mV\cos\beta} \quad (5.14)$$

$$\dot{\beta} = p\sin\alpha - r\cos\alpha - \frac{S + mg\cos\gamma\sin\mu}{mV} \quad (5.15)$$

$$\dot{\mu} = -\frac{p\cos\alpha + r\sin\alpha}{\cos\beta} - \frac{L - mg\cos\gamma\cos\mu}{mV}\tan\beta + \frac{L\sin\mu + S\cos\mu}{mV}\tan\gamma \quad (5.16)$$

The simulation starts by calculating $\dot{p}$, $\dot{q}$ and $\dot{r}$ from the previous state using Equation 5.11 to 5.13. The required roll, pitch and yaw rates to maintain the set angles are calculated using Equation 5.14 to

5.16 at both the previous and the current state. This allows for numerical differentiation of p, q and r, which can then be used in Equation 5.11 to 5.13 to determine the required vehicle torques to maintain the attitude angles. In practice, it was found that the M_y is the only moment significantly effected by the aerodynamic forces. This means that the torque needed to compensate for this is almost exactly M_y when using this method. The advantage of going through all of the aforementioned steps is that this method captures pitch-roll coupling and allows for a much better estimate of the required torque around the x-axis. The required torques around the x-axis and y-axis are shown in Figure 5.7a and Figure 5.7b respectively.

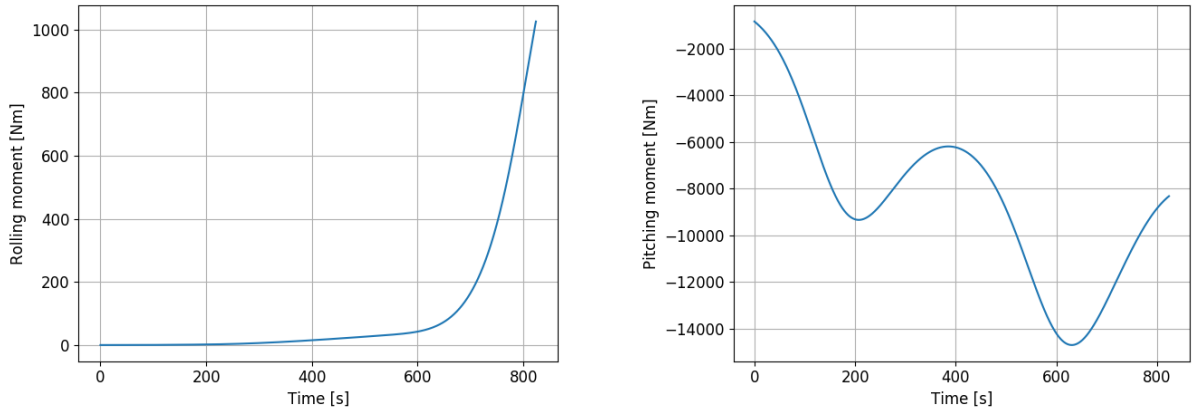

(a) Rolling moment to maintain 3.4° bank angle

(b) Pitching moment to maintain 55.1° angle of attack

Figure 5.7: Required moments for the nominal entry trajectory of Charon

5.7. Aerodynamic Heating

Accurately determining the heat flux through the boundary layer of the flow around the reentry vehicle is very difficult with empirical methods. A highly simplified approach was used in this simulation to calculated the convective heat transfer at the stagnation point of the vehicle according to Fay and Riddell [20]. This method neglects radiative heat transfer and does not account for changes in the chemical species in the boundary layer, due to the high temperatures and pressures. A chemical library [3] is used to calculate the gas properties due to the increase in temperature after the shock wave and at the wall. The heat flux through the boundary layer is given by Equation 5.17.

$$q = 0.94 \left(\rho_e \mu_e\right)^{0.4} \left(\rho_w \mu_w\right)^{0.1} \sqrt{\left(\frac{\mathrm{d}u_e}{\mathrm{d}x}\right)_{\text{stag}}} c_p \left(T_t - T_w\right) \tag{5.17}$$

With

$$\left(\frac{\mathrm{d}u_e}{\mathrm{d}x}\right)_{stag} = \frac{1}{R}\sqrt{\frac{2\left(p_e - p_\infty\right)}{\rho_e}} \tag{5.18}$$

Where the subscripts e, w and t indicate post-shock-wave, wall and total conditions respectively. The bow shock created by the vehicle is assumed to be a normal shock wave. Relations to calculate the post-shock-wave gas properties have been obtained from [21]. The nose radius R is taken as 7 [m], resulting from a design which is further detailed in Section 6.3, and the wall temperature is assumed to be 400 [K]. The stagnation point heat flux over the course of flight is shown in Figure 5.8b, with the Mach number and accelerations shown in Figure 5.8a.

[3] Thermodynamics, phase equilibria, transport properties and chemical database component of Chemical Engineering Design Library (ChEDL), `https://github.com/CalebBell/thermo`, accessed on June 2nd 2020

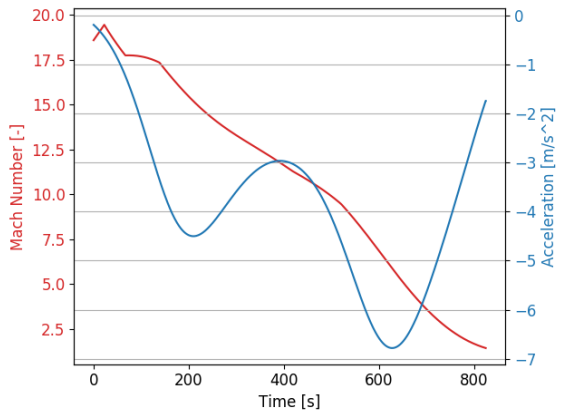

(a) Mach number and Dynamic Pressure

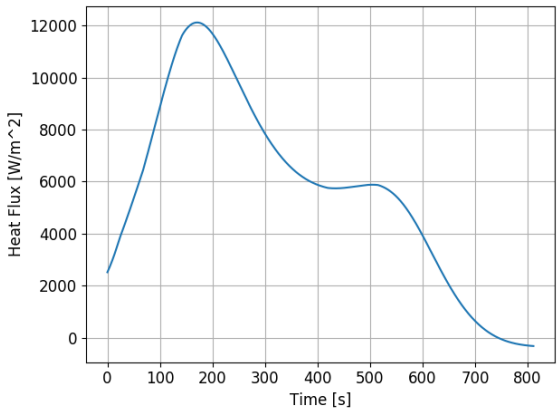

(b) Stagnation point heat flux

Figure 5.8: Nominal entry trajectory of Charon

Data from simulations of the entry of the Mars Science Laboratory (MSL) has been used to assess the validity of the model. The simulations performed in [22] and [23] account for changes in chemical species near the vehicle surface. Wind tunnel experiments referenced in [22] indicated an enthalpy of $5-10$ [MJ/kg] measured on scale models under reentry conditions. This indicates the presence of chemical reactions and species transport phenomena in the boundary layer. A maximum stagnation point heat flux of 128 [W/cm^2] is estimated without accounting for catalytic effects and a heat flux of 193 [W/cm^2] with catalytic effects. Using Equation 5.17 the predicted value lies at only 87.84 [W/cm^2] for the reentry conditions of MSL. Due to this discrepancy, a correction factor of 3 is applied to the heat flux values obtained for the Charon reentry trajectory.

5.8. Propulsive Landing

In the final phase of descent, the vehicle performs a rotation manoeuvre to align the main engines with the flight path angle. The remaining velocity of the vehicle is reduced using three of the main engines. The use of three engines allows for better control of the vehicle while remaining within the requirement ***SRV-CONS-TECH-2.7***: *The maximum g-forces experienced by the crew during nominal operations shall not exceed 4 g*.

With three engines at full thrust, the maximum deceleration does not exceed 2.04 g. For the deceleration burn it is advantageous to perform the burn as late as possible. This allows the rotation to be performed later, at lower velocities, limiting the aerodynamic torque resisting the rotation. As illustrated in Figure 5.3a, the vehicle would impact the ground with 338.3 [m/s] without any additional means of deceleration. The simulation predicts a variance on this final velocity of 2.441 [m/s] based on the atmospheric variation between summer and winter. The Monte Carlo implementation predicts a variance on this impact velocity of only 0.324 [m/s]. With the three main engines at full thrust at 799.6 [s] into the flight the final touchdown velocity is 6.08 [m/s], as shown in Figure 5.9.

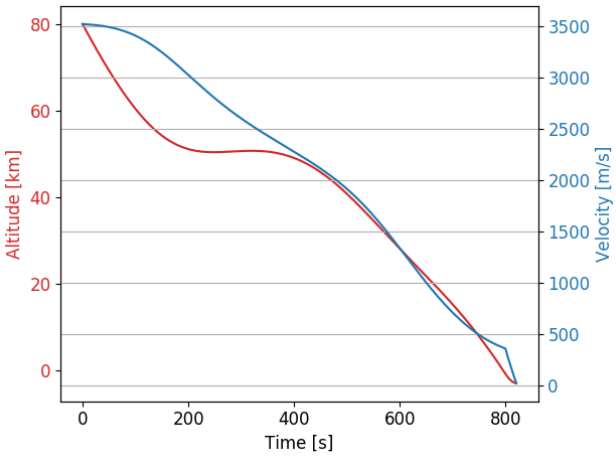

Figure 5.9: Altitude and velocity with propulsive landing

5.9. Verification and Validation of the Reentry Model

To initially verify the reentry trajectory model, the results were compared to the trajectories of the validated two dimensional reentry model presented in the midterm report [2]. Very close agreement was found when controlling for the rotation of Mars and neglecting the J_2 effect. For validation of the simulation, flight data from the Mars Exploration Rover (MER1), ”Spirit”, was obtained from the

Mars Exploration Rover Archive and [18]. This reentry flight data set contains position, velocity and acceleration data, as well as aerodynamic coefficients and atmospheric data for the ballistic reentry phase. Especially the presence of atmospheric data, and the axial and normal force coefficients allow for a very accurate comparison to the simulation model. This way the largest sources of uncertainty can be removed. Specifically, the altitude, velocity, latitude and longitude of the flight path have been compared. For each parameter, the total error is calculated using Equation 5.19.

$$|error| = \frac{(\vec{d} - \vec{n}) \cdot (\vec{d} - \vec{n})}{\vec{d} \cdot \vec{d}} \qquad (5.19)$$

Here, $\vec{d}$ is the flight data vector and $\vec{n}$ is the simulated parameter. The results of this comparison are summarised in Table 5.3. Good conformity with the flight data is observed for all parameters. The absolute difference between the simulation and the data set is below 0.0035. Additionally, the results for the latitude of the flight path are very close to the predicted results.

Table 5.3: Absolute error of the simulation compared to reference data

Parameter	Absolute error
Altitude	0.0034071
Velocity	0.0014004
Latitude	2.1907e-7
Longitude	1.4e-6

A visual comparison of these differences is shown in Figure 5.10. Initially, the velocity, altitude and longitude are very close to the values predicted by the simulation. Only in the latter half of the flight, after 150 seconds the two lines begin to diverge. Only the latitude remains very accurate. Both atmospheric data and aerodynamic coefficients are controlled for in this comparison. Specifically, the simulation predicts a faster deceleration of the vehicle and a flatter trajectory for the final phase of flight. One reason for this discrepancy could be the simplistic gravity model used in the simulation. Only incorporating the J_2 effect means that the major perturbations as a function of latitude are captured well, while the longitudinal perturbations are ignored. This might explain the high accuracy of the latitude data and the deviation in the results for longitude. The flatter trajectory in Figure 5.10a is likely due to a lower flight path angle towards the latter stages of flight. This could account for some of the deviation in velocity and longitude as a flatter trajectory would cause a lower final velocity and a longer downrange distance. The cause of the possible difference in flight path angle is, however, unknown.

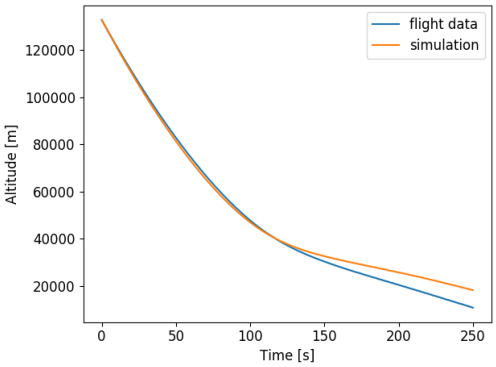

(a) Altitude

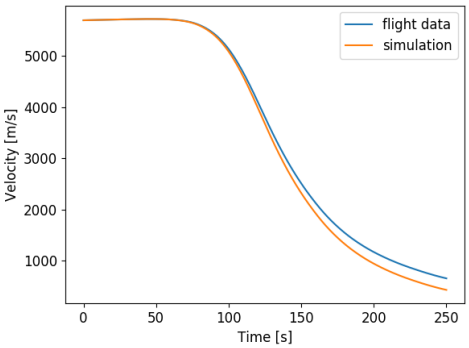

(b) Velocity

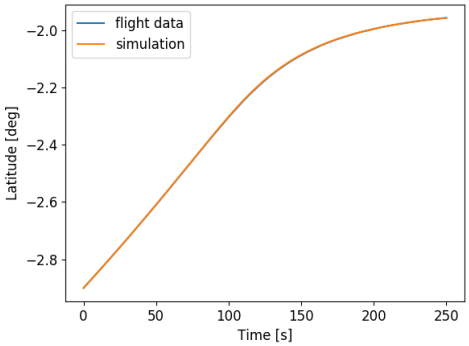

(c) Latitude

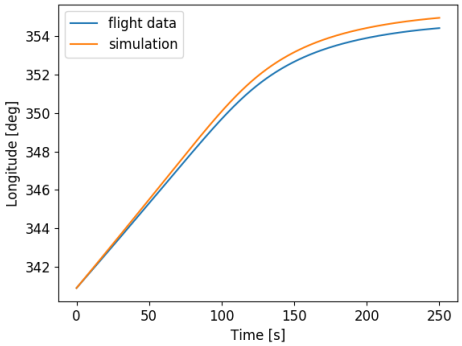

(d) Longitude

Figure 5.10: Comparison of simulated flight path with reentry data form MER1

6

Aerothermodynamics

The design of the aerodynamics of the vehicle is closely linked with the ascent and reentry simulations. The aerodynamic shape of the vehicle is a result of an iterative analysis based on the accompanying demands for stability and aerodynamic performance. In Section 6.1 and Section 6.2, the requirements on the subsystem, along with its global in- and outputs are discussed. In Section 6.3 and Section 6.4, the thermal behaviour is analysed. Then shape design continues and in Section 6.5, the aerodynamic coefficients are detailed, along with an analysis of stability in Section 6.6. Next, a discussion is done on the level of detail in Section 6.7, along with requirement compliance, sensitivity analysis and an analysis of the risks, which are detailed in Section 6.9 and Section 6.8

6.1. Requirements

From the baseline report [1], the following requirements on thermal control have been established:

- **SRV-CONS-TECH-2.5**: [T] The thermal protection hardware shall protect the spacecraft, crew, and cargo during reentry.
- **SRV-CONS-TECH-2.5.1**: [T] The thermal control system shall keep the temperature of the spacecraft structure between 200 [K] and 300 [K].
- **SRV-CONS-TECH-5.2.3**: [T] The thermal protection hardware for reentry shall be maintainable without replacement during nominal refurbishment.

6.2. Analysis; Inputs and Outputs

The inputs to the aerodynamic model have been established in Table 9.1.

Analysis	Inputs	Outputs
Reentry thermal	Heat fluxes, vehicle properties, shape	Temperature changes
Orbital thermal	Heat fluxes, vehicle properties, shape	Temperature changes
Aerodynamic coefficients	Reentry trajectory properties, shape	C_l, C_d, c.p. location
Aerodynamic stability analysis	Atmospheric and vehicle properties, shape	Aerodynamic coefficients

Table 6.1: Inputs and outputs of the aerothermodynamics system

6.3. Thermal Behaviour During Reentry

From an astrodynamics point of view, it was established that Charon should have a somewhat moderate lift to drag ratio during reentry. This was deemed to be the most interesting phase of flight, and therefore it is the phase that is primarily taken into consideration when designing the shape of the vehicle. With the heat fluxes obtained in Section 5.7, the focus of this section is on the design of the thermal protection system.

Within the given reentry profile, the angle of attack has been set to be kept at 50 degrees. Therefore, the stagnation point can be obtained for all moments in flight. As within the heat flux equation for stagnation point the radius of the blunt body at the impact point is of importance, maximising this radius reduces the resulting stagnation point heat flux. A closeup of the blunt

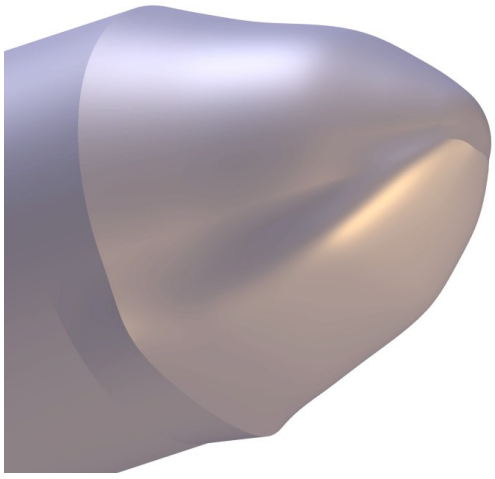

Figure 6.1: Capsule blunt body

aeroshell body can be seen in Figure 6.1. The optimisation of the blunt body shape resulted in a nose radius of about 7 [m].

Now that the stagnation point heating has been established, some additional simplifications can be done, in order to be able to size the thermal protection system.

The heat flux in the stagnation point is relatively low, when comparing it to the heat flux as calculated in [6]. The heating flux on the lower side have therefore been multiplied by a factor of 3, in order to result in comparable heat fluxes, and making sure that the thermal protection system will be designed with sufficient safety margins. Additionally, it is assumed that the stagnation point heat flux is also constant over the whole body facing the flow. This is an overestimation, as the heat flux on other points will be significantly lower because of the lower incidence angle the surface makes with the flow.

Additionally, the heating on the top side of the vehicle is assumed 2 times the heat fluxes that are calculated by our astrodynamic model. This has been done because estimating the heat fluxes on the top side is very complex, as it is mostly dependent on the temperature of the flow around the body, which is highly irregular because of the high temperatures. This estimation was therefore deemed to give a suitable estimation of the expected heat fluxes, while allowing for some margins.

For the analysis of the TPS, material properties of the LI900 tiles that have been used extensively on the Space Shuttle have been taken [24]. Of course, since the Space Shuttle era, various newer and reusable thermal protection systems have been developed. It proofed difficult to find sufficient data for these newer systems however. Therefore, for estimates of the conductivity, emisivity, specific heat and density, it was assumed that these numbers were accurate enough. This means that in all likelihood, the actual weight of the thermal protection system can be lowered, making use of state of the art materials and design principles.

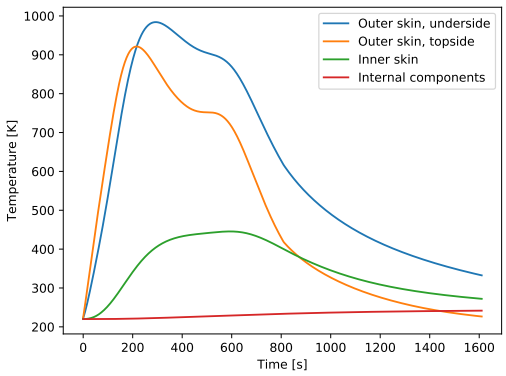

Figure 6.2: The temperatures on the surfaces, plotted over time during reentry

Now that the boundaries have been set, simplifications have been done and material properties have been established, the analysis of the system can be performed. It was established that for sufficient protection, the TPS should be 6 [cm] in thickness on the underside, and 2 [cm] on the top side. The resulting development of temperatures throughout the reentry on the inner side of the TPS and on both of the outer sides of the TPS can be seen in Figure 6.2.

6.4. Thermal Control in Orbit

Another element to be analysed is the thermal behaviour of Charon in orbit. The duration of this period is significant in the mission profile, and if heating of Charon in orbit is required, this means it will contribute significantly to the power budget. Therefore, an analysis of the temperatures obtained in orbit is performed.

The analysis is done on the whole vehicle, by assuming all heat is radiated outward through the outer skin. As input, solar irradiance with an intensity of 590 [W/m^2] [25] is taken on one of the spacecrafts projected areas. On the other side, the heat sourced by the albedo of Mars is taken, which is given to be 0.29 [25]. However, as the orbiter is only perfectly perpendicular to both the sun and Mars for a small period of time, this is divided by 2, for the sake of underestimating a more realistic value. Lastly, IR emissions are included. In literature, these are given to be in the range of 120 to 162 [W/m^2], for which the value of 120 is taken, which is assumed to be uniformly applied to 25% of the surface. Heat generation of all components but the optional thermal control system is deemed negligible.

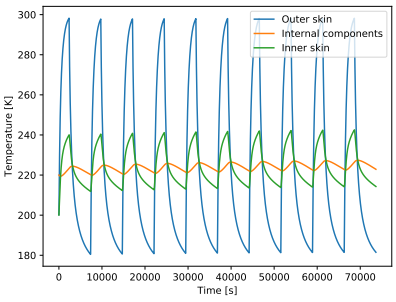

Figure 6.3: Temperatures within and outside the spacecraft during 10 orbital periods

The resulting temperature distribution over a period of 10 orbits can be seen in Figure 6.3. The minimum internal temperature is about 220 [K]. At this temperature, the spacecraft materials will not get damaged. It is too cold however for some electronic components, which will require some additional heating. This is considered to be beyond the scope of this project. Furthermore, the crewed capsule will require additional heating, which is detailed in Section 8.6.

Obviously, most of the numerical values that have been used are taken pretty arbitrarily. For this stage of the design, this was deemed acceptable, as the resulting analysis shows feasibility more than anything else. Far more detailed analysis will have to be performed in order to more accurately estimate the thermal behaviour of Charon in orbit.

6.5. Aerodynamic Coefficients in Hypersonic Flow

When looking at the reentry profile, most of the time is spent at hypersonic velocities. Therefore, the analysis of the aerodynamic behaviour is done within this flow regime. This is done through the Modified Newton Method [21]. This method allows for a relatively accurate analytical estimation of the pressure coefficients on mesh points on a body in hypersonic or supersonic flow. First, an estimation of the pressure coefficient in the stagnation point is obtained, using Equation 6.1 [21].

$$C_{p,\max} = \frac{2}{\gamma M_\infty^2}\left(\frac{p_{0,2}}{p_\infty} - 1\right) \qquad (6.1)$$

$$\mathrm{C_p} = \mathrm{C_{p,max}} \sin^2\theta \qquad (6.2)$$

Here,γ is taken to be 1.37 [25], M_∞ is the calculated Mach number upstream, p_∞ is the calculated pressure upstream, and $p_{0,2}$ is the calculated post-shockwave pressure at zero velocity, which is calculated assuming a normal shockwave. Then, for every element downstream of the stagnation point, c.p. can be obtained through Equation 6.2,in which θ is given to be the angle that the surface makes with the airflow. Additionally, as the shape is given to be curving in 3 dimensions, the area with respect to the flow is projected.

With these calculations set up, all that needs to be done is the creation of a mesh of surface nodes, on which the surface pressures can be analysed. This mesh is created and exported from the CADmodel using the ANSYS Mechanical workbench. The initial conditions are then established, as given by the astrodynamic model. Then, on all of these nodes, representing a small surface element, the magnitude and direction of the pressure force can be obtained. Summing all of these force vectors together, the lift and drag coefficients can be obtained. Furthermore, the location of the centre of pressure can be obtained. A plot of two resulting pressure distributions can be seen in Figure 6.4. The difference between the two plots will be discussed in Subsection 6.6.1

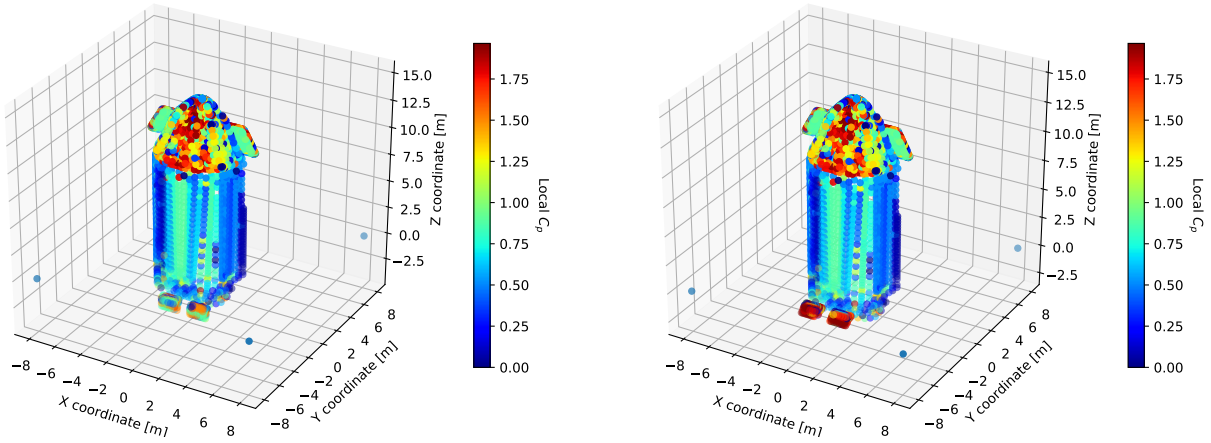

Figure 6.4: Plots of the pressure coefficients distributed along the bottom side of the spacecraft during reentry, with body flaps in neutral (left) and extended (right) position

The resulting model was then used to estimate the changes in lift and drag on different angles of attack, at different Mach numbers, and using different shapes. This was done by constructing force vectors on each of the pressure points, which were then summed to create a resultant force vector, which could be broken up into lift and drag. These results were then used as inputs in the ascent and reentry models.

6.6. Stability and Manoeuvrability in Hypersonic Flow

Now that the aerodynamic model has been set up, some optimisation can take place. For stability and manoeuvrability, it is important that the location of the centre of pressure is close to the location of the centre of gravity. This is important as the aerodynamic forces would otherwise create a significant pitching moment, which would result in a large required correction. In order to reduce this pitching moment, some aerodynamic surfaces have been sized in CATIA for on the nose of the vehicle. Several iterations have been done, and the resulting shape can be seen in Figure 6.5.

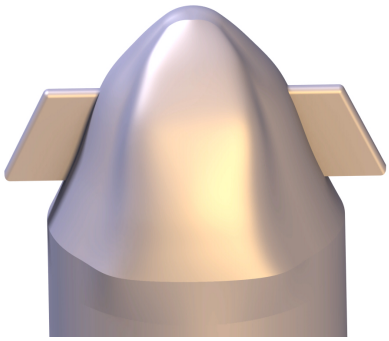

Figure 6.5: Charon's aerodynamic surfaces

6.6.1. Body Flap

Additionally, as the vehicle needs to be controllable during reentry, it was decided that it would be useful to add a body flap to the rear end of the vehicle. This body flap has a controllable angle of attack with respect to the vehicle. It therefore creates an adjustable force, which can move the centre of pressure upwards and downwards. This body flap was sized such that the distance between centre of pressure centre of gravity is minimised. The remaining aerodynamic moment is counteracted by the RCS. The resulting flap in both extended and neutral position can be seen in Figure 6.6. The effect that the body flap has on the pressure distribution on the surface can be seen in Figure 6.4.

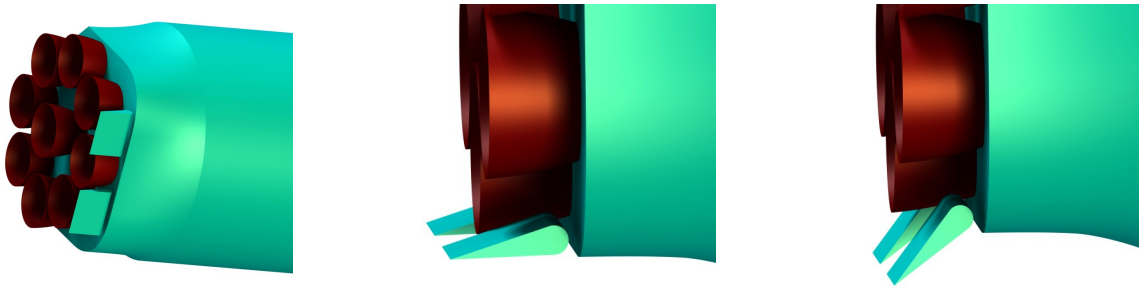

Figure 6.6: Visualisation of the body flaps

A second control mode that would have to be analysed is that of roll. The required roll moments have been established previously in Section 5.6. However, obtaining these through the body flap would require more extensive analysis, which can not be done as of now. It has therefore been checked that the RCS system can supply sufficient torque to enable sufficient roll control.

6.7. Recommendations

Right now the sizing of the aerodynamic body is not consistent with the requirements on pitching moments. For the sizing of the RCS system, it was assumed that the difference between the location of c.g. and c.p. was no more than 10 [cm]. This would however result in the necessity of very large winglike surfaces on the top of the vehicle. Therefore, it was chosen to keep the upper wing surface relatively modest right now, as the location of neither c.g. nor c.p. can be determined to a sufficient accuracy, and the preference is to deliver a feasible design concept. For future analysis, these 2 locations need to be established more accurately, after which the design can be converged further.

6.8. Risk Analysis

The following risks have been analysed and mitigated as part of the Thermal subsystem:

- **SRV-RISK-THERMAL-1** TPS damaged due to surface debris (P=2), results in partial TPS failure (I=3).
  - Probability mitigation (P-1): frequent check-ups.
  - Impact mitigation (I-1): add redundancy layer.
- **SRV-RISK-THERMAL-2** TPS damaged due to space debris (P=2), results in partial or complete TPS failure (I=4).

  - Probability mitigation (P-1): optimise orbital time.
  - Impact mitigation (I-1): design surface for impact resistance.

- **SRV-RISK-THERMAL-3** TPS breaks due to fatigue (P=2), results in partial or complete TPS failure (I=4).
  - Probability mitigation (P-1): frequent check-ups.
  - Impact mitigation (I-1): add redundancy layer.
- **SRV-RISK-THERMAL-4** TPS breaks due to high stress (P=2), results in partial or complete TPS failure (I=3).
  - Probability mitigation (P-1): high strength TPS materials.
  - Impact mitigation (I-1): add a redundancy layer.

From this list, a mitigated risk map has been created. It is shown in Table 6.2. As can be seen, all of the risks have been mitigated to a sufficient extent.

Table 6.2: Risk map of the thermal subsystem, after mitigation

	Very unlikely (1)	Unlikely (2)	Possible (3)	Likely (4)	Very likely (5)
Very high impact (5)					
High impact (4)					
Medium impact (3)	2, 3				
Low impact (2)	1, 4				
Very Low impact (1)					

6.9. Requirement Compliance and Sensitivity Analysis

The requirement compliance matrix for these subsystems can be seen in Table 6.3. The first 2 requirements have been met, as the design is capable of safely protecting the payload and the structure of the vehicle. **SRV-CONS-TECH-5.2.3** could not be verified yet. There are still many different thermal protection concepts available, on which trade-off has to be performed. The current design assumes TPS with similar properties as the Space Shuttle tiles. As these tiles needed a lot of maintenance, they would not be suitable for the design. A different selection will therefore have to be made, which will then result in verification of **SRV-CONS-TECH-5.2.3**.

Requirement	Completion	Explanation
SRV-CONS-TECH-2.5	✓	Section 6.3
SRV-CONS-TECH-2.5.1	✓	Section 6.4
SRV-CONS-TECH-5.2.3	*	To be investigated

Table 6.3: Requirement compliance for the aerothermal subsystem

The inputs of the aerodynamic model can be taken, and a sensitivity analysis can be performed to see what their effect is on the outcome of the model. For this analysis, the Y-coordinate of the c.p. is taken as the measured output variable. 3 input elements were varied, these were the Mach number (standard deviation of $3.33 * 10^{-}3$), altitude (standard deviation of 7.88 [m]), and angle of attack (standard deviation of 0.0041677 (10 times the measuring uncertainty)). It was found that when varying these coefficients separately, or a combination of all of them, the location of c.p. varied by no more than 1 cm in a sample of 100 measurements.

7

GNC

The GNC subsystem provides the guidance, navigation and control of Charon. These are of extreme importance during all phases of flight. High navigational accuracy requirements drive the design of the tracking system, as there is limited satellite coverage available and very little opportunity to have unmanned tracking stations spread out along the Martian surface.

The control system performs all manoeuvres that are not done by the main engines. Accurate manoeuvrability is required as this is a manned mission demanding high reliability. Ascent, docking and reentry manoeuvres are drivers for the sizing of the control system.

Firstly, all requirements with respect to GNC are stated in Section 7.1, after which the inputs and outputs of the analyses are given in Section 7.2. After this, the tracking sensors are determined and sized in Section 7.3. Furthermore, an Extended Kalman Filter (EKF) is used to simulate state determination accuracy for all flight phases in order to judge the accuracy of the sized sensors. This is described in Section 7.4 along with a verification and validation. Furthermore, control modes for the entire flight are identified in Section 7.5. Consequently, an early trade-off is done on the control technique based on these modes and a technique is chosen in Section 7.6. Following this, the manoeuvres are analysed in Section 7.7 and the control configuration is determined and sized in Section 7.8. Having determined the required thrust levels and configuration, the choice on RCS propellant and thrusters is made in Section 7.9. Furthermore, a risk analysis is completed in Section 7.10. Finally, compliance with the requirements is checked and sensitivity is analysed in Section 7.11.

7.1. Requirements

Firstly a list of the Requirements related to the GNC subsystem,

- **SRV-TECH-OPER-1.4**: The absolute position of the spacecraft shall be known within an error of 0.1 [m] RMS.
- **SRV-TECH-OPER-3.3**: The relative position to the orbital node shall be known within an error of 0.1 [m] RMS during the rendezvous process.
- **SRV-TECH-OPER-2.2**: The relative position to the landing site shall be known within an error of 0.1 [m] RMS during the landing process.
- **SRV-TECH-OPER-3.4**: The relative velocity to the orbital node shall be known within an error of 0.035 [m/s] RMS during the rendezvous process.
- **SRV-TECH-OPER-1.5**: The control system shall be able to cause an acceleration of the spacecraft around its longitudinal axis of 0.16 [m/s^2] during rendezvous.
- **SRV-TECH-OPER-1.6**: The control system shall be able to cause an acceleration of the spacecraft around its lateral axis of 0.16 [m/s^2] during rendezvous.
- **SRV-TECH-OPER-1.7**: The ACS shall be able to operate for a 40000 cycles per flight.
- **SRV-TECH-OPER-2.3**: The spacecraft shall be able to land on the pad with an error of 1.5 [m] RMS.

7.2. Analysis; Inputs and Outputs

Table 7.1: Analysis inputs and outputs for GNC

Analysis	Input	Output
EKF - reentry and ascent	Vehicle state over time (reentry, ascent)	State uncertainty (reentry, ascent)
EKF - Orbit	Vehicle state over time in orbit	State uncertainty in orbit
RCS sizing - Ascent pitch control	Pitching moments	thrust and propellant mass
RCS sizing - Ascent rotation	angle, MMOI, cg, burn time, thrust	rotation time, propellant mass
RCS sizing - Rendezvous	angle, MMOI, cg, burn time, thrust	rotation time , propellant mass
RCS sizing - Docking	Navigation errors	thrust, propellant mass
RCS sizing - Reentry rotation	angle, MMOI, cg, burn time, thrust	rotation time, propellant mass
RCS sizing - Reentry pitch control	Pitching moments	thrust, propellant mass

7.3. Sensor Determination and Sizing

First of all, a trade-off of the sensor was made. Then, they have been sized.

7.3.1. Trade-Off

A trade-off must be made between available tracking techniques. Unlike other trade-offs, options do not need to be exclusive and a suite of tracking implements can be chosen to best cover each other's weaknesses. Three distinct groups are considered: rotational sensors, inertial sensors and ground sensor. One particular omission is GPS. It is assumed that the resources required to launch and maintain a network of 24 satellites does not really fit with a colony of the size analysed.

Table 7.2: Tradeoff Rotational sensors

Criteria / Design Concept	Availability, 33.33% (1, 5) High Best, $\sigma = 1.299$	Accuracy, 33.33% (1, 5) High Best, $\sigma = 1.299$	sample rate, 33.33% (1, 5) High Best, $\sigma = 1$	Total
Gyroscope	blue 5 → 1	yellow 3 → 0.5	blue 5 → 1	0.833
Sunsensor	orange 2 → 0.25	blue 5 → 1	yellow 3 → 0.5	0.583
Startracker	yellow 3 → 0.5	blue 5 → 1	yellow 3 → 0.5	0.667
Magnometer	blue 5 → 1	orange 2 → 0.25	blue 5 → 1	0.75

Table 7.3: Tradeoff Inertial sensors

Criteria / Design Concept	Availability, 33.33% (1, 5) High Best, $\sigma = 1.5$	Accuracy, 33.33% (1, 5) High Best, $\sigma = 1$	sample rate, 33.33% (1, 5) High Best, $\sigma = 1$	Total
Optical	orange 2 → 0.25	blue 5 → 1	yellow 3 → 0.5	0.583
Accelerometer	blue 5 → 1	yellow 3 → 0.5	blue 5 → 1	0.833

Table 7.4: Tradeoff Ground based sensors

Criteria / Design Concept	Availability, 33.33% (1, 5) High Best, $\sigma = 1.265$	Accuracy, 33.33% (1, 5) High Best, $\sigma = 1.166$	sample rate, 33.33% (1, 5) High Best, $\sigma = 1.356$	Total
Radar	blue 5 → 1	blue 5 → 1	orange 2 → 0.25	0.75
Radio Interforemter	blue 5 → 1	yellow 3 → 0.5	blue 5 → 1	0.833
Optical (Ground)	orange 2 → 0.25	green 4 → 0.75	yellow 3 → 0.5	0.5
Lidar	yellow 3 → 0.5	blue 5 → 1	orange 2 → 0.25	0.583
Doppler Radar	blue 5 → 1	orange 2 → 0.25	blue 5 → 1	0.75

As can be seen for rational sensors in Table 7.2, the clear choice is the MEMS Gyroscope. To cover for the low accuracy, it seems that the addition of Star cameras would complement the choice well. This allows for attitude determination at a slower rate with rate integration for the prediction. For inertial measurements, accelerometers provide little argument, however the additional accuracy of optical systems will be required for docking and landing. Lastly for ground based systems it seems that radio interferometers have the advantage, however the easy combination of radar and Doppler radar makes this combination more attractive and as such it is chosen as the favoured option for ground tracking. Accelerometers and Star-trackers COTS will be taken from commercially available products for now. [1][2]

7.3.2. Camera Sizing

Cameras will have to be built specifically for the mission. As discussed in Chapter 4 the approach starts at a distance of 1000 [m]. There are a few key parameters for sizing, primarily the Field Of View (FOV) and resolution. Higher FOV yields less accuracy as objects cover fever pixels each, but will be worse at finding the object if it is out of frame. However for FOVs at around 90° the lens assembly will be the lightest. Assuming a 4000x4000 pixel sensor, at 1 [km] the docking hatch can be observed as 0.0011 [rad]. With an FOV of 90 this would make the docking port 3 pixels wide. However, the station will be significantly larger if it is assumed that it is the same size as the ISS, which would be about 200 pixels wide. Thus it is reasonable to assume that the camera can find the node at the 1000 [m] distance. Four cameras are installed to provide increased accuracy and redundancy. This configuration with a frame-rate of 30 [Hz] also yields about $1.3 \cdot 10^{-5}$ [m/s] and $3.9 \cdot 10^{-4}$ [m] resolution at the final moment of docking. With these resolutions it is fair to assume that the error will be within tolerable margins. For landing the positioning is much less of an issue as the radar system allows for high accuracy either way, however the installation of a similar system as the one for docking would be a good addition.

7.4. State Determination

The state of the vehicle can be determined with a higher accuracy using an EKF. It is described in this section.

7.4.1. Description of EKF

As the name suggests, the EKF is an extended version of the regular kalman filter generalised for use with nonlinear driving functions. To achieve this, it linearises the state around the current state and does a normal kalman filter approximation. This is normally done through two separate steps: the prediction step and correction step. The notations from Table 7.5 are used.

Table 7.5: EKF notations

Notation	Size	Description	Notation	Size	Description
$\mathbf{x}_k$	$n \times 1$	State vector	$\mathbf{h}(\cdot)$	$m \times 1$	Observation nonlinear vector function
$\mathbf{w}_k$	$n \times 1$	Process noise vector	$\mathbf{Q}_k$	$n \times n$	Process noise covariance matrix
$\mathbf{z}_k$	$m \times 1$	Observation vector	$\mathbf{R}_k$	$m \times m$	Measurement noise covariance matrix
$\mathbf{v}_k$	$m \times 1$	Measurement noise vector	$\mathbf{P}_k$	$n \times n$	State covariance matrix
$\mathbf{f}(\cdot)$	$n \times 1$	Process nonlinear vector function			

In general, the computed state ($\mathbf{x}_k$) and measured state ($\mathbf{z}_k$) are expressed as shown in Equation 7.1. The prediction step (k iteration) involves updating the state vector using the process vector function and updating the current co-variance estimate, as described in Equations 7.2 and 7.3.

$$\begin{aligned} \mathbf{x}_{k+1} &= \mathbf{f}(\mathbf{x}_k) + \mathbf{w}_k \\ \mathbf{z}_{k+1} &= \mathbf{h}(\mathbf{x}_{k+1}) + \mathbf{v}_{k+1} \end{aligned} \tag{7.1}$$

$$\mathbf{x}^a_{k+1} \approx \mathbf{f}\left(\mathbf{x}^a_k\right) \tag{7.2}$$

$$\mathbf{P}^a_{k+1} = \mathbf{J}_\mathbf{f}\left(\mathbf{x}^a_k\right)\mathbf{P}_k\mathbf{J}^T_\mathbf{f}\left(\mathbf{x}^a_k\right) + \mathbf{Q}_k \tag{7.3}$$

With $\mathbf{J}_\mathbf{f}$ being the Jacobian of function $\mathbf{f}$. The corrector step (a iteration) uses the observation

[1] Analog devices ADIS164900C data sheet, https://www.analog.com/media/en/technical-documentation/data-sheets/adis16490.pdf, accessed on the 8th of June 2020

[2] Terma T1 Star Tracker, https://www.terma.com/media/471442/t1_t2_star_tracker_rev2.pdf, accessed on the 12th of June 2020

and the predicted observation as-well as the current state certainty to correct the predicted state. Afterwards, it uses the more accurate measurements to increase the state certainty. This is shown in Equations 7.4 to 7.6.

$$\mathbf{K}_k^{a+1} = \mathbf{P}_k^a \mathbf{J}_\mathbf{h}^T \left(\mathbf{x}_k^a\right) \left(\mathbf{J}_\mathbf{h} \left(\mathbf{x}_\mathbf{k}^a\right) \mathbf{P}_k^a \mathbf{J}_\mathbf{h}^T \left(\mathbf{x}_\mathbf{k}^a\right) + \mathbf{R}_k\right)^{-1} \tag{7.4}$$

$$\mathbf{x}_k^{a+1} \approx \mathbf{x}_k^a + \mathbf{K}_k^{a+1} \left(\mathbf{z}_k - \mathbf{h}\left(\mathbf{x}_\mathbf{k}^a\right)\right) \tag{7.5}$$

$$\mathbf{P}_k^{a+1} = \left(\mathbf{I} - \mathbf{K}_k^{a+1} \mathbf{J}_\mathbf{h} \left(\mathbf{x}_\mathbf{k}^a\right)\right) \mathbf{P}_k^a \tag{7.6}$$

7.4.2. Landing and Ascent

Landing has by far the strictest requirement for this phase (**SRV-TECH-OPER-2.3**) gives an upper boundary for position deviation at landing. However, the advantage of this phase of flight is clearly that for the large majority of the phase there is line of sight to the Martian colony and thus access to the radar system.

EKF Setup

For this phase it is assumed that two types of the available of position sensors are active, namely a set of phased array radar/Doppler radar tracking stations and on-board IMU data. 4 values are measured by each radar station: r_r (range) ,ϕ (elevation), β (bearing) and v_r (velocity w.r.t. r_{vec}). For this simulation a coordinate system is set up as follows, x towards the starting position of the vehicle (downrange distance) and z as altitude, y (cross range distance) is chosen such that it forms the rhs coordinate system. Since the noise is only state independent in this case if the vector used consists of all the measurements directly This necessitates the use of the EKF state vector described in Equation 7.7 (subscript r denotes measurement space of dimension n, n being the number of radar stations, subscript c denotes a Cartesian coordinate frame x, y, z). The EOMs however are only given in the Cartesian reference frame, as shown in Equation 7.8.

For this simulation, the following function is known: $\mathbf{u}_c^{i+1}\left(\mathbf{u}_c^i\right)$, with $\bar{a}_c\left(t_i\right)$ being the accelerations from the trajectory simulations obtained in Chapter 4 and 5. This function is shown in Equation 7.9.

$$\mathbf{u}_r = [\mathbf{r}_r, \boldsymbol{\phi}_r, \boldsymbol{\beta}_r, \mathbf{v}_r \mathbf{a}_c, t] \tag{7.7}$$

$$\mathbf{u}_c = [\mathbf{x}_c, \mathbf{v}_c, \mathbf{a}_c, t] \tag{7.8}$$

$$\mathbf{u}_c^{i+1} = \begin{bmatrix} \mathbf{x}_c^i + \mathbf{v}_c^i \cdot \Delta t + \mathbf{a}_c^i \cdot \frac{\Delta t^2}{2} \\ \mathbf{v}_c^i + \mathbf{a}_c^i \cdot \Delta t \\ \mathbf{a}_c\left(t_i\right) \\ t^i + \Delta t \end{bmatrix} \tag{7.9}$$

However, as $\mathbf{u}_r$ is the state vector, it is necessary to convert the process $\mathbf{u}_c^{i+1}\left(\mathbf{u}_c^i\right)$ to a process $\mathbf{u}_r^{i+1}\left(\mathbf{u}_r^i\right)$. Using Equations 7.10 to 7.13, a function $\mathbf{u}_r\left(\mathbf{u}_c\right)$ can be obtained.

$$r_i = ||\mathbf{x}_c - \mathbf{p}_i|| \quad i \in [0, n] \tag{7.10}$$

$$v_i = \frac{\mathbf{v}_c \bullet (\mathbf{x}_c - \mathbf{p}_i)}{||\mathbf{x}_c - \mathbf{p}_i||} \quad i \in [0, n] \tag{7.11}$$

$$\beta_i = arccos\left(\frac{(\mathbf{x}_c - \mathbf{p}_i)_x}{||\mathbf{x}_c - \mathbf{p}_i||}\right) \quad i \in [0, n] \tag{7.12}$$

$$\phi_i = arcsin\left(\frac{(\mathbf{x}_c - \mathbf{p}_i)_z}{||\mathbf{x}_c - \mathbf{p}_i||}\right) \quad i \in [0, n] \tag{7.13}$$

with $\mathbf{p}_i$ being the location in Cartesian coordinates of the i'th radio tower. By substitution $\mathbf{u}_r^{i+1}\left(\mathbf{u}_c^i\right)$ can easily be determined. However the determination of $\mathbf{u}_c\left(\mathbf{u}_r\right)$ is not trivial since it is overdetermined. To solve this issue non-linear least squares is used as a triangulation method, which determines $\bar{x}_c$ using the information from $\bar{r}_r$, $\bar{\phi}_r$ and $\bar{\beta}_r$ and $\bar{v}_c$ using $\bar{v}_r$. This results in the closest $\mathbf{u}_c$ for a given $\mathbf{u}_r$. One major issue arising from this approach is that as can be seen in Equation 7.3 $\mathbf{J_f}$ is required and as an analytical expression is no longer available since due to least squares approach it cannot be computed analytically. Therefore $\mathbf{J_f}$ will have to be computed numerically. In this report a central difference scheme is used with $h = 10^{-3}$.

Observation and Process Noise Determination

Next, values for process and measurement noise will be determined. It is assumed that the radar will be operating at 27 [GHz] (K-band). Standard deviations for range and velocity are obtained from [26] assuming that the $\delta_t = 1$ [ns] and $\delta_f = 2$ [Hz] as is the case for for state of the art COTS signal analysers[3]. Standard deviations for ϕ and β are assumed to be $\delta_{ang} = 0.05$ [deg]. This number is obtained from state of the art phased array radar systems[4]. As the primary interest for this

[3]Rigol RSA5000 datasheet, `https://beyondmeasure.rigoltech.com/acton/attachment/1579/f-0816/1/-/-/-/-/RSA5_datasheet.pdf`, accessed on the 3rd of June 2020

[4]MSSR2000 datasheet, `https://www.hensoldt.net/products/radar-iff-and-datalink/mssr-2000-i-secondary-radar`, accessed on the 3rd of June 2020

simulation is the uncertainty of the tracking system over the reentry envelope, it is assumed that the initial uncertainty of the position is $\mathbf{P}_0 = 0$. Additionally it is assumed that there is no process noise $\mathbf{w}_k = 0$, $\mathbf{Q}_k = 0$ and that the observation noise is uncorrelated such that $\mathbf{R_k}$ is a diagonal matrix.

Results

When running the simulation for a single radar station, the low angular precision and high distance mean that the error in the simulation is very high — approximately 100 [km] by final timestep — hence another situation is tried with 6 tracking stations placed at up to 35 [km] away from the base. They are placed in a pattern as shown in Figure 7.1.

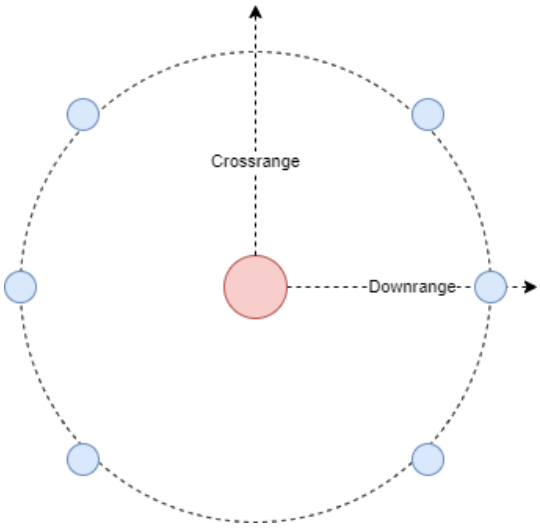

Figure 7.1: Graph of radar station locations, the red circle represents landing site location, blue circles represents radar stations.

This pattern was suggested in [27] as to be optimal for the case of Mars final approach. This approach, with the assumption mentioned above, yields a final $\sigma = 0.51$ [m] for position and a $\sigma = 0.00063$ [m/s] for velocity. Graphs for downrange, crossrange and altitude standard deviations for both velocity and position throughout the flight time are shown in Figure 7.2.

As can be seen in Figure 7.2, as expected, the altitude deviation greatly increases as the vehicle starts approaching the plane of the radar stations while the downrange and cross-range greatly decreases as it gets closer to the stations. Velocity shows similar behaviour. Curiously the inaccuracy of velocity in altitude has a sudden drop as it gets close to the plane, however with the overall deviation in the simulation of velocity it does not matter much.

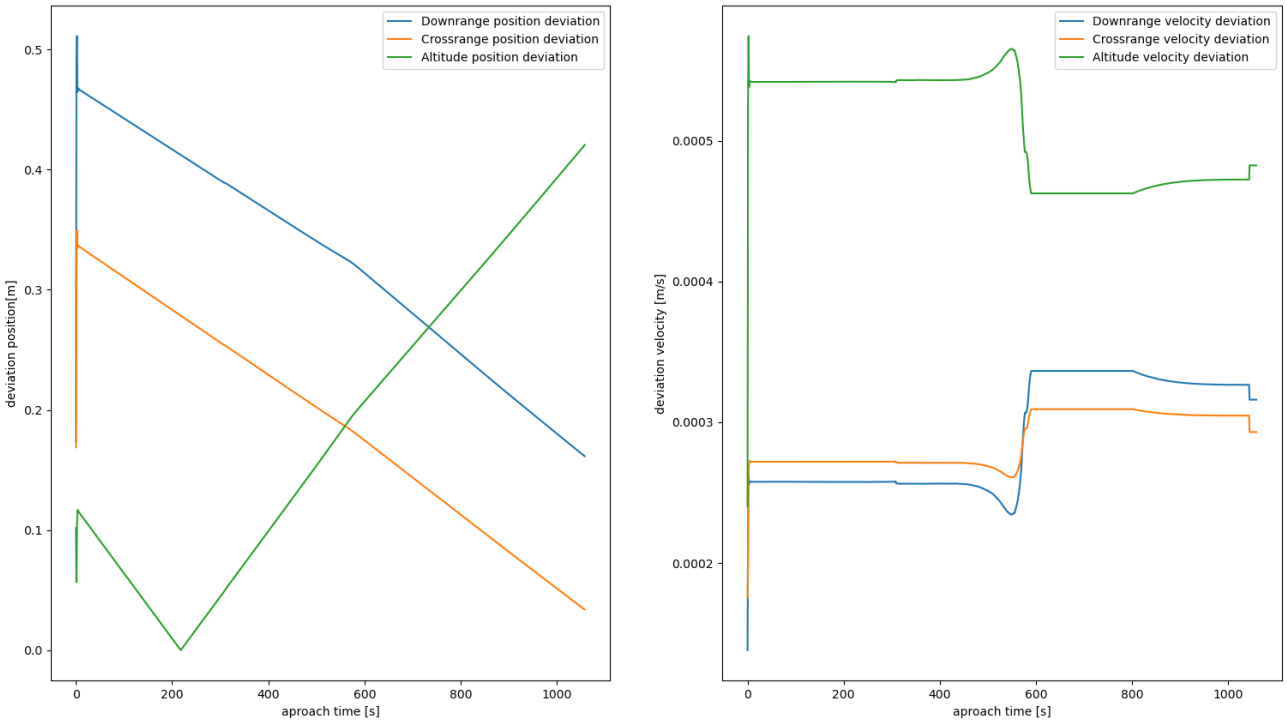

Figure 7.2: Graphs of deviation of position measurements and velocity measurement throughout reentry

7.4.3. Orbit

Next the orbital phase is considered. This phase is important especially as it is the initial condition for the reentry Monte Carlo simulation.

EKF setup

The EKF setup for in orbit state determination is easier as the $\mathbf{u}_c$ state vector can be used directly with $\mathbf{u}_c^{i+1}\left(\mathbf{u}_c^i\right)$ from Equation 7.9 since there is no line of sight to the Martian base. The trajectory is

again taken from Chapter 5. However as there is no line of sight to the Martian base it is assumed that only inertial measurements will be active. The state vector $\mathbf{u}_c$ from Equation 7.8 can therefore be used directly and the process $\mathbf{u}_c^{i+1}\left(\mathbf{u}_c^i\right)$ from Equation 7.9 can as a result also be used directly. The deviation for the acceleration measurements are taken from a COTS tactical accelerometer [28].

Results
Again a similar analysis is performed. This time the considered interval will instead be in between the vehicle leaving the LMO node and until the beginning of the reentry process. The results are shown in Figure 7.3.

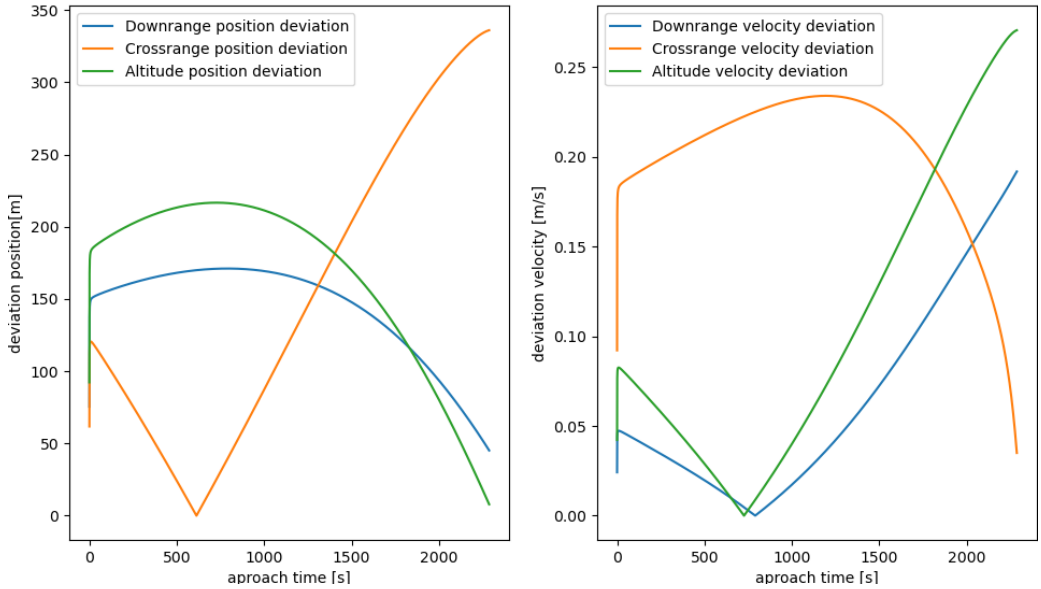

Figure 7.3: Graphs of deviation of position measurements and velocity measurement throughout orbit

As expected the altitude error is low while the planar error is a bit higher. The exact opposite is expected for velocity. It can also be observed that the biggest deviation of all still is within 1km even throughout a full hour runtime.

7.4.4. EKF Verification and Validation

To verify the general implementation of the EKF it was compared to the example in [29]. Each separate type of measurement is tested individually to check if the behaviour matches the expected results. Lastly for validation the current implementation is tested against the case described in [30]. It is important to note that there is a fundamental difference in the approach taken, since the paper uses a radio interferometer and the exact values assumed for variances is presented ambiguously. However the order of magnitude for the most comparable case is within the same order of magnitude (δ_{sim_r}=10.54[m], δ_{ref_r}=9.09[m], δ_{sim_v}=0.18 [m/s] and δ_{ref_v}=0.22 [m/s]).

7.5. Control modes

Before choosing the control technique and sizing of the actuators, control modes are identified for the entire flight. These modes correspond to manoeuvres that the control system will be designed for. These modes are as follows:

- **Orbit-insertion**
  Rotating the vehicle such that it achieves the correct orbital velocity vector
  Control pitch, yaw and roll rates
- **Rendezvous**
  Rotate 180 degrees two times; Within the transfer from phasing orbit to node orbit and before docking approach
- **Docking**
  Approach the node. Control about 3 translational axes in order to align with the target. Furthermore, for attitude alignment it also needs instantaneous rotational control around 3 axis.

- **Reentry**

  Rotate to angle of attack of 180 degrees before landing burn

  Control pitch, yaw and roll rates

7.6. Control Technique Trade-Off

A choice on the control technique has to be made before the design and sizing of the actuators. The first considered techniques are reaction wheels (RW) with thrusters and Control Moment Gyros (CMG) with thrusters. The thrusters in both techniques are used for desaturation and for translational control, while both the RW and CMG are used to maintain rotational control. The two other considered techniques are a full thruster configuration, fixed or gimbaled.

The type and size of all required impulses is estimated for all manoeuvres of the control modes. A low magnitude, angular impulse with 3 rotational DoF is identified for all manoeuvres. The only exceptions are Docking, also requiring high magnitude linear impulse and 6 DoF, and Reentry pitch control, requiring high magnitude angular impulse with 3 DoF. From this it is clear that performance and controllability around all axes are important design drivers. Having completed the trade-off, the chosen control technique is a set of pulsed thrusters.

Table 7.6: Control techniques

Criteria	Controllability, 25.0%	Complexity, 25.0%	Performance, 25.0%	mass, 12.5%	power, 12.5%	Total
Control technique	(1, 5) High Best, $\sigma = 1.479$	(1, 5) High Best, $\sigma = 1.225$	(1, 5) High Best, $\sigma = 0.829$	(1, 5) High Best, $\sigma = 1.09$	(1, 5) High Best, $\sigma = 1.09$	
RW's and thrusters	orange 2 → 0.25	yellow 3 → 0.5	orange 2 → 0.25	orange 2 → 0.25	orange 2 → 0.25	0.312
CMG's and thrusters	red 1 → 0	orange 2 → 0.25	yellow 3 → 0.5	red 1 → 0	orange 2 → 0.25	0.219
Pulsed thrusters	yellow 3 → 0.5	blue 5 → 1	green 4 → 0.75	green 4 → 0.75	green 4 → 0.75	0.75
Gimbaled thrusters	blue 5 → 1	orange 2 → 0.25	green 4 → 0.75	orange 2 → 0.25	red 1 → 0	0.531

7.7. Manoeuvre Analysis

All manoeuvres of the control modes are analysed to obtain the required forces and torques.

7.7.1. Reference Frame

The thrusters create a torque which is defined in the vehicle body reference frame F_b. The reference frame, F_I as defined by the team has another orientation than F_b. Transforming this is done using Equation 7.14.

The required thrust for each manoeuvre is obtained in the Local Orbit Reference frame F_{lo}. Hence, another transformation is required in order to obtain the required thrust levels given by the RCS. This transformation, obtained from [31], is given in Equation 7.15.

$$\begin{bmatrix} x_\mathrm{I} \\ y_\mathrm{I} \\ z_\mathrm{I} \end{bmatrix} = \mathbb{T}_y(\frac{\pi}{4})\Big|_{lo''''} \mathbb{T}_z(-\frac{\pi}{2})\Big|_{lo'''} \mathbb{T}_x(\pi)\Big|_{lo''} \begin{bmatrix} x_\mathrm{b} \\ y_\mathrm{b} \\ z_\mathrm{b} \end{bmatrix} = \begin{bmatrix} \frac{\sqrt{2}}{2} & 0 & -\frac{\sqrt{2}}{2} \\ 0 & 1 & 0 \\ \frac{\sqrt{2}}{2} & 0 & \frac{\sqrt{2}}{2} \end{bmatrix} \begin{bmatrix} 0 & -1 & 0 \\ 1 & 0 & 0 \\ 0 & 0 & 1 \end{bmatrix} \begin{bmatrix} 1 & 0 & 0 \\ 0 & -1 & 0 \\ 0 & 0 & -1 \end{bmatrix} \begin{bmatrix} x_\mathrm{b} \\ y_\mathrm{b} \\ z_\mathrm{b} \end{bmatrix} \tag{7.14}$$

$$\begin{bmatrix} x_\mathrm{b} \\ y_\mathrm{b} \\ z_\mathrm{b} \end{bmatrix} = \mathbb{T}_x(\alpha_x)\Big|_{lo''} \mathbb{T}_y(\alpha_y)\Big|_{lo'} \mathbb{T}_z(\alpha_z)\Big|_{lo} \begin{bmatrix} x_\mathrm{lo} \\ y_\mathrm{lo} \\ z_\mathrm{lo} \end{bmatrix} = \begin{bmatrix} 1 & 0 & 0 \\ 0 & s\alpha_x & s\alpha_x \\ 0 & -s\alpha_x & c\alpha_x \end{bmatrix} \begin{bmatrix} -s\alpha_y & 0 & c\alpha_y \\ 0 & 1 & 0 \\ c\alpha_y & 0 & s\alpha_y \end{bmatrix} \begin{bmatrix} c\alpha_z & s\alpha_z & 0 \\ -s\alpha_z & c\alpha_z & 0 \\ 0 & 0 & 1 \end{bmatrix} \begin{bmatrix} x_\mathrm{lo} \\ y_\mathrm{lo} \\ z_\mathrm{lo} \end{bmatrix} \tag{7.15}$$

7.7.2. Ascent

At the end of the ascent trajectory, the vehicle remains with a pitch angle of 26.7 degrees after it is rotated by means of gimballing main engines and the gravity gradient. This pitch angle is to be reduced to zero during phasing, before entering transfer orbit, such that the ΔV manoeuvre by the main engines for the Hohmann transfer is aligned with the local orbital velocity.

For sizing, Equations 7.16, to 7.18 are used [25]. The thrust level, burn time and rotation angle are used as an input, resulting in the total rotation time. As this rotation has a large window, the required

thrust is considered relatively low. Therefore, the most constraining thrust level, being the maximum thrust the engines are sized for, is given as input with varying burn times, such that the time limit is not exceeded. Phasing time is at most two periods. To allow for a margin, this time constraint is set to half a period. This is computed with Equation 7.19.

$$\ddot{\theta} = \frac{T}{I} \quad (7.16) \qquad \dot{\theta} = \frac{\ddot{\theta}}{t_{burn}} \quad (7.17) \qquad t = \frac{\theta}{\dot{\theta}} \quad (7.18) \qquad t_{limit} = 2\pi\sqrt{\frac{R^3}{\mu}} \quad (7.19)$$

R is the mean radius of Mars and μ is the gravitational parameter. θ, $\dot{\theta}$ and $\ddot{\theta}$ are the slew angle, spin rate and spin acceleration respectively. Finally, I is the mass moment of Inertia of the axis which the vehicle is rotating around. The propellant is calculated with Equation 7.20. Here I represents the impulse given by the thrusters. I_{sp} is the specific impulse, which depends on the type of propellant and engine. The burn time is given by t_{burn}. It should be noted that this has to be multiplied by a factor 2, as an impulse is also required to stop the rotation at the end of the manoeuvre.

$$M_p = \frac{I}{I_{sp}g} = \frac{Ft_{burn}}{I_{sp}g} \quad (7.20)$$

Furthermore, pitch control is required during ascent. Pitch control is needed in order to counteract the aerodynamic torque acting on the vehicle. This is obtained from the ascent model in Chapter 4. The maximum pitch moment is 482.5 [Nm]. The propellant mass required is calculated for each time step in the model, using Equation 7.20.

7.7.3. Rendezvous

During rendezvous, the vehicle needs to approach the node up to a small enough distance, such that it can execute the docking procedure. Rendezvous is initiated by the Hohmann transfer from phasing orbit to node orbit, requiring two ΔV manoeuvres through the main engines. This transfer orbit is reached by speeding up the vehicle. Following this, the nodal orbit is reached by applying retro-thrust. This means that a 180 [°] rotation is required throughout the transfer period. This rotation is computed in exactly the same way as explained in Subsection 7.7.2. The time constraint here is equal to the period of transfer, which is half of the period the Hohmann transfer orbit. This period can be calculated using Equation 7.21.

$$t_{limit} = \pi\sqrt{\left(\frac{h_{node} + h_{phasing} + 2R}{2}\right)^3 \cdot \frac{1}{\mu}} \quad (7.21)$$

Here, h_{node} and $h_{phasing}$ are the height of the node and the phasing orbit respectively. R is the mean radius of Mars and μ is the gravitational parameter.

At the start of the docking phase, the vehicle, from now on referred to as chaser, reaches a go/no go point. Here three outputs are considered:

1. Initiate docking: *the chaser rotates 180 [°] such that it has the right attitude for mating with the target.*
2. Transfer to phasing orbit: *the chaser manoeuvres back to the phasing orbit through the same Hohmann transfer orbit.*
3. Abort: *the capsule is separated from the chaser.*

Looking at outputs 1 and 2, two additional rotations are required. The time limit can be freely chosen, as these rotations occur at zero relative velocity. Hence the time limit from Equation 7.21 is used here as well.

7.7.4. Docking

Approach Strategy

As the Hohmann transfer can be timed accurately, it is assumed that the vehicle is able to initialise the docking phase within 1000 [m] from the node. The rendezvous and docking procedure can be divided into multiple phases, based on the relative distance and navigation source [32]. Looking only at the relative position range of Charon during docking, these phases are shown in Table 7.7.

Table 7.7: Properties of the control modes [32]

Phase	Range [m]	Duration
Proximity-A	1000-250	1 orbit
Proximity-B	250-30	60 min
Docking	25-3	<17 min

For a trajectory approach, a Vbar (along the orbital velocity vector) or a Rbar (along the nadir axis) approach is considered. Incapacity of executing a manoeuvre must not result in a collision. Rbar has a natural breaking effect, as the chaser attains a different altitude. For Vbar this breaking effect is only 5% the value of Rbar [31]. Considering the worst case, a Vbar approach is used. Furthermore a straight line approach is used, as this allows for stops during approach in case of contingencies. In between each phase the vehicle performs a ΔV manoeuvre and stops, such that a go/no go decision can be made in case of a failure. When go is decided, another ΔV manoeuvre will initiate the next phase.

Model

In order to determine the control input needed during this phase, the docking approach is simulated. For this, a model is built in order to monitor the trajectory of the vehicle (chaser) towards the node (target).

For the model, the reference frame is defined as F_{lo} originating in the CoM of the target. This is more convenient in the case of relative navigation, which is used within close proximity of the target during docking. This also means that the Vbar axis is equal to the x-axis of F_{lo} For this the equations of relative motion are used, also known as the Hill equations, as shown in Equation 7.22 [31]. These simplified equations of motion are only accurate for a specified scenario, as they hold some assumptions: the orbit is circular, there are no orbital perturbations, and the distance between chaser and target is very small compared to their areocentric distance.

$$\begin{gathered}\ddot{x} - 2\omega\dot{z} = \frac{1}{m_c}F_x \quad , \quad \ddot{y} + \omega^2 y = \frac{1}{m_c}F_y \quad , \quad \ddot{z} + 2\omega\dot{x} - 3\omega^2 z = \frac{1}{m_c}F_z \\ x_0 = X_0 \quad , \quad y_0 = z_0 = 0 \quad , \quad \dot{x}_0 = \Delta V_{x1} \quad , \quad \dot{y}_0 = \dot{z}_0 = 0\end{gathered} \tag{7.22}$$

The motion can be controlled by input accelerations $\frac{1}{m_c}F_{x,y,z}$. The navigational measurement errors are included in this model, both in position and velocity, obtained from [31]. These result in a change in position as can be seen in Equation 7.23.

$$\begin{gathered}\Delta x = \Delta x_m + 6\Delta z_m(\omega t - sin(\omega t)) + \Delta V_{xm}(\frac{4}{3}sin(\omega t) - 3t) + \frac{2}{\omega}\Delta V_{xm}(1 - cos(\omega t)) \\ \Delta y = \Delta y_m cos(\omega t) + \frac{1}{\omega}\Delta V_{ym} sin(\omega t) \quad , \quad \Delta z = \Delta z_m(4 - 3cos(\omega t))\frac{1}{\omega}\Delta V_{zm} sin(\omega t) \\ X_0 + V_x \cdot t + \Delta x = x(t) \quad , \quad Y_0 + \Delta y = y(t) \quad , \quad Z_0 + \Delta z = z(t)\end{gathered} \tag{7.23}$$

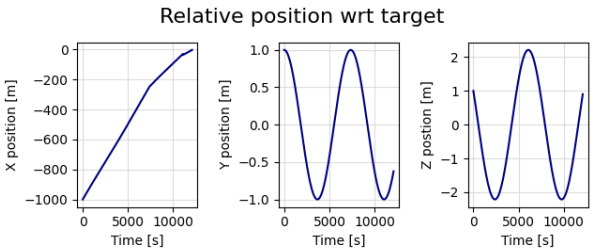

Figure 7.4: Chaser position and propellant mass required by the RCS from the model of the Vbar approach

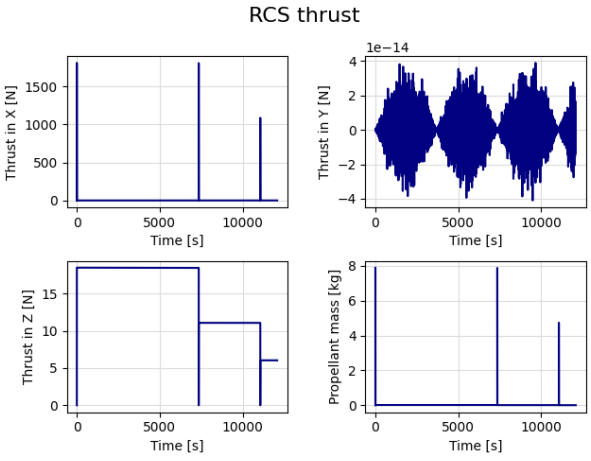

Figure 7.5: Forces required by the RCS from the model of the Vbar approach

Considering a straight line approach with constant velocity, the input for this model is the average velocity for each phase along with the starting positions $X_{0,A}$, $X_{0,B}$ and $X_{0,d}$. The output of the model

are the control forces F_{xyz} that are required for this trajectory. As can be seen, the maximum thrust required is in x-direction and results from the ΔV manoeuvres in between the phases, which is equal to 1807.41 N. Furthermore, the thrust in z also drives the thruster design as this is the minimum thrust level to be designed for and this is equal to 11.21 N.

Model Verification

The chaser motion resulting from the equations of motion in a straight line Vbar approach without any perturbations is a constant motion along the x-axis. This can be analytically computed using Equation 7.24 [31].

$$\gamma_z = \frac{F_z}{m} = 2\omega V_x = 2\sqrt{\frac{\mu}{R + h_{node}}} \tag{7.24}$$

With the determined velocities during each phase and ω determined, the thrust in z-direction can be analytically computed. Considering Proximity-A, the thrust is 9.25 N. For Proximity-B this is 5.55 N. During docking the thrust is 3.02 N. Noting that a 100% safety margin is applied to the required thrust, these values align with the model output thrust values. Additionally for each time step, the propellant mass can be calculated with Equation 7.20.

7.7.5. Reentry

During reentry, a rotation is required such that the angle of attack becomes equal to 180 degrees, in order to initiate the landing burn by the main engines. Computing this is done in the same fashion as the rotations during ascent and rendezvous. The time limit regarding this manoeuvre depends on time of initiation.

Furthermore, pitch and roll control is required in order to stabilize the vehicle and to make sure **SRV-TECH-OPER-2.3** is adhered to. For this, a body flap is designed in combination with a RCS thruster. The thruster is added because the body flap is not able to control the aerodynamic disturbance torque within its sizing constraints. The required rolling and pitching moment that need to be delivered are shown in Figure 5.7. The maximum moments for roll and pitch are 1000 [Nm] and 14500 [Nm] respectively. For calculating the propellant mass, Equation 7.20 is used for each time step in the reentry control model in Section 5.6.

7.7.6. Disturbances

The spacecraft dynamics resulting from the control input will also be affected by external disturbances. This means that they need to be taken into account while sizing the performance of the actuators. Attitude measurement errors are present along with uncertainty of the spacecrafts' principal axis. For this, an error angle of 2 degrees is considered.

Gravity Gradient

A pitch or yaw angle results in a torque applied to the vehicle due to gravity. This torque tends to bring the vehicle back to an attitude which is aligned with the local orbital velocity. It is calculated with Equation 7.25 [11].

$$T_g = \frac{3\mu}{2R^3}\left|I_z - I_y\right|\sin(2\theta)\begin{bmatrix}1 & 0 & 0\end{bmatrix}^T \tag{7.25}$$

Here, I_{yz} are the mass moments of Inertia, θ is the angle between the vertical axis in F_b and the axis pointing from the CoM of the vehicle towards the gravitational centre of Mars. Considering symmetry along x and z, the torque is zero in y and z.

Magnetic Field

Due to the residual dipole moment of the vehicle, a torque is generated while it moves within Mars' magnetic field. The torque is computed with Equation 7.26. D, the residual dipole moment, is estimated to be $3.5x10^{-}3\frac{Am^2}{kg}$ according to [33]. M is the magnetic moment of Mars, which is approximately $1.35Tm^3$ according to [34].

$$T_m = DB = D\frac{2M}{R^3} \tag{7.26}$$

Aerodynamics

Aerodynamic drag acts on the vehicle in the case there is a density. The distance in centre of pressure (cp) and centre of gravity equals the arm of the aerodynamic torque, which is calculated with Equation 7.28. To obtain an estimate of the cp, Equation 7.27 is used [5]. Here, A is the reference area, defined to be projected on the plane normal to the velocity vector and d is the position of each component in F_b. Due to symmetry along x-axis and z-axis, only torque around y-axis is considered.

$$cp_A = \sum_{i=0}^{i=n} d_i A_i = dA_{nose} + dA_{body} + Ad_{flaps} + Ad_{engines} \tag{7.27}$$

$$T_a = 0.5\rho C_d A \bar{V}^2 \left(cp_a - cg\right) = D\left(cp_a - cg\right) \tag{7.28}$$

Solar Radiation

An offset in the solar centre of pressure cp_{ps} and the centre of gravity create a torque. It is calculated using Equation 7.29 [11]. F_s is the Martian solar irradiance, being equal to $586.2\frac{W}{m^2}$ [6]. A_s is the reference area, calculated with Equation 7.27. q is the reflectively of the vehicle, estimated to be 0.6 [7] c is the speed of light, being $3x10^8\frac{m}{s}$ and I is the solar incidence angle, which is set to zero as a worst case scenario.

$$T_{sp} = F\left(cp_{ps} - cg\right) = \frac{F_s}{c} A_s (1+q)\cos(I)(cp_{ps} - cg) \tag{7.29}$$

Assembly Errors

Errors in the assembly of RCS engines are common and it is important that these are taken into account while sizing the thrusters. An error in the angle of the thrust vector will result in a torque around all three axes. It is computed with Equation 7.30. Here, l_x, l_y and l_z are the thruster arms of the specific thruster with respect to principal axes x,y and z.

$$T_{error} = Tsin(\theta)\begin{bmatrix} l_x & l_y & l_z \end{bmatrix}^T \tag{7.30}$$

7.8. Configuration

From the control mode identification in Section 7.5 and control manoeuvre analysis in Section 7.7, it is recognised that instantaneous 6 DoF is required for docking. In order to provide this, decoupling of each DoF is highly favourable. Decoupling usually means adding more weight, as more thrusters are added. However, an advantage of this is that it results in a more robust design, having lower control complexity and more redundancy. Based on these considerations, a complete decoupled thrust configuration is chosen. The thruster configuration is shown in Figure 7.6. For each DoF, at least level 1 redundancy is considered. A separate set of thrusters for each DoF with this configuration results in a total of 32 thrusters. 1 more thruster is added to provide pitch control during reentry. The force- or moment direction each thruster is assigned to provide thrust for is shown in Figure 7.6.

All thrusters used for rotational control are located such that they maintain a thrust arm as large as possible, increasing efficiency. Additionally, the capsule should be able to have manoeuvrability after abort, which leads to all thrusters in the top part of the vehicle being attached to the capsule. Due to aerodynamic constraints, they are attached as low as possible, resulting in a y-coordinate of 15.21 m. Translation in y-direction only occurs during docking. During this phase the bottom and top thrusters need to have an equal arm in order to provide pure translation. The y-coordinate of the bottom thrusters is obtained from this requirement. Considering a constant center of gravity of 7.71 m, this y-coordinate is equal to 1.0 m. Furthermore, the bottom thrusters and top thrusters are located at a distance from the CoG that is equal to the body radius and capsule radius respectively. This can be seen in Figure 7.6.

[5] T. Benson, Determining centre of Pressure, https://www.grc.nasa.gov/www/k-12/rocket/rktcp.html, accessed on 10 June 2020

[6] NASA, Mars fact sheet, https://nssdc.gsfc.nasa.gov/planetary/factsheet/marsfact.html,accessed on 10 June 2020

[7] Alumet Avantgarde in anodizing, https://alumet.nl/wp-content/uploads/2016/05/Solar-Reflectance.pdf,accessed on 10 June 2020

The required control forces and torques for each manoeuvre, along with the disturbance torques are shown in Table 7.8. $T_{e_{xyz}}$ represent the disturbances and engine assembly errors, discussed in Subsection 7.7.6.

Table 7.8: Control forces F_{xyz} and moments T_{xyz} required for each manoeuvre along with the disturbance torques $T_{e_{xyz}}$

Manoeuvres	Time	F_x [N]	F_y [N]	F_z [N]	T_x [Nm]	T_y [Nm]	T_z [Nm]	T_{e_x} [Nm]	T_{e_y} [Nm]	T_{e_z} [Nm]
Ascent										
Rotation	153.8 [s]	-	-	-	5517.1	-	-	0.274	0.274	1.09
Pitch control	-	-	-	-	482.50	-	-			
Rendezvous	157.6 [s]	-	-	-	5517.1	-	-	3.37	0.27	0.27
Docking										
Proximity-A	122.6 [min]	-	1807.41	18.50	- -	-	-	4.81	1.11	1.11
Proximity-B	61.9 [min]	-	1804.63	12.22	- -	-	-			
Docking	17.0 [min]	-	591.63	6.42	- -	-	-			
Reentry										
Rotation	6.95 [s]	-	-	-	5517.1	-	-	1.02	0.27	0.27
Pitch/Roll control	-	-	-	-	16976.6	1000	-	-	-	-

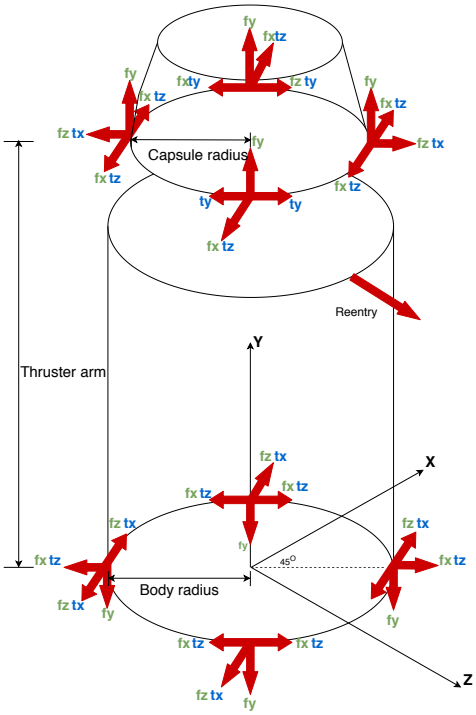

Figure 7.6: Thruster configuration, total of 33 thrusters

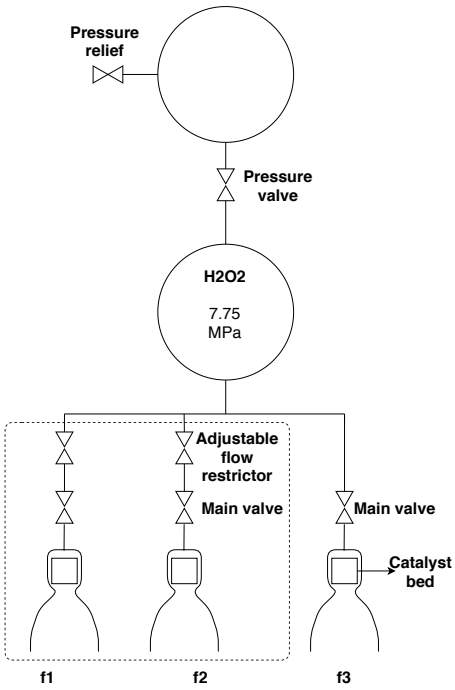

Figure 7.7: Engine feed system

Based on the chosen configuration, the total torques and forces in Table 7.8, obtained from sizing, can be related to the required thrust levels per engine. A margin of 100% is applied to all thrust levels, obtained from [35]. For nominal thrusting, the upper constraint on the thrust levels comes from the first ΔV manoeuvre during docking, requiring 452.60 [N] and is used as input for all rotation manoeuvres with a short burn time such that the rotation time doesn't exceed the time limit. Furthermore, for each manoeuvre the maximum disturbance torque is taken to determine the required thrust for counteracting these. Next to a body flap, high RCS thrust of 2772 [N] for stability pitch control during reentry is required due to the high aerodynamic moment, shown in Figure 5.7. For this thrust level, it is decided to design a separate engine.

Two other thrust levels are identified; 0.31 [N] - 9.25 [N] and 85.13 [N] - 454.37 [N]. An engine with high throttleability is required for this. Furthermore, valves can be used for the engine that regulate the mass flow. For this, two types are considered; a single needle valve and a set of a normal valve combined with an adjustable flow restrictor. Needle valves provide a large range in mass flow, but relatively more pressure loss. The latter may usually provide less range, but allows for less complex design and more redundancy. Considering using a high throttleable engine, the set of the normal valve and adjustable flow restrictor is chosen for all engines. This can be seen in Figure 7.7. Furthermore, flow control valves are used. These provide the possibility to enhance mass flow toward the engine.

This in turn makes the engines throttleable and make it possible to provide a range of thrust levels through a single engine. In Equation 7.31, the relation between the set of thrusters and total force F_{xyz} or total torque T_{xyz} for each DoF is given.

Table 7.9: Trust levels per engine for each cluster (given in Figure 7.6)

Manoeuvres	f_x [N]	f_y [N]	f_z [N]	t_x [N]	t_y [N]	t_z [N]
Ascent						
Rotation	-	-	-	452.60	0.75	0.75
Pitch control	-	-	-	85.13	0.31	0.31
Rendezvous	-	-	-	452.70	0.85	0.85
Docking						
Proximity-A	-	454.37	9.25	2.52	2.52	2.52
Proximity-B	-	273.50	6.11	2.52	2.52	2.52
Docking	-	150.10	3.21	2.52	2.52	2.52
Reentry						
Rotation	-	-	-	452.13	0.55	0.55
Pitch control	-	-	-	2772.18	81.71	-

$$\begin{aligned} \begin{bmatrix} F_x & F_y & F_z & T_x & T_y & T_z \end{bmatrix}^T &= diag(f_x, f_y, f_z, t_x, t_y, t_z) \begin{bmatrix} u_1 & u_2 & u_3 & u_4 & u_5 & u_6 \end{bmatrix}^T \\ &= diag(2f_1, 4f_1, 2f_2, 4(f_1/f_3)l, 2f_1(r_{capsule} + r_{body}), 4f_2) \begin{bmatrix} u_1 & u_2 & u_3 & u_4 & u_5 & u_6 \end{bmatrix}^T \\ f_1 = 84.82N - 454.37N \quad , \quad f_2 = 0.31N - 9.25N \quad , \quad f_3 = 2772.18N \end{aligned} \tag{7.31}$$

7.9. Propellant Trade-Off

For the propellant used by the RCS engines, multiple options are considered. For trading-off these options, main drivers are performance, throttleability, complexity and sustainability. A combination of bi-propellant and mono-propellant is considered as an option. The bi-propellant considered for this option is LCH4/LOX, as the propellant can be stored in the main propellant tank this way. This option has the advantage of more efficiency at higher thrust levels, due to the bi-propellant engines. The disadvantage however is that very high complexity would be included in the feed system, as the tank pressure requirements for the main propulsion are different than for the RCS.

Furthermore, using only mono-propellant RCS engines is also a possible option, having the advantage of decomposing catalytically, resulting in lower combustion temperatures. This usually requires only radiative cooling instead of active cooling for bi-propellant engines. For the mono-propellant, Hydrogen Peroxide (H_2O_2) and Hydrazine (N_2H_4) were considered, because this is also used in the abort system, which means that RCS- and abort propellant can be stored in the same tank in the capsule. A big advantage of H_2O_2 is that it is producible in-situ and it is non-toxic [36]. This lead to going with H_2O_2 for this option. The propellant trade-off is shown in Table 7.10.

Table 7.10: RCS propellant

Criteria / Design Concept	Performance, 25.0% (1, 5) High Best, $\sigma = 1$	Throttleability, 25.0% (1, 5) High Best, $\sigma = 1$	Complexity, 25.0% (1, 5) High Best, $\sigma = 1.5$	Sustainability, 25.0% (1, 5) High Best, $\sigma = 0.5$	Total
Bi-liquid (LCH4 and H2O2)	blue 5 → 1	orange 2 → 0.25	red 1 → 0	yellow 3 → 0.5	0.438
Mono-liquid (H2O2) only	yellow 3 → 0.5	green 4 → 0.75	green 4 → 0.75	green 4 → 0.75	0.688

The trade-off shows that only H_2O_2 mono-propellant is used for the RCS engines.To size these engines, the Rocket Propulsion Analysis software (RPA)[8] was used. The resulting properties and dimensions are shown in Table 7.12. Finally, knowing the specific impulse, the propellant mass can be computed for each manoeuvre, using Equation 7.20. The engine masses of f_1 and f_3 are estimated to be 3.7 [kg], while for f_2

Table 7.11: Propellant mass required for each control mode

Manoeuvres	Propellant [kg]	Redundancy [kg]
Ascent	50.61	2.62
Rendezvous	3.95	0.01
Docking	177.28	11.97
Reentry	975.67	12.21
Total	**1207.51**	**35.81**

[8]RP Software and Engineering, `http://www.propulsion-analysis.com`, accessed the 2nd of June 2020.

this is 0.65 [kg], comparing with similar mono-propellant engines from [37]. Engine properties are shown in Table 7.11, and the propellant mass usage for the trajectories is plotted as seen in Figure 7.8

For simplification, two tanks are used for the RCS system; one is for the top part, placed in the top part of the body, and one for the bottom part, placed in the bottom. Additional RCS propellant for the capsule after abort is stored in the propellant tank in the capsule. The H_2O_2 volume is 1440 [kg/m^3], leading to a tank volume of 0.42 [m^3]. The structural mass per tanks is 40.2 [kg].

Table 7.12: Engine characteristics and Propellant mass required

Engine	V_e $[\frac{m}{s}]$	I_{sp} $[s]$	M_e $[kg]$	A_e/A_t	D_e $[mm]$	l_e $[mm]$	l_c $[mm]$
f_1	1717.29	175.11	4.92	22.0	72.10	85.40	157.26
f_2	1717.29	175.11	8.77	22.0	10.32	12.22	144.97
f_3	1717.15	140.28	13.32	22.0	245.95	291.28	193.21

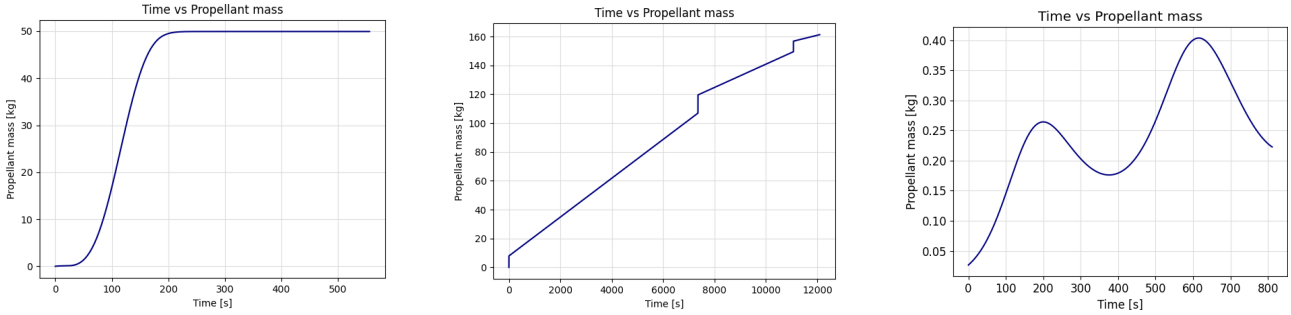

(a) Ascent (b) Rendezvous (c) Reentry

Figure 7.8: Propellant mass usage for control trajectories

7.10. Risk analysis

The following risks have been analysed and mitigated as part of the Gnc subsystem:

- **SRV-RISK-GNC-1** Docking camera failure (P=3), results in LOM: not being able to dock (I=3).
  - Impact mitigation (I-2): redundancy.
- **SRV-RISK-GNC-2** Landing camera failure (P=3), results in possible vehicle damage (I=3).
  - Impact mitigation (I-2): redundancy.
- **SRV-RISK-GNC-3** Star tracker failure (P=2), results in LOC: not being able to successfully reenter the atmosphere (I=5).
  - Impact mitigation (I-3): redundancy.
- **SRV-RISK-GNC-4** Gyroscope failure (P=4), results in LOM: loss of attitude (I=4).
  - Impact mitigation (I-3): redundancy.
- **SRV-RISK-GNC-5** Accelerometer failure (P=4), results in LOM: loss of position (I=4).
  - Impact mitigation (I-3): redundancy.
- **SRV-RISK-GNC-6** Flight computer failure (P=2), results in LOC: loss of control of vehicle (I=5).
  - Probability mitigation (P-1): extensive validation and testing.
  - Impact mitigation (I-2): redundancy.
- **SRV-RISK-GNC-7** Thruster failure (P=4), results in LOV: loss of manoeuvrability (I=4).
  - Impact mitigation (I-3): redundancy.
- **SRV-RISK-GNC-8** Ignition failure (P=4), results in LOM: momentary loss of control (I=4).
  - Impact mitigation (I-3): automatic monitoring system of the engines.
- **SRV-RISK-GNC-9** Valve/feedsystem failure (P=4), results in LOM: loss of single thruster (I=4).
  - Impact mitigation (I-3): redundancy.
- **SRV-RISK-GNC-10** Critical thruster failure (P=2), results in LOV: : vehicle damage (I=5).
  - Impact mitigation (I-2): adding shutoff valves in the feedsystem.
- **SRV-RISK-GNC-11** Propellant leakage (P=1), results in loss of multiple thrusters (I=5).
  - Impact mitigation (I-2): adding shutoff valves in the feedsystem.
- **SRV-RISK-GNC-12** Control algorithm errors (P=2), results in LOV: terminal loss of control and possible ill manoeuvring (I=5).
  - Probability mitigation (P-1): extensive v&v.

  - Impact mitigation (I-2): alternate emergency control software.
- **SRV-RISK-GNC-13** Guidance algorithm errors (P=2), results in LOM: terminal loss of guidance information (I=3).
  - Probability mitigation (P-1): extensive v&v.
- **SRV-RISK-GNC-14** Engine thruster misalignment (P=5), results in the introduction of an extra disturbance torque (I=2).
  - Probability mitigation (P-2): installation checks.
  - Impact mitigation (I-1): compensation.

From this list, a mitigated risk map has been created. It can be seen in Table 7.13. While some risks are still in the orange zone, that is deemed acceptable, as the added redundancy will make these risks almost negligable.

Table 7.13: Risk map of the GNC subsystem, after mitigation

	Very unlikely (1)	Unlikely (2)	Possible (3)	Likely (4)	Very likely (5)
Very high impact (5)					
High impact (4)					
Medium impact (3)	6, 11, 12, 13	10			
Low impact (2)		3			
Very Low impact (1)			1, 2, 14	4, 5, 7, 8, 9	

7.11. Requirement Compliance and Sensitivity Analysis

As can be observed in Table 9.4 the design is not able to meet **SRV-TECH-OPER-1.4**, This is due to the fact that the number given in the baseline was based on state of the art using GPS. As discussed in Subsection 7.3.1 GPS is not assumed to be available and thus it is no longer reasonable to assume this degree of absolute position at all times. The computed deviation has been used successfully for the Monte Carlo simulation in Chapter 5, thus this requirement is no longer needed.

Regarding the control system, requirements **SRV-TECH-OPER-1.5** and **SRV-TECH-OPER-1.6** are also not met. From the Rendezvous and Docking model from Subsection 7.7.3 the accelerations around the longitudinal and lateral axis are obtained by dividing maximum required thrust by the MoI around the x-axis and y-axis. This results in required accelerations of 0.102 [m/s^2] and 0.00535 [m/s^2]. This is significantly lower than stated in the requirement, due to the requirement being based on the Dragon Capsule, whose empty weight is more than a factor 15 lower than Charon's, resulting in a lower MoI. The obtained values are used to correct the requirements, adding a 50% margin, resulting in 0.051 [m/s^2] and 0.0053 [m/s^2]. This margin is used as the model is of simplified nature using numerous assumptions. Lowering this acceleration only leads to a longer δV burn time (12s) during docking, which is still deemed acceptable as the distance between chaser and target during the last burn is initially 25m with a velocity of 0.06 [m/s]. Finally, requirement SRV-TECH-OPER-1.7 can not yet be complied with as an estimation of the number of cycles for the ACS is not yet possible. The amount of cycles of a mono propellant engine is dependant on the valve cycle lifetime, material degradation inside the thruster and lifetime of the catalyst bed. Verifying this requirement can be done by a full life cycle test, pulse trusting the engine the required amount of times, following the procedures described in Section 22.3.

Table 7.14: Requirement compliance for GNC

Requirement	Completion	Determination
SRV-TECH-OPER-1.4	✗	
SRV-TECH-OPER-3.3	✓	Subsection 7.3.2
SRV-TECH-OPER-2.2	✓	Subsection 7.4.2
SRV-TECH-OPER-3.4	✓	Subsection 7.3.2
SRV-TECH-OPER-1.5	✗	
SRV-TECH-OPER-1.6	✗	
SRV-TECH-OPER-1.7	*	
SRV-TECH-OPER-2.3	✓	Subsection 7.4.2

8

Life Support

The first subsystem related to the capsule that has been designed is Life Support, with the goal of keeping the crew well and alive during nominal and non-nominal missions. Section 8.1 first lays out the requirement and inputs of this subsystem. Section 8.2 then presents the architecture of the Life Support that the capsule will be equipped with. From this architecture, the atmospheric control, food and water supply, wast management, thermal control, and radiation shielding have been investigated, in Section 8.3 to Section 8.8. Finally, the requirements of this subsystem have been verified, and the sensitivity of the design to the inputs assessed, in Section 8.9.

8.1. Requirements and Inputs

The following requirements concern the Life Support system:

- **SRV-CONS-TECH-4**: [S] The vehicle shall be able to transport a crew of up to 6 persons.
- **SRV-TECH-PROD-1**: [S] 80 % of all consumables used by the vehicle shall be produced in-situ.
- **SRV-TECH-PROD-2**: [S] All parts that are not designed to survive the entire operational lifespan of the vehicle shall be producible in-situ.
- **SRV-CONS-TECH-2.6**: [T] The spacecraft shall be equipped with human life support system capable of sustaining all crew members for 7 sols.

In addition, multiple parameters influence the life support system. The most important ones being the number of crew members, and the mission duration,

8.2. Architecture

Figure 8.1 shows the global architecture of the life support system of Charon. This life support is exclusively related to the capsule of the vehicle, as the full life support capacity is still required after abort. All of the subsystems described in this architecture diagram will be later described throughout this chapter.

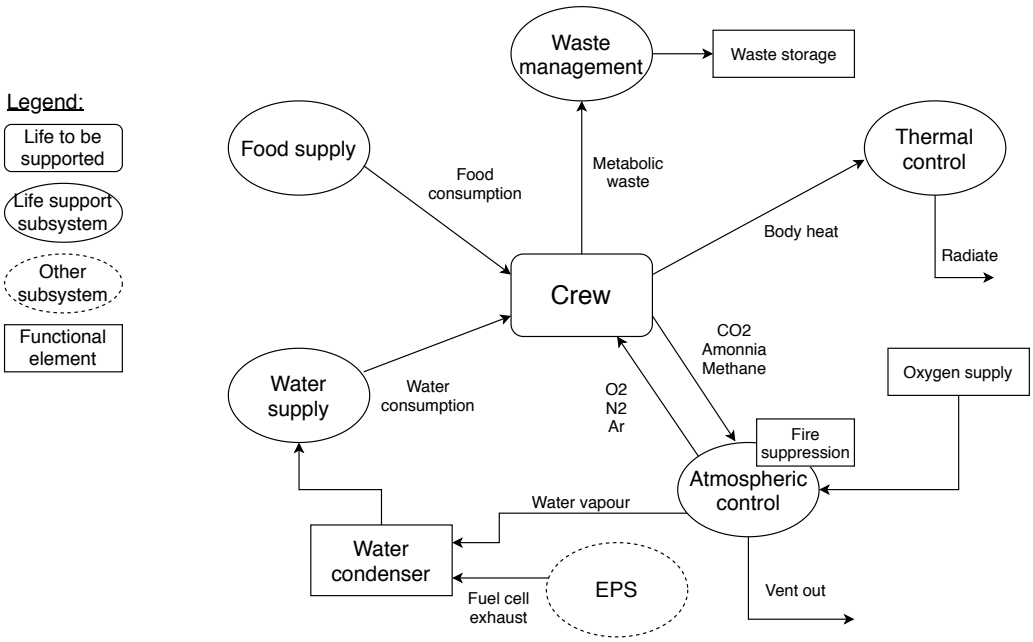

Figure 8.1: Life Support architecture

8.3. Atmospheric Control

It is of utmost importance to constantly control the atmosphere that the crew will be breathing in the capsule. As having a pure Oxygen atmosphere in the capsule would be hazardous, it has been decided to have a similar air composition as the one on Earth. This means that 21% of it shall be Oxygen, and the remaining 79% shall be an inert gas, with trace amounts of CO2.

The Atmospheric filtering system will be developed in Subsection 8.3.1. The method for the pre-launch setup of the atmosphere will be discussed in Subsection 8.3.2.

8.3.1. Filter

It is important to remove the excess CO2 from the capsule, as the crew would otherwise suffocate. In addition, toxic substances such as Ammonia (NH3) and Methane (CH4) also need to be removed from the air. To do so, a chemical filter using Lithium Hydroxide could be used, as it has often been for crewed missions lasting about a week.

However, such chemical filter would need to be changed after each flight, adding to maintenance, and requiring from the Martian base to be able to produce such filters. Physical molecular filtering is thus preferred, as it could be reused. This filter would use a mesoporous silica[38] with pore of 2 [nm] and could either be shipped from Earth, or produced on Mars, as Silica is available in vast quantities in-situ.

Figure 8.2 shows how such a filter operates. Air would come in the inlet of the filter system, and first go trough a dust filter, to catch the biggest particles. A pump is placed after this first filter, to move the air trough the filter system. Molecules smaller than 2 [nm], such as Oxygen (0.15 [nm]), Argon (0.188 [nm]), and Nitrogen (0.15 [nm]), would then go trough the mesoporous silica filter, while bigger molecules, such as CO2 (0.232 [nm]), Ammonia (0.33 [nm]), and Methane (0.38 [nm]), would get stuck in front of this molecular filter.

This filter operates following a dual cycle. First, the inlet and outlet valves open, to make air go trough it. After some time, these valves are closed, and the vent out valve is open, to allow for the bigger toxic molecules stuck in front of the mesoporous silica filter to vent out of the vehicle. Then, the vent out valve would close, and the first cycle would begin again. To ensure the crew safety, an additional safety valve will be present before the vent out one, to prevent air from escaping the capsule unintentionally.

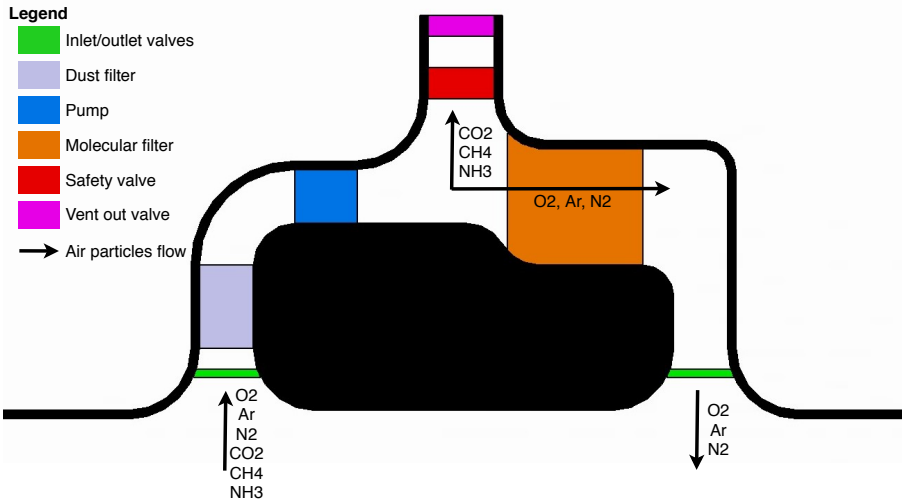

Figure 8.2: Atmospheric filter system

The capsule contains two of these molecular filters, for redundancy, but also so that venting out gases can be done symmetrically under nominal conditions, to avoid changing the attitude of the capsule.

The filter system also has to contain a smoke detection sensor. In case of fire, the crew would thus be urged to get into their spacesuits, if they are not already in it. After this, one crew member would use a CO2 extinguisher to put the fire out. If that does not succeed, the vent out valves and safety

valves would fully open, to completely depressurise the capsule, preventing any fire from developing any further.

Finally, in addition to the molecular filter, a water condenser is needed, to prevent the capsule from having its air saturated with water. A circuit of cooling fluid and a pump is thus needed. This water condenser will be integrated into the capsule cooling system, as further developed in Section 8.6.

8.3.2. Setup

Now that the capsule has a way to filter the atmosphere, it has to have a way to setup this atmosphere. As the crew is going to enter the capsule on Mars, it will be filled with the Martian atmosphere.

One way to pressurise the capsule to 1 [atm] would be by filling it with 21% Oxygen, and 79% Nitrogen, both contained in tanks, and progressively vent out the Martian air. However, it is possible to reduce the amount of Nitrogen necessary, by instead using the Nitrogen and Argon present in the Martian atmosphere.

The crew would thus close the capsule and, while they go trough the launch setup during about an hour, the pressurisation would pump the Martian atmosphere in, keep the Aron and Nitrogen in, and vent the CO2 out of it using the filter. Once the capsule is pressurised at about 0.8 [atm], the Oxygen tank would then fill the capsule until 21% of its air is Oxygen. The final atmosphere in the capsule would thus be of 21% Oxygen, 39.5% Argon, and 39.5% Nitrogen.

This means that $21\% \cdot V_{\text{capsule}} = 7.35$ [m^3] of Oxygen need to be in a tank for the atmospheric setup. In addition, according to [39], an average person breathes about 585 [L/day]. Since there will be a maximum crew count of 6, for a maximum duration of 7 sols, 24.5 [m^3] of Oxygen is needed.

8.3.3. Tank Sizing

With the total required volume of Oxygen known, the Oxygen tank can be sized. It has been decided to add a 30% margin to the Oxygen need, combined with an additional 15% margin for medical contingency. On top of this, a factor of 2 has been applied, and the Oxygen will be split in 3 different tanks. Because it will be stored at a typical pressure of 13 [MPa], at the capsule temperature of 20 [°C], 3 tanks of 3L are required [40].

To size the different tanks, a Python tool has been developed. Specifying the maximum stress allowed by the tank material σ_{max}, the tank pressure P, and the required tank volume V, it uses the hoop stress from Equation 8.1 to link the radius of the tank R and its thickness t. It also uses Equation 8.2 to link the tank radius and its length L. It then outputs a plot of different possible tanks, classified by their length over radius, and their respective masses. The user can then select the tank with the lowest mass, that still has a realistic length over radius for the given application. In the tool, a safety factor of 25% is applied by default on the thickness.

$$\sigma_{\text{max}} = \frac{P \cdot R}{t} \quad (8.1) \qquad V = \pi R^2 \cdot L + \frac{4}{3}\pi R^3 \quad (8.2) \qquad m = (2\pi R \cdot L \cdot t + 4\pi R^2 \cdot t) \cdot \rho \quad (8.3)$$

From the tool it came out that each of the 3 Oxygen tanks has a mass of 1.03 [kg]. With an Oxygen density at the given conditions of 1.43 [kg/m^3], all filled tanks thus have a combined mass of 76.3 [kg].

In addition to this, 3 [kg] are added to account for the Oxygen release system, as well as the connection of the seats to the Oxygen supply. This allows the crew to connect their spacesuit to the Oxygen supply during critical phases of the flight.

8.4. Food and Water Management

In addition to breathing, a second biological need of the crew during up to 7 sols of the mission is to eat and drink.

First, a crew member needs 1.77 [kg] of dry food per day, combined with 0.8 [kg] to hydrate it, according to [39]. Combining the need of the whole crew throughout the entire mission, and adding a margin of 50%, this adds up to 111.5 [kg] of dry food, and 50.4 [kg] of water.

Then, the need for water has been quantified. Following the numbers from NASA [39], an adult needs 1.62 [kg] of water per day. Adding the water needs of the whole crew for the complete mission,

and adding the same 50% margin, there is a need for 102 [kg] of water.

Thanks to the EPS described in Chapter 11, up to 300 [kg] of water will be produced in the capsule. Indeed, the hydrogen fuel cell will produce water vapour. Using a water condenser, the same as the one used to remove water vapour from the capsule atmosphere, part of this water will be condensed, to be drinkable.

The capsule will thus only contain 20 [kg] of water at lift-off. Three different water containers of 20 [L] will be taken inside the capsule: one filled with water as a reserve, one getting progressively filled by the EPS, and one for the crew to progressively drink.

Finally, in case of depressurisation, the spacesuit shall allow the crew to connect to the water supply, in addition to the Oxygen.

8.5. Human Metabolic Waste Management

The last biological need of the crew during the mission is to evacuate their metabolic waste. To do so, a toilet similar to the one of Soyuz will be placed in the capsule. This piece of equipment would take a volume of 16 [L], and have a mass of 80 [kg], according to [41].

As an average human has a stool mass of 0.125 [kg], as investigated in [42], the waste management system shall be able to put a total amount of faeces of 3.5 [kg] in individual air-tight bags. Similarly, the crew will produce a total amount of 68 [L] of urine. Similar containers of 20 [L] as the one used for water storage will be used, except for a clear visual distinction.

Mass-wise, this metabolic waste production is not an issue, as it will only be consumed food and water provisions. It will thus not add any mass to the capsule. Finally, if the capsule was to depressurise, the crew shall always be equipped with diapers in their spacesuits. According to a study from NASA [43], a human could stay in specialised diapers for up to 6 days. The total mission, in case of abort, could last up to 7 sols, so this is deemed acceptable.

8.6. Thermal Control

In addition to the crew needs, it is important to keep the crew heated at a comfortable temperature of about 20°C. To achieve this, the capsule will be thermally insulated by a foil similar to Coolcat 2 Ni from Ruag [44]. This would limit the heat flux of the capsule to 3.4 [W/m^2]. The insulated section of the capsule having a surface area of 45 [m^2], this means that the capsule will lose 153 [W] of heat continuously.

A human produces 100-120 [W] of power[1]. As the crew count is between 3 and 6, there is a need to cool the capsule down due to the excess of 247 to 567 [W] of heat produced. A system of cooling that will carry the heat from the capsule to a radiator, and then radiate that heat away, thus has to be added to the capsule. This same system will also carry the extra heat produced by the fuel cell of the capsule. This produced heat could also be used in case the crew count is even lower than 4.

8.7. Radiation Shield

Finally, the last life support subsystem that was evaluated was the need for radiation shield. However, as the mission would last at most 7 sols, there is no need for such shield. Indeed, according to the Ames Research Center [45], radiation shield is recommended for a mission of more than 30 days.

In conclusion, while radiation shielding will be important on the Mars base and at the station in orbit, none is needed for the capsule.

8.8. Risk Analysis

The following risks have been analysed and mitigated as part of the Life Support subsystem:

- **SRV-RISK-LS-1** Oxygen supply failure (P=2), no more oxygen supplied to the capsule (I=5).
  - Probability mitigation (P-1): have 3 separate overdesigned tanks for oxygen.
  - Impact mitigation (I-2): have the combinations able to directly connect to the supply.
- **SRV-RISK-LS-2** Capsule fire (P=1), results in capsule atmosphere filled with co2 (I=3).

[1]Human Body Heat as a Source for Thermoelectric Energy Generation, `http://large.stanford.edu/courses/2016/ph240/stevens1/`, accessed on 2nd June 2020

  - Impact mitigation (I-2): have a 100% safety margin in oxygen supply.
- **SRV-RISK-LS-3** Vent out valve stuck in open position (P=2), results in loss of atmospheric filtering, possible depressurisation (I=3).
  - Probability mitigation (P-1): add a second safety valve.
  - Impact mitigation (I-1): duplicate the atmospheric filter.
- **SRV-RISK-LS-4** Fuel cells failure (P=2), results in no more water produced (I=5).
  - Probability mitigation (P-1): duplicate the fuel cells.
  - Impact mitigation (I-2): already take 20% of the required water in the capsule.
- **SRV-RISK-LS-5** Capsule radiator failure (P=2), results in crew overheating (I=5).
  - Probability mitigation (P-1): duplicate the number of radiators.
  - Impact mitigation (I-2): isolate the fuel cells from the crew volume.
- **SRV-RISK-LS-6** Waste management failure (P=1), results in toxic vapours (NH_3, CH_4) (I=3).
  - Impact mitigation (I-1): provide hermetic bags in addition to the toilet.

From this list, a mitigated risk map has been created, and can be seen in Table 8.1.

Table 8.1: Risk map of the Life Support subsystem, after mitigation

	Very unlikely (1)	Unlikely (2)	Possible (3)	Likely (4)	Very likely (5)
Very high impact (5)					
High impact (4)					
Medium impact (3)	1, 4, 5				
Low impact (2)	3, 6				
Very Low impact (1)	2				

It can be seen in Table 8.1 that all risks are in the green zone of the map. This can be explained by the fact that all critical subsystems of life support have been duplicated or even triplicated. This is because Life Support is essential to the survival of the crew, thus all risks have been lowered to their minimums, even when that meant reducing the performance of the vehicle by adding mass.

8.9. Requirement Compliance and Sensitivity Analysis

With the Life Support system designed, its compliance with its requirements can be assessed.

Table 8.2: Requirement compliance for Life Support

Requirement	Completion	Explanation
SRV-CONS-TECH-4	✓	Sized for crew of 6
SRV-TECH-PROD-1	✓	Designed for complete production on Mars possible
SRV-TECH-PROD-2	✓	Filter designed to be changeable
SRV-CONS-TECH-2.6	✓	Sized for 4 sols of nominal + 3 non-nominal mission

The Life Support design is linearly related to its inputs for water, food, and oxygen supplies. Indeed, adding more crew or increasing the mission duration will linearly increase the supplies quantity. In addition, the crew number directly influence the amount of thermal shielding needed, as the capsule would require to be designed with more volume, and more shielding. However, this parameter does not influence the capsule mass significantly. The waste management system is a constant, as it will not be resized even if the crew count increases. Finally, the atmospheric filters are only to be resized slightly if the crew count is increased. This would also not change the capsule mass significantly.

9

Main Engine Design and Control

In this chapter, the preliminary design of the main propulsion system for Charon will be discussed. At the high level, the propulsion system opted to use bi propellant liquid rocket engines with Bell nozzles given the large body of experience with the technology. This chapter, while being only a preliminary design, will seek to establish the core components of the rocket engine and address the propulsion system requirements as established in the baseline report [1]. The rocket engine has been codenamed 'Obol' after the Charon's coin.

9.1. Requirements

- **SRV-TECH-OPER-1.1**: [T] The propulsion system shall provide a total ΔV of 6200 [m/s].
- **SRV-CONS-TECH-2.4-B**: [T] The burn program shall limit maximum linear accelerations to 4 g_0 during launch and reentry operations. *Originally stated as 3* g_0
- **SRV-TECH-OPER-1.2**: [T] The propulsion system shall have a minimum thrust-to-weight ratio of 1.5 relative to Martian gravitational acceleration at maximum mass.
- **SRV-CONS-TECH-5.2.1**: [T] The main engine(s) shall be able to operate continuously for 6 minutes before nominal refurbishment.
- **SRV-CONS-TECH-5.2.2**: [T] The propulsion system shall not require disassembly for nominal refurbishment.
- **SRV-CONS-TECH-5.4.1**: [T] The main propulsion system shall be dismountable.
- **SRV-CONS-TECH-5.4.2**: [T] All major components of the feed system shall be replaceable.
- **SRV-TECH-PROD-1.1**: [S] The propellants for propulsion system shall be generated in-situ.
- **SRV-TECH-OPER-3.1**: [F] The engine(s) used for propulsive landing shall be throttleable between 10% to 100% of nominal thrust.
- **SRV-TECH-OPER-3.2**: [F] The main engine(s) shall be able to fully shut off within 0.5 [s]. [46]
- **SRV-TECH-OPER-3.3**: [F] The main engine(s) shall be fully restartable in flight.

9.2. Analysis; Inputs, and Outputs

Table 9.1: The in- and outputs of the aerothermodynamics chapter

Analysis	Inputs	Outputs
Thrust sizing	Vehicle mass, max. acceleration, TWR, propellant selection	Combustion conditions, nozzle dimensions, thrust level
Cooling system	fuel selection, combustion conditions, fuel mass flow	Nozzle material, turbine inlet pressure
Turbomachinery	Chamber pressure, mass flow, turbine inlet pressure	Pump specific speeds, pump power

9.3. Engine Configuration

The propulsion system was first sized with relation to the number of engines and their arrangement at the bottom of the rocket. For high reliability, it was decided to have a redundant number of engines

that could throttle to compensate for various engine out scenarios. Furthermore, a symmetric engine arrangement allows for more responses to an engine out condition, such as preserving stability by cutting off the engine opposite of any failed engine. Thus it was decided to design for a 9 engine configuration with 2 engine out capability. The arrangement can be seen in Figure 16.3.

The current arrangement allows the 8 outer engines to gimbal outwards from the centre up to 10 [deg], while the centre engine can gimbal with a range of 19 [deg]. This led to a maximum exit area. Given the low ambient pressures of 915 [Pa] at the launch site, the engine will always be underexpanded. In order to maximise performance then, the exit area has to be at a maximum. Since Charon will be have to fit on an Earth-based launcher, which imposes constraints on the fuselage diameter, the nozzle exit diameter is set at 1.03 [m] as it is approximated from the thrust vectoring constraints .

9.4. Thrust Sizing

Key characteristics of the engine needed to be chosen in order to complete the detailed design. The bi propellant liquid nature of the engine was decided already in the Midterm, with the main drivers being reliability and maintainability on Mars. Furthermore, a closed expander cycle was chosen for the engine given its relative simplicity to other cycle options, and for its high reliability. For example the closed expander cycle RL-10 LOX/H2 engine has a failure rate under 0.0025. Furthermore, there is less wear on the turbine given that the working gas has not been combusted and is at a lower temperature. The upper bound of thrust for a closed expander cycle engine is around 800 [kN] as larger chambers have proportionally less heat-loss to the cooling jacket in comparison to the required turbine power.

Given requirement **SRV-CONS-TECH-5.2.2**, the propellant mass and burn time were estimated recursively with iterative class II weight estimations and with the Tsiolkovsky rocket equation, using an initial guess of the Isp.

Another crucial parameter for thrust sizing is the thrust to weight ratio ψ_0 (TWR), which was taken from **SRV-CONS-TECH-2.4**, using Equation 9.1.

$$\psi_0 < \frac{1}{\Lambda}\left(\frac{(a_e)_{\max}}{g_{\text{Mars}}} + 1\right) \tag{9.1}$$

Where Λ is the mass fraction and $(a_e)_{max}$ is the maximum linear acceleration of the rocket as limited by **SRV-CONS-TECH-2.4**, taken as $4g_0$. This results in a TWR of 2.08. With a MTOW of 200800 [kg], the max. total thrust delivered by the propulsion system should be 1544 [kN] while the maximum thrust per engine should be 310 [kN].

A thrust sizing program is used to determine the engine size and performance characteristics, whose final values can be seen in Section 9.9. The program relies on the assumption that the flow of the exhaust gas is one-dimensional and isentropic.

The thrust level and mass flow rate were determined as described, while the exit area was limited by the engine arrangement. Furthermore, combustion temperature was set at 3424 [K] and taken from RPA [47]. The chamber pressure was set at multiple values, but a final choice of 20 [MPa] was made. The specific heat ratio was set to vary linearly from 1.17 at the injector to 1.12 at the exit. The molar mass of exhaust gasses is assumed to be 22 [g/mol], taken from RPA.

Establishing the conditions at nozzle exit first requires an understanding of the conditions and dimensions at the nozzle throat. These can be calculated using the conditions at the combustion chamber and the gas specific heat ratio.

9.5. Nozzle Sizing

For the preliminary sizing of the nozzle, the main inputs are the dimensions of the throat, found in Section 9.4, and the expansion ratio of the Obol engine, which was found to be 15. The converging section is composed of two straight contour segments and two arcs, while the diverging section is composed of a slight arc and a Bézier curve. With the contour defined, the nozzle must be sized for structural integrity. The hoop stress from the exhaust gas pressure was calculated at the cross section for each 1 [mm] station along the nozzle, and from this the minimum required thickness was

taken. The material for the outer wall of the nozzle was chosen in Section 9.6 by assessing various material performances for the inner wall. Choosing the same material for the inner and outer chamber walls allows for 3D printing of the nozzle and minimal material waste, important for production and refurbishment when on Mars.

9.6. Cooling System

The adiabatic flame temperature of the methane-oxygen reaction reaches just below 3500 [K] inside the combustion chamber at max. thrust conditions with 200 [bar] chamber pressure. After the throat, the gas temperature decreases as the flow expands. The critical regime of the nozzle is between the injector and the throat where the gas temperature is very high and the surface area of the inner wall is at its smallest.

The Obol engine opted for regenerative cooling as a baseline assumption, similar to the RL-10, RS-25, Merlin, and Raptor engines. Based on a thermodynamic analysis of the cooling effect, further cooling applications may be considered.

Inner wall materials

Before an analysis can be done, a material for the inner chamber must be specified. The choice of material requires that the maximum adiabatic wall temperature with cooling could be kept below a certain threshold, beyond which a given material would lose strength significantly. The two materials considered were Aluminium 2024-T4 with $T_{aw_{max}} = 450$ [K] [48], and Copper-0.65Cr-0.08Zr with $T_{aw_{max}} = 800$ [K] [49]. These temperatures affect the dimensions of the cooling channels, while other properties of the material affect the dimensions of the nozzle itself. Important here is both the Young's Modulus and the Yield Stress of the material. The critical loads considered are buckling due to coolant pressure inside the channels and failure due to the hoop stress from the gas pressure.

The critical buckling stress due to coolant pressure was found from [50] to be the minimum between:

$$\sigma_{2_{\text{buckling}}} = \frac{\pi^2}{3}\left(\frac{\mathrm{t}_i}{w_c + t_r}\right)^2 \mathrm{E}_i, \quad \sigma_{\text{compressive}} \tag{9.2}$$

Meanwhile, the hoop stress resulting from the difference in chamber pressure and coolant pressure must be taken into account:

$$\sigma_{yield} \geq \sigma = \frac{\Delta p}{R t_i} \tag{9.3}$$

For both the buckling and hoop stresses, the maximum value occurs at the nozzle exit, whereas the regimes of highest temperature requiring the most cooling, the throat and combustion chamber, will experience smaller stresses. Thus the thickness of the inner wall should be tapered from exit to injector face in order to save mass on the nozzle. Furthermore, it should be noted that both of these stress estimations are conservative as the contribution of the ribs between cooling channels is not taken into account.

9.6.1. Regenerative cooling

With regenerative cooling, liquid methane is used to cool the inner wall of the chamber. It is chosen due to its availability on board as a main propellant, and because it does not have the risk of oxidising the chamber material, unlike the liquid oxygen. The coolant is injected into the cooling channels from an annular manifold at the rim of the combustion chamber injector. A program was made based on the OMECA program by Luka Denies [51] to analyse the wall temperatures along the nozzle contour. If wall temperatures are too high, it was decided to implement film cooling within the nozzle by injecting liquid methane into the combustion chamber. As expected, wall temperatures peaked at 1500 [K] at the throat of the nozzle, and were similarly high in the combustion chamber. Regenerative cooling would be insufficient to keep either Aluminium or Copper below the required temperatures.

9.6.2. Film cooling

The feasible alternatives to reduce the wall temperature even with regenerative cooling all entail a significant decrease in performance: sufficiently decreasing the chamber pressure, reducing the OF.

The last alternative that meets the minimum TRL of 4 is film cooling, whereby a gas or liquid is injected into the nozzle, forming a film between the exhaust gasses and the wall. This reduces heat flux to the wall material greatly.

Liquid methane is used as opposed to a gaseous film coolant, as it is the more efficient coolant. As only the combustion chamber and converging section must be cooled, the film coolant can be injected through a single manifold at the injector face.

It was determined through variation of the aforementioned program that the adiabatic wall temperature must be reduced to approximately 2200 [K] in order for regenerative cooling to reduce the wall temperature below 800 [K], and 800 [K] to reduce it below 450 [K].

The efficiency of the film in reducing heat flux to the wall is given as [52]:

$$\eta = \frac{T_{aw} - T_{cc}}{T_2 - T_{cc}} \tag{9.4}$$

To reduce $T_{aw_{max}}$ to 2200 [K] requires an efficiency of 0.36, while reducing it to 800 [K] requires 0.79. For a similar sized engine with 120 [bar] combustion chamber, it has been found experimentally that a gaseous hydrogen film will attain an efficiency of 3.6 with a blowing rate of about 3, where the blowing rate is the ratio of film coolant mass velocity to the mass velocity of the exhaust gas [53]:

$$M = \frac{(\rho u)_2}{(\rho u)_{\text{cc}}} \tag{9.5}$$

Whereas liquid methane is much denser than gaseous hydrogen, and is injected at cryogenic temperatures, it is estimated to be a much more efficient coolant, and thus the required blowing rate was given the conservative estimation of 2.

At this stage, it was apparent that the blowing rate required to cool an Aluminium wall below 800 [K] would be infeasibly large. Thus, the inner wall, and outer wall, will be constructed of the Copper alloy.

Such a blowing rate translates into 3.5 [tons] of methane throughout the flight, which is a 2% increase in propellant mass and a 1% decrease in Isp, to 371 [s]. Running the aforementioned thrust sizing and cooling programs again, the addition of such a film cooling system has no significant effect on performance or vehicle mass.

9.7. Feed System

With the closed expander cycle chosen for Obol, the feed system can be designed. Due to the nature of the cycle, the feed system will be less complex compared to engines with other cycles; specifically, the total length of plumbing lines and number of valves will be lower. Figure 9.1 gives an overview schematic of Obol. The fuel and oxidiser pumps are powered by a single turbine, whose working fluid is the methane coolant that becomes gaseous after exiting the cooling system.

Throttling is possible by reducing the pump speed and thus decreasing the mass flow. This keeps the specific speed low enough, while increasing the total pressure difference. Thus, the chamber pressure can be kept constant, and the extra pressure difference from the pumps can compensate for the great pressure loss at the injector.

Injector

Because the methane will be gaseous when injected into the combustion chamber, it was chosen to use an array of coaxial hollow post injectors. This is commonly used when one propellant is gaseous while the other is liquid, as it results in good mixing of the propellants and entrainment of the oxygen in the methane flow.

When throttling, the mass flow through the injector decreases, which increases the pressure loss. Because of this, it is proposed to have multiple concentric injector manifolds, at least 2, so that the mass flow for any single injector element can be kept sufficiently high. As can be seen in Figure 9.1, the LOX pump and turbine exhaust are designed for an exit pressure 100 [bar] greater than the chamber pressure, to allow for some variation in injector pressure loss when throttling.

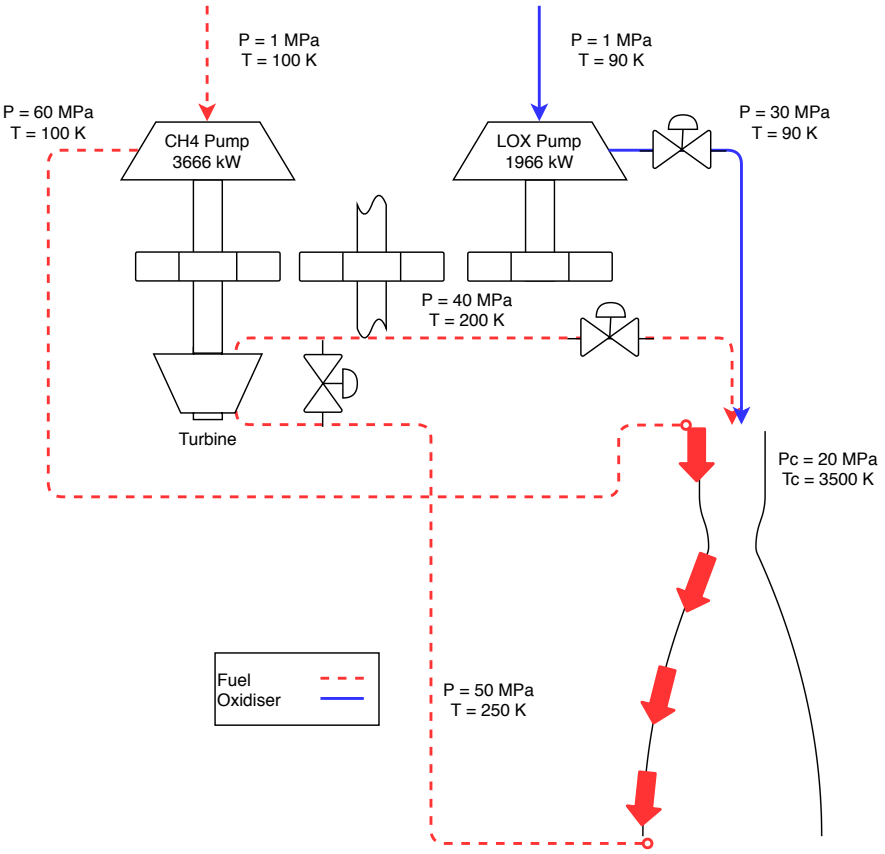

Figure 9.1: Closed expander engine schematic for Obol

9.8. Thrust Vectoring and Control

The thrust vector control (TVC) system of Charon controls the 9 engines during nominal flight, 3 engines during reentry, and the 5 engines in the case of max. engine out condition. The 8 outer engines are hinged with the hinge line perpendicular to the radius from the central engine, and the center engine is itself on the X axis, so there is no roll control capability from the TVC. Only pitch and yaw can be affected by gimballing and hinging of the engines.

For maintenance and refurbishment, it is important for the engine to be dismountable and modular in its mounting. Thus all engines, with turbomachinery included, shall be mountable on either a hinge joint or a gimbal bearing.

Hinges and Actuator

As mentioned, the 8 outer engines will be connected to the thrust structure by a hinge whose axis tangential on the circle from the central engine where the outer engines sit. The engine is rotated using a linear actuator with water as the hydraulic fluid, whereas recent technological progress for fusion reactors has developed water hydraulic actuators on par with oil hydraulic actuators [54]. The main concern here is the power supply for hydraulic fluid pressurisation and heating of the actuator to keep the fluid temperature above 273 [K]. Both of these will be supplied by tapping off the turbine exhaust through a flexible hose. The pressure loss resulting from this heating is expected to be negligible.

Gimbal Bearing and Actuator

The central engine gimbal is more complex, but is not unlike the mechanism used for the Saturn V F-1 and the Falcon 9 Merlin engines. A dual axis bearing will be fixed to the thrust structure, and each engine will have its joining mechanism at the top, above the hinge joining mechanism. This ensures that the central engine exit will be lower than the outer engines, which is advantageous for manoeuvring during the landing burn.

Gimballing of the engine will require two linear actuators, attached at locations that are $90\,\mathrm{deg}$

apart measured from the central axis of the nozzle.

9.9. Performance and Dimensions

Table 9.2 shows the engine parameters.

Table 9.2: Engine parameters

Parameter	Unit	Value (full thrust)	Parameter	Unit	Value
Thrust	kN	310	Chamber area	m^2	0.112
Specific impulse	-	381	Throat area	m^2	0.00626
Chamber pressure	MPa	20	Exit area	m^2	0.877
Chamber temperature	K	3424	Ae/At	-	141
Exit Mach	-	5.00	Engine length	m	2.11
Exit pressure	MPa	23,500	Converging section length	m	0.448
			Diverging section length	m	1.17

9.10. Verification and Validation

For the analysis performed in Section 9.4 and Section 9.6 and the custom programs therein, verification was performed using unit tests, system tests, and sensitivity tests that proved the program worked and gave feasible outputs. For validation, the outcome of the code was compared to [47] and [51]. Both software are considered validated, and comparison between results have validated the programs created.

9.11. Risk Analysis

The following risks have been analysed and mitigated as part of the Propulsion subsystem:

- **SRV-RISK-PROP-1** Catastrophic engine failure (P=1), results in explosion, loss of all engines and vehicle (I=5).
  - Impact mitigation (I-1): responsive abort system, quick separation system from vehicle for engine eject.
- **SRV-RISK-PROP-2** Controlled failure (P=2), results in loss of thrust vectoring or throttleability (I=3).
  - Probability mitigation (P-1): rigorous inspections and lower complexity.
  - Impact mitigation (I-1): multiple engines.
- **SRV-RISK-PROP-3** Ignition failure (P=2), results in engine does not start, or takes too long to start (I=4).
  - Probability mitigation (P-1): robust igniter design, inspection and maintenance.
  - Impact mitigation (I-1): multiple engines.
- **SRV-RISK-PROP-4** Fluid leak (P=2), results in localised engine failure (I=3).
  - Probability mitigation (P-1): sensors, inspections, and maintenance.
  - Impact mitigation (I-1): multiple engines.
- **SRV-RISK-PROP-5** Fuel pump failure (P=3), results in failure of high pressure methane pump (I=3).
  - Probability mitigation (P-1): inspection, maintenance.
  - Impact mitigation (I-1): multiple engines.
- **SRV-RISK-PROP-6** Oxidise pump failure (P=2), results in failure of lower pressure lox pump (I=3).
  - Probability mitigation (P-1): inspection, maintenance.
  - Impact mitigation (I-1): multiple engines.
- **SRV-RISK-PROP-7** Turbine failure (P=3), results in no power to pumps (I=3).
  - Probability mitigation (P-1): inspection, maintenance.
  - Impact mitigation (I-1): multiple engines.

- **SRV-RISK-PROP-8** Gimbal bearing failure (P=2), results in main rocket mounting is destroyed, engine separates from vehicle (I=3).
  - Probability mitigation (P-1): inspection, maintenance.
  - Impact mitigation (I-1): multiple engines.
- **SRV-RISK-PROP-9** Combustion instability (P=2), results in an annoying to catastrophic effect (I=5).
  - Probability mitigation (P-1): testing, inspection, maintenance, damping.
  - Impact mitigation (I-2): multiple engines, quick separation system from vehicle for engine eject, abort system.

From this list, a mitigated risk map has been created. It can be seen in Table 9.3.

Table 9.3: Risk map of the Propulsion subsystem, after mitigation

	Very unlikely (1)	Unlikely (2)	Possible (3)	Likely (4)	Very likely (5)
Very high impact (5)					
High impact (4)	1				
Medium impact (3)	3, 9				
Low impact (2)	2, 4, 6, 8	5, 7			
Very Low impact (1)					

All of the risks presented above are for a single engine, while the propulsion subsystem has 9 engines. Thus, many of the risk impacts as shown in Table 9.3 are decreased given the multiple engine out capability.

9.12. Requirement Compliance

Table 9.4: Requirement compliance for propulsion

Requirement	Completion	Determination Location
SRV-TECH-OPER-1.1	✓	Section 9.4
SRV-CONS-TECH-2.4-B	✓	Section 9.4
SRV-TECH-OPER-1.2	✓	Section 9.4
SRV-CONS-TECH-5.2.1	✓	Section 9.4
SRV-CONS-TECH-5.2.2	*	To be investigated
SRV-CONS-TECH-5.4.1	✓	Section 9.8
SRV-CONS-TECH-5.4.2	*	To be investigated
SRV-TECH-PROD-1.1	✓	Section 15.6
SRV-TECH-OPER-3.1	✓	Section 9.7
SRV-TECH-OPER-3.2	*	To be investigated
SRV-TECH-OPER-3.3	*	To be investigated

Still to be verified are the requirements relating to the mounting of the engine, the feed system reliability, and the ignition system. The ignition system will have to be looked at in more depth, and in general the interface of the engine components will have to be mapped out. The interface design will determined whether requirements SRV-CONS-TECH-5.2.2, SRV-CONS-TECH-5.4.2, SRV-TECH-OPER-3.2 and SRV-TECH-OPER-3.3.

Regarding the sensitivity of the results obtained it was determined that the system was the most sensitive to changes in the propellant and dry mass of the vehicle, and the delta V requirements, as these are the core inputs to the thrust sizing program. Increases in vehicle mass require larger maximum thrust, resulting in an engine with a lower Isp. A low Isp means more propellant mass (derived from the delta V budget), and more vehicle mas, leading to a positive feedback loop. Thus above a certain threshold, the engine design is very sensitive to increases in the mass and delta V budgets.

10

Structures

With the astrodynamic and propulsion analysis performed, the structural analysis of the vehicle could start. Section 10.1 includes the requirements connected to the structure of the vehicle followed by the design loads and the worst case that the vehicle experiences during its mission in Section 10.3. The material choices and the initial vehicle layout and analysis are then presented in Section 10.4 and 10.5. Section 10.6 to 10.9 include the structural analysis performed for the various components of the vehicle, followed by the risk analysis and requirement compliance in Section 10.10 and 10.11.

10.1. Requirements

The structural analysis and the design of the different structural elements of Charon's vehicle had to be performed in such a way that the following requirements, as they were determined in previous phase of the design, were met:

- **SRV-CONS-TECH-2.1**: [T] The structure of the spacecraft shall withstand a sustained acceleration of 6 g in longitudinal direction.
- **SRV-CONS-TECH-2.2**: [T] The structure of the spacecraft shall withstand a sustained acceleration of 9 g in lateral direction.
- **SRV-CONS-TECH-2.3**: [T] The structure of the spacecraft shall have a natural frequency higher than 35 [Hz] in axial direction. [11]
- **SRV-CONS-TECH-2.4**: [T] The structure of the spacecraft shall have a natural frequency higher than 10 [Hz] in lateral direction. [11]
- **SRV-TECH-OPER-1.3**: [T] The aerodynamic structure needs to withstand a dynamic pressure of 1500 [Pa] [11].
- **SRV-CONS-NONT-3.1**: [T] The structure of the spacecraft shall make sure the spacecraft does not tip over due to winds up to 45 [m/s].
- **SRV-CONS-NONT-3.2**: [T] All mechanical components shall be able to withstand the impact of dust particles entering the spacecraft.
- **SRV-TECH-OPER-2.1**: [T] The structure of the spacecraft shall make sure the spacecraft does not tip over due to landing on inclined surfaces up to 10 degrees.
- **SRV-CONS-TECH-2.8**: [T] The structure of the spacecraft shall withstand impact of objects with <TBD> [J] of kinetic energy.

10.2. Analysis; Inputs and Outputs

Table 10.1 includes the required inputs and outputs of all the different analyses that are described in the next sections.

Table 10.1: Inputs and Outputs of the structural analyses

Analysis	**Input**	**Output**
General (Used in all analyses)	Material Properties	-
Loading cases	Mass distribution, loads	Design loads
Vehicle Layout	Mass distribution	MMOI & CG
Crew Compartments	Impulse & Sustained Accelerations	Injury Risk
Capsule Analysis	Loads	Dimensions, Mass
Docking Mechanism	Approach velocity & Mass	Performance, Dimensions
Tank Analysis	Loads, propellant volume & pressure	Mass, Dimensions
Skirt Analysis	Loads, subsystems dimensions	Mass, Available volume
Thrust structure	Engine numbers & dimensions	Mass, dimensions
Landing Legs	Vehicle mass and approach velocity	Mass, landing performance
Vibrational Analysis	Vehicle characteristics	Natural Frequency

10.3. Design and Input Loads

10.3.1. Critical Cases

Sizing of any structure components requires the design loads to be defined, otherwise it is not known if the structure is strong enough. Hence the loading conditions were identified and analysed, namely the launch from the surface of Mars and the location of maximum thrust during ascent.

Assuming the misalignment of two engines at the beginning of the launch of about 10 [deg], as it was determined in Chapter 9, a lateral component of the thrust is present. This lateral component creates a moment and, as a result, an angular acceleration around the centre of gravity of the vehicle. As a result, the loads acting on the vehicle are different compared to the case where no misalignment would exist, introducing of a moment and shear force to the structure.

Having those conditions defined, it was obtained from the ascent model that the maximum attainable thrust is equal to 175284 [kg], which is obtained at launch with the total wet mass, as presented in Chapter 17. From this, the loading diagrams could be created. To begin with, the exact mass distribution is needed as the forces change depending on the variation of mass. With the function for mass distribution known, the normal force diagram could be created using Equation 10.1 for the case of maximum thrust [55]. It can be seen in Figure 10.1.

$$A(x) = -T + D + a_x \sum_{X0}^{X} m_x \tag{10.1}$$

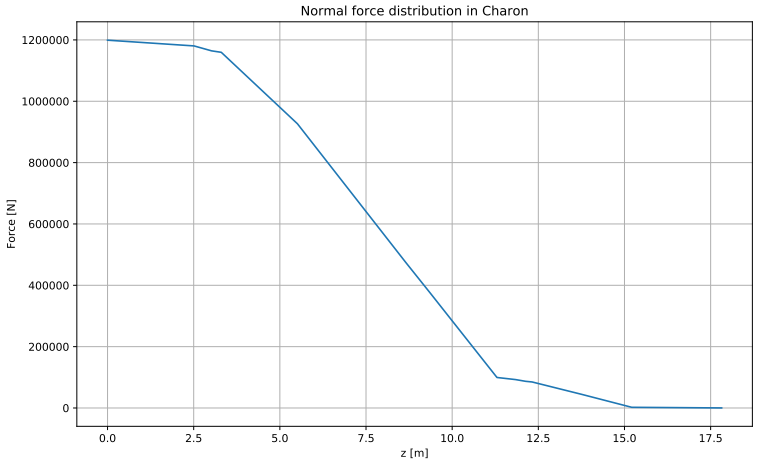

Figure 10.1: Normal force distribution in Charon at maximal thrust

Similarly, the moment acting on the structure can be obtained. In this case the vehicle has to have infinite stiffness, or it is needed to transform the problem to the static solution, disregarding dynamic loading [56]. With the first option being unrealistic, the second one is performed, using the angular acceleration from the thrust misalignment. Furthermore to account for the acceleration, fictitious forces were added by moving the coordinate system from the bottom of the vehicle to the c.g. location. In this reference frame Charon is experiencing the fictitious forces due to the accelerations. This means that the model is only working for one specific c.g. and as a result it has to be reevaluated different stages of flight. For this specific case it was decided to analyse only previously stated critical condition, using it to determine maximal stresses in the structure. To obtain those fictitious forces, Equations 10.2 and 10.3 were used [56].

$$dF^* = dM^* a_x = \frac{dM^*}{dz} a_x dz \quad with \quad a_x = \alpha * \left(z - z_{cog}\right) \tag{10.2}$$

$$\frac{dF^*}{dz} = q^*(z) = \frac{dM^*(z)}{dz} a_x(z) \quad then \quad \tau(z) = \int_0^z q^*(z) \left(z - z_{cog}\right) dz \tag{10.3}$$

With the moment acting along the z axis determined the shear force could also be obtained using that shear is the slope of the moment curve ($V = \frac{dM}{dz}$). The shear force is obtained using the central difference scheme. Doing so, Figure 10.2a and Figure 10.2b were obtained.

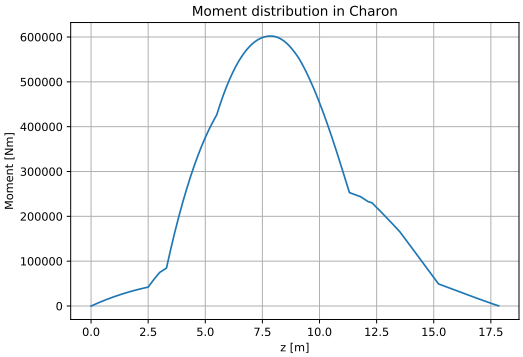

(a) Moment distribution

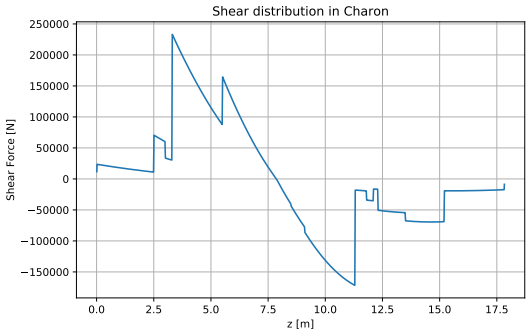

(b) Shear distribution

10.3.2. Launch Loads from Earth

To check the requirement for the launch loads during the transportation from Earth to Mars Equation 10.4 is used. In this expression the stresses exerted by the structure can be obtained. Taking the worst case scenario with vehicle partially fuelled and maximum values for accelerations it was discovered that stresses are above the limit. However it was already anticipated that vehicle that is optimised for Mars will be not strong enough to sustain the launching loads in Earth environment. If the vehicle would be designed for Earth loads, the whole mission would be very unsustainable, given all the extra non essential structural components. Hence, a supporting structure has to be used to decrease the induced stresses and safely launch Charon to Earth orbit. To transport one Charon to Mars, two SLS launches or launchers with similar capabilities have to be used. In this case total payload mass is equal to about 260 [t], which is more than a fully fuelled Charon. Thanks to this margin there is a spare performance for the supportive structure.

$$\sigma_{tot} = \frac{a_y MLc}{I} + \frac{a_x M}{A} \tag{10.4}$$

10.4. Material Selection

Before any structural analysis can be done, the material selection has to be performed. Normally the material could be chosen based purely on performance and perhaps cost. However, for this mission one of the driving requirements is that some components have to be producible on Mars surface, meaning that only materials available on Mars can be taken into account. Given the corrosion on Mars being an issue [57], the choice of material is of high importance. Advanced alloys are not considered as their production is difficult and energy intensive, requiring sophisticated infrastructure that will not be available on Mars. Considering these constraints, composites, titanium alloys, advanced ceramics and laminates can not be used as material for components producible in situ.

To achieve required performance, hence low structural mass the possible solution for material was narrowed down only to aluminium alloys. Based on the availability of metal ores in the Martian crust Aluminium 2024-T4 was chosen. In case of the tank design however, it was concluded that usage of graphite composite IM-7 is more suitable as the tank will be produced on Earth without the need for reproducibility [1] [58][59][60].

Table 10.2: Material Properties [61]

Property	Density	Elasticity Modulus	Shear Modulus	Poisson's ratio	Tensile strength
Symbol	ρ [kg/m^3]	E [GPa]	G [GPa]	ν [-]	σ [Mpa]
IM7-977 Carbon Epoxy Composite	1770	84.1	4.37	0.456	5300
Alum. Alloy-QQ-A-250/4	2740	73	28	0.33	312

[1] Aluminum 2024-T4; 2024-T351, http://asm.matweb.com/search/SpecificMaterial.asp?bassnum=MA2024T4, Accessed on the 6th of June 2020

10.5. Initial Vehicle Layout

Based on the Class II mass estimation performed in the previous phase of the design [2], the initial vehicle layout, such as initial dimensions, centre of gravity and MMOI, can be determined. With the different subsystems defined and a more detailed and accurate mass budget, the vehicle's dimensions and characteristics can be updated through an iterative process. After one iteration the following vehicle characteristics presented in Table 10.3, were determined and used for the design of Charon.

Table 10.3: Initial Vehicle Layout

Parameter	Value	Parameter	Value
Diameter [m]	6	No. Landing Legs	4
Length [m]	17.82	Capsule Length [m]	5.87
No. Engines	9	Oxidiser Tank Length [m]	8.45

10.5.1. Mass Moment of Inertia

With every subsystem sized after the first iteration the Mass Moment Of Inertia of the vehicle can be calculated. Together with MMOI, the centre of gravity is obtained for different stages of mission. Looking at Figure 10.3, one can notice six different stages of the vehicle's mission. They were chosen as they provide the necessary MMOIs for control and astrodynamics analysis.

In order to calculate the required MMOIs the vehicle was divided into simplified geometrical shapes, such as spheres and cylinders with certain mass assigned to them, as it was taken from the individual subsystems. Through this approach the calculations were simplified while the results remained realistic. Equations 10.5 to 10.10 were used for the determination of the MMOIs at different stages of the mission [62]. It can be observed that the trend of both the centre of gravity as well as that of the moments of inertia follow what was expected for a rocket in motion. With more fuel consumed the c.g. location is moving closer to the nose while at the same time the MMOI decreases. This verifies, to an extent, that the model used for the determination of those parameters is working correctly.

Configuration	Axis	MMOI wrt. Datum	MMOI wrt. C.G.	C.G. Location [m]
Fully fueled vehicle	Ixx	3013959,763	8530759,575	5,275876596
	Izz	898017,039	898017,039	
	Iyy	3013959,763	8530759,575	
Empty vehicle (no payload, no fuel)	Ixx	1503226,979	3752716,398	8,969527501
	Izz	344883,4005	344883,4005	
	Iyy	1503226,979	3752716,398	
Empty vehicle (no fuel)	Ixx	1565109,837	4053828,763	9,238266683
	Izz	374401,1792	374401,1792	
	Iyy	1565109,837	4053828,763	
Vehicle at 100 m	Ixx	3670884,578	8951886,095	5,310850335
	Izz	845561,3391	845561,3391	
	Iyy	3670884,578	8951886,095	
Vehicle at MAX fuel flow	Ixx	2404899,465	6799979,682	5,381694926
	Izz	803747,0872	803747,0872	
	Iyy	2404899,465	6799979,682	
Vehicle at the end of ascent	Ixx	2259398,968	4321654,768	6,120803919
	Izz	407613,6669	407613,6669	
	Iyy	2259398,968	4321654,768	
Vehicle at the orbital node (after the ascent)	Ixx	1693769,723	4124615,776	9,00731289
	Izz	433619,6909	433619,6909	
	Iyy	1693769,723	4124615,776	

$$I_{hollow_{sphere}} = \frac{2}{3}mr^2 \tag{10.5}$$

$$I_{solid_{sphere}} = \frac{1}{2}\rho\pi \int_{-R}^{z} (R^2 - z^2)^2 dz \tag{10.6}$$

$$I_{xx_{hemisphere}} = I_{yy_{hemisphere}} = \frac{2}{5}mr^2 \tag{10.7}$$

$$I_{zz_{hemisphere}} = \frac{83}{320}mr^2 \tag{10.8}$$

$$I_{xx_{Cylinder}} = I_{xx_{Cylinder}} = \frac{1}{2}mr^2 \tag{10.9}$$

$$I_{zz_{Cylinder}} = \frac{1}{12}mL^2 \tag{10.10}$$

Figure 10.3: Mass moment of inertia at different stages of the flight

10.6. Crew and Cargo Compartment

10.6.1. Allocated Volume

The design of the crew and cargo compartment begins with the determination of the required space needed to accommodate a crew of 6 for the whole duration of the mission. While designing the habitable environment for the crew one shall always take into account the different demands of launch, on-orbit operations, reentry, and recovery as well as the constraints given by the initial mass budget.

It is easily understood that the required pressurised volume and the free volume strongly depend on the number of crew members and the mission duration. The pressurised volume is the confined volume defined by the dimensions of the pressurised capsule while the free volume refers to space in which the crew can be mobile. Based on statistical data from other crew missions the following pressurised volume estimations are obtained, as they are presented in Figure 10.4. It can be observed that, for the case of Orion and Kliper, both being 6 crew missions, the allocated pressurised volume

is equal to about 30 to 40 [m^3]. For Charon the required pressurised volume for crew is 28 [m^3]

Similarly to the statistical relationships used for estimating the pressurised volume, u_p can also be correlated to the volume parameter ld^2 with l being the total length and d the maximum diameter of the capsule. Using Figure 10.4 it can be seen that pressurised volume is connected to the volume parameter with $u_p \sim k \cdot ld^2$, with k being in the range of 0.25 to 0.65. By using the above relationship an initial capsule layout can be determined so that further analysis can take place [63].

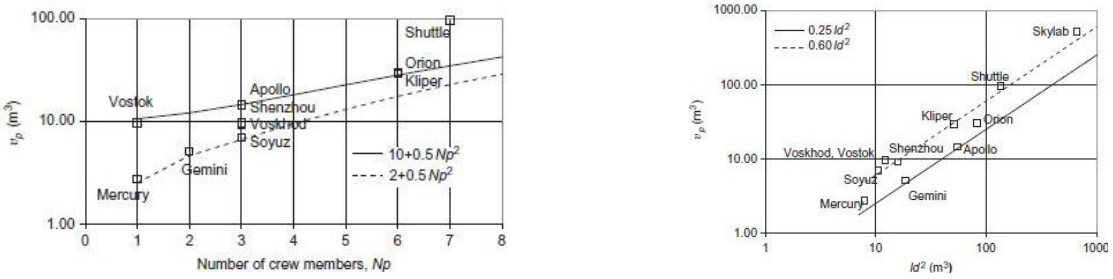

Figure 10.4: Empirical relationships between pressurised volume, crew members and volumetric coefficient [63]

From literature, it is obtained that the free volume of a spacecraft is about $40\% \pm 10\%$ of the pressurised volume. Given that the regular duration of Charon's mission is about 4 sols, with 3 additional sols in case of abort, the specific free volume per person is about 2 [m^3].

Finally, the required volume for 1000 [kg] cargo was estimated. It was decided that only pressurised volume would be used for the cargo on board Charon . To obtain the required volume, data from the resupplying vehicle of ISS, Cygnus[2], were used. Obtaining that the average mass of each resupply is about 2000 [kg] included in a pressurised volume of about 18,9 [m^3] it is determined that for a cargo of about 1000 [kg] the required pressurised volume should be equal to 9.8 [m^3]. It was chosen the cargo to be placed bellow the floor of the capsule and be accessible through another hatch at the floor. Using the fact that the bottom radius of the capsule is 2.3918 [m] in order to obtain the required cargo volume the floor would have to be raised about 0.61 [m] from the bottom of the capsule. The final pressurised volume for the capsule should be equal to about 38 [m^3].

10.6.2. Seat Layout and Design

The seat layout and design is mainly based on medical and operational/orthopometric factors. Medical considerations are acceleration exposure and intolerance concerns while operational are connected to the operability of the system and anthropometric factors.

Orthopometric Considerations

Given that Charon is going to be used as a regular transport vehicle for multiple people, the seats should be designed for a range of sizes of crew members. Generally,seats should accommodate from the 5^{th} percentile Japanese female to the 95^{th} percentile American male while more recent ones are able to support from the 1^st percentile American female to the 99^{th} percentile American male [64].The common dimensions used for seat sizing and the layout were ultimately taken from [63].

With Charon's dimensions it would be beneficial to consider either a stacked seat configuration, with three seats on top of each other or a configuration consisting of all of them on the same plane in such a way that the allowable volume can be used for the benefit of the crew. It is very important to space the seats based on torso depth and stage them according to buttocks to knee height. In order to account for the duration of the mission and for the case of emergency it was determined that seats along a row have a spacing equal to half the forearm-to-forearm distance and the two stacks to have a distance equal to about two times the buttock-to-knee length. With this spacing, modularity is achieved allowing removal of some system components in the case of a mission with less crew members. In order to fit the second seat configuration into the capsule given its dimensions it was also determined that it would be beneficial to have four of them on the same level and two of them below them at an angle of 15°. The spacing considered is half the distance from forearm-to-forearm.

[2]About the Northrop Grumman Cygnus, `https://www.nasa.gov/mission_pages/station/structure/elements/cygnus_about.html`, accessed on the 5th of June 2020

Acceleration Limits & BDRC

During the different phases of the mission of Charon the acceleration direction and magnitude change significantly, affecting the ability of the vehicles occupants to sustain the loads. In order for the occupants to be able to sustain higher loads for bigger amount of time it is of high importance to be able to alter the seat pitch, yaw and roll [65].

The limit on the tolerable acceleration is strongly dependant to the ability of the cardiovascular system to keep the blood flow constant while supplying all the vital organs. As a result the cardiovascular system is affected the most by the G-forces. Depending on the way that the acceleration is oriented along the body different effects are expected.

During sustained acceleration exposure it is important for the highest acceleration to be perpendicular to the chest of the occupants such that higher tolerance is achieved. However, apart from the sustained accelerations experienced during the flight the impulse accelerations should be considered while ensuring that limits set by NASA are not exceeded[66]. Those accelerations are considered to be the driving considerations for the design of the seats. Their analysis is assessed using the Multiaxial Dynamic Response Criteria or Brinkley Dynamic Response Criterion (BDRC). This is succeeded by firstly solving the ODE shown in Equation 10.11 for the displacement of the occupant under an impulse acceleration of A(t). Once the displacement is determined, the dynamic response can be obtained for each axis at time t, after which the injury risk $\beta(t)$ is obtained corresponding to Injury Risk Criterion using Equation 10.12 with the DR limits presented in Figure 10.5. If the IRC is bigger than one the above methodology is performed again, with the next highest DR limit from the table, up to the point that the IRC<1 [66]. Once this is achieved the obtained β corresponds to the risk level of the applied acceleration.

$$\ddot{\delta(t)} + 2\zeta\omega_n\dot{\delta(t)} + \omega_n^2\delta(t) = A(t) \tag{10.11}$$

$$\beta(t) = \sqrt{\left(\frac{DR_x(t)}{DR_x^{lim}}\right)^2 + \left(\frac{DR_y(t)}{DR_y^{lim}}\right)^2 + \left(\frac{DR_z(t)}{DR_z^{lim}}\right)^2} \quad where \quad DR(t) = \frac{\omega_n^2\delta(t)}{g} \tag{10.12}$$

Axis	Direction	Low (<0.5%)	Medium (0.5% to 5%)	High (5% to 50%)
X	Eyeballs out	$-28 \le DR_x < 0$	$-35 \le DR_x < -28$	$-46 \le DR_x < -35$
	Eyeballs in	$0 \le DR_x < 35$	$35 \le DR_x < 40$	$40 \le DR_x < 46$
Y	Eyeballs left	$-15 \le DR_Y < 0$	$-20 \le DR_Y < -15$	$-30 \le DR_Y < -20$
	Eyeballs right	$0 \le DR_Y < 15$	$15 \le DR_Y < 20$	$20 \le DR_Y < 30$
Z	Eyeballs up	$-13.4 \le DR_Z < 0$	$-16.5 \le DR_Z < -13.4$	$-20.4 \le DR_Z < -16.5$
	Eyeballs down	$0 \le DR_Z < 15.2$	$15.2 \le DR_Z < 18.0$	$18.0 \le DR_Z < 22.8$

Figure 10.5: Dynamic Response Limits for BDRC [66]

Using the fact that the maximum longitudinal and lateral acceleration experienced by the vehicle momentarily is equal to about 9.45 and 6 g_{earth} respectively, as it is obtained from Chapter 14 and the requirements, and obtaining the natural frequency and damping coefficient for the aforementioned seat design from [66], the IRC is equal to 1.0092 for a risk less than 0.5%. By re-applying the above-mentioned methodology, it is obtained to be 0.8649 for a medium risk (0.5%-5%).

Truss structure & Attenuation System

In both scenarios of the seat configurations considered an attenuation system is required to absorb the loads experienced by the crew due to the accelerations. This system shall be able to provide rotation and translation of the seat configuration in such a way that the highest acceleration is perpendicular to the chest of the seated person. By determining the allowed distance that the seats could move along the x,y and z axis and assuming that the attenuation system acts as a spring the total stiffness along each axis can be obtained through Equation 10.13.

$$K = \frac{F}{\delta} = \frac{m \cdot a}{\delta} \tag{10.13}$$

Allowing for less that 0.1 [m] along the x and y axis, the seats being able to rotate 45^o along those axes and the fact that the maximum longitudinal and lateral accelerations that the vehicle experiences during its nominal operations are 2.83 and 0.94 $g_{martian}$, from Chapter 4, it is obtained that the attenuation system shall have a total stiffness of 20.56 and 72.19 [kN/m] in the longitudinal and the lateral direction respectively.

10.6.3. Capsule Analysis

Several assumptions were used to simplify the capsule analysis while ensuring that the results are realistic and representative of the actual cases.

The capsule was analysed as a simple cone with dimensions constraint from the required allowable volume and the abort system considerations. This means that a base radius of 2.39 [m] , top radius of 1.4 [m] and a convex angle of 20 ° were used. At this phase of the design no stiffening elements were considered for the design of the structure, meaning that the results of the analysis show the minimum structural characteristics for a cone consisting of only the skin.

The loads applied correspond to the normal force, shear force and moment that are presented in Section 10.3 while at the same time an internal pressure of 1 [atm] is present in the capsule. Such a structure consisting of thin, curved isotropic sheet, whether or not it includes stiffening elements should be designed in such a way that buckling of the structure resulting in collapse or affecting its function does not occur. Equation 10.14 to Equation 10.16 show the critical axial force, moment and pressure under which buckling occurs at a conical shaped structure, with $\bar{\rho}$ indicating the average radius of curvature of the cone given by Equation 10.17. For each of the equations below the knockdown factor γ is assumed to be equal to 0.33, 0.41 and 0.75 as it is obtained from [67].

$$P_{crit} = \gamma \frac{2\pi E t^2 cos(\alpha)}{\sqrt{3(1-\nu^2)}} \quad (10.14) \qquad M_{crit} = \gamma \frac{\pi E t^2 r_1 cos(\alpha)^2}{\sqrt{3(1-\nu^2)}} \quad (10.15)$$

$$p_{crit} = \frac{0.92 E \gamma}{(\frac{L}{\bar{\rho}})(\frac{\bar{\rho}}{t})^{\frac{5}{2}}} \quad (10.16) \qquad \bar{\rho} = \frac{r_1 + r_2}{2cos(\alpha)} \quad (10.17)$$

By equating the critical loads to the actual applied loads with a safety factor of 1.5, so that buckling occurs at higher loads, the minimum thickness can be obtained.The shear flow in the structure and then the stresses can be determined. By doing so the maximum critical stress under which buckling occurs at the capsule is obtained to be 95 [MPa]. This value seems reasonable, given the fact that the structure is not stiffened. At the same time the shear flow induced to the structure as a result of the shear force acting on the vehicle can be obtained using Equation 10.18.

$$q = \frac{F \cdot Q}{I} \quad (10.18)$$

Once the total shear flow distribution in the structure is determined cutouts can be added to the structure to determine the total maximum shear flow and obtain the maximum stress. The hatch dimensions are chosen in such a way that would allow the transfer of cargo and crew while allowing the removal of seats in case of missions with smaller number of crew members. The driving parameter for the cutout dimensions is actually the width and the height (back to front of feet) of the seats. As a result the hatch was determined to have a width and height of 0.65 [m] respectively. At the same time a square window with sides of 0.2 [m] was also simulated, in order to determine the shear flow around each of the windows, in case they would be introduced to the structure.

To determine the shear flow around the cut-outs, the equilibrium of forces on small increments along the length was taken so that the shear flow within the cutout would be equal to 0. The locations around the cut-outs would likely be reinforced so that they would be able to sustain the new shear flow, while trying to keep it the same at the rest of the structure. Hence, only the locations around the cutouts were investigated. The diagrams presented in Figure 10.6, showing the stress distribution in the capsule without and with cutouts included, were created.

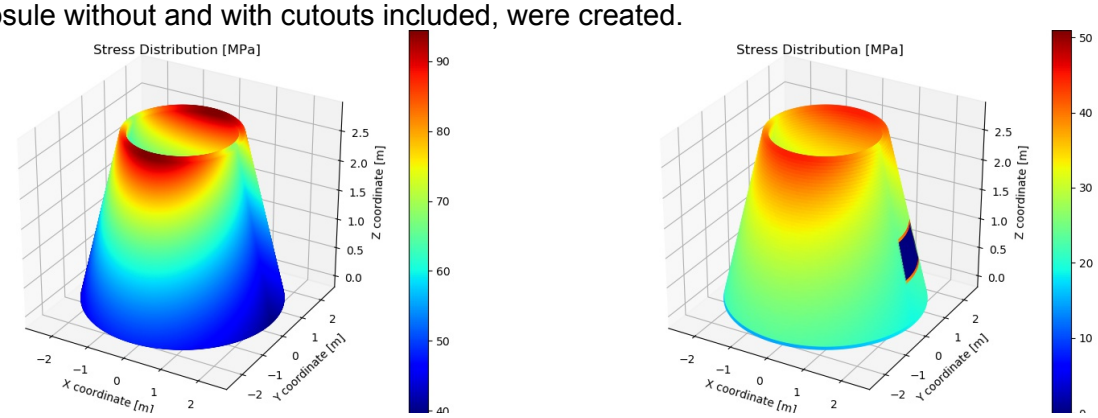

(a) Stress distribution in the capsule without cutouts (b) Actual stress distribution in capsule with cutouts

Figure 10.6: Stress distribution at the capsule

With the total stress on the structure determined whether or not the limit imposed by the maximum tensile and yield stress of the material is met can be checked. By designing the structure in such a way that the maximum stress in the final capsule structure is equal to the maximum allowable buckling stress ,which was determined to be equal to about 95 [MPa], reduced by a safety factor of 1.5 the required thickness of the structure can determined. Given that the cone was simply modelled without the existence of any stiffening elements it is then obtained that the required thickness of the skin should be equal to about 27.2 [mm]. However, as it is certain that in further phases of the design stiffening materials will be considered for the optimisation and reduction of mass of the structural component, a reduction factor will be applied to the obtained thickness in order to get a better estimate for the mass of the capsule at later phases of the design.

10.7. Docking Mechanism

Both the design and sizing of the docking and mating mechanism depends on the mission objectives and the conditions during the contact of the chaser and the target. The docking mechanism shall allow for transfer of crew and cargo. This means that a tunnel should be formed after successful capture so that a pressurised passage is present. In order to size the hatch, as a result of the required tunnel, one has to design it in such a way that an astronaut in his spacesuit is able to pass through it.

The designed docking mechanism has to be androgynous. This kind of design is really beneficial for the rescue of the vehicle and it provides a bigger operational flexibility. Furthermore, the reliability of the system increases as in case of failure of one of the sides the roles can be easily reversed.

A central design is dismissed as valuable tunnel volume is reduced due to the rod and the capture mechanism being in the way of the transfer tunnel even after capture. The central docking mechanism does not allow for an androgynous design. For that reason, only peripheral docking mechanisms are considered which allowing for androgynous design and better use of the transfer tunnel.

Finally, the docking mechanism will be located at the front of the capsule, protected by the thermal and aerodynamic loads during ascent and reentry by the nosecone and the aerodynamic shell. During docking and un-docking the nosecone shall be able to ”open” such that the docking mechanism is exposed and fully operational, so that all the required procedures can be performed optimally.

10.7.1. Considered Concepts

Given the aforementioned considerations, translated from the different requirements, two docking mechanisms are considered as applicable for Charon’s vehicle. Those concepts are the Apollo-Soyuz androgynous docking system [68] and the Androgynous Peripheral Docking System (APDS) [69]. Finally, the APDS design was chosen for Charon, given its reliability considering the number of missions it has been used for connection to the ISS.

Apollo-Soyuz Androgynous Docking System

This docking mechanism is considered the first attempt to design an androgynous docking mechanism to be used for the Apollo–Soyuz . Its functions are quite simple . Firstly, contact is achieved, using the flanks of the guiding pedals located on the outside of contact ring. The contact ring, used for the soft capture, is extended through six dampers around its circumference in a ”Stewart platform” arrangement, with an angular difference of 60^o, allowing that way six Degrees Of Freedom and ensuring that capture takes place [70]. Connection is achieved through capture latches-catches on the petals and the ring, which are engaged after contact and alignment .

Once capture is achieved the contact ring is retracted, through dampers and cables from each side. Once the soft capture ring is aligned with the hard capture ring they are structurally connected through 8 double-hook type latches. At the end seals along the circumference of the rings are used to ensure that there are no leaks and that pressure difference remains constant.

Androgynous Peripheral Docking System

The APDS function is pretty similar to the one of the Apollo-Soyuz docking system. Given its more improved design it was used for the docking of the Space Shuttle to the ISS. Contact between the chaser and target happens through the contact rings of each side and the three petals mounted on them. Between the contact ring and the docking ring a spring-damper system in ”Stewart platform” configuration is present. However,the petals of the ring point towards the centre creating that way the barriers of the transfer tunnel itself. Similarly to the previous design capture latches, engaging on a latch-catch, are mounted in the petals. The contact ring is also retracted in to the docking ring,

once capture is achieved, through the damper system. Finally, in contrast to the previous design 12 double-hook type structural latches are required as the seal diameter of the docking ring is bigger. In this design the connections for transfer of power,data and fluid are automatically [71].

10.7.2. Attenuation System

The movement of the system chaser- target, once the connection is achieved, can be calculated using the momentum law. Assuming that the orbital node is designed so that central impact/contact takes place with the chaser the total velocity of the system can be obtained using Equation 10.19.

$$V_{total} = \frac{m_a V_{a_0} + m_b V_{b_0}}{m_a + m_b} \tag{10.19}$$

During capture and docking the structure shall be able to sustain high loads for a short period of time. The forces introduced to the structure and the available time for capture can be adjusted by including a shock absorber. The travel after contact can be increased as part of the kinetic energy is absorbed by viscous damping or even friction.

In order to determine the required spring and damping coefficients the system can be simulated as a simplified model of central impact with a spring-damper system. The mass of the shock absorber system is assumed to be very small compared to the masses of Charon and the orbital node. Then the equation of motion is given by $F_x(t) = m\ddot{x} = -D\dot{x} - Cx \pm F_f$ with D being the damping coefficient, C the spring constant, and F_f the constant friction force. By disregarding the idea of friction braking due to its high risk, the equation of motion becomes, with a and b the mass of chaser and target :

$$\Delta\ddot{x} = -(D\dot{x} + Cx)\frac{1}{m_e} \quad where \quad m_e = \frac{m_a m_b}{m_a + m_b}$$

The following ways of reducing the kinetic energy of the system are considered:

Shock Attenuation by Spring

In this case the equation of motion simply becomes $m_e\ddot{x} = -Cx$ meaning that the solution is of the form of Equation 10.20.

$$x(t) = c_1 cos(\omega_1 t) + c2 sin(\omega_1 t) \quad with \quad \omega_1 = \sqrt{\frac{C}{m_e}} \quad , \quad c_1 = x_0, c_2 = \frac{u_0}{\omega_1} \tag{10.20}$$

Shock Attenuation by Dampers Only

In this case the equation of motion becomes $m_e\ddot{x} = -D\dot{x}$ for which the solution is as Equation 10.21.

$$x(t) - x_0 = \Delta x(t) = -\frac{m_e}{D} u_0 (e^{-\frac{D}{m_e}t} - 1) \tag{10.21}$$

Combination of Damping and Spring

Finally, for this case the equation of motions becomes $m_e\ddot{x} = -D\dot{x} - Cx \Rightarrow \ddot{x} + 2\delta\dot{x} + \omega_1^2 x = 0$ for which the solution is as Equations 10.22 and 10.23.

$$\Delta x(t) = e^{-\delta t}[\Delta x_0 + (u_0 + \delta\Delta x_0)t] \quad , \quad \Delta\dot{x}(t) = e^{-\delta t}[u_0 - (u_0 + \delta\Delta x_0)\delta t] \tag{10.22}$$

$$\Delta\ddot{x}(t) = \delta e^{-\delta t}[(u_0 + \delta\Delta x_0)\delta t - 2u_0 - \delta\Delta x_0] \tag{10.23}$$

Allowing for a maximum displacement of 1 [m] after contact with an approach velocity of about 0.0333 [m/s], a mass and moment of inertia of the orbital node being the same as the one of ISS and the mass of Charon equal to the vehicle's mass reaching the node the following graphs presented in Figure 10.7 were obtained for the linear displacement.

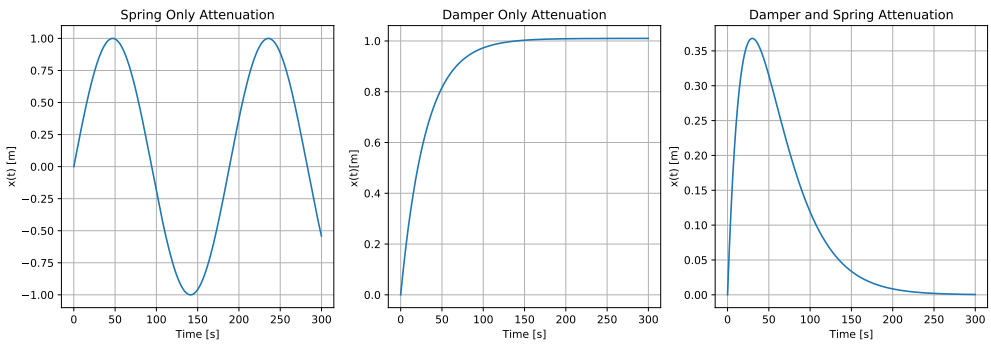

Figure 10.7: Travel after impact for spring only, damper only and combination of cases.

It can be observed that, for the case of a combination of spring and dampers, the maximum travel is about 0.37 [m] after 25-30 [s] while the whole system comes to a rest after about 250 [s] . It is also determined that the maximum absolute acceleration of the system is equal to about 0.00222 [m/s^2] resulting at a maximum force experienced at the beginning of the impact of $F_{\text{max}} = \Delta\ddot{x}m_e = 0.00222 \cdot 31788.56 \approx 70.64$ [N].

The method used for the above analysis was verified and validated using data from rendezvous and capture of re-supply vehicles to the ISS. Using a chaser with a mass of $10{\cdot}10^3$ [kg] and an approach velocity of 0.1 [m/s], similar results as the ones presented in [31] were obtained.

10.7.3. Connection

The structural components, such as the structural latches and seals required to ensure that the loads are transferred throughout the structure and that the connection is sealed should also be looked into.

Structural Latches

The structural latches present in the docking mechanism shall be able to sustain the loads introduced to the structure while providing the required strength and stiffness. The structural latches in the case of manned missions shall provide the compressive force required to ensure optimum function of the seals around the circumference of the docking ring. The total force to be carried by the structural latches can be determined using Equation 10.24 and is strongly related to the inner pressure and the diameter of the sealing ring.

$$F_p = pd^2\frac{\pi}{4} \tag{10.24}$$

As the inner pressure is about 1 [atm] , the diameter of the sealing ring is equal to about 1.2 [m] and diameter of the transfer tunnel is 800 [mm] [69], the total compressive force to be carried by the structural latches is equal to 114.6 [kN]. Furthermore,for a sealing ring with a diameter of 1.2 [m] the mechanism would require 12 structural latches with 12 more for redundancy [69]. This seems to follow the empirical rule, obtained from the different designs of docking mechanisms according to which an increase by a factor of n of the sealing diameter would result in an increase of n^2 to the number of the required structural latches given the same design.

Seals

The seals of the docking ring should be arranged so that the forces required from the latches to compress them are as low as possible. The sealing rings should be located at the smallest possible diameter of the docking ring. At the same time to increase the reliability of the system and make it redundant two concentric seal rings are used. By including a pressure measurement device the leak-tightness of the seals can be checked regularly .

Given the fact that grease and metallic seals are not that suitable choices for space a different kind of seal had to be considered. Such material, able to provide the required mechanical properties, is some synthetic elastomer. However, given this material's properties and the fact that they wear during long term exposure to space conditions it is of high importance to check it during the mission's duration [72].

10.8. Propulsive Stage

To fulfil the mission objective, the capsule has to be transported from the surface of Mars to the orbital node and back. It can achieve this as it is connected to the propulsive stage of the vehicle, where main propulsion, propellant and landing legs are placed. The design and analysis of the structural components of those elements will be presented in this section, starting from tanks going through skirts design and finishing with landing legs.

10.8.1. Propellant Tanks

Propellant tanks are the main structural elements of any launchers, and shape and size of almost every vehicle are determined around them. Hence in order to start analysis of propellant tanks, several decisions had to be made beforehand. Firstly it was decided that tanks will be used as a load carrying structure to optimise weight and performance consequently. It is a common practice in the industry as tanks on its own provide enough structure support and such a solution has most often the lowest weight, as it doesn't require separate structure to support the loads. However, such a decision requires a special care on the analysis of tanks to ensure that they won't fail under the subjected load, so not

only internal pressure has to be taken into account. Furthermore it was decided that vehicle L/D is equal to 3.2, similarly to reference vehicle such as: Hercules[5], Cobra [6] and Lockheed MADV[7]. Comparing this value to other current Earth launchers it may seem that this value is too low. However due to the Mars low density atmosphere, the highest advantage of the sleek vehicle, low drag is negligible and more chubby design is beneficial for landing and reentry. In order to keep the vehicle in this desired L/D ratio, the tanks were designed with elliptical caps, to decrease the overall length. According to the [63] most suitable value of semi-minor axis in this case is around 0.7R and the final value for this design was chosen to be 0.707. To even further decrease the length of the tanks, the common bulkhead design was chosen as seen in the Figure 10.8a. In this way oxidiser and fuel tanks are sharing one of the bulkheads, saving material and space. The main disadvantage of common bulkhead approach is the insulation issues but for this case both the oxidiser and fuel have similar temperature and extensive insulation is not necessary.

When the overall shape of the tank was determined, the actual analysis could start. Firstly the material was chosen ,in Section 10.4, as this determines the production approach and gives the constraint for stresses. According to the latest NASA research the composite tanks are 30 percent lighter than state of the art aluminium tanks, hence the IM7-977 carbon epoxy composite was chosen [61], similarly to other designs like the X-33 or Hercules [73]. As was mentioned before, usage of composite in the tank design can significantly decrease the overall structural mass and save propellant, decreasing in the same way pollution. As a reference design the proposal from Lockheed Martin was chosen from the same NASA studies. This choice was purely made due to usage of stiffeners as reinforcement, making the preliminary calculations more straightforward and more accurate, not requiring FEM analysis for example. Furthermore, the weight difference between other concepts from the study was negligible. Following this design concept the stiffeners shape was kept the same , as it can be seen in Figure 10.8b, made from the same material as the tank itself and with pi-preform attachment to the skin which provides stable and reliable connection [74]. The shape and dimensions of the end cups were adjusted to previously mentioned characteristics with a/b=0.707. To optimise the performance the following composite fibre layup was chosen: [45/90/90/-45/0/45/90/-45]s, taken from the X-33 tank design [73], as the material for both designs is the same. The design pressure was chosen to be 10 [bar], following the main engine design and mass of the propellant was determined in Chapter 17. With the above the tank parameters presented in Table 10.4 were determined.

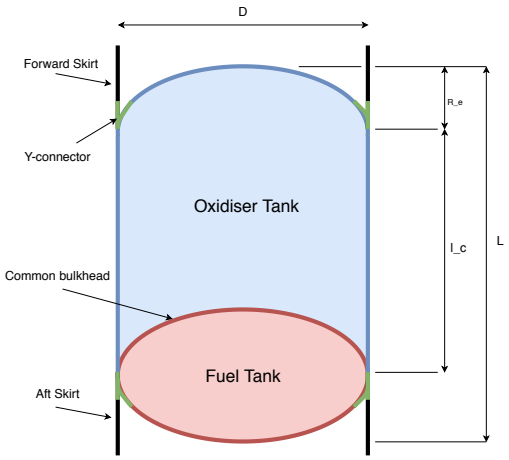

(a) Propellant Tank design

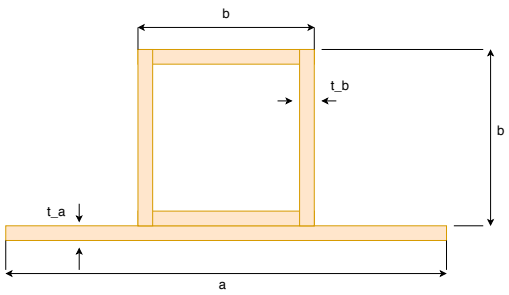

(b) Cross section of the tank stiffener

Figure 10.8: Tank layout

Table 10.4: Tank design parameters

Param.	Value [m]
h_w	1.121
l_c	4.243
D	6
b	0.021
t_b	0.003
t_a	0.001
a	0.01625
L	8.485

Forces Analysis

With the design characteristics defined, sizing of the tanks could start. Following the given equations the length of the cylindrical part could be determined, together with the thickness of the skin [63]. Then the actual volume of the tank material could be calculated and with the density of the material the mass could be obtained too. Furthermore, the critical stress was calculated from the equation Equation 10.28 and then the critical force that tank can sustain before it starts buckling.

$$v_w = 2\pi\left[R_c l_c t_c + R_c^2 t_d + \frac{1}{4}\frac{R_c^2 t_d}{e}\ln\left(\frac{1+e}{1-e}\right)\right] \quad (10.25) \qquad v_t = 2\left[\frac{2}{3}\pi R_c^2\,(0.707R_c)\right] + \pi R_c^2 l_c \quad (10.26)$$

$$t_d \approx \frac{1}{2}\frac{pR_e}{(\sigma_y/k_d)} \quad , \quad t_c = \frac{pR_c}{(\sigma_y/k_d)} \quad (10.27) \qquad \frac{\sigma_{crit}}{E} = 9\left(\frac{t}{R_c}\right)^{1.6} + 0.16\left(\frac{t}{L}\right)^{1.3} \quad (10.28)$$

$$F_{a,crit} = (\pi dt)\sigma_{crit} \quad (10.29) \qquad e = \sqrt{1-\frac{a^2}{b^2}} \quad (10.30) \qquad l_c = v_t/(\pi * R_c^2) \quad (10.31)$$

This analysis took only into account pressure force and necessary volume for the propellants. To completely analyse this structure the stresses caused by other forces has to be considered as well. Looking at the most critical conditions introduced in Section 10.3, the magnitude of the normal and shear force can be obtained, together with the moment force at exact location along the z-coordinate. The applied forces can be seen in Figure 10.10a with normal force acting through z-coordinate. To analyse stresses induced by shear and moment the idealisation method was chosen, in which stiffeners are sized as a point areas and to which the skin contribution is added following Equation 10.32 to 10.35 [75]. As a outcome of this the entire cross-section of the tank is simplified to point areas distributed around the circumference as in the Figure 10.10a. When the structure was idealised the mass moment of inertia of the cross section could be computed and later used to calculate normal stresses due to the moment and change in shear flow due to the applied shear force. The outcomes of those calculation can be seen in the plots Figure 10.9. However to determine the maximum stresses both load cases have to be combined using the Von-Mises stresses approach. Furthermore the normal force contribution was also added by dividing applied force by cross-section area. The final result is then presented in Figure 10.10b.

$$\sigma_z = \frac{\left(M_x I_{yy} - M_y I_{xy}\right)y + \left(M_y I_{xx} - M_x I_{xy}\right)x}{I_{xx}I_{yy} - I_{xy}^2} = \frac{M_x y}{I_{xx}} \quad (10.32)$$

$$\Delta q = -\left(\frac{V_y I_{yy} - V_x I_{xy}}{I_{xx}I_{yy} - I_{xy}^2}\right)B_r y - \left(\frac{V_x I_{xx} - V_y I_{xy}}{I_{xx}I_{yy} - I_{xy}^2}\right)B_r x = -\frac{V_y}{I_{xx}}B_r y \quad (10.33)$$

$$B_1 = \frac{t_{skin} b}{6}\left(2 + \frac{\sigma_2}{\sigma_1}\right) \quad (10.34) \qquad I_{xx} = \sum^{n} y_i^2 B_i \Rightarrow (I_{xx})_{B_r} = y_r^2 B_r \quad (10.35)$$

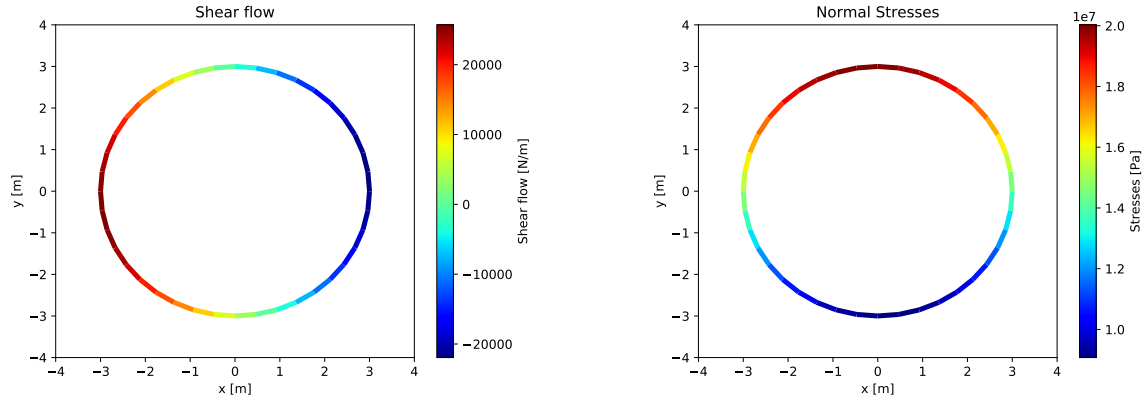

(a) Shear flow (b) Normal stresses

Figure 10.9: Shear flows and Normal stresses in the tank

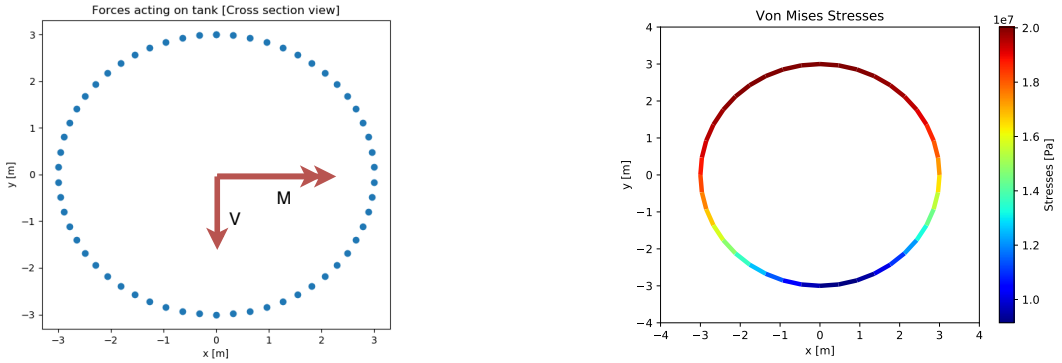

(a) Tank forces

(b) Von Misses stresses

Figure 10.10: Forces applied to the tank and final Von Misses stresses in the tank

Looking at the plots, the maximum stress value can be obtained. It is equal to 20 [MPa]. It is a very low number, however structural loads on Mars are very low in comparison to Earth conditions. Thrust levels, air resistance and gravity forces are all higher for Earth launchers. Furthermore this analysis consists of only Quasi-Static conditions and vibrational loading is omitted, which should be performed in later stages of the design to confirmed that loads are still within safety margin.

Buckling

Thin cylinder structures, like the tanks or skirts are most often failing due to the buckling [63], sometimes way before reaching the yield stress of the material. Hence reinforcements like stiffeners or rings are necessary to increase critical buckling load. Therefore, the magnitude of the critical buckling load has to be checked to be higher than the subjected load. To calculate the critical buckling load the semi-empirical relation was used [76], for which the critical stress for the bare skin can be computed using Equation 10.36, where K_c factor can be taken from the Figure 10.11. For this tank design r/t = 450 and Z= 170, hence the buckling constant used = 150. As it can be seen the critical buckling stress for skin alone is very low and tank would certainly fail without any reinforcements. Hence the stiffeners contribution has to be added by calculating firstly the the maximum crippling stress of singular stiffeners and then the combined crippling stress of stiffeners by cross-sectional area scaling. When this is done the w_e parameter has to be obtained as it provides the information about the effective width for which crippling load of the skin is increased by the presence of the stiffeners. Finally the total buckling load can be computed using Equation 10.41. [75]

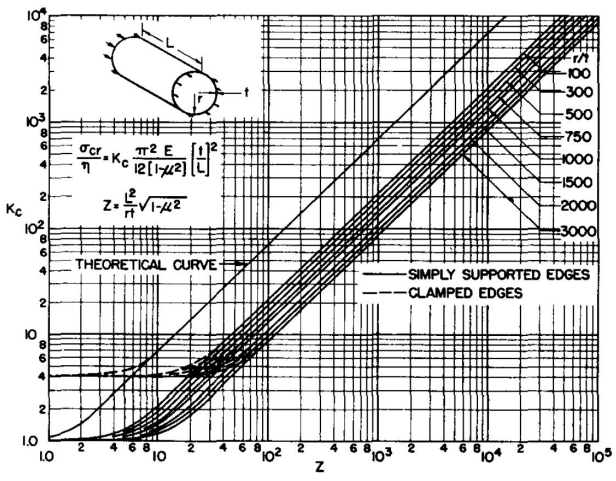

Figure 10.11: Empirical relations to obtain the buckling constant [77]

$$\sigma_{\text{cr}} = K_c E \pi^2 / 12\left(1-v^2\right) * (t/L)^2 \quad (10.36)$$

$$\frac{\sigma_{cc}^{(i)}}{\sigma_y} = \alpha\left[\frac{C}{\sigma_y}\frac{\pi^2 E}{12\,(1-v^2)}\left(\frac{t}{b}\right)^2\right]^{1-n} \quad (10.37)$$

$$\sigma_{cc} = \frac{\sum \sigma_{cc}^{(i)} A_i}{\sum A_i} \quad (10.38)$$

$$\sigma_{cr} = \frac{P_{cr}}{A} = \frac{\pi^2 E I_{\text{sx}}}{A L_c^2} = \pi^2 E \cdot \frac{I_{\text{xx}}}{A L_{\text{c}}^2} \quad (10.39)$$

$$w_e = \frac{t}{2}\sqrt{\frac{C\pi^2}{12\,(1-v^2)}}\sqrt{\frac{E}{(\sigma_{cc})_{\text{stiffener}}}} \quad (10.40)$$

$$(\sigma_{cc})_{\text{panel}} = \frac{\sum \sigma_{cc}^{(i)} A_i}{\sum A_i} \quad (10.41)$$

From those equations, several values have been obtained. Firstly, the maximum buckling stress for the cylinder without the stiffeners is equal to 9.9 [MPa]. As it is half the value obtained for the structure load Figure 10.10b, the structure would fail by buckling soon after launch. This confirms

the decision of using stiffeners as a reinforcement. To check how the maximum buckling stress improves by adding stiffeners, the rest of the equations were used. It was clear that the structure can sustain a much higher load, as the maximum buckling stress is equal to 185 [MPa], much higher then what structure is experiencing during the mission. It could be argued that such a margin of safety is excessive. However, it is important to remember that other loads like handling loads will be also present, but are now unknown. Furthermore if the structure would be even weaker, any imperfection or fault could cause failure by buckling at lower loads than calculated, as buckling phenomenon are very sensitive to defects that can arise during production or handling. Finally, adding stiffeners does not increase the mass significantly: 40 stiffeners have a mass of 44.31 [kg]. Moreover the calculated tank mass is an underestimation as more components like: insulation[78][79], pipes, fasteners, and extra reinforcement go into the tank assembly, and their weight also have to be taken into account. Since the exact estimation was not possible, the analytical value for the membrane and stiffeners was simply multiplied by two, as suggested by [63]. All the dimensions determined are presented in Table 10.5.

Table 10.5: Propellant tank

Parameter	Oxidiser volume	Fuel volume	Number of stiffeners	Thickness (cylindrical part)
Value	119.97 [m^3]	85.08 [m^3]	40	0.0041 [m]
Parameter	Thickness (elliptical part)	Fuel tank mass (structure)	Fuel tank mass (total)	Oxidiser tank mass (structure)
Value	0.0029 [m]	466.7335 [kg]	933.45 [kg]	1086.06 [kg]
Parameter	Oxidiser tank mass (total)	Max stress	Max allowable stress	
Value	2172.12 [kg]	20 [MPa]	185 [MPa]	

Maintenance

The propellant tank has to withstand many cycles during its lifetime, especially since it is decided that it can't be reproducible in-situ. According to the research done by Technology Laboratory for advanced composites [73], the composite tank of X-33 under the fatigue testing showed very promising results. Changes in ultimate stress and young's modulus vs number of cycles can be seen in Figure 10.12. It is pretty obvious from them that changes in the tank properties across the life-time are pretty negligible, also in the same studies a leak test was performed that showed no issues with propellant penetration. Hence it is fair to assume that tanks made out of carbon epoxy laminate are safe to use in many cycles throughout the life-time. However, certain control still has to be taken, especially for manned mission where safety is the highest priority. Since the tank is a closed structure, usage of NDT is necessary. The tests that are suitable for such a design can include: optical examination using microscopes and X-radiography using die-penetrant.

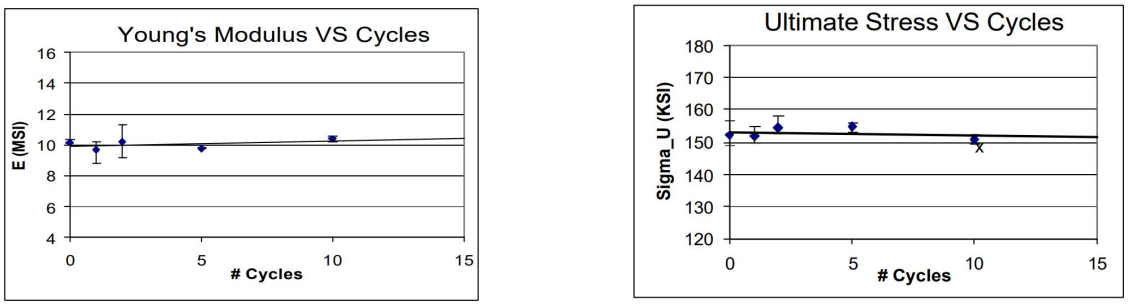

Figure 10.12: Fatigue analysis on the cryogenic tank of the X-33 [73]

Future recommendations

Due to the time constraints, certain analysis were not possible to perform but they would be extremely valuable at later phases of the design. Hence, as a recommendations, a FEM analysis of the entire tank assembly should be performed to validate the analytical calculations. Moreover, the layup should be optimised for this specific design to achieve better performance and confidence [80]. One way to do this is the netting analysis, which uses fibre orientation as an input. One can also add the detailed

loading analysis and possibly testing of the elliptical caps, similarly to how it was done in [81].

10.8.2. Skirts

To accommodate other subsystem inside the vehicle structure, two skirt were added to the tanks assembly, one at the top and a second one at the bottom of the vehicle, as it can be seen in Figure 10.8a. The aft skirt provide connections and load transfer from the engines to the tanks and forward skirt connects capsule to the tanks and similarly provide load path. To calculate the loads in both of those structures the loading diagrams presented in Section 10.3 were used, similarly to the propellant tank design. Hence the combined stress during mission could be obtained following the same analysis as for the tank. Then as it was mentioned before the critical buckling load had to be calculated as skirts are thin cylinders structures. This time however, other method was used to obtain the critical buckling load. Following the method presented in [82] and [83] for isotropic reinforced cylinders with rings and stiffeners, the buckling load can be computed with Equation 10.42.

$$\mathrm{N_X} = \left(\frac{l}{\mathrm{m}\pi}\right)^2 \begin{vmatrix} \mathrm{A_{11}} & \mathrm{A_{12}} & \mathrm{A_{13}} \\ \mathrm{A_{21}} & \mathrm{A_{22}} & \mathrm{A_{23}} \\ \mathrm{A_{31}} & \mathrm{A_{32}} & \mathrm{A_{33}} \end{vmatrix} / \begin{vmatrix} A_{11} & A_{12} \\ A_{21} & A_{22} \end{vmatrix} \tag{10.42}$$

Where the elements of the matrix are as follows:

$$A_{11} = \bar{E}_X \left(\frac{m\pi}{l}\right)^2 + \overline{G}_{XY} \left(\frac{n}{r}\right)^2 \quad , \quad A_{22} = \bar{E}_y \left(\frac{n}{r}\right)^2 + \bar{G}_{Xy} \left(\frac{m\pi}{l}\right)^2 \quad , \quad A_{12} = A_{21} = \left(\bar{E}_{xy} + \bar{G}_{xy}\right) \frac{m\pi}{l} \frac{n}{r}$$

$$A_{33} = \bar{D}_X \left(\frac{m\pi}{l}\right)^4 + \bar{D}_{xy} \left(\frac{m\pi}{l}\right)^2 \left(\frac{n}{r}\right)^2 + \bar{D}_y \left(\frac{n}{r}\right)^4 + \frac{\bar{E}_y}{r^2} + \frac{2\bar{C}_y}{r} \left(\frac{n}{r}\right)^2 + \frac{2\bar{C}_{xy}}{r} \left(\frac{m\pi}{l}\right)^2$$

$$A_{23} = A_{32} = \left(\bar{C}_{xy} + 2\bar{K}_{xy}\right) \left(\frac{m\pi}{l}\right)^2 \frac{n}{r} + \frac{\bar{E}_y}{r} \frac{n}{r} + \bar{C}_y \left(\frac{n}{r}\right)^3$$

$$A_{31} = A_{13} = \frac{\bar{E}_{XY}}{r} \frac{m\pi}{l} + \bar{C}_X \left(\frac{m\pi}{l}\right)^3 + \left(\bar{C}_{Xy} + 2\bar{K}_{Xy}\right) \frac{m\pi}{l} \left(\frac{n}{r}\right)^2$$

For which the different variables are the following:

$$\bar{E}_x = \frac{\mathrm{Et}}{1-\mu^2} + \frac{\mathrm{E_s A_s}}{\mathrm{b}} \quad , \quad \overline{\mathrm{E}}_\mathrm{y} = \frac{\mathrm{Et}}{1-\mu^2} + \frac{\mathrm{E_r A_r}}{\mathrm{d}} \quad , \quad \overline{\mathrm{E}}_\mathrm{xy} = \frac{\mu \mathrm{Et}}{1-\mu^2} \quad , \quad \overline{\mathrm{G}}_\mathrm{xy} = \frac{\mathrm{Et}}{2(1+\mu)}$$

$$\overline{\mathrm{D}}_\mathrm{x} = \frac{\mathrm{Et}^3}{12\,(1-\mu^2)} + \frac{\mathrm{E_s I_s}}{\mathrm{b}} + \tilde{z}_\mathrm{s}^2 \frac{\mathrm{E_s A_s}}{\mathrm{b}} \quad , \quad \overline{\mathrm{D}}_\mathrm{y} = \frac{\mathrm{Et}^3}{12\,(1-\mu^2)} + \frac{\mathrm{E_r I_r}}{\mathrm{d}} + \tilde{z}_\mathrm{r}^2 \frac{\mathrm{E_r A_r}}{\mathrm{d}}$$

$$\overline{\mathrm{D}}_\mathrm{xy} = \frac{\mathrm{Et}^3}{6(1+\mu)} + \frac{\mathrm{G_s J_s}}{\mathrm{b}} + \frac{\mathrm{G_r J_r}}{\mathrm{d}} \quad , \quad \bar{C}_x = \tilde{z}_S \frac{E_S A_S}{b} \quad , \quad \bar{C}_y = z_r \frac{E_r A_r}{d} \quad , \quad \bar{C}_{xy} = \bar{K}_{xy} = 0$$

Using these equations the theoretical buckling load could be obtained, which is the lowest possible value of N_x for all values of variable n and m. Furthermore, the final outcome could be quickly changed for different parameters like: skin thickness, shape of the rings or stiffeners, and the number of them. In this way the optimal solution could be obtained where the structure can withstand higher loads than the applied one but at the same time has the lowest possible weight. To summarise this iteration process the final characteristics of both skirts are presented in Table 10.6. It is good to point out that for both skirts the same stiffeners and rings were used.

Table 10.6: Final parameters for the forward and aft skirt

Parameter	Length [m]	Radius [m]	Skin thickness [m]	Stiffener Iyy [mm⁴]	Ring Iyy [mm⁴]
Forward Skirt	3	3	0.002	333,900	333,900
Aft Skirt	2.5	3	0.002	333,900	333,900
Parameter	Number of rings	Number of stiffeners	Mass [kg]	Max Stress [MPa]	Max allowable Stress [Pa]
Forward Skirt	5	40	778.2	16	45.97
Aft Skirt	4	30	625.5	30	57.91

From Table 10.6, it can be seen that, for both skirts, the maximum value of stress is small, and smaller than the allowable value. It is crucial that there is some margin between the two values, as the analytical solution for buckling tends to underestimate the true stress at which the structure will fail. According to a research from NASA [84], the analytical solution sometimes has to be scaled down to 65% of the computed value. Most of the times, it is caused by imperfections in the materials or defects from manufacturing. 65% of the allowable stress for both skirts is still above the maximal stress. It can thus be concluded that the structure will not fail under loading during the mission. Finally, the distribution of the Von Mises stresses is presented in Figure 10.13a and the theoretical critical buckling is plotted in Figure 10.13b for different numbers of buckle half waves in the axial direction -m, and numbers of buckle waves in the circumferential direction -n.

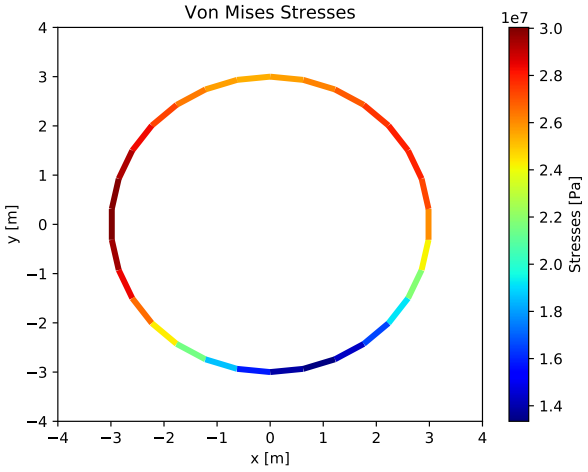

(a) Von Mises stresses in the aft skirt

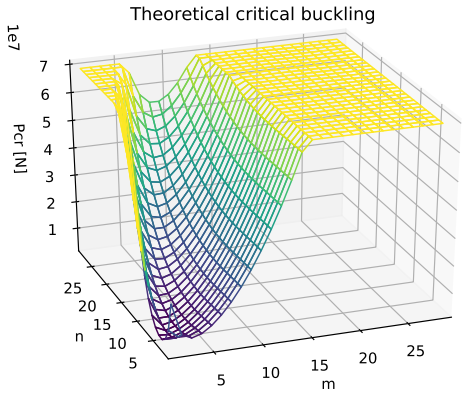

(b) Theoretical buckling force for the isotropic cylinder reinforced with stiffeners and rings

Verification and Validation

To verify and validate this analysis, the outcome of the code was compared to the solution form [63]. Here, the problem was simplified to a simple cylinder without any reinforcement with following dimensions: 1 [m] radius, 2 [m] length, 0.002 [m] thickness. Obtaining maximum theoretical buckling force of 450 [kN] and minimum of about 180 [kN]. Then the results were presented in a 3D plot, where theoretical critical buckling was plotted against n and m values. As it can be seen in Figure 10.14 for both cases the result is the same, meaning that the code has been verified and validated.

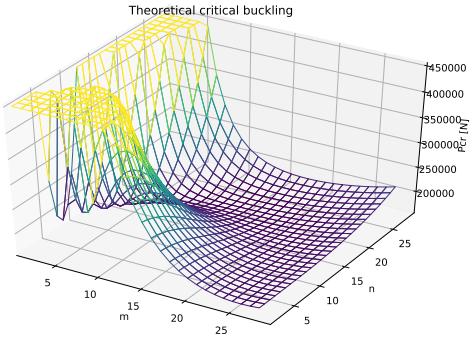

(a) Theoretical buckling force for the isotropic cylinder from the presented model

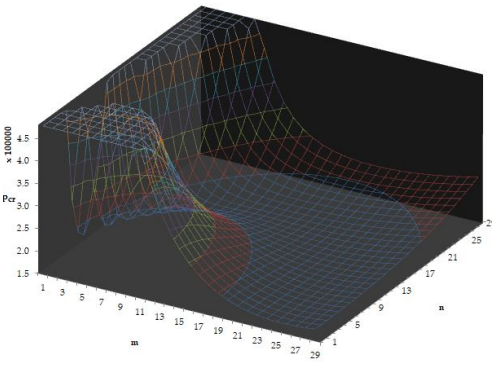

(b) Theoretical buckling force for isotropic cylinder from [56]

Figure 10.14: Comparison between two models for theoretical buckling

10.8.3. Adapter

To connect propulsive stage with the capsule an adapter is needed to match two different diameters. Inside this adapter the separation system is placed that allows for the abort in case of the emergency. As both propulsive stage and the capsule have different radius, the shape of the adapter is conical similar to many inter-stages in other launchers. To analyse the loads inside this structure, thanks to

similar overall shape, the same calculation were performed as for the pressurised part of the capsule. The loads were taken once again from the loading diagram at z-coordinate of about 12 [m] and for a determined critical buckling stress of about 61 [MPa]. Similar to the capsule the inner angle is equal to 20 °, while the bottom and the top radius are equal to 3 and 2.97 [m] respectively. Under the actual loads the stress distribution in the adapter is expected as in Figure 10.15.

To ensure that the stress in the structure is at least a factor of 1.5 smaller than the buckling stress, the thickness of the adapter, without any stiffeners, should be equal to about 14.9 [mm]. As it can be seen the maximum stress in the structure is significantly lower than yield stress of the material that was chosen, which proves that the structure will not fail due to external forces. Apart from providing the support for the capsule, adapter has to provide also a way to separate it from the bottom stage if something goes wrong. Looking at similar systems in other vehicles several solutions were identified: electrical pin pullers[3], quick release latches[4] and pyrotechnic bolts[5]. Then the trade-off was made between those solutions based on the following parameters: reliability, mass, and power requirement to arrive at the best possible system for this mission.

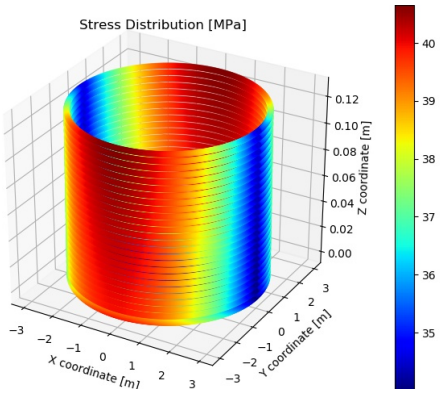

Figure 10.15: Stress distribution to the adapter under actual loads

Table 10.7: Separation Mechanism trade-off

Criteria / **Design Concept**	**Reliability, 56.25%** (1, 5) High Best, $\sigma = 1.247$	**Mass, 18.75%** (1, 5) High Best, $\sigma = 0.816$	**Power requirement, 25.0%** (1, 5) High Best, $\sigma = 1.633$	**Total**
Pyrobolts	blue 5 → 1	green 4 → 0.75	blue 5 → 1	0.953
Pin-pullers	orange 2 → 0.25	yellow 3 → 0.5	yellow 3 → 0.5	0.359
Latches	green 4 → 0.75	orange 2 → 0.25	red 1 → 0	0.469

As it can be seen pyro-bolts performed the best in the trade-off, hence they were chosen as a separation method for the capsule in case of abort.Moreover releasing or changing the capsule shouldn't be an issue too, as even though bolts have a pyrotechnic charge inside them, they are still behaving as normal bolts and can be simply unscrewed, which is also helpful for the maintenance.

10.8.4. Landing legs

To launch and safely recover Charon, reusable and retractable landing legs are necessary. They have to sustain the static loads from the fully fuelled vehicle at the launch pad, but more importantly they must not fail during landing, when dynamic loads are applied to them. Apart from that, they have to be able to fold just after take-off and deploy before touch-down, which implies high reliability and redundancy, as failure of landing legs could result in LOV. To fulfil those goals, a certain landing legs configuration was chosen, namely a set of 4 landing legs, with double hydraulic telescopic extension for redundancy, and a leg shell. For re-tractability, electric motors were added at the bottom of each leg, and pushers at the top of them. Furthermore, each telescopic extension has a dampener which dissipates some of the kinetic energy during landing, also making the touch-down more pleasant for the crew. During the entire flight, but most importantly at ascent and reentry, the legs will be kept in place by the latches mounted at the tip of a leg. Such a system is fairly simple, and delivers satisfactory

[3]TiNi^{TM} Pin Puller, `https://www.ebad.com/tini-pin-puller`,accessed on 17 June 2020
[4]TiNi^{TM} Subsea Shackle Release, `https://www.ebad.com/tini-subsea-shackle-release`, accessed on 17 June 2020
[5]Explosive Bolts | Separation Bolts | Sep Bolts | Pyro Bolts, bolts,`https://psemc.com/products/explosive-bolts-sep-bolts`, accessed on 17 June 2020

reliability as it does not consist of too many movable parts, and has a lot of redundancy. Furthermore, it may seem that four legs is a bad design choice, as if one leg fail then the whole vehicle can fall down. While this is true, extra redundancy with the double hydraulic extensions lowers the probability of this occurring significantly. Also, the crew in such a situation is not in danger because it can still safely abort. Finally, the chance of one leg failure has been calculated and presented in the risk table in Section 18.5. Even without the extra leg, the LOV is lower than the given requirement. Hence, it was concluded that 4 legs is enough for this mission.

To properly size the landing legs, several analysis had to be performed. Firstly, the angle θ between the ground and the landing shell had to be determined. This angle determines the amount of clearance between the engines and the Mars surface obtained through Equation 10.43. Following previous mission designs [85] it was assumed that 0.5 [m] of clearance is suitable. Secondly this angle also determines the maximum tilt-angle of the vehicle in case of rough landing through Equation 10.44. Having both of those constraints determined, functions were implemented into Python and possible angles were determined. Although it was obtained that vehicle can land at the ground slope of 28 [deg], the analysis was done for static condition only. In case of the dynamic motion the rotation might take place around the point of contact with the ground and this was later investigated for the performance envelope .

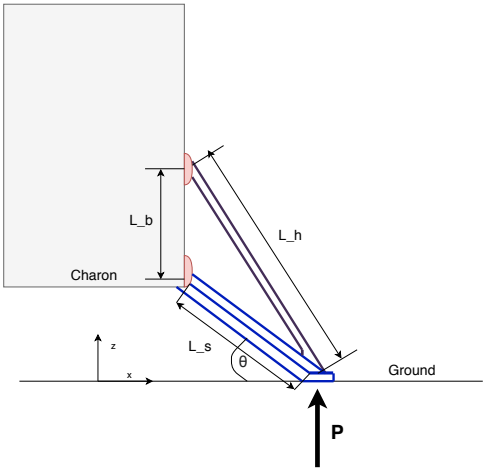

Figure 10.16: Landing legs layout

$$\sin\theta >= \frac{h}{L_s} \tag{10.43}$$

$$\sin\beta >= \frac{L_s\cos\theta}{(z_{cog} + L_s\sin\theta)\sqrt{2}} \tag{10.44}$$

$$\sum F_x = 0 \tag{10.45}$$

$$\sum F_y = 0 \tag{10.46}$$

$$\sum M = 0 \tag{10.47}$$

After the angles were determined the load analysis could take place. Several critical loading conditions were identified and the landing legs were analysed for them as they are presented in Table 10.8. Firstly the static load was checked using Figure 10.16 in which stresses are distributed evenly and it was concluded that taking off from the landing legs is possible as the maximal stress is 10.7 [MPa] for 50 tons of mass, substantially lower than tensile strength of the chosen material 324 [MPa]. Then the stresses during landing were checked using Equation 10.48 and 10.49 [86][87].

$$n = 1 + \sqrt{1 + \frac{2h}{\delta_{\text{st}}}} \tag{10.48}$$

$$n = \sqrt{\frac{\eta v^2}{g\delta_{\text{static}}}} \tag{10.49}$$

It was discovered that loads in this case are significantly larger, especially if one of the legs would hit the ground sooner than the other. In that case the entire load from the vehicle is concentrated in one leg. It is an example of an off-nominal condition, where possibility of such a landing is low but still possible, hence landing-legs system should still be able to withstand this load.

Table 10.8: Critical loading conditions exerted by landing legs

Loading conditions	Angle of slope [deg]	Max. Normal Stresses [MPa]
Static Load (fully fuelled)	0	10.69 [MPa]
Landing Vv = 16 [m/s]	0	293.81 [MPa]
Landing Vv = 16 Vh =5 [m/s]	2	288.77 [MPa]

To complete the design of the landing leg, the cross-sectional view is present in Figure 10.17 together with the list of parameters of Table 10.9.

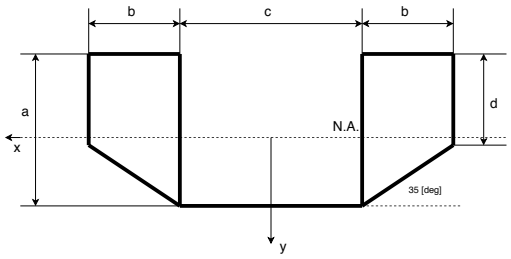

Figure 10.17: Cross-sectional view of the leg shell

Table 10.9: Leg shell design parameters

Parameters	Value
a	237.5 [mm]
b	125 [mm]
c	500 [mm]
d	150 [mm]
t	6.6 [mm]
Mass	195.66 [kg]

When all the dimensions were determined according to a given loads, the performance envelope was created was created as can be seen in Figure 10.18. In which the deviation in Charon's horizontal and vertical velocity is plotted as a yellow ellipse. Boundary of this ellipse are defined by 3σ deviation both in horizontal and vertical direction, for which it was assumed that σ for vertical velocity is equal to 2[m/s], while for the horizontal velocity is equal to 0.5 [m/s]. Blue lines are representing the landing-legs constraints, meaning that for higher velocities the legs will fail or the whole vehicle will be unstable. It is worth to point out that negative horizontal velocity indicates the negative slope during landing, while positive velocity corresponds to positive slope. This analysis was based on an Apollo document [85].

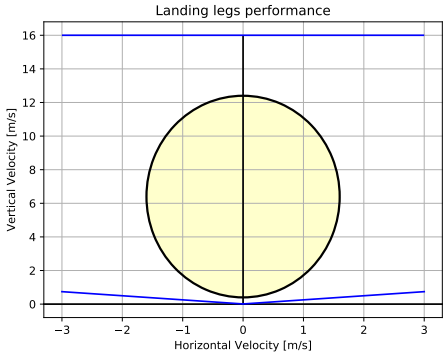

Figure 10.18: Landing Leg Velocity envelope

The top blue line describes the structural constraint after which the leg structure would yield due to forces higher then material allowable ones. This constraint was obtained by gradual increase of vertical velocity to the point at which the stresses in the structure exceeded the proof stress of the material. The blue lines at the bottom of the Figure 10.18 correspond to the stability criterion, at which vehicle would tilt over due not high enough vertical velocity. Stability constraint were calculated using Equations 10.50 to 10.52.

$$r = \sqrt{cg_x^2 + cg_z^2} \quad (10.50) \qquad \frac{1}{2}\left(I_{yy} + m \cdot r^2\right) \cdot \omega^2 < (1 - cos\,(\theta)) \cdot r \cdot m \cdot g_m \quad (10.51) \qquad \omega = v_x \cdot cg_z + v_z \cdot cg_x \quad (10.52)$$

Looking once again at the Figure 10.18 it is clear that legs constraints are outside of the vehicle envelope, confirming that landing legs system is safe to use in this mission.

Wind Consideration

One of the consideration that have to be addressed for landing legs design is the effect of the wind on the stability of the vehicle, namely vehicle can not tilt more than a design value due to the wind force. To prevent that from happening, first the wind pressure and the resulting force have to be calculated. Taking a rectangular shape with an area of 108 [m^2] as a cross section for simplicity, and multiplying it by the dynamic pressure, the force of the wind is equal to about 2187 [N], taking the density of the Martian atmosphere at around 0.02 [kg/m^3].

As it can be seen the force exerted on the vehicle by the wind is fairly low and can be simply disregarded, especially as the wind pressure acts on the whole surface, hence the force is distributed and do not act as a point load, even further decreasing the possibility of any tilt. In case of the Earth atmosphere this situation would be completely different as the force for this case is almost 700 [kN]. Similarly, given that the acting force exerted on the vehicle is low, it is easily understood that impact with dust particles on Mars would not affect the structural integrity of the Charon significantly.

10.9. Vibrational Analysis

In order to ensure the safety of the crew and the integrity of the vehicle the structural elements must not resonate at the same frequency with the vibration loads during the mission and transportation of the vehicle from Earth to Mars. Following the requirements presented in Section 10.1 the natural frequency of the vehicle shall be higher than 35 [Hz] and 10 [Hz] in the axial and in the later direction.

The vibrations analysis was performed for two different cases . Firstly the whole system of the vehicle/capsule was simulated as a simple cantilevered beam with a total mass the mass of the vehicle, length of 17.822 [m] and a diameter of 6 [m] using Equation 10.53 and then secondly as a beam with the capsule as a separate mass on top using Equation 10.54. For both cases the Young's Modulus is estimated to be equal to be a combination of Young modulus of Aluminium and of the Bulk modulus of methane, approximated to be similar to that of water; 2.2 [GPa]. Using the mass ratio, obtained from the mass budget, it was determined that E would be equal to about 13.87 [GPa].

$$f_{nat} = 0.56\sqrt{\frac{EI}{m_b L^2}} \quad \& \quad f_{nat} = 0.250\sqrt{\frac{AE}{m_b L}} \tag{10.53}$$

$$f_{nat} = 0.276\sqrt{\frac{EI}{m_{caps}L^3 + 0.236ML^3}} \quad \& \quad f_{nat} = 0.160\sqrt{\frac{AE}{m_{caps}L + 0.333ML}} \tag{10.54}$$

For the first case in the natural frequency in the longitudinal and lateral direction are 78.19 and 14.81 [Hz] while for the second case 99.61 and 24.79 [Hz] respectively. It can be observed that for both cases the natural frequency is higher than the limit imposed by the requirements.

10.10. Risk analysis

The following risks have been analysed and mitigated as part of the Structures subsystem:

- **SRV-RISK-STRUC-1** Propellant tank rupture (P=2), results in vehicle explosion (I=5).
  - Probability mitigation (P-1): design with safety margins, inspection before every mission.
  - Impact mitigation (I-1): have an abort system.
- **SRV-RISK-STRUC-2** Thrust structure failure (P=2), results in possible damage of the tanks, unwanted side thrust, engine damage (I=4).
  - Probability mitigation (P-1): overdesign structure with safety margins, regular inspections.
  - Impact mitigation (I-1): design for specific failure modes.
- **SRV-RISK-STRUC-3** Pipe leakage (P=2), results in loss of the propellant, depressurisation of the propulsion system, vehicle explosion (I=5).
  - Probability mitigation (P-1): plumbing testing before mission, system redundancy.
  - Impact mitigation (I-1): have an abort system.
- **SRV-RISK-STRUC-4** Landing leg collapsing (P=3), results in vehicle with tilt angle after landing, possible falling over (I=4).
  - Probability mitigation (P-1): redundancy, overdesign structure with safety margins.
  - Impact mitigation (I-2): special crumple zones, designing for specific failure modes.
- **SRV-RISK-STRUC-5** Skirt buckling (P=2), results in structure damage (I=4).
  - Probability mitigation (P-1): overdesign structure with safety margins, .
  - Impact mitigation (I-1): designing for specific failure modes.
- **SRV-RISK-STRUC-6** Separation mechanism failure (P=2), results in launch abort failure (I=5).
  - Probability mitigation (P-1): redundancy, inspection before every mission, fail-safe system.
- **SRV-RISK-STRUC-7** Hydraulics system failure (P=2), results in propulsion system failure, landing legs failure (I=4).
  - Probability mitigation (P-1): redundancy, regular inspections.
- **SRV-RISK-STRUC-8** Legs not deploying (P=2), results in rough landing, damage of the vehicle, crew abort (I=4).
  - Probability mitigation (P-1): redundancy, regular inspections.
  - Impact mitigation (I-1): special crumple zones in case of rough landing.
- **SRV-RISK-STRUC-9** Depressurisation of the capsule (P=2), results in lack of breathable atmosphere, possible rupture of the capsule (I=4).
  - Probability mitigation (P-1): Design structure with safety margins, leak testing before missions.
  - Impact mitigation (I-1): have pressurised combinations for the crew.
- **SRV-RISK-STRUC-10** Buckling of the capsule (P=2), results in structure failure, possible depressurisation and rupture of the capsule (I=4).
  - Probability mitigation (P-1): Design the structure with safety margins, testing before missions.
  - Impact mitigation (I-1): design for specific failure modes.
- **SRV-RISK-STRUC-11** Attenuation system failure (P=3), results in crew injuries (I=5).

  - Probability mitigation (P-2): redundancy, overdesign structure with safety margins,
  - Impact mitigation (I-1): designing for specific failure modes.
- **SRV-RISK-STRUC-12** Side hatch not opening (P=3), results in only main hatch usable (I=2).
  - Probability mitigation (P-1): redundancy, inspections before missions, .
  - Impact mitigation (I-1): ability to perform entire mission through main hatch.
- **SRV-RISK-STRUC-13** Docking hatch not opening (P=2), prevent transport of anything through the hatch (I=3).
  - Probability mitigation (P-1): redundancy, possibility for manual opening.
- **SRV-RISK-STRUC-14** Capsule ring not deploying (P=2), results in incapacity to dock to the orbital node (I=3).
  - Probability mitigation (P-1): redundancy, possibility for manual deployment.
- **SRV-RISK-STRUC-15** Non-sealed connection (P=2), results in depressurisation of the system, incapacity to open main hatch (I=3).
  - Probability mitigation (P-1): redundancy, repeating docking procedure.

From this list, a mitigated risk map has been created, and can be seen in Table 10.10. Looking at it, it can be noticed that some of the risks are still in the unwanted red zone. This is however caused due to the scale for the probability being only from 1 to 5. Certain failure have a real world probability even lower than 1. This explains the presence of some critical conditions in the red zone. This issue is further addressed in the chapter about risk, where probability values can take any value.

Table 10.10: Risk map of the Structures subsystem, after mitigation

	Very unlikely (1)	Unlikely (2)	Possible (3)	Likely (4)	Very likely (5)
Very high impact (5)	6				
High impact (4)	1, 3, 7, 11				
Medium impact (3)	2, 5, 8, 9, 10, 13, 14, 15				
Low impact (2)		4			
Very Low impact (1)		12			

10.11. Requirement Compliance and Sensitivity Analysis

With all the analyses of the different structural components finished whether or not the requirements are met could be checked. Table 10.11 shows the compliance matrix for the structural requirements while including the location in which those requirements are investigated. Some of the requirements, such as **SRV-CONS-TECH-2.8**, are still to be investigated in later phases of the design. At the same time, during the analysis is was determined that requirements **SRV-CONS-TECH-2.1** & **SRV-CONS-TECH-2.2** can be considered as killer requirements in the essence that would make the design unfeasible if they were actually met by the vehicle itself. It was decided to go with supportive structure to full-fill those requirements but the analysis of it should be performed in the later stages of the design.

Table 10.11: Requirement compliance for Structures

Requirement	Completion	Explanation	Requirement	Completion	Explanation
SRV-CONS-TECH-2.1	*	Subsection 10.3.2	**SRV-CONS-NONT-3.1**	✓	Equation 10.8.4
SRV-CONS-TECH-2.2	*	Subsection 10.3.2	**SRV-CONS-NONT-3.2**	✓	Equation 10.8.4
SRV-CONS-TECH-2.3	✓	Section 10.9	**SRV-TECH-OPER-2.1**	✓	Equation 10.8.4
SRV-CONS-TECH-2.4	✓	Section 10.9	**SRV-TECH-OPER-2.8**	*	To be investigated
SRV-TECH-OPER-1.3	*	To be investigated			

Regarding the sensitivity of the results obtained and of the models generated to perform the required structural analyses it was determined that the system was the most sensitive to changes in the propellant and dry mass of the vehicle. Given that those are inputs to all the different simulations used, the output is expected to be affected. However, given the contingencies and safety factors (1.5 safety factor applied to maximum loads for example) applied throughout the design as well as the margins obtained between the results and the actual designed ones it can be determined that changes are allowed and can be performed, without having big effect on the structural design of the vehicle. Furthermore, from the simulations it is also obtained that most of the input-output relations are linear meaning that in the case of an increase by a factor of 2 of the tank pressure a similar increase is expected to be seen for the thickness and the mass as well.

11

Power

The goal of the power subsystem is to supply and distribute power to the various subsystems of the spacecraft. The power requirements and the inputs & outputs are firstly stated in Section 11.1 and 11.2, after which the power budget is updated in Section 11.3. A trade-off is performed in Section 11.4 and the subsystem is sized in Section 11.5 to Section 11.7. The chapter is closed with a risk- and sensitivity analysis in Section 11.9 and 11.10.

11.1. Requirements

Although no formal requirements were set up for the power system, its function is to be able to meet the power needs of the spacecraft. When designing the power system, it is key to keep in mind that the entire vehicle has to be powered during a nominal mission, but the capsule should also be powered after an abort. This means that there should be power generation systems in both the propulsive part and in the capsule, or all the power generation should be done inside the capsule. This latter option would concentrate more mass and volume inside the capsule, which is not desired as this would increase the mass of the abort system.

11.2. Analysis; Inputs and Outputs

Table 11.1 shows the inputs and outputs of the power subsystem design process.

Table 11.1: Power Inputs and Outputs

Analysis	**Input**	**Output**
Fuel cell sizing	Power requirements, nominal mission and abort duration	Fuel cell mass
Required water production	Water consumption	Fuel mass

11.3. Updated Power Budget

In previous reports, an initial estimate of the power budget had already been made [2]. With more details of subsystems known, a more correct estimate of the power budget can be made. This can be seen in Table 11.2. It was difficult to make better estimates of the power budget with respect to the midterm report, meaning that the power needed for some subsystems has stayed the same, which were based on reference vehicles such as Orion or the Space Shuttle. It was found that because of the strong insulation around the capsule, the required power for thermal heating and life support could be reduced significantly. Since this power budget is still not very detailed, there is still quite some uncertainty regarding these power values, which is why a 25% margin is used.

Table 11.2: Power Budget with design margins

Subsystem	**Power [W]**	**Margin [%]**	**Power [W]**
Guidance and Navigation	1200	25	1500
Life Support	1500	25	1500
Communications	150	25	187.5
Avionics	2400	25	3000
Active Thermal control	1000	25	1250
Total	**6250**	**25**	**7812.5**

When sizing the power system, it was assumed 2/3s of the avionic power loads lie in the capsule, and 800 of the 1250 [W] required for thermal control would go to the capsule. This would bring the power required for the capsule to approximately 6000 [W].

11.4. Trade-Off

Since there are many methods of providing power to the vehicle, a trade-off will be conducted to choose the most suitable method for this mission.

11.4.1. Power Generation Methods

The following power generation methods will be taken into account for the trade-off. Note that some methods will need to be paired with power storage systems.

- **Solar arrays**: Solar panels which would deploy after abort has been initiated.
- **Non-rechargeable (primary) batteries**: One-time use batteries which would be used in case of an abort. These are the standard source of power for most current unmanned launch vehicles.
- **Hydrogen fuel cell**: Fuel cells which operate on hydrogen and oxygen to generate power and water. These were used on manned missions before like Apollo and the Space Shuttle [88] [89].
- **Solid Oxide Fuel Cell(SOFC)**: Fuel cells in development which can run on natural gases such as methane and operate at highly elevated temperatures, above a 1000 [K]. [90].
- **Internal Combustion Engine(ICE)**: A combustion engine which would intake boil off propellant from the main propellant tank to generate power. This system would be based on the Integrated Vehicle Fluids (IVF) system recently developed by United Launch Alliance (ULA) for their new Vulcan rocket [91]. Although the IVF system that ULA has developed uses an ICE that runs on liquid oxygen and liquid hydrogen, they have stated that the system should also work with other fuels such as methane [92].

In the case that power storage would be needed, secondary batteries would be used. Some other promising power storage methods were looked into, such as flywheel storage, but all the TRL of each of these different methods was deemed too low, meaning that ultimately they were not considered as options.

11.4.2. Power Generation Criteria

The following 5 parameters are important criteria factors when quantifying the performance of a power generation method: mass, time dependency, ease of integration, slew rate (how fast it can increase and decrease current flow) and flight heritage on launch vehicles. Table 11.3 gives an overview of how well certain methods perform with respect to these criteria.

Table 11.3: Power generation characteristics

Power generation	Mass	Time dependency	Integration	Slew rate	Flight heritage
Hydrogen Fuel cell	++	-	+	+	++
Solid Oxide Fuel Cell	+	+/-	+	- -	- -
Internal Combustion Engine	+/-	+	+	+	+/-
Primary battery	-	- -	++	++	++
Solar arrays	-	++	- -	-	+/-

11.4.3. Possible Configurations

Since different power generation methods can be used at different parts of the vehicle and at different stages, the trade-off will be performed on configurations instead of one power generation method specifically.

To narrow down all the possible configurations, for the power generation in the propulsive stage, it must be done by a power generation method that can use the boil-off from the main propellant tanks. This leaves only an SOFC or an ICE as possibilities. Between these two options, the ICE is always favoured, as it has a much higher TRL and can deal with peak powers better.

With this in mind, 5 possible configurations were made. Sketches of these configurations can be found in Figures 11.1 to 11.5.

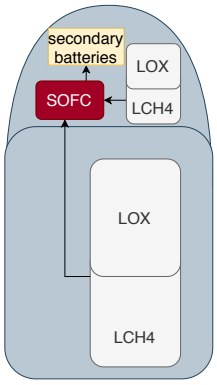

Figure 11.1: Power configuration 1

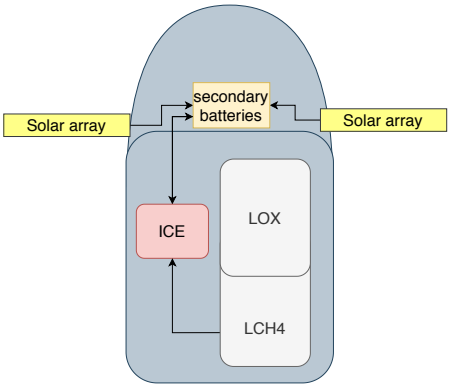

Figure 11.2: Power configuration 2

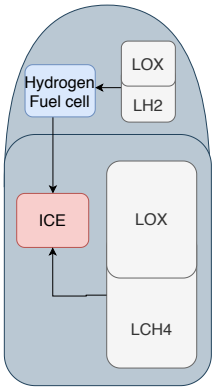

Figure 11.3: Power configuration 3

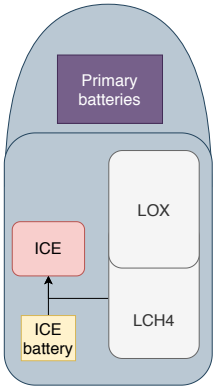

Figure 11.4: Power configuration 4

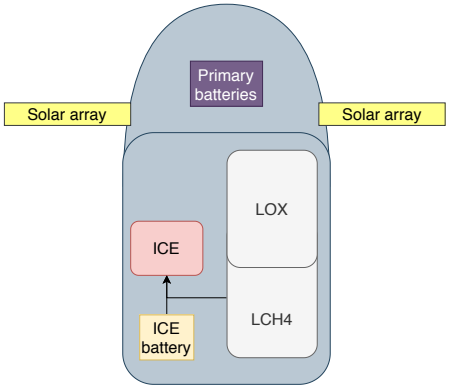

Figure 11.5: Power configuration 5

11.4.4. Trade-Off Result

For the trade-off, only the mass, integration and flight heritage parameters are used. Highly time constrained systems will need more mass added to them to take into account certain design margins, and systems with poor slew rates need extra sources of power to account for peak powers which also add to the mass. These two parameters are thus already accounted for in the mass parameter. The trade-off result can be seen in Table 11.4.

Table 11.4: Trade-off Power generation configuration

Criteria / Design Concept	Mass, 50.0% (1, 5) High Best, $\sigma = 1.02$	integration, 30.0% (1, 5) High Best, $\sigma = 1.47$	Flight heritage, 20.0% (1, 5) High Best, $\sigma = 1.356$	Total
Configuration 1	blue 5 → 1	orange 2 → 0.25	red 1 → 0	0.575
Configuration 2	yellow 3 → 0.5	red 1 → 0	green 4 → 0.75	0.4
Configuration 3	green 4 → 0.75	green 4 → 0.75	blue 5 → 1	0.8
Configuration 4	orange 2 → 0.25	blue 5 → 1	green 4 → 0.75	0.575
Configuration 5	yellow 3 → 0.5	orange 2 → 0.25	green 4 → 0.75	0.475

As can be seen in Table 11.4, configuration 3, the combination of hydrogen fuel cells and an IVF engine, wins the trade-off with a score of 0.8. Although configuration 1, which was based on the SOFC, has the best mass performance, it is difficult to integrate with the rest of the vehicle for many reasons, such as the highly elevated temperatures or the feed system needed between the capsule and the propulsive stage. Therefore configuration 3 will be the chosen power generation method for Charon. Seeing as the next closes score is 0.575, slight changes in weighting factors will not lead to different configurations winning.

11.5. Fuel Cell Characterisation

Now that the power configuration is known, the fuel cells can be sized. Firstly, which type of hydrogen fuel cell will be used is decided upon in Subsection 11.5.1, after which the fuel cells are sized in Subsection 11.5.2.

11.5.1. Alkaline vs PEM

When it comes to hydrogen fuel cells for space applications, mainly alkaline fuel cells have been used. These have shown to have exceptional efficiencies and high specific energies with their applications in the Space Shuttle missions [89]. However, the general consensus is that these will be replaced by the promising Proton-Exchange Membrane(PEM) fuel cells. PEM fuel cells have shown to be able to have the potential for higher specific energy and increased lifetimes when compared to alkaline fuel cells [90]. Alkaline fuel cells do have the capability of having higher efficiencies, but PEM fuel cells can accommodate much higher current densities, meaning peak powers are dealt with easier. PEM fuel cells also have higher lifetimes than alkaline cells, meaning that they could be reused once a vehicle is retired. Since Charon is designed to be operational in 2040, it is thus the logical choice to use PEM fuel cells due to their high potential.

11.5.2. Sizing

The fuel cells consist of an anode and a cathode, at which chemical reactions take place. At the anode, the reaction: $H_2 \longrightarrow 2\,H^+ + 2\,e^-$ occurs, while the cathode reaction is $\frac{1}{2}\,O_2 + 2\,H^+ + 2\,e^- \longrightarrow H_2O$.

Thus the total reaction is $H_2 + \frac{1}{2}\,O_2 \longrightarrow H_2O$ with 2 electrons moving between the anode and the cathode, creating a current. At 100% efficiency, the fuel cell creates a maximum voltage of 1.23 [V] [93]. Therefore, the specific fuel consumption, defined as power generated per fuel mass consumed [kWh/kg] can be defined by Equation 11.1. For the sizing of the fuel cells a 70% efficiency was assumed, which is slightly less than that of the Space Shuttle fuel cells [89].

$$F_{sp} = \frac{\eta \cdot V_{max} \cdot 2 \cdot q_e \cdot N_A}{(MH_2 + \frac{1}{2} \cdot MO_2) \cdot 3.6} = \eta \cdot 3661[Wh/kg] \tag{11.1}$$

To determine the mass of the entire fuel cell system, Equation 11.2 is used.

$$M_{Fuelcellsystem} = 2 \cdot M_{PEMFC} + M_{fuel} + M_{H2tank} + M_{O2tank} \tag{11.2}$$

With Equation 11.3 the mass of the fuel cell itself is calculated. PEM fuel cells are predicted to reach high specific (>500 W/kg)[94], but since it is unsure when such technology would be available, a value of 400 [W/kg] was used for this analysis. The mass of the fuel cells will be doubled, since there will be an extra fuel cell needed for redundancy. The fuel cell mass is calculated with Equation 11.4. There needs to be enough fuel to power the capsule after abort, but also to provide enough water to the crew during nominal missions, since the fuel cells also function as the water source of the spacecraft.

$$M_{PEMFC} = \frac{P_{capsule}}{P_{sp}} \tag{11.3}$$

$$M_{fuel} = M_{water} + \frac{P_{capsule} \cdot t_{abort}}{F_{sp}} \tag{11.4}$$

The required liquid hydrogen mass is found with Equation 11.5 by calculating the ratio of the molar masses of the two reactants. Finally the liquid oxygen mass is determined with Equation 11.6.

$$M_{LH2} = \frac{MH2}{\frac{1}{2} \cdot MO2} \cdot M_{fuel} \tag{11.5}$$

$$M_{LOX} = M_{fuel} - M_{LH2} \tag{11.6}$$

For the mass of tanks, the same method was used as in Subsection 8.3.3. However, when compared to the mass of the tanks of the Space Shuttle the masses were considerably smaller, around a factor 2, taking into account the difference in total stored fuel. Therefore a 100% margin was taken on the mass of both tanks. Again, in total two fuel cells will be used, with one being able to provide all the power needed for the capsule and the other one being redundant. If high peak powers arise, both fuel cells can function at the same time to accommodate the power needs of the vehicle.

11.6. IVF Characterisation

The IVF system is based on the concept of using wasted energy sources for other activities such as generating power or pressurising tanks. The IVF engines consume boiled off CH4 and O2 from the main propellant tank to create shaft power, which powers a generator to create electrical power [91].

Exhaust heat at higher power settings can also be used to vaporise liquid propellant which can be pumped to the main propellant tank to pressurise it [91].

When running at the highest power setting, the engine can produce up to 20 [kW] in electrical power, which is more than sufficient to deal with any peak loads. The system is considered to be an off the shelf product, which means it will not be sized specifically to accommodate the peak powers of Charon. For a mass estimation, the IVF mass estimation for Hercules is used, as the IVF system for this concept also uses methane instead of hydrogen for fuel [5]. With 2 engines in total, one for redundancy, the total mass of the IVF system is 209 [kg].

11.7. Power Distribution and Control

With the power generation method known, the needed power distribution system can be determined. The power distribution will be handled by a Power Distribution Unit (PDU). To make sure the design has enough redundancy, a similar approach will be taken as was done in the Space Shuttle, which was done by having each power source connected to their own separate electrical bus [89]. This means that the vehicle will need a total of 4 PDUs, with 2 in the capsule and 2 in the propulsive stage. These PDUs will be connected to the main computer of the vehicle, which will handle the power control and electrical fault detection in the vehicle. All PDUs will distribute the power to the loads at 24 VDC, as this is the general standard and most electrical equipment operates at this voltage level [25]. Wire mass could be saved by distributing at 120 VDC, but this would also mean more DC/DC converters would be needed to supply the power to the different loads, which could offset this initial mass saving. An overview of the power subsystem is shown in the electrical block diagram in Figure 11.6.

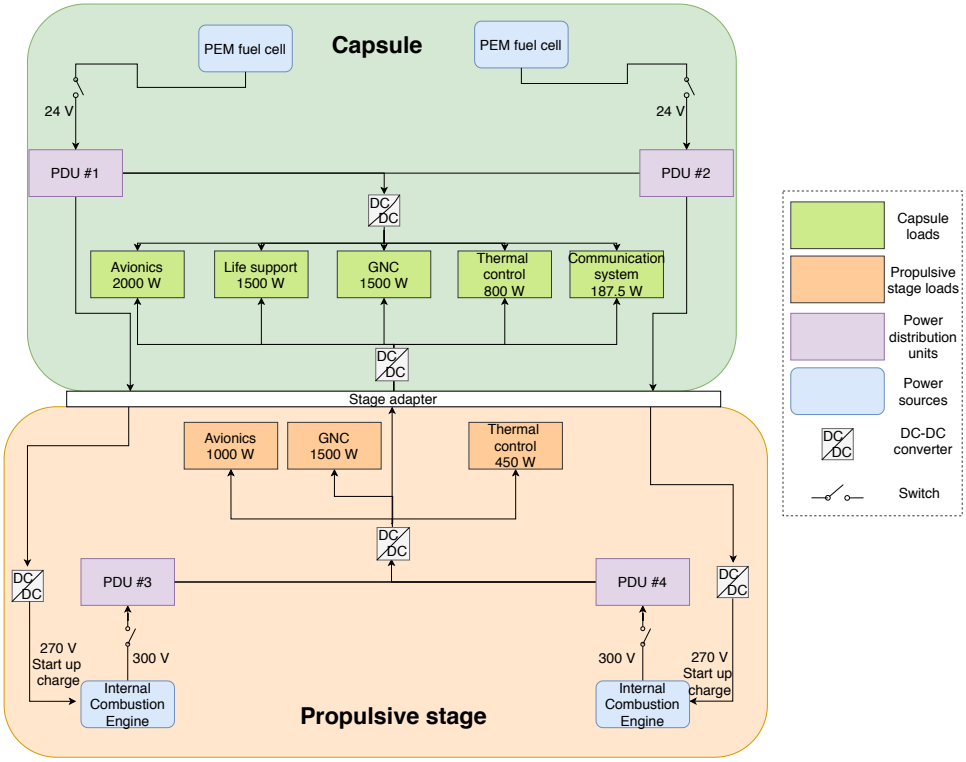

Figure 11.6: Electrical block diagram

Note that the GNC system can be seen in both the capsule and the propulsive stage. During nominal conditions the GNC power loads lie entirely in the capsule, since this is where the flight computers are located. However after abort, the propulsive stage will switch to its own flight computers, which would also require power and are shown as the GNC box in the propulsive stage.

In summary, the mass of the fuel cells themselves is 30 [kg], 25.17 [kg] and 201.40 [kg] for LH2 and LOX and 23.64 andd 45.32 [kg] for their respective fuel tanks. The mass for the IVF system is 209 [kg] and the mass for the PDUs together is 80 [kg], seeing as a PDU generally weighs around 20 kg[95]. Finally, for the mass estimation of the harness of the entire spacecraft, 5% of the dry mass is used, following ESA standards [35].

11.8. Verification and Validation

All equations used in this chapter can be solved in an exact manner, meaning that no error is induced by numerical methods. The V&V process is also simple. For verification, the computations were compared and verified to be correct with a hand made calculation. For validation, comparisons were made with the Space Shuttle fuel cells. From previous mission data it is found that the Space Shuttle fuel cells required approximately 1500 [kg] to produce 4260 [kWh] [96]. With the constructed tool used to size the power system, a fuel mass of 1684 [kg] is calculated to produce this energy, with a fuel cell efficiency of 70 %. The exact efficiency of the Space Shuttle fuel cells is not known, but it is confirmed to be higher than 70% [94], which would explain why it requires less fuel.

11.9. Risk Analysis

The following risks have been analysed and mitigated as part of the Power subsystem:

- **SRV-RISK-POWER-1** PDU failure (P=2), results in vehicle loss of power (I=5).
  - Probability mitigation (P-1): 4 separate PDUs.
- **SRV-RISK-POWER-2** Fuel cell failure (P=2), results in loss of power source for abort (I=5).
  - Probability mitigation (P-1): redundant fuel cell.
- **SRV-RISK-POWER-3** ICE overheating (P=3), results in temporary loss of power (I=2).
  - Probability mitigation (P-2): ice designed for very high peak powers.
  - Impact mitigation (I-1): redundant ICE.
- **SRV-RISK-POWER-4** Ice failure (P=3), results in propulsive stage power loss (I=4).
  - Probability mitigation (P-1): extra redundant ICE.
  - Impact mitigation (I-1): fuel cells can shortly take over.
- **SRV-RISK-POWER-5** Short circuit (P=3), results in loss of power to critical subsystems (I=5).
  - Probability mitigation (P-1): extensive fault detection, fuses and short circuits in the electrical BUS.
  - Impact mitigation (I-3): multiple PDUs give more electrical paths to subsystems.

From this list, a mitigated risk map has been created. It can be seen in Table 11.5.

Table 11.5: Risk map of the Power subsystem, after mitigation

	Very unlikely (1)	Unlikely (2)	Possible (3)	Likely (4)	Very likely (5)
Very high impact (5)	1, 2				
High impact (4)					
Medium impact (3)		4			
Low impact (2)		5			
Very Low impact (1)	3				

As can be seen in the table, two risks still lie in the red section, which are PDU and fuel cell failure. With regards to total PDU failure, although this will always lead to LOC, since there are 4 separate PDUs available the probability of this happening is very unlikely. Furthermore, fuel cell failure is deemed as an LOC event, but this would only be the case if an abort would be required. Combined with the fact that a redundant fuel cell is available, the likelihood of this event happening is also deemed sufficiently low.

11.10. Sensitivity Analysis

Regarding the sensitivity of the power system to input changes, it is most sensitive to changes in the maximum mission and abort duration, as well as the maximum capsule power. These inputs heavily influence the mass of the fuel needed for the fuel cells. All the relations however are linear, meaning that no exponential mass growth in the power system will occur by increasing the power or time requirements linearly.

12

Communication

Communication between the spacecraft and the ground station or node is of the essence to ensure mission success. The requirements for this system, and its inputs and outputs, are first lay out in Sections 12.1 and 12.2. The architecture of the communication system is then presented in Section 12.3, followed by the link budget in 12.4. The communication flow diagram is then presented in Section 12.5. Finally, the risk analysis and compliance with the requirements can be found in Sections 12.6 and 12.7.

12.1. Requirements

The following requirements have been set on the communication system.

- **SRV-TECH-OPER-5 [F]** The vehicle shall be capable of sharing telemetry data with operators.
- **SRV-TECH-OPER-6 [F]** The spacecraft shall maintain communication with the orbital node and the ground station at all times (excluding reentry blackout).
- **SRV-TECH-OPER-6.1 [F]** The communications subsystem shall be able to handle a bitrate of 20 Mbps at a distance of 8966 [km].

12.2. Analysis; Inputs and Outputs

Apart from the given requirements, the only input to the communication calculations is the height of the phasing orbit.

12.3. Required Architecture

In the previous report, a link budget had already been made for the three needed links. This means that there is already a general idea on what will be needed from the communication system. Parts of the budget were already sufficiently detailed, however some parameters for which a value was assumed at the time can now be further investigated. With this in mind, the communication architecture can be determined.

12.3.1. Antenna Configuration

Before the communication design can be further detailed, an antenna configuration needs to be decided upon. Typically for launch vehicles, omnidirectional antennas are placed on the sides of the upper stage of the vehicle, which then transmit telemetry to the ground station or an existing relay satellite system, e.g the Space Shuttle [89]. SLS is supposed to have a phased array configuration[97], which would result in higher gain and thus improved data rates. However, little technical detail is known about how this configuration would work and if such a system can provide coverage for the entire mission of Charon. Since from initial estimates it was possible to close the link budget with a 0 dB gain antenna, it is decided that a complex phased array configuration would not be required for such a mission. Flight proven configurations like that of the Space Shuttle or Ariane 5 will be chosen instead. If during later phases of the design the data rate requirement is significantly increased, a phased array configuration could be considered.

Thus, the antenna constellation will consist of 4 omnidirectional S-band antennas mounted 90 degrees away from each other on the capsule, as sketched in Figure 12.1.

An off the shelf antenna is selected to obtain more detailed parameters needed for the link budget calculations.

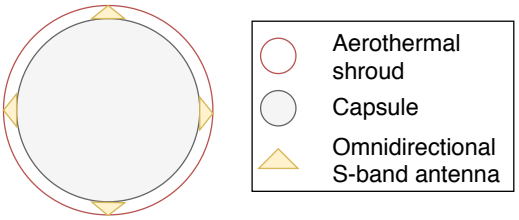

Figure 12.1: Antenna configuration

An antenna from L3Harris was chosen, as they provide antennas which are designed for launch vehicle applications. These antennas thus have certain favourable qualities, such as being able to be flush with the aerothermodynamic shroud of the capsule. The AS-49034 was chosen as it is an omnidirectional antenna made specifically for the telemetry of launch vehicles [98]. The mass of these antennas can be taken straight from their datasheet [98].

12.3.2. Relay Satellites

Furthermore, as was determined in the previous report, a relay satellite system must be in place in order to maintain continuous communication links with the base or the orbital node. The Mars Data Relay Satellites (MDRS) system will consist of three satellites. To keep continuous contact with Charon, these satellites must have the same or very similar orbital inclination as that of the orbital node. The minimum orbital radius of the relay satellites to have line of sight with each other is found to be 6778 [km]. This is found by drawing an equilateral triangle in which a circle with the radius of Mars fits exactly, and then calculating the sides of that triangle. There must also be an elevation angle present between the triangle sides and the Martian surface. Through visual inspection, by increasing the radius by 50% it was deemed that sufficient elevation was present, bringing the orbital radius to 10167 [km]. Another function of the relay satellites is to bypass the typical communication blackout during reentry. This is because instead of the signal having to travel through the plasma sheet on the bottom of the vehicle, it can travel upwards to the MDRS, meaning the communication link can be upheld. The MDRS system is shown in Figure 12.2.

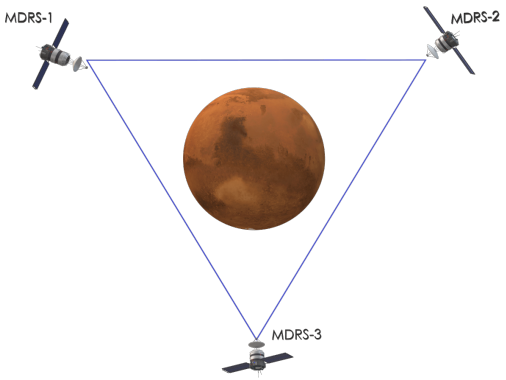

Figure 12.2: Relay satellites

12.3.3. Additional Hardware

In addition to the antennas, the communication subsystem of Charon will consist of the following hardware:

- **Transmitter and receivers**: 2 pairs of transmitters and receivers which can switch between the 4 antennas, making 1 of the pairs redundant. The mass of these components is taken from reference commercial equipment [99].
- **Diplexers**: 4 diplexers are needed in total, with one connected to each antenna. The diplexers are needed to be able to transmit and receive signals with the same antenna.
- **Multi- and demultiplexer**: Multiplexers function to combine signals coming from different channels into one signal, which can then be transmitted. This is needed when transferring multiple signals such as video, voice or telemetry. The demultiplexer then does the opposite, by breaking up the received signal into multiple kinds of signals.
- **Distress beacon**: One distress beacon will be placed inside the capsule in case of an abort landing. This distress signal can then be picked up by the rescue rover in order to locate the crew faster.

The mass of this other hardware is estimated to be around 20 [kg] [25].

12.4. Final Link Budget

With the antenna parameters known, a more detailed link budget can be made. Equation 12.1 is used to calculate the signal to noise ratio [25].

$$E_b/N_o = P + L_l + G_t + L_{pr} + L_s + L_a + G_r + 228.6 - 10\log T_s - 10\log R \tag{12.1}$$

Equation 12.1 can be further broken up into Equation 12.2-Equation 12.5.

$$\lambda_S = \frac{c}{4\pi \cdot S \cdot f} \tag{12.2}$$

$$G = -159.59 + 20log(D) + 20log(f) + 10log(\eta) \tag{12.3}$$

$$T_S = T_{ant} + \frac{T_0(1-L_r)}{L_r} + \frac{T_0(F-1)}{L_r} \quad (12.4) \qquad L_{pr} = -12 \cdot (\frac{21 \cdot e}{f[GHz] \cdot D})^2 \quad (12.5)$$

The main parameters used for the link budget calculation are shown in Table 12.1. The antenna Voltage Standing Wave Ratio (VSWR) shows how much power is reflected by the antenna, with a larger VSWR meaning a less efficient antenna. A VSWR of 2.5 corresponds to a return loss of around -0.88 dB [1]. Although the antenna has quite a wide 3dB beamwidth of 80 °, a 0 dB gain is still used to take into account scenarios with poor line of sight. The space loss is calculated for each link based on the largest possible distances with line of sight, which can be found through simple geometry. For the modulation, the Binary Phase Shift Keying (BPSK) method is assumed. The Bit Error Rate (BER) requirement is set at a low $1 \cdot 10^{-7}$. This is done to mitigate the additional noise that will be generated when the signal is cross linked from Charon to the relay satellites and the ground station. The BER is calculated using Equation 12.6.

$$BER = 1 - \Phi(\sqrt{2\frac{E_b}{N_0}}) \quad (12.6)$$

The final downlink budgets can be seen in Table 12.2 for all communication links. Note that only the downlink is interesting to analyse, since for the uplink the power of the ground or relay communication satellites can simply be increased, since these systems will have fewer power limitations for their communication.

Table 12.1: Link budget inputs

Inputs	**Description**	**Value**	**Source**
f	Frequency	2.2 GHz	Antenna data [98]
R	Data rate	20 Mb/s	SLS as reference [97]
VSWR	Voltage Standing Wave Ratio	2.5	Antenna data [98]
D_{ground}	Ground antenna diameter	6 m	Estimation
D_{relay}	Relay antenna diameter	3 m	Estimation
D_{node}	Node antenna diameter	2 m	Estimation
L_a	Path loss	0.45 dB	Source [100]
T_{ant}	Ground antenna temperature	185 K	Source [101]
T_{orb}	Orbit antenna temperature	9 K	Source [101]
R_{relay}	Relay satellite orbit radius	10167 km	Subsection 12.3.2
$R_{phasing}$	Phasing orbit radius	610 km	Section 4.1
R_{node}	LMO Node orbit radius	500 km	Subsection 15.3.1

[1] Return Loss and VSWR for your antenna, H. Naumann, `https://www.gsm-modem.de/M2M/antenna-test/return-loss-vswr-antenna`, accessed on the 16th of June 2020

Table 12.2: Calculation of Eb/No ratios and BER

Element [dB]	Charon to ground	Charon to relay	Charon to node
Transmitter power	18.5	18.5	18.5
Line loss	-0.88	-0.88	-0.88
Transmitter gain	0	0	0
Point loss receiver	-0.12	-0.12	-0.12
Space loss	-165.8	-178.3	-171.4
Path loss	-0.45	-0.45	-0.45
Receiver gain	40.2	24.2	30.7
Boltzmann	228.6	228.6	228.6
System noise temp	-26.0	-12.8	-12.8
Data rate	-73.0	-73.0	-73.0
Margin	-2	-2	-2
Eb/No	19.0	13.6	17.0
BER ($*10^{-7}$)	0.0035	0.91	0.027

12.5. Communication Flow Diagram

The flow of communication during the operation of Charon is visualised in Figure 12.3. As can be seen, Charon is capable of forming a direct communication link with the ground station, LMO node and the MDRS, either directly or indirectly. These three systems also give Charon the opportunity to have contact with the Earth, although this would have some time delay.

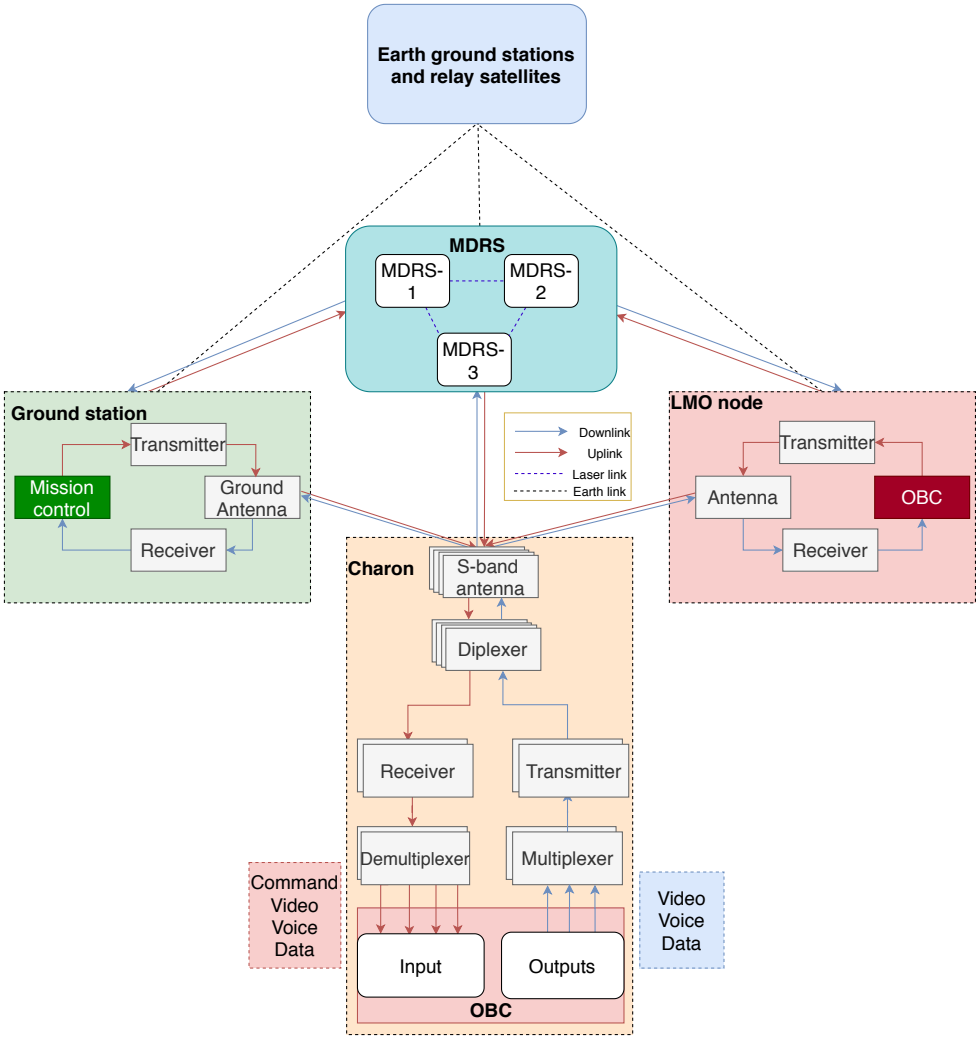

Figure 12.3: Communication flow diagram

12.6. Risk Analysis

The following risks have been analysed and mitigated as part of the Communication subsystem:

- **SRV-RISK-COM-1** Poor or no line of sight (P=5), results in reduced or total loss of communication (I=3).
  - Probability mitigation (P-3): combination of 4 antennas and relay satellites ensure some line of sight is always possible.
  - Impact mitigation (I-1): only transmit critical mission information.
- **SRV-RISK-COM-2** Antenna failure (P=2), results in loss of communication (I=3).
  - Probability mitigation (P-1): redundant antennas.
  - Impact mitigation (I-1): only transmit critical mission information.
- **SRV-RISK-COM-3** Transmitter/receiver failure (P=2), results in loss of communication (I=3).
  - Probability mitigation (P-1): system redundancy.
- **SRV-RISK-COM-4** Extensive noise from cross-link (P=3), results in poor communication (I=2).
  - Probability mitigation (P-1): system designed for low BER.
- **SRV-RISK-COM-5** No line of sight post abort landing (P=3), results in extended search time for crew (I=5).
  - Probability mitigation (P-1): 4 antenna configuration gives more opportunities for signal transmission.
  - Impact mitigation (I-4): beacon on the vehicle and personal locators for each crew member.

From this list, a mitigated risk map has been created. It can be seen in Table 12.3.

Table 12.3: Risk map of the Communication subsystem, after mitigation

	Very unlikely (1)	Unlikely (2)	Possible (3)	Likely (4)	Very likely (5)
Very high impact (5)					
High impact (4)					
Medium impact (3)	3				
Low impact (2)	2	1, 4			
Very Low impact (1)		5			

12.7. Requirement Compliance and Sensitivity Analysis

Table 12.4: Requirement compliance for communicaion

Requirement	Completion	Determination Location
SRV-TECH-OPER-5	✓	Section 12.4
SRV-TECH-OPER-6	✓	Subsection 12.3.2
SRV-TECH-OPER-6.1	✓	Section 12.4 Subsection 7.4.2

Regarding the sensitivity of the communication system to input changes, it is not sensitive to changes in the phasing orbit height, since the maximum space loss is determined by the relay satellite orbital radius. This radius can be increased by 50% before the BER starts to increase beyond 10^{-6}, which is undesired as this would decrease the quality of the signal, although communication would still be possible. The outcomes are also not very sensitive to increases in the required data rate, This is because the link budget works on a logarithmic scale, meaning that unless the data rate is increased exponentially, it will not have a significant effect on the final signal to noise ratio.

13

C&DH

The Command & Data Handling (C&DH) subsystem is central to command and transfer data within the vehicle. Section 13.1 and 13.2 describe the hardware needed to command the vehicle. The data handling and software diagrams are shown in Section 13.3 and 13.4 respectively, after which the human interface analysis is performed in Section 13.5.

13.1. Computer

An off-the-shelf computer is chosen for the C&DH system. This assures that the computer system will contain all needed functions. For the On Board Computer(OBC), the Phoenix flight computer is chosen, produced by L3Harris [102]. This computer is currently being developed for use on the Vulcan rocket and thus is seen as a current state of the art flight computer. Not much data is available on European developed flight computers. There is data available on certain on board computers which are produced by Airbus Space & Defence, such as the OSCAR. However, this computer has only flown on satellite missions and not on launch vehicles, thus making it not the most suitable choice for Charon. The Phoenix flight computer has 3 cross channel data link ports, meaning that 3 extra flight computers can be linked to it for high design redundancy. The fault tolerant OBC will function with the four computers operating in hot redundancy with a voting mechanism to ensure nominal operations of all elements, which is similar to the fault tolerant system used on the space shuttle [89], of which a schematic is shown in Figure 13.1. An additional two flight computers will be placed inside the propulsive stage, such that in case after an abort it is still possible to land or control this stage, these computers will still be available to command this stage. Currently, this flight computer is designed to operate with the LEON3FT processor, which is also to be used for the Ariane 6. However, by 2040 this processor will likely be outdated and thus a more recently developed processor would be a better fit. Such a processor is ESA's next generation microprocessor, the GR740 [103]. This processor is a better representation of the future state of the art and is assumed to be flight proven by 2040.

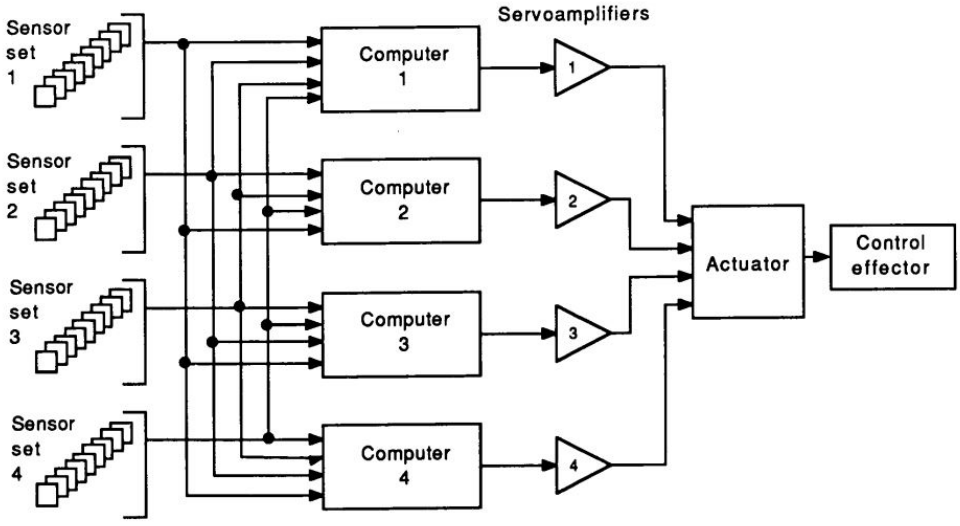

Figure 13.1: Shuttle computer redundancy [104]

13.2. Data Links

The C&DH system must also provide links for data transfer between the different subsystems. There are different standards in place for such data buses. Most notable is the MIL-STD-1553 data bus, which is a military standard made by the United States and is widely used in many spacecrafts. The Phoenix flight computer is equipped with three MIL-STD-1553 data terminals which can provide data transfer links within the vehicle. ESA has also developed their own data bus architecture, SpaceWire and even more recently SpaceFibre, which uses optical fibres to accommodate very high data rate links within the spacecraft of up to 1 Gb/s. While a system such as SpaceFibre is not necessary for Charon, the MIL-STD-1553 links will not be able to handle certain high data links, such as the data generated by the crew camera. The computer is also equipped with ethernet ports, which means ethernet can be used for these larger data links.

13.3. Data Handling Diagram

To get an overview of how the computer interacts with the rest of the system, a data handling diagram is constructed, which is presented in Figure 13.2. With red lines, the flow of data within the vehicle is shown. This data flows to the computer system which then executes commands. The flight computer is not the only system that can transmit command signals, since commands can also flow from incoming communication signals or from the crew controls. Note that since it is difficult to get a good estimate of how much data each separate subsystem generates, the data rates are not shown in the diagram.

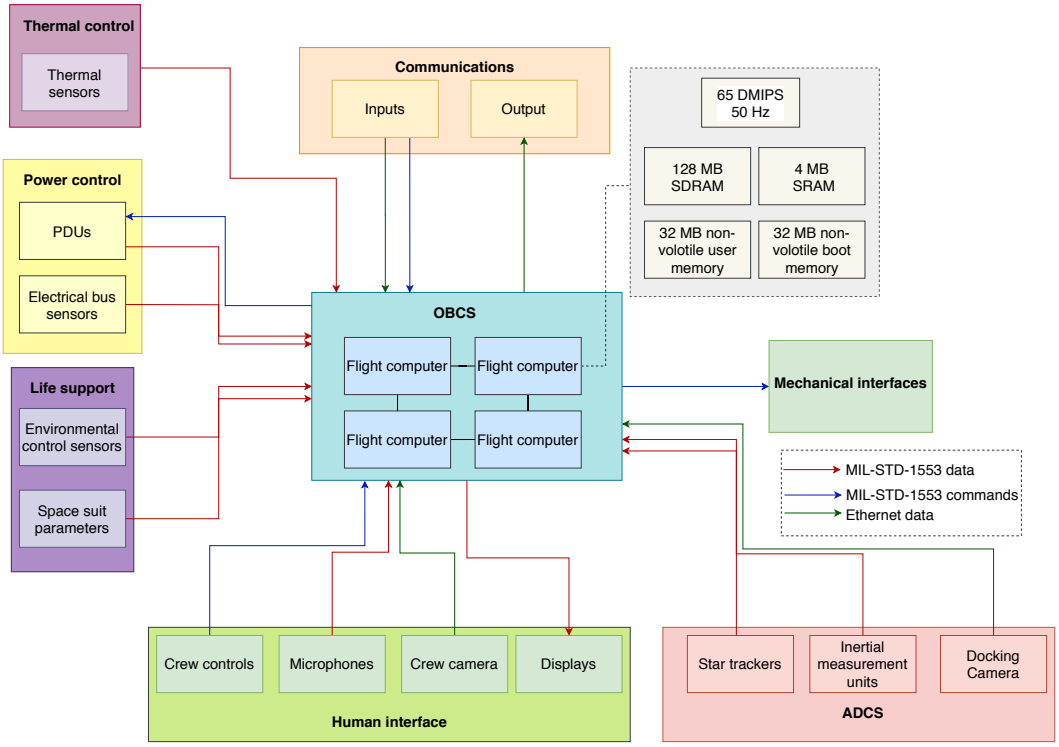

Figure 13.2: Data handling block diagram

13.4. Software Diagram

In addition to the data handling diagram, the software diagram is constructed to show the vehicle uses data generated by other subsystems to operate correctly. This diagram is shown in Figure 13.3. On the left side, the different subsystems and their respective measured values can be seen. These values either first go through certain calculations, or go directly to the flight computer which compares it to reference values, which is depicted as the diamond shaped box. Based on the results of this comparison, commands are sent to certain mechanical interfaces to perform corrective actions. If an error exists such that it can not be solved, either an emergency correction is executed, such as engine shutdown, or the abort system is initiated.

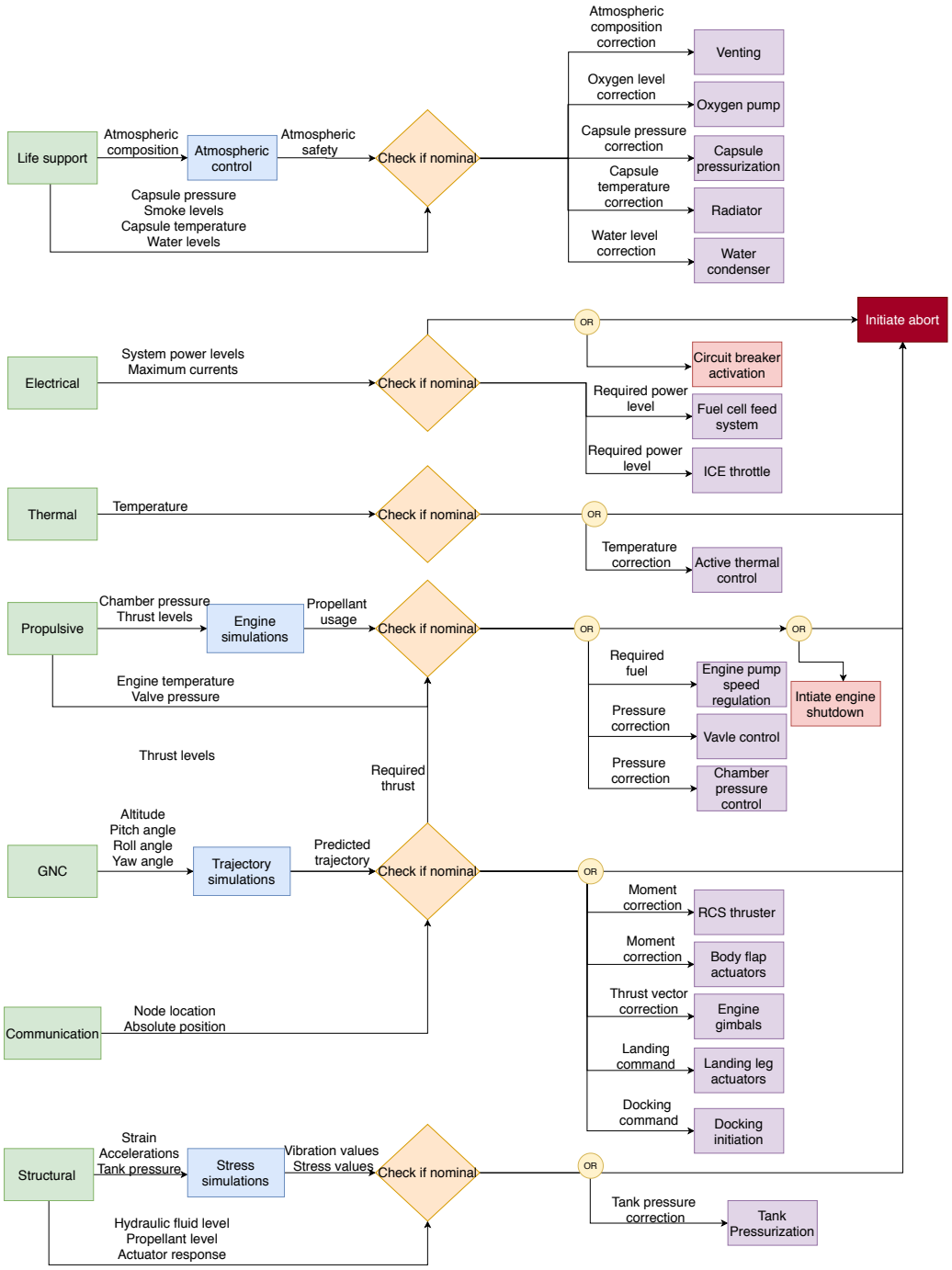

Figure 13.3: Software diagram

13.5. Human Interface Analysis

One requirement relating to the human interface for the crew is:

- **SRV-TECH-OPER-7.1** The GNC of the vehicle shall be fully autonomous, with manual overrides for crewed missions.

To verify this requirement several things have to be considered with respect to the human interface. The most important function of this system is to relay the most important information to the correct astronauts and to allow them to correctly control the vehicle while in flight. To this end a FAMT (Function allocation matrix tool)[105][106] is used to correctly identify these functions. Each function is assigned two parameters dictating placement reach zone (RZ) and criticality (CRT). Reach zone describes the reach of the astronauts throughout different phases of flight. Reach zones are defined as in [106]:

- RZ1: Accelerations above 3G, restraints limit operator to hand and wrist motions only

- RZ2: Accelerations between 2G to 3G, restraints limit operator to hand/wrist motions only with forward reaches within forward +/-30 degree cone
- RZ3: Accelerations less than 2G, restraints limit operator to hand/wrist/arm/shoulder motions only
- RZ4: During on-orbit manoeuvres (Zero-G). Operators have full motion around point of restraint.

The second parameter illustrates the importance of information being displayed in high vision areas and controls being easily accessible. They are defined as in [105]:

- CRT1: eye movement only, controls as at primary resting position. Defined as a field of view of less than $30°$ facing straight ahead. Information/control available on two astronauts control panels and on one panel for backup,
- CRT2: may require head motion, slight hand motion may be required. Defined as a field of view of less than $70°$ facing straight ahead. Information/control available on one astronauts control panel and on one panel for backup,
- CRT3: May be towards limits of field of view with head movement, arm motion might be required. Defined as a field of view of less than $130°$ facing straight ahead. Information/control available on one astronauts control panel

Both RZ and CRT place constraints on hand motion and in each case the strictest requirement apply. For the FAMT three astronaut roles are assumed to be available, Commander: primary pilot, in charge of mission and crew safety, Pilot: assists commander with flight and trajectory monitoring and Flight engineer: in charge of monitoring subsystems

	Flight Phase						function type				interaction Type			CRT grades					allocation							
																			Commander		Pilot		Shared		Fligth engineer	
	ascent	phasing	rendevousz	deorbit	Reentry	Landing	CTRL flight	NAV	COMM	SYS MNG	Control	Display	Alert	Hazard criticallity	S/C Direct ontrol	Operational criticallity	Freq of use	CRT	Controls	Display	Controls	Display	Controls	Display	Controls	Display
Monitor burn																										
Monitor acceleration	x	x	x	x	x	x		x				x	x	5	1	5	5	16		RZ1		RZ1		(RZ1)		
Monitor aerodynamics	x				x	x		x		x		x	x	5	1	5	5	16		RZ1		RZ1		(RZ1)		
monitor Projected trajectory	x	x	x	x	x	x		x				x	x	5	1	5	5	16		RZ1		RZ1		(RZ1)		
Monitor vehicle attitude	x	x	x	x	x	x		x				x	x	5	1	5	5	16		RZ1		RZ1		(RZ1)		
manual control																										
Rotational control	x	x	x	x	x	x	x				x	x		5	5	5	3	18	RZ1	RZ1	RZ1	RZ1	(RZ1)	(RZ1)		
Translational control	x	x	x	x			x				x	x		5	5	5	3	18	RZ1	RZ1	RZ1	RZ1	(RZ1)	(RZ1)		
Main engine control	x	x		x		x	x				x	x		5	5	5	2	17	RZ1	RZ1	RZ1	RZ1	(RZ1)	(RZ1)		
Monitor/control systems																										
Capsule atmoshphere	x	x	x	x	x	x				x	x	x		4	2	5	2	13					(RZ1)	(RZ1)	RZ1	RZ1
Capsule temprature	x	x	x	x	x	x				x	x	x		2	2	3	2	9							RZ1	RZ1
EPS charectaristics	x	x	x	x	x	x				x	x	x	x	3	1	4	2	10					(RZ1)	(RZ1)	RZ1	RZ1
Propulsion Charectiscs	x	x	x	x	x	x				x	x	x	x	4	1	5	2	12					(RZ1)	(RZ1)	RZ1	RZ1
Abort diagnostics	x	x	x	x	x	x				x		x	x	5	1	5	2	13						(RZ1)		RZ1
Heat loading	x	x	x	x	x	x				x		x	x	5	1	5	2	13						(RZ1)		RZ1
Ullage	x	x	x	x	x	x				x	x	x		3	1	5	2	11					(RZ1)	(RZ1)	RZ1	RZ1
read and call out procedures																										
Flight milestones	x	x	x	x	x	x			x	x		x		3	1	4	4	12						(RZ1)		RZ1
Pre-start procedures	x								x	x		x		3	1	4	4	12						(RZ1)		RZ1
docking procedures			x						x	x		x		3	1	4	4	12						(RZ3)		RZ3
monitor comms																										
Telemetery	x	x	x	x	x	x			x	x	x	x		4	3	5	5	17	RZ1	RZ1	(RZ1)	(RZ1)			RZ1	RZ1
Command	x	x	x	x	x	x			x	x	x	x		4	3	5	5	17	RZ1	RZ1	(RZ1)	(RZ1)			RZ1	RZ1
Voice internal	x	x	x	x	x	x					x	x		5	1	5	5	16	RZ1	RZ1	(RZ1)	(RZ1)			RZ1	RZ1
Voice external	x	x	x	x	x	x					x	x		3	1	5	5	14			(RZ1)	(RZ1)			RZ1	RZ1
Video	x	x	x	x	x	x		x		x	x	x	x	1	1	3	3	8							RZ1	RZ1
Monitor comm points		x		x			x				x		x	3	1	3	3	10					(RZ2)	(RZ2)	RZ2	RZ2
abort																										
Monitor abort warning	x					x								5	2	5	4	16	RZ1	RZ1	RZ1	RZ1	(RZ1)	(RZ1)		
Manual abort actuation	x					x								5	5	5	1	16	RZ1	RZ1	RZ1	RZ1	(RZ1)	(RZ1)		

Figure 13.4: FAMT Red indicates highest RZ/CRT (1) while green indicates lowest

As the vehicle shall be capable of operating autonomously the addition of astronauts to the vehicle requires that all the vehicle functions can be monitored and operated manually from the vehicle as a matter of crew safety. This requires certain crew training. Looking at the Shuttle operation it

was only required that the commander was an experienced astronaut, while both the pilot and flight engineer were trained for the task but did not have flight experience. As can be seen the operation of a vehicle such as Charon requires quite a few tasks to be done. Under Earth operating conditions there would be a significant amount of people monitoring the subsystems, however, as mentioned in Subsection 15.10.1 there is a comparatively small ground staff for the operation of Charon. It is therefore deemed necessary for the vehicle to have a flight engineer to monitor the performance of subsystems for anomalies. Its is possible that over the next 20 years the efficacy of autonomous control has evolved to a point where astronaut intervention is no longer a safety requirement. However it has, since the start of human spaceflight, been required to have people capable of performing all the tasks performed by the computer in case of an emergency. Therefore all three roles are deemed necessary for the flight. It can be assumed that people will be trained for these roles by the organisation sending them to Mars. as can be seen in Figure 13.4 the large majority of functions should be located in RZ1, requiring a quite advanced cockpit. It is recommended that a state of the art Glass cockpit like the ones used on Space X Dragon or Orion. In addition all commands should be reachable in a constrained position so a combination of joysticks, buttons and pointing devices should be placed on the astronaut armrests. This discussion concludes that **SRV-TECH-OPER-7.1** is verified.

13.6. Risk Analysis

The following risks have been analysed and mitigated as part of the C&Dh subsystem:

- **SRV-RISK-CDH-1** Computer failure (P=2), results in total loss of commanding in the vehicle (I=5).
  - Probability mitigation (P-1): 4 computers in the capsule provide high redundancy.
- **SRV-RISK-CDH-2** Critical software errors (P=3), results in wrong in-flight calculations (I=5).
  - Probability mitigation (P-2): use flight proven and redundant computer systems.
  - Impact mitigation (I-2): crew manual override or vehicle commanded from the ground.
- **SRV-RISK-CDH-3** Sudden processing errors (P=4), results in errors in spacecraft commanding (I=3).
  - Probability mitigation (P-2): processors are equipped with watchdogs that can reset and reboot the system when errors occur, system redundancy.

From this list, a mitigated risk map has been created. It can be seen in Table 13.1.

Table 13.1: Risk map of the C&DH subsystem, after mitigation

	Very unlikely (1)	Unlikely (2)	Possible (3)	Likely (4)	Very likely (5)
Very high impact (5)	1				
High impact (4)					
Medium impact (3)	2	3			
Low impact (2)					
Very Low impact (1)					

The event of computer failure still remains in the red zone, as this would mean the spacecraft is no longer controllable. However, with 4 flight computers in the capsule and 2 in the propulsive stage, enough redundancy is available to ensure that the probability of this event is sufficiently low.

14

Abort System

With Charon's capsule sized, the abort system has been designed. This system is critical to the safety of the crew, as it offers the means of escape in case a failure would lead to the vehicle becoming hazardous.

Section 14.1 describes the inputs that were used to size the abort system. Section 14.2 then assesses all of the different abort modes of the vehicle. With the abort modes assessed, the abort engines and deceleration methods have been designed in Sections 14.3 and 14.4. The method for rescuing the crew after landing is then discussed in Section 14.5. Section 14.6 then presents a safety discussion of the abort system. Finally, the effects of the abort system on the other systems and the sensitivity of the abort design are presented in Sections 14.7 and 14.9.

14.1. Analysis; Inputs and Outputs

The main input of the abort system is the capsule mass. However, as the abort system contributes to the capsule mass, it was required to know the mass of all of the capsule components. The sum of their mass is 9117 [kg]. An iteration was required to size the abort system, as it has to propel its own mass in case of abort, in addition to the mass of the capsule. In the end, the capsule has a mass of 14230 [kg], abort system included.

Another input required for the abort system is the vehicle mission profile: the ascent and reentry simulation profiles were used to assess the conditions of the critical abort modes.

14.2. Abort Modes

Throughout the flight of the vehicle, different abort modes have been assessed, depending on the related flight phase. In these sections, each phase is defined, and the respective abort mode is developed.

14.2.1. Escape to Surface During Ascent

This phase of the flight starts as soon as the crew is inside of the capsule, that it is locked, and that they are properly connected to life support. The abort system is then armed, and any catastrophic event would separate the capsule from the vehicle, even from the pad. This phase then stops when the Mach number is above 8, as required from Apollo abort modes [107, p.7]. This upper limit on the Mach number allows for the detached capsule to slow down enough into the atmosphere before getting to the ground.

The requirement for the engine thrust flows from the fact that the capsule needs to be at a velocity of 225 [m/s] from the vehicle in 3 seconds, as for Orion [108, p.15]. This means that, taking into account the contribution of the Martian gravity, the abort engine shall provide an acceleration of 78.8 [m/s^2]. In term of Martian g, that would mean that the crew will be subjected to 21 g_{Mars}. However, their body will still be used to the Earth gravitational acceleration, so it is fair to assume that they would resist the load of 8 g_{Earth} without being injured [109].

This flight phase is the most demanding case for the abort engines, as they have to propel the capsule away from the vehicle, and perform a propulsive landing. Indeed, all other flight phases will later require fewer thrust, and fewer propellant. The two most critical times from the abort to surface during the ascent phase are abort from the launch pad, and abort at Mach 8. With the abort system being capable of handling these two scenarios, the crew could abort at all time from the launch pad to Mach 8.

Abort from the Launchpad

Even if the capsule needs to abort from the launch pad, it needs to get to a high enough altitude so that the deceleration systems later described in Section 14.4 can operate as intended. To ensure this, a simulation of the capsule accelerating from the pad, reaching its maximum altitude, and deploying its parachutes has been conducted. All simulations from this chapter have utilised the trajectory simulation tool developed in Section 5.4.

This simulation can be seen in Figure 14.1. It can be seen in Figure 14.1a that the maximum altitude of the capsule would be of 5.9 [km], and that the capsule would get to ground level at a velocity of 98 [m/s]. However, the abort system would still have enough propellant for a propulsive landing of up to 178 [m/s]. It can also be seen in Figure 14.1b that there are two vertical spikes in the acceleration at 68 and 97 seconds after abort initiation. These represent the deployment of the drogue chutes, and of the main parachutes, opening at a dynamic pressure of 10 and 100 [Pa] respectively. Finally, the simulation showed that, requiring from the RCS system to keep the capsule at 5 [deg] from the vertical, the capsule will touchdown at 2 kilometres from the pad. This would thus not require a complex rescue, but would steer the crew away from the hazardous launch pad by a sufficient distance.

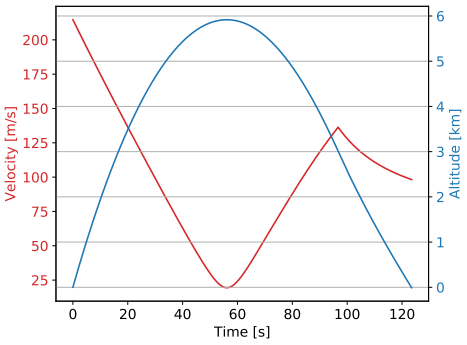

(a) Simulated velocity and altitude

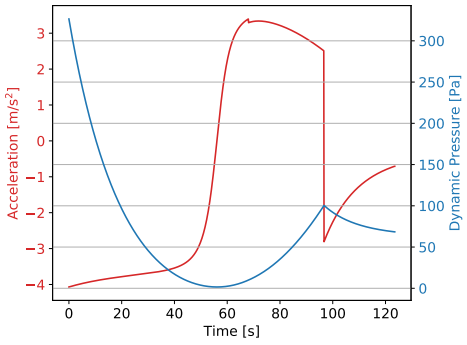

(b) Simulated dynamic pressure and acceleration

Figure 14.1: Simulation of the capsule during abort from the launch pad

Abort at Mach 8

The maximum Mach number that the vehicle shall have for the abort system to safely land the crew on the surface is 8. Beyond that limit, the velocity of the capsule would be too high, and the atmosphere too thin for the abort system to be able to slow it down by means of parachutes and propulsive landing.

Similarly as for the abort from the launch pad, a simulation of the launch abort at Mach 8 has been carried. This Mach number is acquired 86 seconds after liftoff, at an altitude of 37.7 [km] and a velocity of 1644 [m/s].

During this abort mode, the drogue chutes would deploy 106 seconds after abort initiation, once the capsule starts falling back to the ground, at a dynamic pressure of 850 [Pa]. The main parachutes deploy 28 seconds after, at a dynamic pressure of 922 [Pa]. These deployments can once again be seen by the vertical spikes in acceleration in Figure 14.2b. The maximum acceleration that the crew is going to feel from the main parachute opening is of about 6 g_{Earth}. From Figure 14.2a, it can also be observed that the capsule will get at ground level with a velocity of 95.5 [m/s]. Hopefully, the abort engines can decelerate it as they still have propellant for a 178 [m/s] landing burn.

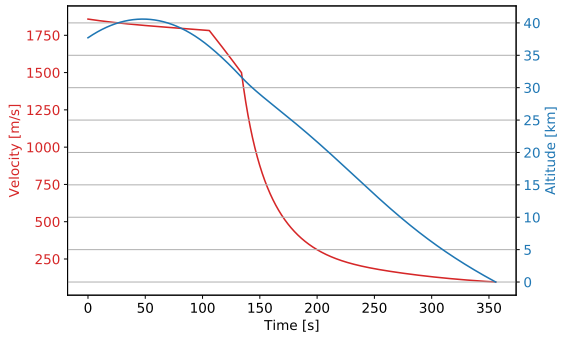

(a) Simulated velocity and altitude

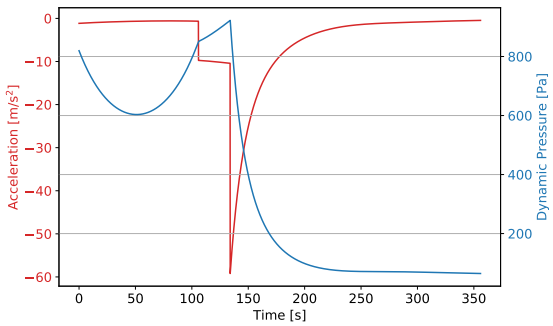

(b) Simulated dynamic pressure and acceleration

Figure 14.2: Simulation of the capsule during abort during ascent, at Mach 8

14.2.2. Escape to Orbit During Ascent

Once the Mach number is increased over 8 during ascent, abort to surface is no longer possible. The possibility of abort to orbit has thus been assessed.

The minimum orbital height that the capsule should reach after abort to orbit has been simulated. Assuming that it would take a maximum of 4 days for another vehicle to get from the station to the capsule, and dock with it to transfer the crew, a simulation of the orbital decay due to atmospheric drag has been conducted.

Progressively reducing the orbital altitude by increments of 5 kilometres, it has been found that an orbital altitude of 170 [km] would offer the capsule a time in orbit of 4.12 days. Below this altitude, the capsule would reenter the atmosphere in less than 4 days.

Figure 14.3 shows the simulation that was carried. It shows the orbital altitude of the capsule decaying due to the atmospheric drag.

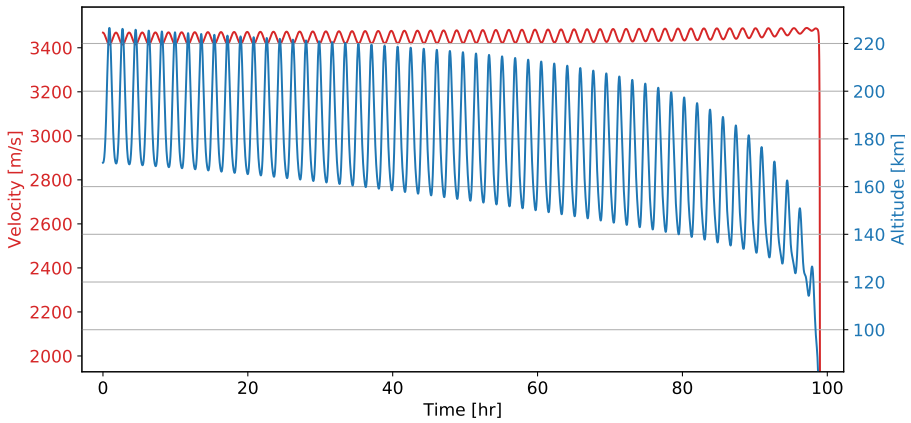

Figure 14.3: Simulation of the orbital decay after abort to orbit

To get to this altitude of 170 [km], at abort just after Mach 8, the capsule would need 3468.7 [m/s] of ΔV. Using the vacuum I_{sp} of the abort engines from Section 14.3, this velocity increment would require 12,450 [kg] of propellant. This is deemed too high to be included in the capsule for an abort to orbit capability.

This means that Charon will not have the capability of aborting the launch during its ascent after Mach 8. However, this is not deemed as a high safety issue, as the maximum dynamic pressure experienced by Charon during the launch will be 54 seconds after lift-off, 32 seconds before Mach 8. It can thus be assumed that, after Mach 8, the need for an abort system is considerably lowered as the structural load will be considerably decreased, and the engines will have performed nominally for 86 seconds.

14.2.3. Escape to Orbit Before and after Docking

Abort is possible again once Charon reaches the phasing orbit, and up to 1 [km] away from the station. At all times during this flight phase, the vehicle shall point the capsule away from the station, so that abort could be triggered without the need for the vehicle to rotate first.

In this abort mode, the capsule would detach from the vehicle and first use 1200 [kg] of propellant to increment the velocity of the capsule by 225 [m/s]. This will thus increase the orbital velocity of the capsule. Half an orbit later, the capsule will use most of the 1133 [kg] of propellant left to circularise its orbit.

As the vehicle will be left behind the capsule, possibly on the same orbit as the LMO node, this causes issues for the space station. To ensure that the station does not suffer from any damage caused by a catastrophic failure from the vehicle, the orbit of the LMO node will thus be increased as soon as the abort has been initiated. Potentially, this orbit could be lowered again later if the vehicle does not present a threat anymore; if it was still capable of autonomously either go to a graveyard orbit, or impact a graveyard on Mars with high velocity, or even better land by itself on Mars.

Later, another Charon docked to the LMO node would thus need to rendezvous with the capsule

containing the crew in orbit. It would thus either rescue the crew and land on Mars, or dock to the space station.

14.2.4. Escape to Orbit Before Reentry

Once the reentry burn is completed, Charon will be at an orbital altitude of 500 [km], and an orbital velocity of 3057 [m/s]. This configuration is meant for Charon to reenter the atmosphere, effectively slowing it down up to landing. For the abort system to prevent this atmospheric reentry, it has to increase the orbital altitude enough for the vehicle to orbit Mars for 4 days before reentry.

To achieve this, the same orbit as the one described in Subsection 14.2.2 is needed. A simulation of the capsule aborting Charon at different altitudes has been generated, each time decreasing the abort altitude until the capsule would be in this orbit. This prevents the atmospheric drag from decaying the orbital altitude of the capsule back to Mars within 4 days. From the simulation, the lowest altitude for which abort before reentry is possible was found to be 246 [km].

The capsule would thus abort from the vehicle 19 [min] after the reentry burn, and use 80% of its abort propellant to increase its orbital velocity by 365 [m/s]. This would increase the periapsis of its orbit enough so that the atmospheric drag on its first orbit would not de-orbit it. However, the atmospheric drag would be too high for the capsule to stay in this orbit for 4 days. The remaining 20% of propellant would thus be used once the capsule reaches its apoapsis, to increase its orbital velocity by an additional 91 [m/s]. This would effectively increase the periapsis of the capsule and prevent a high atmospheric drag each time the capsule is at its periapsis.

These two velocity increments can be seen in Figure 14.4, at 0.32 [hr] and 1.3 [hr]. Once these two burns have been executed, the capsule reaches an orbit with a periapsis of about 250 [km]. This is much higher than the minimum 170 [km] discussed in Subsection 14.2.2, due to the high first burn required for the capsule to increase its orbital altitude before entering the atmosphere for the first time.

Finally, a more efficient orbital manoeuvre should be investigated. This better manoeuvre would increase the orbital altitude of the capsule at its first pass into the atmosphere by lowering the apoapsis. This would effectively place the capsule on the minimum 170 [km] circular altitude with two more efficiently used burns, allowing for the abort to orbit before reentry to be initiated longer after the reentry burn.

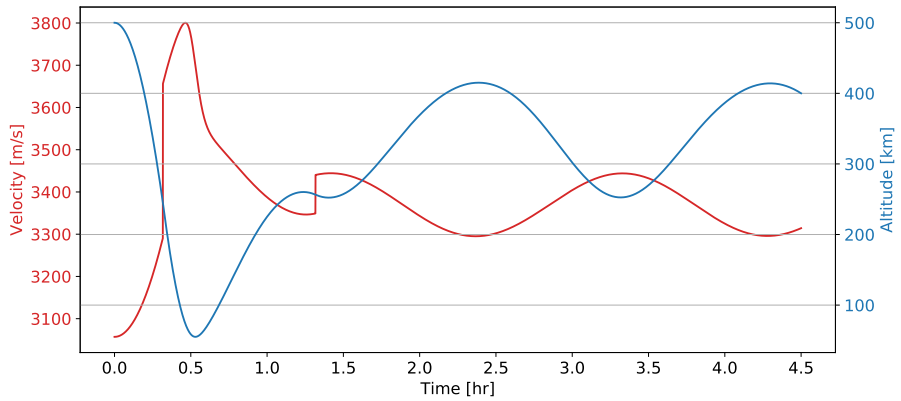

Figure 14.4: Simulation of the capsule altitude and velocity following abort from reentry

14.2.5. Escape to Surface After Reentry

Once the vehicle has bled enough velocity in the atmosphere, abort can be triggered again. This abort mode starts when the heat flux generated by the atmospheric drag gets lower than 2 [kW/m^2]. At this point, the vehicle will have a velocity of 1009 [m/s], at an altitude of 22.9 [km]. The end of this abort mode is characterised by the vehicle shutting down, and the crew disconnecting from life support. For this abort mode to be safe, Charon should never point below the horizon at the end of its reentry, and below 70 [deg] during the last landing phase. This is because the capsule has to escape to a safe altitude at all times.

Abort from such an altitude and at such a velocity, requires the drogue chutes and main parachutes to decelerate the capsule before landing. To ensure that these would be enough for the capsule to bleed enough velocity, a simulation similar to the one of Subsection 14.2.1 has been carried.

From the simulation, it appears that the parachutes only would be insufficient to decelerate the

capsule. It has thus been decided to increase the abort ΔV from 225 [m/s] to 300 [m/s], as this would slow down the capsule at high altitude, leaving more time for the parachutes to bleed out more velocity.

Following the abort burn, the drogue chutes would then deploy at a dynamic pressure of 450 [Pa], followed by the main parachutes at 350 [Pa], 24 seconds later. This can be seen from Figure 14.5b. From Figure 14.5a, it can be observed that the simulated velocity at touchdown would be of 93 [m/s]. Hopefully, the abort system would still have enough propellant for a landing burn of 106 [m/s].

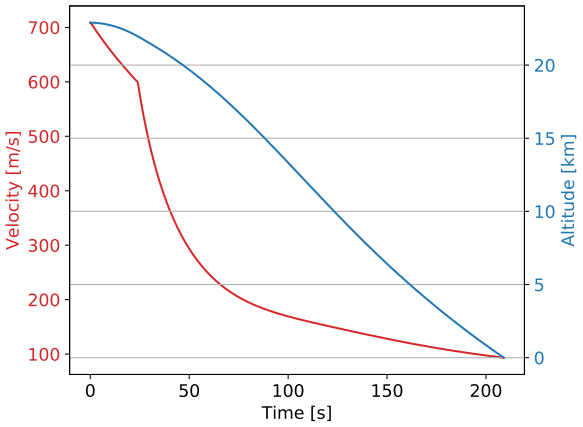

(a) Simulated velocity and altitude

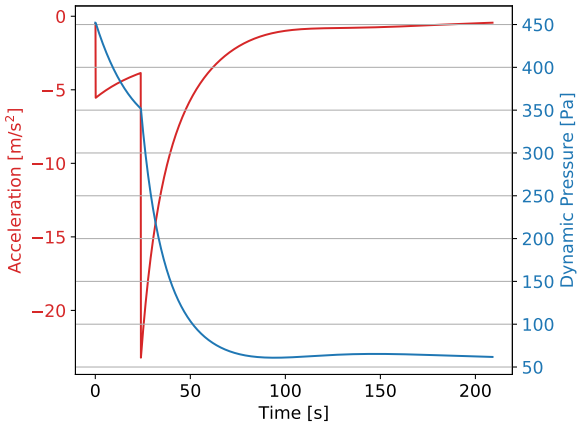

(b) Simulated dynamic pressure and acceleration

Figure 14.5: Simulation of the capsule during abort after reentry

14.3. Abort Propulsion System

From Subsection 14.2.1, it has been computed that the abort system shall provide an acceleration of 78.8 [m/s^2]. With few mass iteration of the complete capsule system, its final mass was computed to be 14,200 [kg]. This means that the thrust provided by the abort engines shall be 1065 [kN].It has been decided that the engine configuration shall be of 3 clusters of 2 engines, placed at 120 [deg] from each other. A number of combustion chamber of 6 was decided upon, as to diminish their footprint. Taking into account that the engines are going to be parallel to the side of the capsule, hence inclined at 20 [deg], the thrust provided per engine shall be of 189.04 [kN].

To size these engines, the Rocket Propulsion Analysis software (RPA)[1] was used. As explained in the midterm report [2], the propellant used by the abort system is a mixture of Hydrogen Peroxide for the oxidiser, and of Hydrazine for fuel. This mixture allows for fast ignition, as it is self-igniting, and allow for a pressure fed combustion cycle, meaning that there is no need for turbo-machinery, making the operation of the abort system faster. Also, the chamber pressure was set to be of 7.25 [MPa], at 20% higher than SpaceX's SuperDraco engines. Finally, the engines have been optimised for an atmospheric pressure of 500 [Pa], which represents an altitude of about 5 [km] on Mars, and the throat to exit ratio was decided to be of 2.5, thus minimising the footprint of the nozzle. Running RPA with these inputs, the engine parameters of Table 14.1 have been computed.

Table 14.1: Abort engine parameters

Parameter	Symbol	Value	Unit
Optimum specific impulse	$I_{sp_{opt}}$	221	[s]
Vacuum specific impulse	$I_{sp_{vac}}$	259.61	[s]
Mass flow	$\dot{m}$	74.37	[kg/s]
Mixture ratio	O/F	1.793	[-]
Chamber radius	R_c	164.65	[mm]
Throat radius	R_t	75.15	[mm]
Exit radius	R_e	118.83	[mm]
Engine mass	m_{eng}	118.83	[mm]

Following the engine parameters from Table 14.1, the total mass flow of the abort system is of 446.22 [kg/s]. Having a burn time of 3 seconds during abort, this totals to a propellant mass of

[1]RP Software and Engineering, `http://www.propulsion-analysis.com`, accessed the 2nd of June 2020.

1338.66 [kg]. On top of this, an additional 997.36 [kg] of propellant has been added, to allow for a propulsive landing capability of at least 175 [m/s]. These combine to a total propellant mass of 2336 [kg], from which 1499.6 [kg] is the Hydrogen Peroxide, and 836.38 [kg] is the Hydrazine.

As the abort propellant tanks both need to be kept at temperatures between 2 and 113 [°C], they will be placed in the same isolated volume as the crew, and thus be at a constant temperature of 20 [°C]. Also, the propellant will be kept at a pressure of 8.75 [MPa], 1.5 [MPa] above the chamber pressure, to ensure that the combustion does not backfire to the tanks. Given this, the Hydrogen Peroxide and Hydrazine tanks need to have a volume of 1.08 [m^3] and 0.83 [m^3] respectively. Using aluminium tanks, and a safety margin of 25%, the mass of the tanks are thus of 207 [kg] and 159 [kg], respectively.

It is important to ensure that the tanks will be kept at the designed 8.75 [MPa]. For this, Helium as pressurant is used. A mass of 37.7 [kg] is needed for it to be able to keep the oxidiser and fuel tanks at the same pressure. Keeping the required Helium in a tank at a pressure of 300 [MPa], the tank mass would be of 276.6 [kg] to accommodate for the 0.42 [m^3] of pressurant. To compute these tanks masses, the same method as in Subsection 8.3.3 has been followed.

While Helium is not producible on Mars, this is not an issue, since the abort system would presumably be used at maximum once during the lifetime of the vehicle.

Finally, the 3 tanks required for abort propulsion are placed in the capsule, under the pressurised volume containing the crew, but still within the insulated volume of the vehicle. They are located in such a way that, when full, the centre of gravity of the capsule is along its central line. They will thus not affect the equilibrium of the vehicle.

In summary, the abort propulsion system consists of a total mass of 425 [kg] for the engines and piping. In addition, the Hydrogen Peroxide has a mass of 1706.4 [kg], the Hydrazine of 995.4 [kg], and the Helium of 314.3 [kg], each including their respective tanks.

14.4. Deceleration Methods

As it has been developed in Section 14.2, parachutes are required from all abort modes for which the goal is to land the capsule on the surface of Mars. These parachutes are one of the ways used for the capsule to safely decelerate before getting the crew back to the surface of Mars.

Drogue chute

To begin with, the use of a hemisflo drogue chute [110] has been investigated.

This drogue chute can be used at a Mach range of 1.5 to 4, and offers a low shock and a drag coefficient of 0.35. It will be used as a first method of decelerating the capsule, before the main parachutes are deployed. The simulations described in Section 14.2 helped determine that a total number of 5 of these used simultaneously, at a nominal diameter of 10 [m], would be optimum. Deployed at a maximum dynamic pressure of 850 [Pa], as established in Subsection 14.2.1, each of these drogue chutes would experience a load of 66.7 [kN].

Main parachute

After the drogue chutes have deployed, they will detach from the capsule to lead to the deployment of the main parachutes. According to [110], they offer a drag coefficient of 0.55, and a medium shock following their opening. They have once again been sized during the simulations carried in Section 14.2, and a total of 3 main parachutes of a nominal diameter of 25 [m] offered a good combination for the required deceleration.

As described in Subsection 14.2.1, the main parachutes would open at a maximum dynamic pressure of 922 [Pa]. The maximum load per parachute would thus be of 452 [kN], below the maximum allowable load of this type of parachute [111, p.6-96].

An additional drogue chute and one main parachute will be added to this, as the capsule shall safely decelerate even in the event that one of these chutes would malfunction. From [111, p.6-95], the mass of one drogue chute is of 20 [kg], and the one of a main parachute is 30 [kg]. Having a total

of 6 drogue chutes, and 4 mains parachutes, and taking an additional 25% margin to account for the ribbons and ejection mechanism, the total mass of the parachutes is 300 [kg].

It is important that the parachutes do not interfere with each other once they are deployed. According to [112], having a clutter of up to 6 canopies deployed at the same time does not lead to interference reducing the parachutes performances.

Finally, it is also important to ensure that these fit at the top of the capsule. According to [113], parachutes have a pack density of about 640 [kg/m^3]. This thus leads to the drogue chutes taking a volume of 31 [L], and the main parachutes of 47 [L]. Putting these volumes in the CAD model of Charon confirmed that this deceleration configuration is realistic.

Propulsive landing and airbags

The final landing of the capsule after abort will be damped by five airbags. These are inflating under the capsule in such a way that, in the event that one of them fails, this system would still damp the majority of the landing load.

Taking the same landing velocity of $V_{\text{land}} = 7.85$ [m/s] as the airbag system studied for Orion [114], the suicide burn for landing shall bring the capsule at a zero velocity at $h_{V_0} = V_{\text{land}}^2/(2 \cdot g_{\text{Mars}}) = 8.3$ [m].

The landing burn in itself will use the abort engines, throttled at 25%, to have more control over the velocity, and give a more gentle landing to the crew. This means that the capsule will decelerate at 15 [m/s^2] during propulsive landing. Taking the case for which the landing velocity was the highest, 95.5 [m/s] from abort at Mach 8, the abort engines would thus need a burn time of 6.37 seconds.

Finally, this means that the abort engines need to start the landing burn 312.3 [m] above the surface, to have the time to decelerate the capsule to a zero velocity at 8.3 [m] from the ground.

14.5. Crew Rescue

During the first 3 seconds of the abort, the crew will experience an acceleration of 8 g_{Earth}. Added to the maximum 1.45 g_{Earth} experienced due to the main engine propulsion, this combines to an acceleration of 9.45 g_{Earth} that the crew will have to sustain. While this acceleration would not be lethal, the probability that one or more crew members would be at least lightly injured is high[109]. This means that, after landing, the crew should be rescued from the capsule as fast as possible.

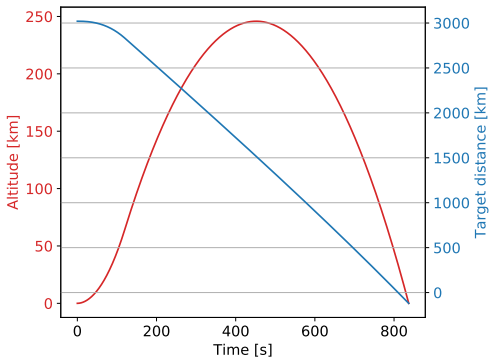

Figure 14.6: Simulation of a suborbital flight, as part of a rescue mission

In the worst case, after abort at Mach 8, the capsule would land at about 3020 [km] from the base. To rescue the crew at such a distance within 4 days, as required by the life support and power budget, a rover departing from the base would need to move at a velocity of 31.5 [km/hr]. This would be 26% higher than one of NASA's concepts for a crewed rover on Mars[2]. This velocity increase, while possible using Hydrogen fuel cells, would be at the limit of safety, due to the rocky surface of Mars. However, an un-crewed rover could be posted beforehand in the relative zone where the capsule would land after abort. This way, the crew could be rescued by the autonomous rover within the required time, and the rover would provide additional life support as well as a medical kit.

To get to the base faster than 4 days, the possibility of using a Charon that would launch from the base has been assessed. With this goal, a simulation has been carried to ensure that Charon could complete a sub-orbital surface to surface mission. A modified ascent profile has been setup for such mission: the vehicle would take-off at a tilt of 4 [deg], so that Mars' gravitational acceleration would accelerate it sooner as to increase the downrange.

From the simulation, a downrange of 3140 [km] could be attained by Charon with this mission profile, using 51,650 [kg] of propellant for the ascent. The propellant mass for the propulsive landing further has a higher estimate of 6000 [kg]. The vehicle would later need to complete the same mission

[2]Mars Rover to Help Visitor Complex Kick Off New Exhibit, NASA, `https://www.nasa.gov/feature/mars-rover-to-help-visitor-complex-kick-off-new-exhibit`, accessed the 11th of June 2020.

to return the crew back to the base. As the vehicle would be lighter, only 27040 [kg] of propellant would be required for ascend, and a higher estimate of 3000 [kg] for landing. This means that a rescue mission would require a total of 87,690 [kg] of propellant. With Charon capability to have about twice that amount of propellant, such rescue mission is possible. Figure 14.6 shows the simulation of the altitude of the vehicle and its distance from the crew to be rescued 3020 [km] from the base.

14.6. Safety Analysis

Now that all different abort modes have been evaluated, and that the engines and deceleration system have been sized, the safety of the abort system can be analysed.

The safety of the crew is first of all supported by the very existence of the abort system. It offers a final option in case the vehicle behaves catastrophically. Without this system, most events leading to LOV would otherwise directly lead to LOC.

The crew can utilise this abort capability at all time during the flight with the exception of 3 flight phases. The first one being during ascent from Mach 8 to the phasing orbit, as aborting ascent at a higher Mach number would not leave enough atmospheric density to slow down the capsule effectively.

The second section of the mission for which no abort is possible is when the Charon is closer than 1 [km] to the space station. At that distance, it will start the final docking manoeuvres, and orient itself towards the LMO node. If abort was to happen at this moment, the risk of the capsule colliding with the station would be too high.

Finally, the crew does not have any abort capability from 19 [min] after the reentry burn, up to a heat flux of 2 [kW/m^2], at an altitude of about 23 [km]. Before this, the capsule would not be capable of slowing down without being connected to the complete body of the vehicle.

The following risks have been analysed and mitigated as part of the Abort subsystem:

- **SRV-RISK-ABORT-1** Failure to detect need to abort (P=2), results in the capsule attached to hazardous vehicle (I=5).
  - Probability mitigation (P-1): multiple redundant sensors at all possible failure points, crew override.
- **SRV-RISK-ABORT-2** Abort engine failure (P=2), results in not enough thrust to detach from the vehicle or to land (I=5).
  - Probability mitigation (P-1): have an engine layout of 3x2 instead of 3x1.
- **SRV-RISK-ABORT-3** Suicide burn starting too early or late (P=3), results in capsule impact on the ground (I=5).
  - Probability mitigation (P-2): continuously compute the best burn time.
  - Impact mitigation (I-1): equip the capsule with additional airbags.
- **SRV-RISK-ABORT-4** Too high load (P=2), results in capsule structural failure, potential crew internal damage (I=5).
  - Probability mitigation (P-1): limit the engine thrust to 8 g_{earth}, and the parachute deployment to 1 [kPa].
  - Impact mitigation (I-2): equip the crew seats with shock absorbers.
- **SRV-RISK-ABORT-5** Parachute deployment failure (P=2), results in high energy impact of the capsule (I=5).
  - Probability mitigation (P-1): add an extra parachute of each type.

From this list, a mitigated risk map has been created. It can be seen in Table 14.2.

Table 14.2: Risk map of the Abort subsystem, after mitigation

	Very unlikely (1)	Unlikely (2)	Possible (3)	Likely (4)	Very likely (5)
Very high impact (5)	1, 2, 5				
High impact (4)	3				
Medium impact (3)	4				
Low impact (2)					
Very Low impact (1)					

As it can be seen from Table 14.2, most of the critical failures modes still have a very high impact, even after mitigation. This is due to the fact that the abort system is the most critical subsystem of

Charon, as it is the last hope of the crew to avoid LOC in case of catastrophic failure. Having no more backup system in case of failure, the failures of the abort system are expected to have such a high impact. For instance, if the abort engines fail, there is no more way for the crew to safely finish their mission.

However, while the picture depicted here may seem sinister, the probability of all failures modes of the abort system has been mitigated to the lowest possible level. And such mitigation has put strict constraints on the abort subsystem, so that the low probability of failure would compensate its high impacts.

Finally, as the abort system is only used in case the vehicle experiences a catastrophic failure, the probability that such failures are experiences are lowered even more. For these reasons, it is deemed acceptable, and expected, to have such high impacts in case of abort failure. The abort system is a last resort in terms of crew safety, meaning that the risks cannot be further mitigated.

14.7. Effect on Other Subsystems

In case of abort, the capsule will be separated from the rest of the vehicle. This means that all critical subsystems should be included in the capsule itself.

The CD&H, Communication and Life Support subsystems are thus all included in the capsule. In addition, the Power subsystem includes a redundant fuel cell in the capsule, in addition to the ICE power generation. Also, this subsystem includes the PDUs in the capsule itself.

Finally, the Communication subsystem also had to include a distress radio beacon, to localise the capsule on the ground after abort.

14.8. Verification and Validation

All simulations carried out in this chapter have been verified and validated as part of the V&V effort carried in Chapter 5. Additionally, the modifications that were required for parachute opening and propulsive landing were verified by setting inputs to artificially high values, and verifying their effects on the simulation. Finally, the propulsive landing calculations were also computed analytically for comparison.

14.9. Sensitivity Analysis

The abort system is mainly sensitive to the mass of the capsule. Indeed, the heavier the capsule, the heavier the abort system required to propel it away from the potentially hazardous vehicle. With the capsule mass increasing, the abort system mass increases linearly, due to the additional propellant mass required to keep the abort velocity increment the same.

15

Ground Operations

In this section, Charon's journey on the surface of Mars is followed to determine everything necessary for the vehicle to be operational and reusable within its life cycle. This includes the launchpad infrastructure, propellant manufacturing and energy requirements, maintenance and many other details deemed vital for this vehicle.

15.1. Requirements

The following requirements were needed to be complied with for the ground base:

- **SRV-CONS-TECH-1**: [S] Vehicle operations shall be non-hazardous for the Mars base.
- **SRV-CONS-TECH-5.1**: [T] The vehicle shall be able to conduct 10 launches before requiring extensive refurbishment.
- **SRV-CONS-TECH-5.2**: [T] Vehicle turnaround time shall not exceed 22 sols under nominal refurbishment.
- **SRV-CONS-TECH-5.3**: [T] Vehicle turnaround time shall not exceed 130 sols under extensive refurbishment
- **SRV-CONS-NONT-1**: [T] The required launch personal for a single launch shall not exceed 18 people.
- **SRV-TECH-MAIN-1**: [T] The required time for total refurbishment shall not exceed 40000 man-hours.
- **SRV-CONS-NONT-2**: [M] The combined cost of nominal refurbishment and extensive refurbishment for one operational period shall not exceed 20% of the cost of building and delivering a new vehicle.
- **SRV-TECH-PROD-1**: [S] 80 % of all consumables used by the vehicle shall be produced in-situ.
- **SRV-TECH-PROD-2**: [S] All parts that are not designed to survive the entire operational lifespan of the vehicle shall be producible in-situ.
- **SRV-TECH-MAIN-2**: [T] Nominal refurbishment shall be performed in a non-pressurised environment.
- **SRV-TECH-MAIN-3**: [T] Extensive refurbishment shall be performed in a pressurised environment.
- **SRV-CONS-NONT-3**: [T] The vehicle shall not require any storage infrastructure on Mars.

These requirements are addressed throughout the chapter, however, some need to be changed. As discussed later, Martian dust storms can be hazardous for the vehicle integrity, hence the requirement SRV-CONS-NONT-3 is changed to not require any pressurised storage, as the time is sufficient to transport the vehicle to a nearby facility for nominal refurbishment.

15.2. Analysis; Inputs and Outputs

Table 15.1 presents the inputs and outputs of the operations.

Table 15.1: Inputs and outputs of the relevant calculations

Analysis	Inputs	Outputs
Propellant Manufacturing	Propellant mass	Relevant component masses
Transporter and facilities size	Vehicle size	-
Flight without refurbishment time	Engine burn time	-
Energy requirements	Propellant mass	Propellant manufacturing power budget

15.3. Orbital Node

Before ground operations can be discussed, the orbital node has to be specified. This node is vital for the mission, as it affects the flight profile (and hence, the amount of propellant needed). The amount of crew and cargo that it can accommodate will affect the number of Charon launches. Finally, the functions of the node will affect the operations on the base..

15.3.1. Orbital parameters

As specified in the midterm report [2], the orbital node is located at an altitude of 500 [km] above the Martian surface. Seeing as the Mars base is located at a latitude of 42.5 degrees, a minimum inclination of 42.5 degrees is required to pass over the base. A further requirement is that the node passes over the Mars base approximately once every sol, to allow for a large number of possible launch windows and for the node to perform additional functions such as weather forecasts. Choosing the lowest inclination allows for less propellant use on ascent, making best possible use of the rotation of Mars. Equation 15.1 can be used to determine the number of days and orbits after which the same ground path is covered.

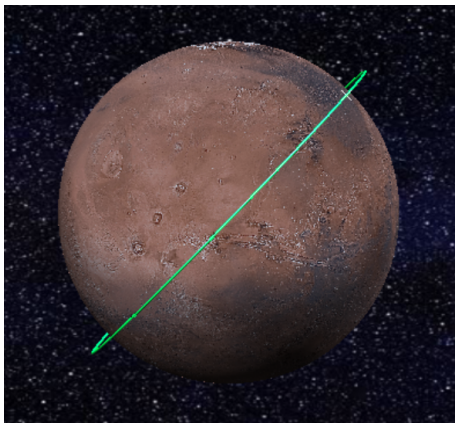

Figure 15.1: Orbit of the Martian node

$$j\,|\Delta L_1 + \Delta L_2| = j\left|-2\pi\frac{2\pi\sqrt{\frac{a^3}{\mu}}}{T_E} - \frac{3\pi J_2 R_e^2\cos(i)}{a^2\left(1-e^2\right)^2}\right| = k2\pi \quad , \quad \Delta L_1 = -2\pi\frac{T}{T_E} \quad , \quad \Delta L_2 = -\frac{3\pi J_2 R_e^2\cos(i)}{a^2\left(1-e^2\right)^2} \tag{15.1}$$

Where j is the number of orbits and k is the number of days. i is the orbital inclination and T_E is the time of one sidereal day. The inclination selected using Equation 15.1 is 44.96 degrees with a 1.02 Sidereal day repeat orbit. This orbit is visualised in Figure 15.1.

15.3.2. Capabilities of the Node

The node is assumed to be capable of docking three vehicles simultaneously (one coming from Earth and two Charons for redundancy). The vehicles coming from Earth are expected to carry about 100 people and 50 tons of cargo. Therefore, the node is assumed to provide the additional facilities and the capacity to process 100 people and 50 tons of cargo down to the Martian surface. As specified in subsection 15.5.4, the node is assumed to be able to perform some weather forecast in the region of Deuteronillus Mensae and to predict dust storm movement and severity in the region. The node is thus a very large station, that would most likely require an RTG to power. Since such a station would be huge, a case could be made that an artificial gravity setup, similar to Wernher von Braun's Gateway system could be designed. In that case, the station would be able to incorporate some production laboratories working in microgravity, such as medication.

15.4. Launchpad

First thing to consider is the launch infrastructure that Charon utilises. While Charon does not need a launch tower to launch, it does need some infrastructure due to large possible impact by dust particles on the vehicle. Therefore, dust and safety of Martian habitat are two things mainly considered for launchpad.

As discussed in the midterm report [2], the Martian base was chosen to be present in the Deuteronillus Mensae region in the Northern hemisphere of Mars, due to significance of scientific research on the river delta nearby and abundance of resources. As shown in Figure 15.3 made by NASA Reconnaissance Orbiter , this region has plenty of near-surface glacial ice, which makes it easier to mine such vital resource both for human needs and for the propellant manufacturing. Such location also proves a lot of

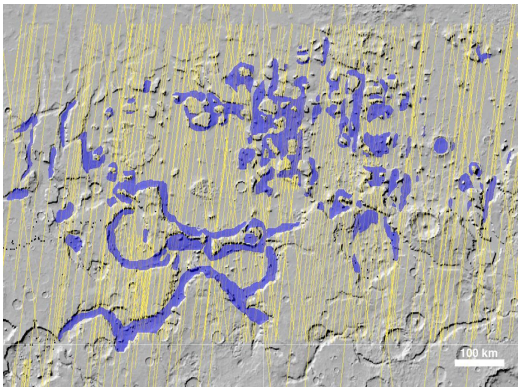

Figure 15.2: Location of sub-surface ice deposits near Deuteronillus Mensae[1]

[1] Ice deposits on Deuteronillus Mensae, NASA JPL, https://www.jpl.nasa.gov/spaceimages/details.php?id=PIA12861, accessed the 2nd of June 2020.

other advantages. It's elevation, being 3 kilometres below Martian sea level, gives the vehicle more time to slow down during descent to the Martian base. Additionally, regional topography is very suitable for a construction of a launch site with sufficient protection to the Martian habitat posed by hills.

As such, it was decided to build the launchpad in the crater located at 42.5 degrees North latitude and 25.5 degrees East longitude, visible in the picture below with a lizard-shaped hill in the centre of the crater, as seen in figure Figure 15.3. This location allows for easy access to the crater without high slopes, allowing for construction of two landing pads in the crater and a launchpad on a slope on the lizard hill itself. Moreover, the nearby hills could serve as a natural protection from any debris for the Martian base located nearby, opposite of the launch direction. The crater diameter of almost 20 kilometres allows sufficient spacing between launchpad and landing pads with an appropriate safety zone from the habitat, assumed to be located somewhere behind one of the red-marked hills in figure Figure 15.3.

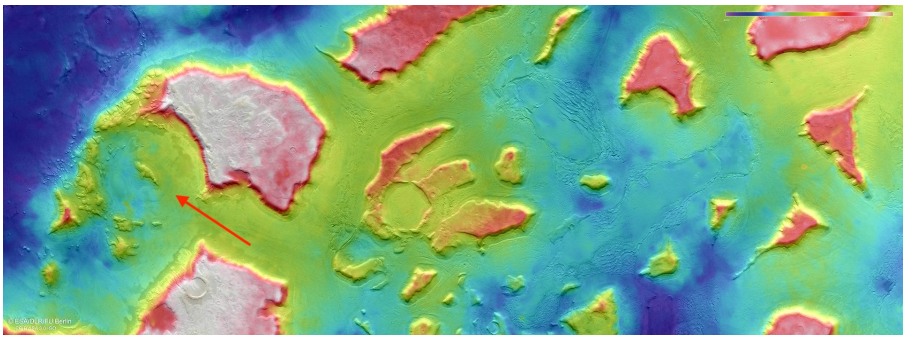

Figure 15.3: Topographic map and proposed location for Martian base

The three pads could be constructed of sulfur concrete, which is producible on Mars[115] and is assumed to be manufactured before Charon's operational use. Additionally the launchpad is equipped with propellant fuelling and other umbilical cords from a nearby storage facility. The launchpad would also have some solar arrays that could deliver power to the rocket while it is on the launchpad. Using values from section Section 15.7, the estimated area for such solar arrays is 39.5 [m^2] (assuming the 7.8 [kW] requirement), constructed on the elevation as well to have them out of shade. A battery storage facility could also be accommodated to have more energy stored in case of an emergency (or night-time launch).

The location of the habitat is assumed to be 40 [km] back-range, behind the mountain North-East of the crater. This was done to protect the habitat in case of launch failure as much as possible, while also considering the transportation costs. Due to rough terrain and additional life support and power systems, any vehicle transportation on Mars will be much slower than on Earth, with an average distance travelled assumed to be 10 kilometres per hour on a plateau. Therefore, even though back-range safe distance is usually considered bigger on Earth, and a more detailed debris-analysis was not available for Charon at this time, the trade-off between safety and logistical constraints had to be made, further assuming that the steep mountain near the base would provide sufficient protection. The crew will still be advised to stay inside the habitat for the whole duration of launch.

15.5. Transportation, Crew and Cargo discharge

15.5.1. Crew and Cargo Discharge

The first consideration after the vehicle has landed is getting the crew and cargo out of the vehicle safely. A few types of disembarking were considered. These were: a movable stairway, a pressurised sleeve connected to a nearby building (possibly a manufacturing facility), a ladder with a separate crane to take the cargo out, and a pulley elevator system on the spacecraft itself.

A pressurised sleeve can be considered unfeasible due to necessity to build long sleeves to nearby facilities from multiple landing spots. A movable stairway would require an additional motorised vehicle to be assembled, which adds unnecessary complexity. Some initial estimations were performed for the pulley elevator system. It was established that a motorised elevator capable of moving a 1000 kilograms up and down the height of the vehicle in less than a minute would utilise less than 3 kW of instantaneous peak power when accelerating. This was deemed feasible, however, such an ele-

vator would need at least a few square meters of platform size. Due to structural vulnerability it was decided that it couldn't be extended from below the capsule and that it also was impossible to extend such a platform from the capsule hatch due to its size, computed in Chapter 10. It was decided that the best option is to have a simple ladder for the astronauts, while a crane, which is used to later transport the vehicle to the manufacturing facility, discharges the cargo to the motorised crew and cargo transportation vehicle.

15.5.2. Crew Transport Vehicle

Many different crew transport vehicles have been so far proposed for Martian habitat, of which 8 open and pressurised vehicles were looked at [116]. Most proposed vehicles of this size are pressurised and have a cargo compartment at the back, powered by either a fuel cell or a small RTG. A similar concept has been suggested by NASA [117] and Mars Society Australia [118]. Interestingly, it plans to fuel the vehicle by Sabatier process with methane/oxygen combination in an IC engine. Further studies are needed to estimate the feasibility, as a huge methane plant will be primarily focused on Charon propellant manufacture, hence possibly leading to a need of an electrical engine powered by smaller solar array plant. Therefore, the methane consumption of this vehicle was not considered in the propellant production. Considering a 40 kilometre distance to the base that is needed for 6 people and cargo to be transported, it is thus more efficient to have multiple vehicles, each having 2-3 people on board as well as the cargo, thus allowing spare space for ground support personnel. Since the crew will be accompanied by launch support crew (discussed in section Section 15.10, a minimum of 3 vehicles with 4 people on board + 350 kilogram cargo capacity are considered.

15.5.3. Transportation

After landing, the vehicle is connected to the umbilical cords to drain all the fuel left, allowing for safe vehicle transportation to the refurbishment facility. Considering the transportation of the vehicle itself, with its dry mass of 33 tons, a few options were considered again: a single vehicle capable of lowering, clamping and transporting the rocket and get it back up once in a manufacturing facility, such as a Mobile Transporter-Erector-Launcher system used for Minuteman III ICBM; a double vehicle, with one part towing and the other erecting the system; a crane that would rotate the vehicle in-air and transport it, and finally, a stationary erector near launchpad with a rail system transporting the vehicle to the maintenance facility and back.

Any of these systems requires transporting another vehicle to Mars with a weight similar to Charon itself. Therefore, while mass was considered, the trade-off performed was mostly based on the performance. For instance, an MTEL used for ICBMs would not be useful, as a vehicle of this size would require more assembly equipment on Mars and would not be able to place the rocket on the launchpad. Moreover, transporting a rocket to the maintenance facility after landing would also be impossible with such vehicle [2]. Furthermore, there would be a need to redesign the engine to accommodate for fuel resources available on Mars. Quite similar considerations with respect to difficulty of assembly disqualified a double vehicle idea and an idea of multiple stationary cranes with a railroad assembly.

Therefore, it was decided that the best option for Charon would be a crane-type vehicle, capable of lifting and rotating Charon to a horizontal position and transporting it to the maintenance facility. The main advantage is that the same crane could be used to discharge cargo from the vehicle. While it would still have to be assembled from multiple parts, it allows for transportation of Charon in and out of the maintenance facility, as well as even lifting the vehicle inside of such facility to perform necessary refurbishment. Assuming some robotic arm being present on the base since the construction of initial habitat, an assembly of such vehicle seems least complex. Also it is comparable by weight to any other towing systems. Finally it is much better in transportation on Martian surface compared to regular transporter-erector systems.

15.5.4. Dust Protection

An important consideration for Charon on Mars is the dust storms, which impact the vehicle and its coating during the launch procedures or at any moment during transportation. While the location of the launchpad in a crater does provide some protection from frequent dust storms, these are still very possible, and some consideration needs to be put into protection against it. The first protection is

[2] Minuteman III TEL System, `https://www.globalsecurity.org/wmd/systems/lgm-30-tel.htm`, accessed on the 3rd June 2020

weather forecast. A Martian node itself, and a few reconnaissance orbiters on the planet would map a weather forecast for the area, protecting against launching or doing any operations during storms. If a storm or any smaller dust cloud was to appear during transportation or fuelling of the vehicle, some other protective equipment is necessary. For this, launcher transportation crane would have to load a protective cover over the vehicle. Many rockets on Earth are transported in a protective layer, so a similar plastic cover is thought to be suitable on Mars.

15.6. Propellant Manufacturing

In this section, the process for manufacturing the propellant for Charon is considered, along with its energy requirements. The section on energy will then sum those requirements and consider the energy production.

15.6.1. Water Mining

Multiple studies have been made on water mining on the Martian surface, utilising various methods from mechanical or electrical drilling [119] to jets of hot water melting the ice on the surface [120]. Considering that not all water at the location will be available on surface as seen in Figure 15.4 [120], a drilling method would be necessary. Further considering the amount of water needed for propellant, as well as Martian habitat requirements, the assumed production capacity is 220 tons of water in 83 days using 40 [kW] of power, allowing for fast propellant production.

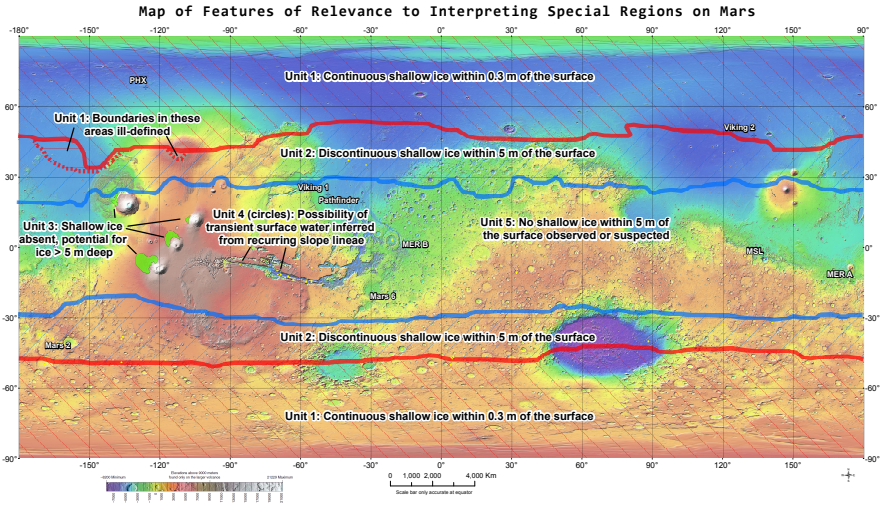

Figure 15.4: Ice deposits by average location under surface

170 tons of water is needed for the first launch propellant production, with around half of that needed for all subsequent propellant production. This leaves 50 tons of water for human use in the 83 days, the requirements for which will also increase with the amount of crew needed. Therefore, multiple mining setups are needed, ideally one fully devoted to Martian habitat requirements and a few more mining water for subsequent electrolysis and propellant manufacturing.

15.6.2. Manufacturing

Possibly the most important consideration of all ground operations on Mars, propellant manufacturing is vital for any mission on Mars, as it allows significant cost reduction and reuse of vehicle.

As mentioned in midterm report [2], the propellants used are Liquid Methane and Oxygen, produced through Sabatier reaction with subsequent water electrolysis. The reaction is described in [116] and its reaction formula is shown in Subsection 15.6.2.

$$CO_2 + 4\,H_2 \xrightarrow{400\,^\circ C} CH_4 + 2\,H_2O$$

It is initialised once the reactants are heated to 400 degrees Celsius over a nickel or palladium catalyst. As the reaction produces heat of 165 [kJ/mol], it is self-sustainable once such heat is achieved. A detailed design of the plant has already been considered [121] and lead to a similar design for Charon, with the setup being described in Figure 15.5.

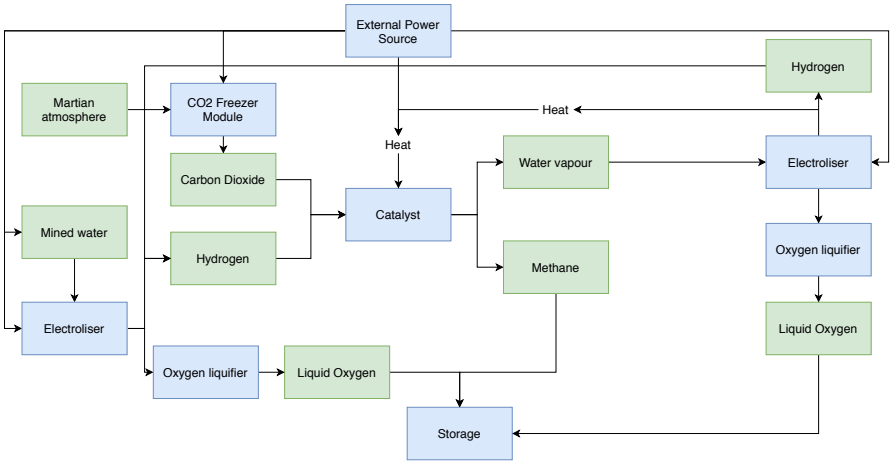

Figure 15.5: Sabatier plant overview (blue boxes consider infrastructure to be brought, green boxes indicate substances)

For calculations, this section contains values for one vehicle refuelling, performed over 130 days due to a limit in water mining and carbon dioxide capturing. The scale-up considerations are performed later in Section 15.8.

As has been calculated in Chapter 9, single launch of Charon utilises up to 38 tons of methane and 143 tons of oxidiser, including boil-off and thrusters. As will become evident from subsequent calculations, due to water electrolysis for initial hydrogen resources and subsequent water produced electrolysis, there is oxygen surplus produced, meaning that the reaction is methane critical. Masses of the sabatier reaction components are shown in Table 15.2.

Table 15.2: Sabatier reaction components and masses

Substance	Molar Mass [g/mol]	Total mass [tons]	No. of moles
Methane	16.0425	38.0	2368708
Hydrogen	2.01588	19.1	9474832
Carbon dioxide	44.009	104.2	2368708
Water	18.01528	85.4	4737416

Subsequent water electrolysis $2\,H_2O \longrightarrow O_2 + 2\,H_2$ produces 9.55 tons of hydrogen and 75.885 tons of oxygen. However, water electrolysis for initial hydrogen amount already produces 151.59 tons of LOX, enough for the launch. Since half of hydrogen is reused, less water will then be required to be mined for next propellant batch. Further water electrolysis produces 75.885 tons of liquid oxygen, which combined with 75.885 tons from the reaction, is sufficient for another launch and with a possibility to mine some more for reserves.

15.6.3. Carbon Dioxide capture

As can be noticed, the reaction requires 104 tons of carbon dioxide extracted from the Martian atmosphere. While the atmosphere does consist mostly of this substance, there are trace amounts of nitrogen, oxygen, argon and other substances, which need to be filtered out beforehand. A few methods exist for this, such as carbon freezing or absorption through porous materials [122], although temperature manipulation is most desirable due to high power requirements. While porous molecular sieves and membranes were suggested for carbon extraction, none of those are capable of producing such amount of carbon dioxide in a short notice, usually producing a few grams per hour. Carbon dioxide freezing requires less power than compression pumping and is more reliable and reusable than membrane-based carbon dioxide solution. Extrapolating from the Carbon Dioxide capturing system produced by NASA [121], which produces 88 grams of purified CO2 per hour at 500 [W], to produce 104 tons of carbon dioxide in 130 days (refurbishment time), or 802 [kg] per day, one would need 189.87 [kW], which is a significant power requirement.

15.6.4. Liquifying Oxygen

The products of the reaction are sent to storage, with oxygen first going through a copper tube, where it will cool down to an atmospheric temperature, usually -20 [°] to -100 [°C], to reduce the amount of

energy needed to liquify it. Copper has very good thermal conductivity, leading to fast cooling, and is of abundance on Mars, allowing fast production of new parts. [123]

Industrial oxygen liquifiers currently are capable of producing 2 tons of liquid oxygen per day using 300 kW of power [3]. While this does assume a room temperature of oxygen gas, using a specific heat of oxygen at constant pressure (assumed constant of 920 [J/kg K]), shows that cooling from 20 [°] to -60 [°C] of 2 tons of oxygen over a span of a day only requires 1.7 [kW] of power, deeming it an insignificant reduction in required power compared to the rest of power budget.

15.6.5. Boil-off considerations

Since production of methane is the limiting factor here, any boil-off of methane has to be prevented during the storage phase for fuel. For that, the solution could be in the boiling point. For methane, it is at -161.5 [°C] at 1 atmosphere pressure, whereas for liquid oxygen it is at -183 [°C]. One could thus store methane in liquid state in a tank inside a larger liquid oxygen tank, cooling the whole system. However, methane also has a solidification point of -182 [°C] at standard pressure, hence the system would have to be pressurised accordingly to have both oxygen and methane liquid. This can happen at any pressure above 5 [bar] [4], which does not pose many constraints on tank material.

15.6.6. Abort System and Thruster fuel

While the abort system is only used once in spacecraft and the fuel for it does not need to be produced on Mars, it is important to discharge the fuel from the vehicle for the maintenance purposes. Therefore, both hydrogen peroxide and hydrazine have to be stored on ground, with both of them needing room temperature for storage. For that, steel tanks would have to be imported from Earth, chosen for its low thermal conductivity of 45 [W/(m*K)] and relative small weight compared to other low thermal conductivity materials [5]. The tanks chosen for storage are identical in size to the ones used in Charon Chapter 8, having a surface area of 4.937 [m^2] for hydrogen peroxide and 7.408 [m^2] for hydrazine. Having those values, further assuming 20 [°C] storage and taking values for -60 [°] and -100 [°] (average and peak cold temperature on Deuteronillus Mensae) the values for power requirements were for peroxide 9 [kW] and 13.3 [kW] respectively, while for hydrazine these were 13.3 [kW] and 20 [kW].

A separate small plant will be made for production of hydrogen peroxide for thrusters. While trace amounts have been found naturally on Mars [124], production of 150 [kg] per launch for thruster operation would require a man-made plant. Hydrogen peroxide is manufactured from hydrogen and oxygen molecules, whereby hydrogen atoms go through a palladium catalyst to form an anthrahydroquinone [125], which is later oxidised to form hydrogen peroxide. To get this amount of peroxide, the amount of water needed was computed in Table 15.3.

Table 15.3: Hydrogen Peroxide reaction components and masses

Substance	Molar Mass [g/mol]	Moles	Mass [kg]
Hydrogen Peroxide	34.0147	4409.858	150
Hydrogen	2.01588	4409.858	8.89
Oxygen	32	4409.858	141.1
Water	18.01528	8819.716	158.89

This will produce waste 8.89 kilograms of hydrogen, which could be used for Sabatier plant. While water mining has already been accounted for, there is still need to take a look at electrolysis and heating for production of peroxide. As explained in section Section 15.7, water electrolysis is assumed to consume 286 [kJ/mol] and to have a 75% efficiency of the process. Assuming a production process of 65 days (half of 130 days refurbishment period), the power requirement for this is 0.6 [kW], small in comparison to main propellant production. While the exact power requirements for hydrogen peroxide

[3] Air Liquide LOX Producing System, `https://advancedtech.airliquide.com/liquid-oxygen-lox-plant`, accessed on 8th of June 2020

[4] Graphic representation of methane and oxygen state for varying temperatures and pressures, `https://www.engineeringtoolbox.com/oxygen-d_1422.html`, accessed on the 8th June 2020

[5] Conductivity of various materials, `https://engineeringtoolbox.com/overall-heat-transfer-coefficient-d_434.html`, accessed on the 8th June 2020

production are hard to estimate, one can assume from previous studies a 0.9 [g/kWh^1] energy yield [126]. Again assuming 65 day production time, the power required is mere 29.7 [W], hence a much faster process is possible with increased power.

15.7. Energy requirements

In this section, some more energy requirements for propellant production are considered, the total sum is then computed and different methods for acquiring this amount of power are discussed.

15.7.1. Heating

As was mentioned in Section 15.6.2, the Sabatier reaction requires carbon dioxide and hydrogen to be heated to 400 °C. Therefore, the power required to get those substances to this temperature is computed assuming carbon dioxide freezing temperature of -80 °C and hydrogen vapour coming out of electrolysis at temperature of 5 °C. The result of this can be seen in Table 15.4.

Table 15.4: Heating Sabatier reaction components

Substance	Mass [tons]	Isochoric specific heat [J/ (kg*K)]	Temperature change	Power needed [W]
Carbon dioxide	104.2	848.7	480	3800
Hydrogen	19.1	10.16	395	6.8

There is still a need to consider the electrical power required to break up water into hydrogen and oxygen. Theoretically, the water electrolysis can happen with 286 [kJ/mol] [127], however, steam reforming electrolysis (happening since our reaction will produce water vapour) can still only produce 74-85% efficiency. For preliminary power budget, a 75% efficiency is assumed. Water electrolysis for propellant manufacturing requires breaking apart 14.2e6 moles of water molecules, which assuming 286 [kJ/mol] energy, of output (at 75% efficiency), further assuming 130 days of production (many processes in production will run simultaneously, hence a standard period is chosen to have a reasonable estimation of power required) gives 482.5 [kW] of power required. This is by far the most power consuming process.

Finally, the Sabatier reaction itself releases 165 [kJ/mol], which is equivalent to 34.8 [kW] of power, of which further assuming methanation efficiency of 80%, 27.8 [kW] can be reused in the system.

15.7.2. Total Power Budget

Finally, the total power budget for production of fuel for one launch is generated in Table 15.5.

Table 15.5: Total Power Budget

Process	H2O Electrolysis	Sabatier reaction	H2O2 production	H2O2 electrolysis	N2H4 heating	H2O2 heating
Power [kW]	483	-27.8	0.03	0.60	20.0	13.3
Process	LOX plant	CO2 capture	CO2 heating	H2 heating	H2O mining	**Total**
Power [kW]	300	190	3.80	0.01	40.0	**1023**

Showing a total of 1.02 [MW] of power required constantly. Moreover, considering electrolysis, oxygen liquifying and carbon dioxide capture to be electrical processes, 972 [kW] of this power needs to be electrical, while 50 [kW] is thermal.

15.7.3. Energy Generation

In this subsection, the power generation methods are discussed. Considering Martian environment, which lacks fossil fuels and fast winds, three methods are discussed: solar arrays, nuclear power and geothermal power.

Solar Power

To generate this amount of power, a huge area of solar arrays is needed. Firstly, the solar irradiance on Mars is roughly equal to 590 [W/m^2]. However, considering instantaneous irradiance, its value G can be obtained using Equation 15.2[128].

$$G(ob) = 590 * [1 + e * cos(L_s - 248°)]^2/(1 - e^2)^2 \tag{15.2}$$

Where 590 [W/m^2] is the average value, e is the eccentricity of the orbit (equal to 0.093377 for Mars) and $(L_s - 248)$ is the true anomaly, with 248 being the areocentric longitude of Martian Perihelion. Since this value changes with orbit, the minimum value will be considered to determine the solar array

area needed. Such value occurs at cosine of -180, meaning that areocentric longitude is equal to 68 °. This gives minimum solar irradiance of 493.5 [W/m^2].

Current technologies cannot exceed 30% efficiency of solar arrays, however, there are reports of successful 40% efficiency array tests [6]. As such, considering the time of the mission to be in a few decades, 40% efficiency falls under TRL 4.

Finally, the area of solar arrays can be estimated by $A = P/(G * \eta)$ [116]. The power requirement is further doubled to account for no power at night. Thus, at minimum irradiance value, the area of solar arrays required is 10357 [m^2]. Moreover, the solar arrays would have to be placed in a non-shaded area, being quite far from the Martian base. Considering the dust storms on Mars that will require frequent array cleaning, and their life cycle of up to 25 years, solar arrays alone are not a realistic option for this design.

Nuclear Power

The 1 [MW] electrical power requirement immediately makes one consider a scaled-back nuclear power plant to provide the energy needs. While small scale projects exist on nuclear reactors on Martian surface [7], the mission concepts with a megawatt-rated nuclear power plant were suggested long time ago - both by Soviet Union [8], as well as NASA [129]. Such reactor would require 1.1 kilogram of Uranium-235. This could be either imported from Earth or found on Mars, where, although no hard-proven data exists, mathematical models predict an abundance of Uranium resources, as it predicts formation of already found radioactive potassium traces from the Uranium [130]. Therefore, while additional studies are needed on feasibility of uranium mining on Mars, a nuclear reactor of such scale is a realistic and highly probable concept for Martian base, as it is easier to construct and operate than 10,000 square meters of solar arrays.

Geothermal Power

Mars is a planet with rich volcanic activity in the past, yet it is currently very poor in terms of heat flow from its crust, estimated to be in the range of [mW] per meter squared [131]. While others [132] argue that the presence of localised hyper thermal areas cannot be ruled out, there is currently no evidence for any such area to be present anywhere on the planet, let alone within a vicinity of Deuteronillus Mensae. Furthermore, even if such location does exist, it would directly contradict the presence of glacial water on the surface, thus deeming the location unsuitable for Martian habitat. Therefore, until further information is present, geothermal activity cannot be considered as a possible heat and power source for Martian habitat.

15.8. Accelerating Production

As explained in Section 15.12, Charon will have 3 vehicles operational at all times, all of which need to be fuelled and ready for the launch at all times. This means creating multiple water mining setups, multiple carbon dioxide capturing and oxygen liquefying setups to facilitate the Sabatier reaction plant. Ultimately, it is safe to assume that the energy requirements for propellant manufacturing will increase linearly with the amount of fuel needed to produce, as the key drivers in power requirements (Water electrolysis, CO2 capture, LOX plant, water mining and substance heating) depend directly on the amount of fuel needed. Furthermore, setups such as the LOX liquifier have limited capacity, hence more setups with the same power requirement are preferred over costly scale-up. For 30 launches per operational period of 260 days, this means a 15 time increase in power output, which could be brought down to 10 times the power output if refurbishment period of 130 days is also included in the cycle. Therefore, the final power budget for propellant manufacturing is around 10-15 [MW], effectively requiring either hundreds of thousands of square meters of solar arrays, or a scaled-up nuclear reactor.

15.9. Refurbishment

In this section, the maintenance of Charon is discussed in terms of facilities, tools and time needed.

[6] Record breaking solar array efficiency, `https://www.popularmechanics.com/science/a32202373/solar-panel-record-efficiency`, accessed on the 9th June 2020

[7] Project Kilopower, `https://www.nasa.gov/directorates/spacetech/kilopower`, accessed on the 9th of June 2020

[8] Soviet Martian Mission Chronology, `https://www.energia.ru/en/history/mars/chronology.html`, accessed on the 9th of June 2020

15.9.1. Facilities

As discussed in the Midterm report [2], the vehicle has to be refurbished in a maintenance facility which is protected from the Martian environment, is capable of suspending a rocket to allow for engine disassembly and has all tools necessary for a fast maintenance. Moreover, such facility has to be within an aforementioned crater, to allow for fast transportation to and from the launch/landing pads, while also needing a connection to a source of power. For this reason, the facility is planned to be located in the south-east of the crater, right next to a mountain, while also being close enough to a power plant somewhere between the crater and the base. A facility is planned to be at least 50 meters wide, to contain a vehicle in horizontal position, while also having enough room to disassemble the engine and perform any work necessary. Moreover, the vehicle would only occupy one side of the facility, the other being then left for machines and other necessary equipment for part manufacturing and assembly. Lastly, facility size needs to account for a transporter crane to enter the facility, lower the rocket on a platform and switch crew and cargo-only capsules. A few clamps underneath the rocket would fix it in the position, and would be located at places that do not require direct access, such as in a few places near fuel tanks.

15.9.2. Tools

As mentioned previously, the vehicle requires some tools for maintenance. It requires clamps to hold the rocket, as well as forklift and suspension system for a disassembled engine. Afterwards, equipment for cleaning the engine is necessary, as well as various sensors and cameras to perform checks for cracks and displacements. Some basic tools are needed to fix any displacements, mainly in turbo pumps, while some machinery, like lathes and mills, are required to produce some of the parts to be replaced. Moreover, 3D printing machines are required for the same reason. All of those machines then required a connection to the power grid, achieved by cable connections to either a solar array plant or the nuclear power plant. Given that such tools would be used for all of Charon vehicles, it is safe to say that the requirement on refurbishment cost not to exceed 20% of total Charon cost (so approximately a 100 million US Dollars) is complied with.

15.10. Personnel Considerations

In this section, the amount of manpower needed for Charon operations is discussed. The section is further split into launch procedures crew and the maintenance crew, giving a preliminary overview of requirements needed for such vehicle to work.

15.10.1. Launch Crew

Any rocket launch on Earth requires hundreds of people working outside of the vehicle. On Mars, Earth assistance during the launch is impossible due to long signal delay, hence a much higher degree of automation is required. Nevertheless, some crew will still need to oversee the launch procedures, making sure that they are done correctly and safely. Therefore, assuming all of fuelling, rocket raising and pressurisation of tanks is automated, the vehicle launch will be supervised by a Launch Director, a Test Director with tank test and support test managers, a launch processing system coordinator, safety console coordinator, ground launch sequence engineer, as well as five subsystem specific controllers: communications, propulsion, guidance and navigation, electrical/environmental and maintenance/mechanical supervisors. Depending on the exact system configuration, some of those tasks can be merged under one position, hence the required personnel for the launch supervision will be ranging from 8 to 12 people, primarily focusing on checking whether automated systems are behaving correctly. Additionally, 4-6 people are assumed present at the launchpad to help astronauts get seated and prepared for launch and driving the Martian transporter vehicles away from the launchpad.

15.10.2. Maintenance

The Space Shuttle, the first reusable space vehicle, had an estimated 750 000 labour hours of refurbishment before every flight. [9]. While it is difficult to estimate the actual amount of hours needed for the vehicle refurbishment before its construction (the same Space Shuttle only planned 2 months of refurbishment between every launch), some considerations can be made. Firstly, Charon is 10 times lighter than the space shuttle, which can be assumed in linear proportion with the labour hours due

[9] Processing the shuttle, NASA, `https://www.nasa.gov/centers/johnson/pdf/584723main_Wings-ch3b-pgs74-93.pdf`, accessed the 29th of May 2020

to lighter system disassembly, part manufacturing and lowered complexity. Moreover, unlike Space Shuttle, Charon does not need any heat shield refurbishment, which is the most difficult part of such repair. Furthermore, the designs are separated by over 40 years of technological advancements (and even more considering the beginning of operational time), hence leading to a much higher automation of the process. Many inspections can be done with a computer aid, many parts, such as landing legs, the skirt and truss structure can be 3D printed. Therefore, total man-hours of refurbishment can be reduced to 20-40 thousand, which assuming 130 sol work period and 8 hour workdays, implies a crew of 20-40 people, with a possible addition of a few to account for days off and sick leaves. Another point needed to consider is the amount of launches before an extensive refurbishment is required. While the exact number of launches is difficult to estimate without extensive fatigue testing of structures and the engine, an assumption is made that a vehicle will be able to perform 10 launches with only quick visible checks and refuelling. This roughly corresponds to 4000 seconds of total Charon engine burn time, which is already a requirement for some currently built engines like the Vulcain engine family [133]. Each of these vehicles would have to perform a short refurbishment, including visual checks and basic engine cleaning. Assuming a 260 sol period, with 10 launches per vehicle, this gives a 26 sol land-refurbish-launch period, 4 of which are taken for the mission, and 22 for inspection, cleaning and refuelling.

15.11. Launch Number

Estimating from the size of the colony needed to facilitate such launches (both in terms of crew as discussed in section Section 15.10 and the power requirements, it is fair to assume that the amount of crew and cargo needed to transport in one operational period is roughly equal to what is planned to be transported in SpaceX Starship - 100 people with around 50 tons of cargo [134]. This means, that having 6 people and 400 kilograms of cargo on board per launch, Charon will need 17 trips to transport all personnel down. Within these 17 trips, people can also be transported up to the station. Some additional trips will have to be added as people might want to be transported both up and down in one operational period, which adds an additional estimated 5 trips. Further assuming cargo-only missions to take 9-10 tons of payload, 5 launches would have to be made to transport all cargo down to surface. Additionally, some cargo can be moved to orbit within these missions to provide provisions and other items for the present crew. This is therefore assumed to increase the required amount of trips by another 5. With a total of 27 launches per operational period, keeping around 3 more launches planned in reserve, this brings the total flight amount to 30 launches, with 10 launches conducted by a vehicle during the operational cycle. As such, three vehicles need to be operational at all times, of which one would have a cargo capsule, and two for crew.

15.12. Vehicle Fleet

During the life-cycle of Charon, many unforeseen circumstances, not necessarily related to the vehicle, may happen. Since the vehicle will be operational on Mars, to have the possibility of saving crew members a need for a fleet of multiple vehicles arises. After considerations with the client, it was determined that one needs to account for at least one vehicle being in orbit, one ready for launch if the need arises, and one in maintenance at all times. However, these considerations can be expanded further, as a possibility of rescue mission abort is also present, hence requiring another backup vehicle. Moreover, if some vehicle needs rapid refurbishment before the part can be manufactured (or if it cannot be manufactured at all), a need for another vehicle, used for scrap parts, arises. This brings the total number of the initial vehicle fleet to 5 vehicles, which can later be increased to account for a growing Martian colony.

15.13. Requirement Compliance

Table 15.6: Requirement compliance for ground operations

Requirement	Completion	Determination	Requirement	Completion	Determination
SRV-CONS-TECH-1	✓	Section 15.4	SRV-CONS-NONT-2	✓	Section 15.9
SRV-CONS-TECH-5.1	✓	Section 15.11	SRV-TECH-PROD-1	✓	Section 15.8
SRV-CONS-TECH-5.2	✓	Subsection 15.10.2	SRV-TECH-PROD-2	✓	Section 15.9
SRV-CONS-TECH-5.3	✓	Subsection 15.10.2	SRV-TECH-MAIN-2	✓	Section 15.9
SRV-CONS-NONT-1	✓	Section 15.10	SRV-TECH-MAIN-3	✓	Section 15.9
SRV-TECH-MAIN-1	✓	Subsection 15.10.2	SRV-CONS-NONT-3	×	Section 15.9

16

Vehicle Layout

Once all the different subsystems and components of Charon were determined, an initial CAD model of the vehicle could be generated. Before that, different components of the vehicle, as well as their relations, are presented in Section 16.1. The capsule layout is then summarised in Section 16.2. Finally, the complete vehicle layout is presented in Section 16.3.

16.1. Hardware Block Diagram

The existing hardware/architecture diagram presented in the midterm report [2] has been updated to include more subsystems and interfaces, based on the work performed in this report. Figure 16.1 shows the hardware diagram for Charon.

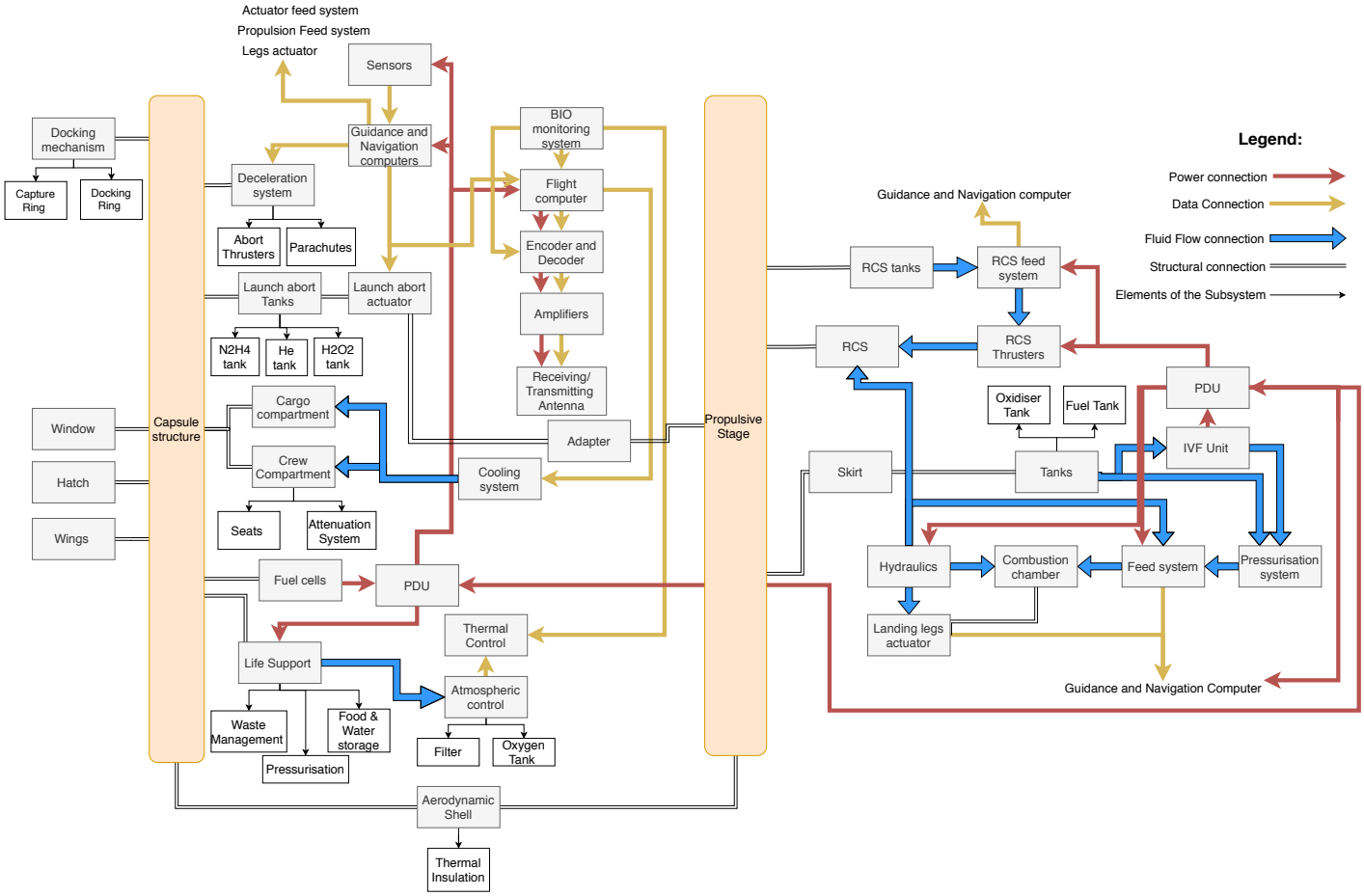

Figure 16.1: Hardware Block Diagram of the vehicle

In the Figure 16.1, the connection and the type of connection between the different components of Charon are illustrated. Based on this diagram, as well as the subsystem sizing and interface design performed in the preceding chapters, an initial CAD model of Charon could be made.

16.2. Capsule Layout

The capsule layout can be seen in Figure 16.2. Further, the interior of the capsule is presented in Figure 16.2a, in the form of a section cut.
The following elements can be seen from it:

- The pressurised volume of the capsule can be seen in grey. It contains a volume for the cargo, one for the crew, and a cylindrical section accommodating the docking port.
- The docking port can then be seen in dark green, linking the pressurised volume to the space station.
- The seats are presented in dark blue. They are placed with their backs on the ground, the closest possible to the wall of the pressurised volume.
- On the top of the capsule, the parachutes can be seen in fuchsia, placed in such a way that explosively detaching the nose cone would give them a direct opening to deploy. Also, the drogue chutes are placed above the main parachutes, to help with their deployment.
- Different life support elements are presented in light green. Namely, the Oxygen tank, water supply, food supply, and urine tanks can be seen. Additionally, the toilet has also been placed on the other side of the capsule.
- The abort engines, as well the propellant and pressurant tanks, can be seen in orange. The abort engines additionally have an aerodynamic shroud surrounding them. They are placed in couples, at 120 [deg] from each other.
- The EPS can be seen in yellow, with the fuel cells, PDUs, and the Hydrogen and Oxygen tanks powering the fuel cells.
- The RCS system can finally be seen in salmon. Two tanks contain the RCS propellant, and 4 different thrusters assemblies can be seen at 90 [deg] angles from each other.

Figure 16.2b shows the exterior on the capsule. The abort engines and RCS thrusters can once again be seen in it. In addition, the aerodynamic shell can be fully seen in light blue, with its TPS on the right, inducing a bump in the shell. The hatch can also be seen, here presented open to the pressurised volume. Finally, the window is invisible on the picture, positioned at 90 [deg] from the hatch.

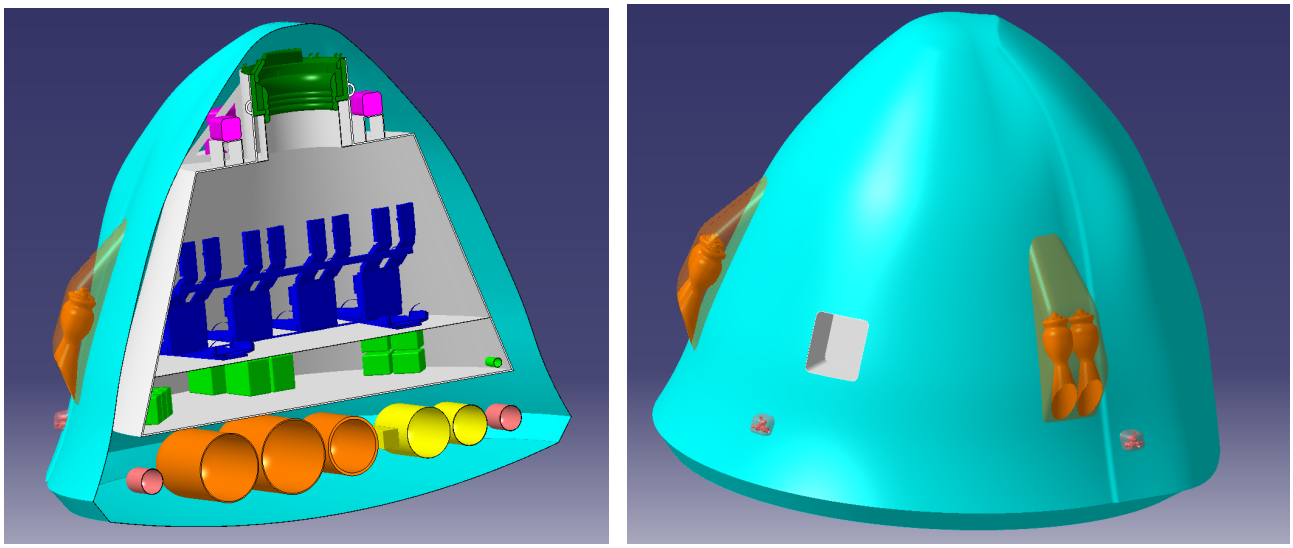

(a) Section cut of Charon's capsule

(b) Charon's capsule exterior

Figure 16.2: Charon's capsule layout

16.3. Vehicle Layout

Figure 16.3 shows the complete vehicle layout. First, Figure 16.3a presents the internal layout, using a section cut. In addition to the components in the capsule, the followings elements can be seen:

- The tanks are represented in blue. They are reinforced and bearing most of the forces exerted

on the vehicle. The oxidiser tank is at the top, and the fuel tank at the bottom. In the same colour, the skirts present at the top and the bottom can be seen, which transfer the load from the engine and the capsule to the tanks.

- The propulsion system can be seen in red, with the engines, their turbo-machinery, and the thrust structure transferring the loads from the engines to the tanks.
- The landing legs are presented in fuchsia, in their deployed position.
- The aerodynamic shell of the vehicle is once again represented in light blue.
- The RCS tanks powering the bottom thrusters, and the reentry thruster can be seen in salmon.

Figure 16.3b shows the external layout of the vehicle. Two additional systems can be seen:

- The wings are shown at the top of the vehicle, attached to the capsule. Their emplacement causes constraints for the positioning of the windows, the hatch, the RCS thrusters, and the abort engines.
- The RCS thrusters assemblies can be once again seen on the capsule, and also at the bottom of the vehicle.

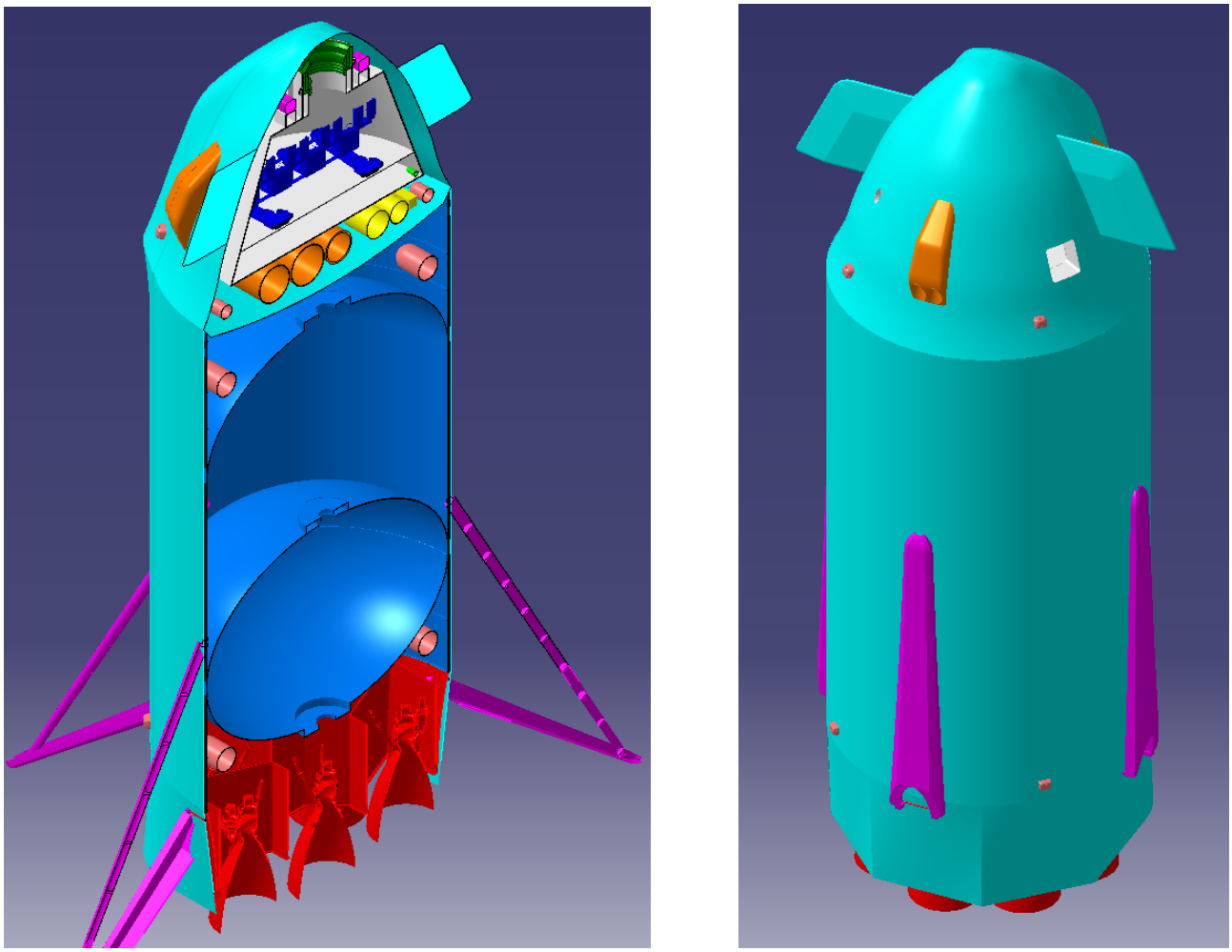

(a) Section cut of Charon

(b) Charon's exterior

Figure 16.3: Charon's layout

17

Detailed Budgets

17.1. Detailed Mass Budget

With the analysis, sizing and design of the different subsystems finished the mass budget could be refined and updated based on actual calculations and component characteristics instead of empirical relations and assumptions. Table 17.1 presents the refined mass budget for Charon. Once again it was important to include some margins on the calculated masses in order to account and as a result allow for an increase of the mass in later phases of the design. It is important to note that as dry mass of the vehicle is taken into account all the mass without the propellant mass stored in the main tanks, so without the mass of the methane and the oxidiser. However, the propellant mass required for abort and RCS is included in the determination of the dry mass of the vehicle. Within the design of all subsystems, mass margins have been taken already, as described in the respective chapters. However, to ensure the convergence of the design, an additional margin of 20% has been taken, following the guidelines from the European Space Agency [35]. On the other side, the margins applied to the propellant mass depended a lot on the number and assumed severity of assumptions used for their determination, presented in Chapter 4 and 5.

Table 17.1: Detailed mass budget of the different components

Subsystem	Component	Component mass [kg]	Component MGA mass [kg]
Total Dry Mass		**30221.22**	**36025.48**
Abort		***4259.08***	***5110.896***
	Engine (x6)	*425.00*	*510.00*
	H2O2 tank	*206.80*	*248.16*
	H2O2	*1499.60*	*1799.52*
	N2H4 tank	*159.00*	*190.80*
	N2H4	*836.38*	*1003.66*
	He	*37.70*	*45.24*
	He tank	*276.60*	*331.92*
	Drogue chute	*120.00*	*144.00*
	Main chute	*120.00*	*144.00*
	Chute deployment	*60.00*	*72.00*
	Airbags	*500.00*	*600.00*
	Sensors	*10.00*	*12.00*
	Computer	*3.00*	*3.60*
	Insulation	*5.00*	*6.00*
Life support		***456.35***	***547.62***
	O2	*73.20*	*87.84*
	O2 tank	*3.09*	*3.71*
	O2 distribution	*3.00*	*3.60*
	Food	*111.50*	*133.80*
	Water	*20.30*	*24.36*
	Urine tanks	*0.40*	*0.48*
	Toilet	*80.00*	*96.00*
	Water condenser	*30.00*	*36.00*
	Thermal heating	*50.00*	*60.00*
	Insulation	*13.86*	*16.63*
	Light	*15.00*	*18.00*

	Filter	*6.00*	*7.20*
	Pressurisation	*50.00*	*60.00*
Chassis		***15517.34***	***18620.81***
	Ox Tank	*2272.12*	*2726.54*
	Fuel Tank	*933.45*	*1120.14*
	Upper skirt	*778.20*	*933.84*
	Lower skirt	*625.50*	*750.60*
	Thrust structure	*637.73*	*765.28*
	Landing legs	*3600.00*	*4320.00*
	Piping	*850.00*	*1020.00*
	Seats	*190.00*	*228.00*
	Docking Mechanism	*325.00*	*390.00*
	Pressurised Capsule	*2925.34*	*3510.41*
	Adapter	*700.00*	*840.00*
	Hydraulics	*1100.00*	*1320.00*
	Capsule main shell	*500.00*	*600.00*
	Capsule nose shell	*80.00*	*96.00*
Power		***1046.58***	***1255.89***
	Fuel cells	*30.00*	*36.00*
	H2	*25.17*	*30.20*
	H2 tank	*23.64*	*28.37*
	O2	*201.40*	*241.68*
	O2 tank	*45.32*	*54.38*
	2x PDU capsule	*40.00*	*48.00*
	Harness (wires)	*432.05*	*518.46*
	IVF system	*209.00*	*250.80*
	2x PDU low stage	*40.00*	*48.00*
Thermal		***2399.04***	***2878.85***
	TPS chassis downstream	*1203.84*	*1444.61*
	TPS chassis upstream	*216.00*	*259.20*
	TPS capsule downstream	*806.40*	*967.68*
	TPS capsule upstream	*172.80*	*207.36*
Propulsion		***2621.25***	***3145.50***
	Thrust chamber	*2097.00*	*2516.40*
	Gimbal	*314.55*	*377.46*
	Turbopumps	*209.70*	*251.64*
Telemetry		***30.96***	***37.15***
	S-band Antennas	*4.60*	*5.52*
	Transmitters & receivers	*6.36*	*7.63*
	Other	*20.00*	*24.00*
Avionics		***220.00***	***264.00***
	Flight computers	*20.00*	*24.00*
	C&C bus and sensors	*200.00*	*240.00*
RCS		***1713.30***	***2055.96***
	Monoprop engines	*151.80*	*182.16*
	H2O2	*1220.50*	*1464.60*
	H2O2 tank	*81.00*	*97.20*
	Body flap	*260.00*	*312.00*
Payload		***1200.00***	***1200.00***
Propellant Mass		**137886.00**	**164806.50**
Wet mass		**168107.30**	**200832.00**

From the Table 17.1 it is obtained that the total wet mass of Charon is equal to around 201 [tons] with about 36 [tons] corresponding to dry mass and 165 [tons] to the propellant mass. The capsule payload mass is equal to 1200 [kg], enough for six astronauts and their personal belongings. With the detailed mass budget determined and with a knowledge of the location of each of the components along the longitudinal axis of the vehicle the mass budget distribution could also be performed.Figure 17.1 shows the mass distribution and the mass above each z location along the length of the vehicle.

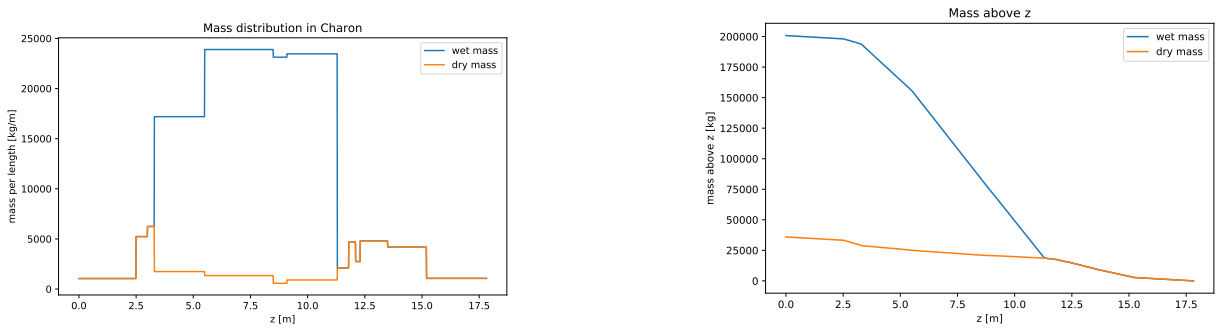

(a) Mass per length distribution

(b) Mass distribution above z

Figure 17.1: Charon's mass distribution

17.2. Delta V Budget

The ΔV budget is taken primarily from the midterm report [2]. The values for ascent and reentry are adjusted based on the more advanced simulations performed in Chapter 4 and Chapter 5. The margins have also been adjusted according to [35].

Table 17.2: Final delta V budget

Phase of flight	Delta V [m/s]	MGA	MGA Delta V [m/s]
Gravity turn	*4532.69*	*5%*	*4759.32*
Vertical flight	*91.67*	*25%*	*114.5875*
Hohmann transfer	*45.84*	*5%*	*48.134*
Inclination change	*289.485*	*5%*	*303.96*
Reentry insertion	*261*	*25%*	*274.045*
Landing burn	*338.3*	*25%*	*422.875*
Flight Reserves	*0*	*5%*	*277.95*
Total	**5558.98 [m/s]**		**6200.875 [m/s]**

17.3. Cost Breakdown

In this section, the cost breakdown of Charon vehicle is presented. This includes most subsystems, as well as considerations on Martian infrastructure.

17.3.1. Requirements

- **SRV-CONS-NONT-5**: [T] The vehicle shall be launchable from an existing and flight proven launcher in 2040.
- **SRV-CONS-NONT-6**: [T] The production of the spacecraft shall follow the labour laws of that facility's location.
- **SRV-CONS-NONT-10**: [M] The total number of launches required for vehicle transport to Mars shall not exceed 2.

These requirements are not directly related to cost, but rather, the cost follows from them, since the chosen vehicle for launch was NASA's SLS.

It is always a difficult task to predict the cost of a newly designed vehicle before its production. Many vehicles are susceptible to redesign, additional testing and delays, which all propel the cost upwards. However, to overcome this, the Project Cost Estimating Capability software from NASA was used [135], as they have much experience with delayed projects and project financing. Therefore, the cost breakdown of the Charon vehicle is based on cost per weight of a subsystem, estimated using NASA reference values for a base fiscal year of 2015. Note that these values include production of one vehicle and do not include system test operations (which add another 507.92 million USD to development), as well as ground operations, which are going to be analysed next.

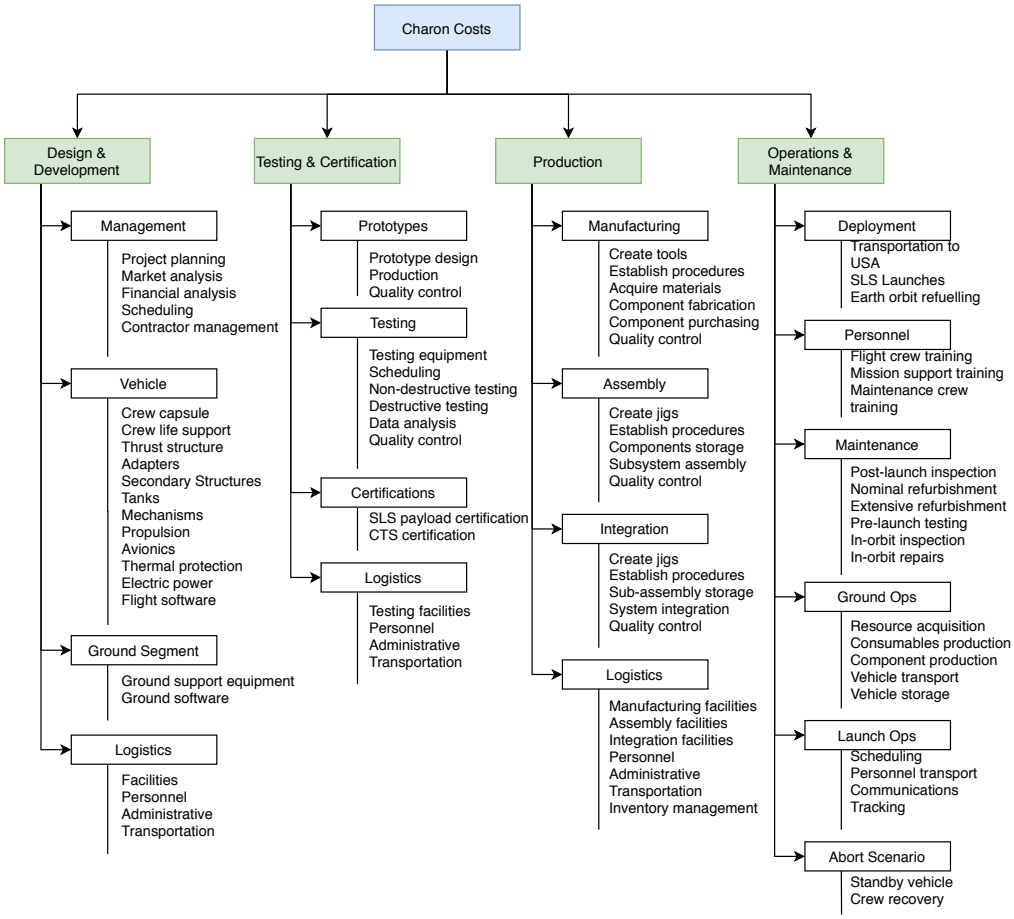

Figure 17.2: Cost breakdown structure for Charon

Subsystem	**Production** [M] $	Design & Development [M] $	**Test & Hardware** [M] $
Launch Vehicle Management	33.44	181.47	-
Launch Vehicle Systems Engineering	49.76	477.19	-
Crew Capsule Fuselage/Body	50.83	340.98	66.08
Crew Capsule Structures	108.87	509.96	141.53
Crew Life Support	39.73	79.02	51.65
Thrust Structure	2.78	14.52	3.61
Adapters	4.38	19.91	5.70
Secondary Structure	20.53	128.36	26.69
Tanks	26.05	92.18	33.86
Mechanisms	4.45	28.80	5.78
Main Propulsion Systems	28.60	251.51	37.17
Avionics	89.99	65.60	116.99
Thermal Protection	11.14	64.66	14.48
Electric Power	18.38	275.76	23.90
Flight Software	-	105.22	-
Integration & Assembly	59.11	52.07	-
Total	548.04	2687.2	527.44

Above, Figure 17.2 considers the cost of only one vehicle. Optimal operation necessitates 5 Charon vehicles on Mars simultaneously, and so it is expected that the cost of production will be multiplied by 5 and thus the total project cost until delivery will be approximately 8.2 billion USD in FY2015. It is important for stakeholders to understand how these costs are distributed over the project lifecycle. The NASA Cost Estimating Handbook [136] recommends a 60:40 Beta Curve for preliminary phasing of cost estimates, whereby 60% of the project budget is expended at the halfway mark. This curve was adopted for Figure 17.3 below, with the costs of the SLS launches being appended onto the last 5 years of the project. The production schedule begins quite early because of there being only 1 SLS launch per year, as current estimates predict between 2 and 4 total SLS launches per year once it becomes operational.

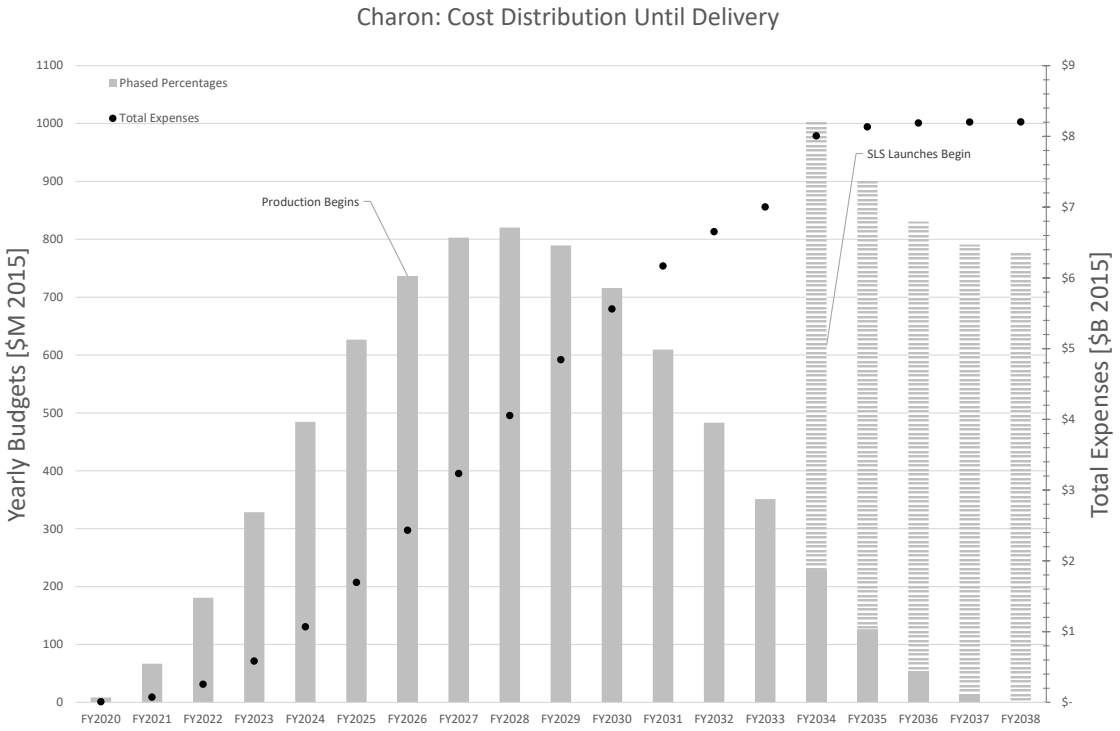

Figure 17.3: Projected vehicle costs over project lifespan on Earth. Note that the bars use the left axis, while the points use the right axis.

This cost does not include the cost of ground operations and ground segment. The developnment of infrastructure and tools for ground segment is estimated to cost 965.89 million USD. This value was computed for Earth operations, which would be slightly different on Mars, due to lack of need for a launch tower (instead, one crane is used for both transportation, erection and cargo discharge). This value is further increased by a cost of transportation of this equipment to Mars, assumed to be 776.52 million dollars, similar to a cost of Charon transportation, albeit most likely on a different vessel.

Further costs of propellant manufacturing depend mostly on the cost of equipment and power source, as resources on Mars are not paid for. While no comparable sources have been found, one can estimate two launches together with transfer to Mars - one for propellant plant and the other for the nuclear plant. Such costs, assuming similar weight and launcher, would amount to 1.6 billion dollars in total. However, the design, development and assembly of such infrastructure is also needed. The development of a smaller RTG reactor used in Jupiter missions costs around 3 billion US dollars[1]. On Earth, current nuclear power plants cost around 6 billion US Dollars, albeit being bigger than the scale needed on Mars. While it is difficult to estimate a design cost, it should be somewhere between 6-12 billion dollars. Propellant manufacturing plant is also assumed to have a multibillion dollar development cost, despite having no estimations at this point. However, on Mars, the costs would only be of maintenance of the whole plant and process, estimating to take up to two full-time engineers for both the propellant and RTG reactor combined, adding up to 112 labour hours per week. For refurbishment, the cost is once again mostly dependent on equipment and its transportation to Mars, while also affected by resources needed on Mars. It was assumed that the exact economics of a Martian colony are not of importance for Charon operations, hence the manpower requirement was not translated into economic value. The equipment, however, can be mostly assumed to be transported together with crane and other ground operations tools, or with one additional launch. Together with equipment cost, total budget should increase by up to 2 billion dollars, assuming up to 500 million dollars of equipment cost and design, together with two launches. Additionally, relay satellites cost would be similar to cost of Mars Reconnaissance Orbiter [2], equal to 420 million dollars for development, around 90 million dollars per launch and 210 million dollars per production and operation of one satellite. Since there are three satellites, total cost rises to 1.32 billion dollars. Altogether, adding to a 8.2 billion dollar Charon mission cost, ground operations with equipment would take up to 12.62 - 18.62 billion US Dollars, most of which include transfer of equipment to Mars. More research has to be done on decreasing the costs of energy and propellant manufacturing plant, especially for future Martian missions.

[1]RTG Systems in Space, `https://www.world-nuclear.org/information-library/non-power-nuclear-applications/transport/nuclear-reactors-for-space.aspx` [accessed on 18th of June 2020]
[2]Mars Reconnaissance Orbiter cost, `https://www.planetary.org/explore/space-topics/mro-cost.html`

Such cost is considered taking into account previous NASA missions (hence, the cost+ funding structure), while also considering production of the first vehicle only. Subsequent vehicle production, if done on a bigger scale, will reduce costs for every subsequent vehicle due to learning curve present. Moreover, a private company in a competitive market will try to diminish costs as much as possible, hence most likely bringing the costs down in comparison to this estimation. That being said, the costs do not include the transportation of ground segment equipment to Mars or the building of any infrastructure related to operations, such as orbital node, the habitat, propellant manufacturing plant and power plants. The cost of each of these will be directly dependent on the amount of resources needed to be transported from Earth, the vehicle chosen for such transportation and the design choices made for Martian mission independent of Charon specifications.

17.3.2. Economic Analysis

Mission Needs Statement for Charon: *Provide an economical continuous transportation service vehicle for crew and cargo between a Low Mars Orbit orbiter (node) and a Mars base.*

One of the main objectives for Charon outlined in the mission needs statement and project goal is for the vehicle to be economical. This, as understood by the design team, encompasses more than the objective and relative cost of the project but also the impact from peripheral requirements for development, production, maintenance, and disposal.

The objective costs of the 5 vehicle Charon project top out at approximately 13.8 billion USD in FY2015, distributed over 17 years of funding. Undoubtedly a large figure, the peak year costs are equivalent to 25% of ESA's 2020 budget. Relative to large scale projects such as the Space Shuttle or the ISS, Charon funding is not impractical.

Relative to competition in the market, any analysis is hard given the lack of knowledge about launch vehicles operational in 2040. The only known vehicle that could satisfy the mission needs statement is SpaceX's Starship, however there is again a lack of knowledge about its launch capabilities in 2040. Starhip is currently advertised with a $2 million launch price. The ability to sign multiple clients and amortize development and production costs over hundreds of launches is not something that this project can do in its current state. Airbus Defense and Space is the sole client, and only 5 vehicles will likely be produced, so optimisation of production procedures will be limited. Developing more commercial applications for Charon is thus crucial for becoming competitive with NewSpace companies.

With regard to peripheral requirements, this report considers two that have a significant affect on this project's economic feasibility. These are: the required industrial capacity on both Earth and Mars to source materials, manufacture and assemble components, and refurbish components; and the amount of skill and labour hours required from technicians for operations and maintenance. Much of the relevant material has been discussed in Chapter 15. Industrial and labour capacity and proficiency on Earth is not a problem for this project. The limited factors, however, are the industrial infrastructure on Mars and the required personnel for operations and maintenance.

Firstly, effective vehicle operation requires 8-12 people supervising the launch, 4-6 people present on the launchpad, and 20-40 people available for refurbishment. This already limits the size of the colony for which Charon can service. The investments required to establish a long-term colony of this minimum size is likely to be in the billions. Furthermore, the industrial capacity required for resource mining and component production must all be transported from Earth initially. This will likely cost upwards of tens of billions of dollars. In short, Charon is only viable if governments and the private sector have devoted enormous capital to establishing the peripheral infrastructure, very probably on a larger scale than the Apollo program. The financial convenience and political will to accomplish this should not be underestimated.

18

RAMS

In this chapter risk, availability, maintainability and safety of Charon vehicle are assessed. The majority of the vehicle specific risk and reliability analysis is performed in Section 18.5 with a detailed analysis of the probabilities of the possible failure events and their consequence. Sections 18.1, 18.2 and 18.3 discuss the general availability, maintainability and safety aspects of operations.

18.1. Availability

The crew and cargo discharge has been discussed in subsection 15.5.1, leaving accessibility discussion to any subsystem of the vehicle prior to the launch. The vehicle will have a few ports located roughly at the top of the fuel tank, allowing umbilical chords to be connected to the tanks and the electronic systems above, therefore allowing a power connection prior to the launch, as well as fuelling done on the launchpad. Any other accessibility, for instance, during maintenance, would have to be done with partial disassembly of the vehicle, for which a crane as a lifting equipment is made available, as further discussed in chapter 15.

18.2. Maintainability

The maintenance of Charon is already discussed in subsection 15.10.2, where the amount of crew is estimated for the extensive refurbishment. This subsection is thus focusing on specifying the tasks that need to be performed rather than means to achieve it. As already discussed in the Midterm Report [2], the first part of maintenance is the inspection of the vehicle to determine any damage. This includes visual inspection, as well as more detailed sensor-aided inspection for cracks in outer skin and inside the nozzle. Should no problems be detected, the quick refurbishment is performed, consisting of engine cleaning of any soot and dust left after the mission, as well as checks on life support system in the capsule. Longer refurbishment, performed after the scheduled operational window or in case of any issues detected, starts with engine disassembly, allowing to access the inside of the vehicle. Such disassembly then allows for visual checks on turbopumps and fuel tanks, as well as manufacturing and replacement of any part of structure necessary.

18.3. Safety

As mentioned throughout this report, several different propellants are used on Charon, some of which present a large safety risk to operations personal[1]. The three primary areas of concern are LOX and HTP for the main engines and RCS system, as well as Hydrazine from the launch abort system. Firstly the Safety hazard of LOX and HTP are mostly related to accidental combustion or decomposition with metals or organic compounds. This requires well thought out and practised procedures specifically with regards to cleaning during and after refurbishment [137]. Hydrazine on the other hand is highly toxic and hypergolic with many things. It has been deemed necessary for a reliable abort system, however, working with this propellant requires proper facilities, procedures and training for personnel, according to [138]. The feed systems within Charon make extensive use of high pressures to ensure the controlled flow of propellants for the main, abort and RCS engines. High pressure enclosed volumes generally pose a safety risk, as rupturing tanks or piping can release a lot of energy. In addition, the high pressures also increase the probability of propellant leaks. It is therefore vital that once the tanks inside the vehicle are being pressurised, that all non essential personal is removed from the vicinity of the vehicle. Regular inspection and maintenance of any pressure bearing system is essential. The launch and operation of Charon pose some danger to the Mars base itself. Close proximity to the base could result in falling debris damaging the base or injuring personal. As a result the launch site is to be located $40[km]$ away from the base, with the launch trajectory leading the vehicle away from any critical areas, as outlined in Chapter 15.

18.4. Quantitative Risk Assessment

Qualitative risk analysis has been performed for each subsystem. In this section these risks are quantified and the possibility of several events occurring at the same time is analysed. In this analysis combined events were considered that would increase the severity of the outcome, using the hardware block diagram in Section 16.1. This means a combination of events of a certain outcome leading to a more severe outcome if they occur simultaneously. An example of this is the failure of the abort system engines in conjunction with any event that would result in loss of vehicle, in turn leading to loss of crew. The probabilities for the individual events

[1]Lox Safety video, `https://www.youtube.com/watch?v=rUKcHe0-m_I`, accessed the the 18th of June 2020

are calculated from single component failure and taking into account the total number of components, as well as redundancy in the system. Some of these values are taken from [2], while the majority are focused on the subsystem level.

18.5. Fault Tree Analysis (FTA)

The results of the quantitative risk assessment are presented in Table 18.1. Here the Events are split into LOM, LOV and LOC. The count and redundancy are used to arrive at the final probability in the column on the right. The total LOM, LOV and LOC probabilities are computed, as well as a 3σ confidence interval for this final value. A 50% margin is added to the maximum value of the confidence interval. In Table 18.1 $\mathbf{F_s}$ is the failure probability for a single component, $\mathbf{N_c}$ is the total number of components, $\mathbf{N_r}$ is the number of redundant components and $\mathbf{F_c}$ is the combined failure probability considering both the total number of components and the number of redundant components.

Table 18.1: FTA for the entire design, all confidence intervals are presented as 3σ confidence intervals, 10000 samples

LOM						
ID	**Source**	**Description**	**F_s [-]**	**N_c**	**N_r**	**F_c [-]**
$e3_s$	[139]	Pipe leakage	1.10E-5	1	0	1.10E-5
$e5_s$	[140]	Skirt buckling	3.40E-6	2	0	6.80E-6
$e6_s$	[140]	Separation mechanism failure	5.00E-4	1	0	5.00E-4
$e11_s$	[140]	Buckling of the capsule	3.40E-6	1	0	3.40E-6
$e13_s$	Negligible	Side Hatch not opening	0E0	1	0	0E0
$e14_s$	Negligible	Docking hatch not opening	0E0	1	0	0E0
$e15_s$	[141]	Capsule ring not deploying	6.96E-5	1	0	6.96E-5
$e16_s$	Negligible	Not sealed connection	0E0	1	0	0E0
$e1_{th}$	[142]	TPS damaged due to surface debris	3.00E-6	1	0	3.00E-6
$e4_{en}$	[139]	Fluid leak	1.10E-5	9	2	6.71E-13
$e5_{en}$	[143]	Fuel pump failure	3.33E-6	9	2	1.87E-14
$e6_{en}$	[143]	Oxidise pump failure	3.33E-6	9	2	1.87E-14
$e7_{en}$	[144]	Turbine failure	1.34E-6	9	2	1.22E-15
$e1_{gnc}$	[1]	Docking camera failure	8.04E-5	4	2	1.25E-11
$e2_{gnc}$	[1]	Landing camera failure	8.04E-5	4	2	1.25E-11
$e8_{gnc}$	[145]	Ignition failure	2.27E-5	1	0	2.27E-5
$e12_{gnc}$	[140]	Control algorithm errors	3.71E-5	1	0	3.71E-5
$e13_{gnc}$	[140]	Guidance algorithm errors	3.71E-5	1	0	3.71E-5
$e14_{gnc}$	Negligible	Engine thruster misalignment	0E0	32	0	0E0
$e2_{com}$	[146]	Antenna failure	8.69E-3	4	2	1.53E-5
$e3_{com}$	[146]	Transmitter/receiver failure	2.53E-2	2	1	1.26E-3
$e5_{com}$	Estimation	No line of sight post abort landing	5.00E-3	1	0	5.00E-3
$e2_{pow}$	[147]	Fuel cell failure	2.50E-4	4	3	9.37E-14
$e3_{pow}$	[147]	ICE overheating	1.25E-3	1	0	1.25E-3
$e4_{pow}$	[147]	ICE failure	1.50E-3	2	1	4.50E-6
$e5_{pow}$	Estimation	Short circuit	3.33E-4	1	0	3.33E-4
$e2_{ls}$	[140]	Capsule fire	6.19E-6	1	0	6.19E-6
$e3_{ls}$	[140]	Atmospheric control failure	2.48E-5	2	1	1.23E-9
$e5_{ls}$	[140]	Waste management failure	4.95E-5	1	0	4.95E-5
$e2_{ab}$	[140]	Abort engine failure	1.09E-3	6	1	3.55E-5
$e3_{ab}$	[148]	Suicide burn starting too early or late	1.10E-5	1	0	1.10E-5
$e4_{ab}$	Estimation	Too high load	1.00E-4	1	0	1.00E-4
$e5_{ab}$	[149]	Parachute deployment failure	4.00E-3	4	1	1.90E-4
$e3_{comp}$	[2]	Sudden processing errors	8.33E-4	1	0	8.33E-4
ID		**Description**				**F_c [-]**
Total LOM, Format Value (min , max)			**9.75E-3 (4.67E-3 , 1.51E-2)**			
Max LOM Including 50% margin			**2.27E-2**			
LOV						
ID	**Source**	**Description**	**F_s [-]**	**N_c**	**N_r**	**F_c [-]**
$e2_s$	[140]	Thrust structure failure	3.40E-6	9	2	1.98E-14
$e4_s$	[150]	Landing leg collapsing	5.00E-5	8	1	1.40E-7
$e8_s$	[141]	Hydraulics system failure	6.96E-5	9	2	1.70E-10
$e9_s$	[151]	Legs not deploying	1.67E-3	8	1	1.54E-4
$e10_s$	[152]	Depressurisation of the capsule	7.23E-5	1	0	7.23E-5
$e12_s$	[141]	Attenuation system failure	6.96E-5	1	0	6.96E-5
$e1_{en}$	[140]	Catastrophic engine failure	1.09E-3	9	2	6.45E-7
$e2_{en}$	[145]	Control system failure	1.37E-4	9	2	1.29E-9
$e3_{en}$	[145]	Ignition failure	2.27E-5	9	2	5.89E-12
$e8_{en}$	[145]	Gimbal bearing failure	5.50E-4	9	2	8.34E-8
$e9_{en}$	[145]	Combustion Instability	3.03E-3	9	2	1.36E-5
$e3_{gnc}$	[1]	Star tracker failure	7.50E-6	3	2	2.55E-15

[1] Blackfly S Datasheet, https://flir.app.boxcn.net/s/mj27am7zik371ivyzv352gmt390yqt6z, accessed on the 16th of June 2020.

$e4_{gnc}$	[153]	Gyroscope failure	1.29E-3	4	3	6.62E-11
$e7_{gnc}$	[140]	RCS Thruster failure	4.00E-3	32	6	1.88E-7
$e9_{gnc}$	[148]	Valve/Feedsystem Failure	5.60E-4	32	6	2.77E-13
$e10_{gnc}$	[140]	Critical thruster failure:	1.09E-3	32	2	3.67E-5
$e11_{gnc}$	[139]	Propellant leakage	1.10E-5	2	0	2.20E-5
$e1_{pow}$	[147]	PDU failure	6.25E-4	4	3	3.66E-12
$e1_{comp}$	[2]	Computer failure	1.67E-4	4	3	1.87E-14
$e2_{comp}$	[2]	Critical software errors	8.33E-4	1	0	8.33E-4
ID		**Description**				**F_c [-]**
($e3_s$ AND $e5_s$)		Pipe leakage with skirt buckling				7.48E-11
($e2_{gnc}$ AND $e13_{gnc}$)		Wrong attitude/position during landing				4.44E-16
($e1_{gnc}$ AND $e13_{gnc}$)		Wrong attitude/position during docking				4.44E-16
Total LOV, Format Value (min , max)			**1.20E-3 (4.22E-4 , 2.04E-3)**			
Max LOV Including 50% margin			**3.05E-3**			
LOC						
ID	**Source**	**Description**	**F_s [-]**	**N_c**	**N_r**	**F_c [-]**
$e1_s$	[140]	Propellant tank rupture	8.20E-6	2	0	1.64E-5
$e2_{th}$	[152]	TPS damaged due to space debris	7.23E-4	1	0	7.23E-4
$e3_{th}$	[142]	TPS breaks due to fatigue	1.20E-7	1	0	1.20E-7
$e4_{th}$	[142]	TPS breaks due to high stress	1.44E-8	1	0	1.44E-8
$e5_{gnc}$	[153]	Accelerometer failure	1.29E-3	4	3	6.62E-11
$e6_{gnc}$	[140]	Flight computer failure	7.41E-4	4	3	7.22E-12
$e1_{ls}$	[140]	Oxygen supply failure	2.48E-5	3	2	9.15E-14
$e4_{ls}$	[140]	Capsule radiator failure	1.86E-5	2	1	6.92E-10
$e1_{ab}$	[154]	Abort detection need failure	5.00E-3	2	1	4.99E-5
ID		**Description**				**F_c [-]**
($e2_s$ AND $e6_s$)		Thrust structure failure and capsule not separating				0E0
($e2_s$ AND $e6_s$)		Landing legs not deploying and capsule not separating				0E0
($e4_{en}$ AND $e13_s$ AND $e14_s$)		Fluid leak with malfunctioning hatches				0E0
($e2_{en}$ AND $e6_s$)		Control System failure and capsule not separating				6.47E-13
($e2_{en}$ AND $e2_s$)		Engine control system failure and thrust structure failure				0E0
($e8_{en}$ AND $e2_s$)		Gimbal bearing failure and thrust structure failure				0E0
($e9_{gnc}$ AND $e1_{gnc}$)		Shutoff valve and critical failure				0E0
($e4_{en}$ AND $e1_{th}$)		Propellant leak with damaged TPS				0E0
($e11_{gnc}$ AND $e1_{th}$)		RCS propellant leak with damaged TPS				6.60E-11
($e12_{gnc}$ AND $e15_s$)		Guidance algorithm errors and capsule ring not deploying				2.58E-9
($e2_{gnc}$ AND $e4_s$)		Lading camera failure and Landing leg collapsing				0E0
($e7_{gnc}$ AND $e4_{en}$)		RCS thruster failure and propellant leakage				0E0
($e13_{gnc}$ AND $e8_{en}$)		Gimbal bearing failure and guidance algorithm errors				3.09E-12
($e5_{com}$ AND $e1_{ls}$)		No line of sight post abort landing and Oxygen supply failure				4.44E-16
($e5_{com}$ AND $e4_{ls}$)		No line of sight post abort landing and Capsule radiator failure				3.46E-12
($e5_{pow}$ AND $e4_{en}$)		Short circuit and propellant leakage				2.22E-16
($e2_{ab}$ AND $e2_s$)		Abort engine failure and thrust structure failure				0E0
($e2_{ab}$ AND all LOV)		Abort engine failure and LOV event				4.26E-8
($e6_s$ AND all LOV)		Capsule not separating and LOV event				6.01E-7
Total LOC, Format Value (min , max)			**7.90E-4 (1.41E-4 , 1.45E-3)**			
Max LOC Including 50% margin			**2.18E-3**			

18.6. Sensitivity Analysis

The requirement on LOC probability has been identified in the baseline report [1] as a driving design requirement. Hence, a sensitivity analysis of the values presented in Table 18.1 is vital to assess the impact of uncertainty in the event probabilities. For the sensitivity analysis of the final LOM, LOV and LOC probabilities, the individual event probabilities were assumed to be normally distributed. The standard deviation was chosen to be 30% of the mean value. The calculation of the final probabilities was run 10000 times, varying all parameters simultaneously according to their respective normal distributions. The results of this analysis are presented in Table 18.2.

Table 18.2: Sensitivity analysis of the LOM, LOV and LOC probabilities

Parameter	LOM	LOV	LOC
σ	17.37E-4	27.02E-5	21.84E-5
$1-\mu+3\sigma$	15.11E-3	20.39E-4	14.49E-4
$1-\mu-3\sigma$	46.83E-4	41.81E-5	13.91E-5

A standard deviation of 30% in all input parameters still results in the LOM probability below the required 5.5%, an LOV below the required 1.5% and an LOC probability below the required 0.5%. This means that the requirements **SRV-TECH-OPER-6**,**SRV-TECH-OPER-7** and **SRV-TECH-OPER-8** can be considered verified.

19

Sustainability approach

A sustainable design approach has been a driving parameter for the design of Charon. This extends to the design of vehicle subsystems and the mission envelope. In the midterm report [2] sustainability aspects are identified, as shown in Figure 19.1. Consequently, integration was discussed with regards to the preliminary concept trade-off and main propellant trade-off and finally End-of-Life strategy options were identified. In this chapter, considerations made at this stage of the life cycle (phase A & B) are analysed and discussed and strategies for a sustainable approach in future phases are given.

19.1. Requirements

Firstly, a list of the requirements related to vehicle and mission sustainability.

- **SRV-TECH-EOL-1**: [S] 50% of the total dry mass of the vehicle shall be recycled at the end of life.
- **SRV-TECH-PROD-1**: [S] 80% of all consumables used by the vehicle shall be produced in-situ.
- **SRV-TECH-PROD-2**: [S] All parts that are not designed to survive the entire operational lifespan of the vehicle shall be producible in-situ.
- **SRV-CONS-NONT-7**: [T] The production of the spacecraft shall be carbon-neutral.
- **SRV-CONS-NONT-8**: [T] No byproducts of the production of the spacecraft shall contaminate ground soil or water.
- **SRV-CONS-TECH-9**: [S] The technology used shall be at least TRL-4 according to 2020 specifications.

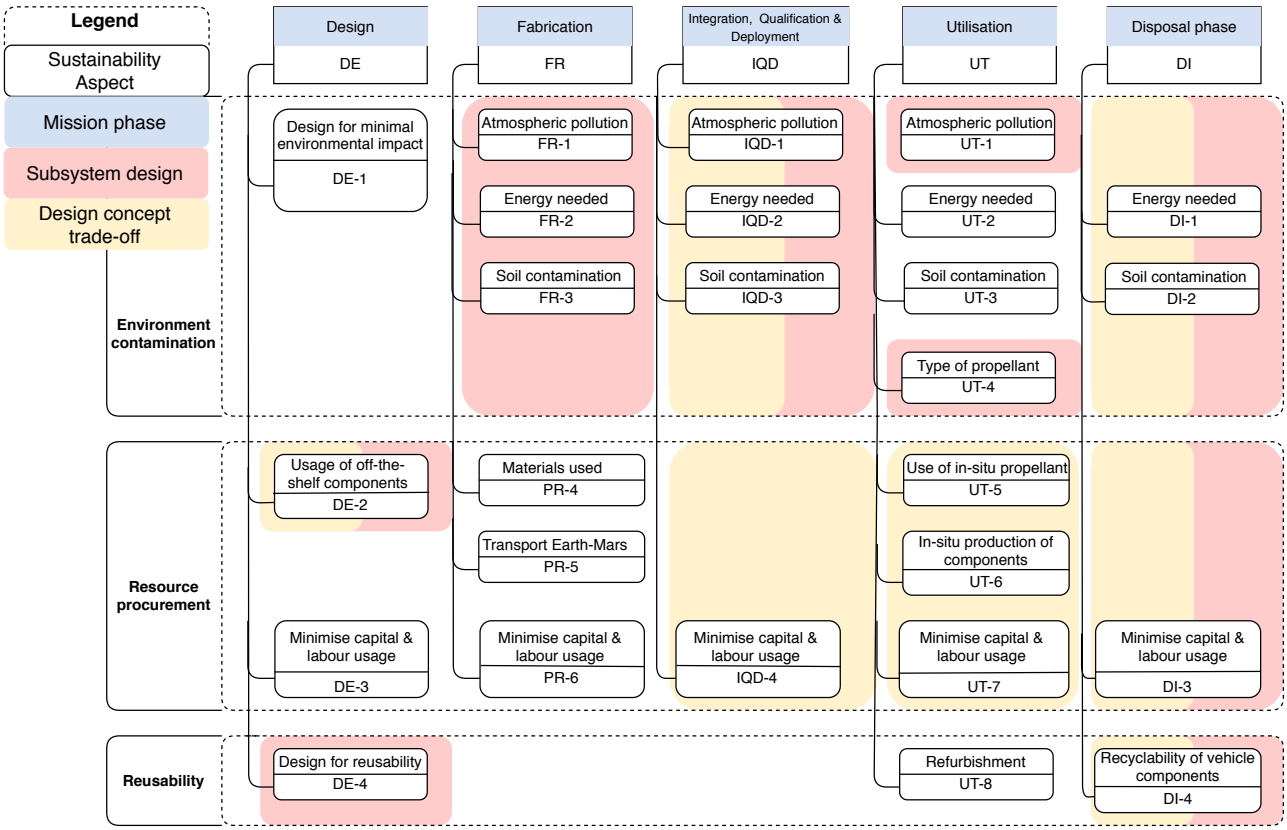

Figure 19.1: Sustainability aspects throughout mission life cycle

19.2. Life Cycle Analysis

A sustainability flow diagram is constructed in order to analyse the sustainability aspects in terms of inputs and outputs of the system and is shown in Figure 19.2. The phases are determined in Chapter 22. This project is limited to phase A and B. Sustainability aspects that are implemented in the system up until now have an impact through out the entire life cycle. In this diagram, these impacts are visualised.

19.2.1. Subsystem Design

Impact factors are implemented on multiple areas on subsystem level. This section discusses the design choices driven by these factors and the implementation in subystem design.

TRL

For all subsystems, importance of TRL is taken into account with regard to requirement **SRV-CONS-NONT-9**.

Weight Strategy

The structures subsystem has many exchangeable components that can be replaced during refurbishment. As the components are favourably lightweight, a large part of the material used for non-exchangeable components are composites. Being lightweight, they will contribute in reducing the dry mass, requiring less resources and resulting in a more sustainable vehicle all together.

Waste Reduction

To ensure waste reduction during phase C and D, 3D printing is advised for certain structural and propulsion parts and assemblies. Furthermore, the fuel cells used by the power distribution subsystem use LH2/LOX bi-propellant with its single byproduct being drinkable water for the crew. This reduces waste, in terms of amount and level of toxicity.

Refurbishment Strategy

The majority of the material used in Charon has been chosen with in-situ production in mind. Structural components consist largely of aluminium. Additionally, the propulsive stage uses aluminium and copper alloys that can be produced on Mars.

Propellant Strategy

The main propellant, LCH4/LOX, is producible in-situ. Abort propellant hydrazine, is not producable in-situ, has negative environmental impact and is highly toxic. However, important safety considerations led to still going with this propelant. However, redundancy and reliability is implemented in the design, such that use of hydrazine is minimal. Furthermore RCS propellant, H2O2, is also producable in-situ and has lower toxicity than more commonly used RCS propellants, as well as exhausting only water. Additionally, the use of a body flap during reentry allows for minimal use of the RCS thrusters for pitch control, thereby reducing required propellant mass.

Reusability

Considerations regarding reusability are taken into account for life support, where a molecular filter is used instead of a chemical filter to scrub carbon dioxide. This allows for less replacement of components that would be very difficult to produce on Mars.

19.3. End-of-Life Strategy

An End-of-Life (EoL) strategy is required for completing the Disposal phase in a sustainable and responsible manner. In the midterm report, three options were chosen, analysed and discussed in more detail in this section.

Looking at Figure 19.2, four factors are driving for this EoL strategy design. These are *Energy from Mars*, *Human Resources (HR)*, *New function* and *Solid Waste*. The last factor is bound to driving requirement **SRV-TECH-EOL-1** and puts an upper boundary on the amount of solid waste, which is 50% of the total dry mass. The sustainability impacts of each strategy can be seen in Table 19.1.

Table 19.1: End-of-Life strategy impacts

Strategy	HR	Energy	Solid waste	New function
Container	+	+	+-	+
Facility	+-	+-	++	++
Disassembly & Disposal	+	++	-	–

Using Charon as a facility for training of astronauts or flight simulations, comparably large HR and energy is required, as more requirements and design constraints are present for this application. However, considering the reusability of the entire vehicle in the case of a facility, the facility strategy is highly advantageous with respect to solid waste output. When reusing Charon as a container, mainly the propellant tanks are of interest

for the propellant manufacturing plant and some of the smaller components of the vehicle would be less useful. Furthermore, disassembling the vehicle and recycling and reusing parts probably results in quite a large solid waste output. Finally, using Charon as a facility results in a very high functionality with respect to the other strategies. Given these considerations, the use of a facility for training astronauts as a flight simulator is advised for the first disposed vehicles. Subsequent vehicles can be reused as containers or scrapped for recycling on a component level.

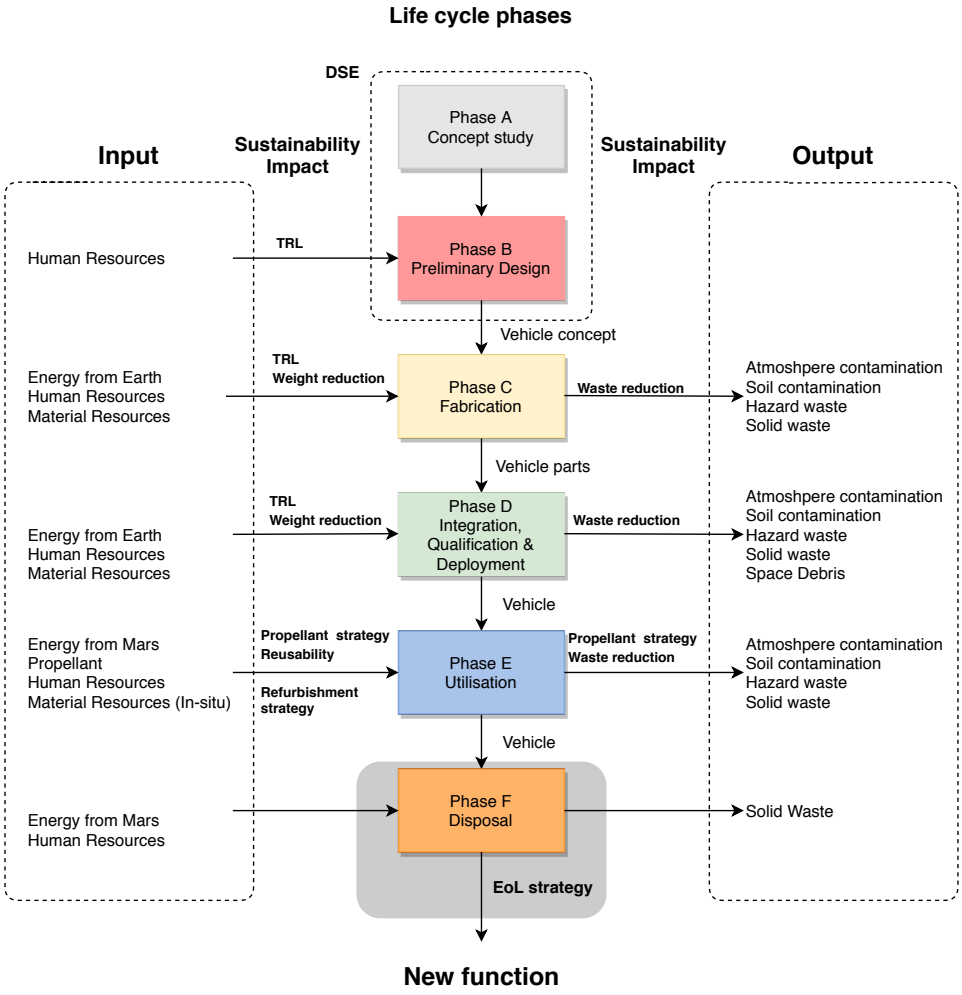

Figure 19.2: Life Cycle flow with inputs and outputs influencing sustainability

19.4. Requirement Compliance

In Table 19.2 it can be seen that **SRV-TECH-EOL-1** is completed, considering the advised EoL strategy. Furthermore, **SRV-CONS-NONT-7** is not completely guaranteed yet, as Earth production is not yet entirely proven to be carbon-neutral. However, the entire propellant production is carbon-neutral. The only used propellant emitting carbon, LCH4/LOX, has a carbon neutral production, as all emitted carbon is initially taken from the atmosphere for the Sabatier reaction, explained in Section 15.6. Finally, **SRV-CONS-NONT-8** is not fully guaranteed yet either.

Table 19.2: Requirement compliance for sustainability

Requirement	Completion	Determination Location
SRV-TECH-EOL-1	✓	Section 19.3
SRV-TECH-PROD-1	✓	Subsection 19.2.1
SRV-TECH-PROD-2	✓	Subsection 19.2.1
SRV-CONS-NONT-7	*	To be investigated
SRV-CONS-NONT-8	*	To be investigated
SRV-CONS-TECH-9	✓	Subsection 19.2.1

20

Requirement Compliance Matrix

Given the performed subsystem analysis, sizing and design it is determined whether or not the requirements developed and set by the stakeholders in the initial phase of the design are met. The results are summarised in the generated compliance matrix presented in Table 20.1 in which ✓ indicates that the requirement is met, * refers to requirements that need to be investigated further to ensure compliance and ✗ to requirements that are not met and that would have to either be modified or change the design itself in order to be met.

Table 20.1: Requirements Compliance Matrix

Requirement ID	Comp.	Explanation		Requirement ID	Comp.	Explanation
SRV-CONS-TECH-1	✓	*Chapter 15*		*SRV-TECH-OPER-1.1*	✓	*Chapter 9*
SRV-TECH-OPER-1	✓	*Chapter 4,15*		*SRV-CONS-TECH-2.4*	✓	*Chapter 4*,9
SRV-TECH-OPER-2	✓	*Chapter 5*		*SRV-TECH-OPER-1.2*	✓	*Chapter 4* ,9
SRV-TECH-OPER-3	✓	*Chapter 5,7*		*SRV-CONS-TECH-5.2.1*	✓	*Chapter 9*
SRV-CONS-TECH-2	✓	*Chapter 10*		*SRV-CONS-TECH-5.2.2*	*	*Chapter 9*
SRV-TECH-OPER-4	✓	*Chapter 10,15*		*SRV-CONS-TECH-5.4.1*	✓	*Chapter 9*
SRV-TECH-OPER-5	✓	*Chapter 12*		*SRV-CONS-TECH-5.4.2*	*	*Chapter 9*
SRV-TECH-OPER-6	✓	*Chapter 12*		*SRV-TECH-PROD-1.1*	✓	*Chapter 9*
SRV-CONS-TECH-3	✓	*Chapter 4*		*SRV-TECH-OPER-3.1*	✓	*Chapter 9*
SRV-CONS-TECH-4	✓	*Chapter 4,8*		*SRV-TECH-OPER-3.2*	*	*Chapter 9*
SRV-CONS-TECH-5	✓	*Global*		*SRV-TECH-OPER-3.3*	*	*Chapter 9*
SRV-CONS-TECH-5.1	✓	*Chapter 15*		*SRV-CONS-TECH-2.1*	*	*Chapter 10*
SRV-CONS-TECH-5.2	✓	*Chapter 15*		*SRV-CONS-TECH-2.2*	*	*Chapter 10*
SRV-CONS-TECH-5.3	✓	*Chapter 15*		*SRV-CONS-TECH-2.3*	✓	*Chapter 10*
SRV-CONS-TECH-5.4	✓	*Global*		*SRV-CONS-TECH-2.4*	✓	*Chapter 10*
SRV-CONS-TECH-6	✓	*Chapter 18*		*SRV-TECH-OPER-1.3*	*	*Chapter 10*
SRV-CONS-TECH-7	✓	*Chapter 18*		*SRV-CONS-NONT-3.1*	✓	*Chapter 10*
SRV-CONS-TECH-8	✓	*Chapter 18*		*SRV-CONS-NONT-3.2*	✓	*Chapter 10*
SRV-CONS-NONT-1	✓	*Chapter 15*		*SRV-TECH-OPER-2.1*	✓	*Chapter 10*
SRV-TECH-MAIN-1	✓	*Chapter 15*		*SRV-CONS-TECH-2.8*	*	*Chapter 10*
SRV-CONS-NONT-2	✓	*Chapter 15*		*SRV-TECH-OPER-1.4*	✗	*Chapter 7*
SRV-TECH-PROD-1	✓	*Chapter 8,15*		*SRV-TECH-OPER-3.3*	✓	*Chapter 7*
SRV-TECH-PROD-2	✓	*Chapter 8,15*		*SRV-TECH-OPER-2.2*	✓	*Chapter 7*
SRV-TECH-MAIN-2	✓	*Chapter 15*		*SRV-TECH-OPER-3.4*	✓	*Chapter 7*
SRV-TECH-MAIN-3	✓	*Chapter 15*		*SRV-TECH-OPER-1.5*	✗	*Chapter 7*
SRV-CONS-NONT-3	✗	*Chapter 15*		*SRV-TECH-OPER-1.6*	✗	*Chapter 7*
SRV-TECH-EOL-1	✓	*Chapter 19*		*SRV-TECH-OPER-1.7*	*	*Chapter 7*
SRV-TECH-OPER-7	✓	*Chapter 4,10*		*SRV-TECH-OPER-2.3*	✓	*Chapter 7*
SRV-TECH-OPER-7.1	✓	*Chapter 7*		*SRV-CONS-TECH-2.5*	✓	*Chapter 6*
SRV-CONS-NONT-4	✓	*Chapter 17*		*SRV-CONS-TECH-2.5.1*	✓	*Chapter 6*
SRV-CONS-NONT-5	✓	*Chapter 2*		*SRV-CONS-TECH-5.2.3*	*	*Chapter 6*
SRV-CONS-NONT-6	✗	*Chapter 2*		*SRV-TECH-OPER-6.1*	✓	*Chapter 12*
SRV-CONS-NONT-7	*	*Chapter 19*		*SRV-CONS-TECH-2.6*	✓	*Chapter 8*
SRV-CONS-NONT-8	*	*Chapter 19*		*SRV-CONS-TECH-2.7*	✓	*Chapter 4*
SRV-CONS-NONT-9	✓	*Chapter 19*		*SRV-TECH-OPER-4.1*	✓	*Chapter 10*
SRV-CONS-NONT-10	✓	*Chapter 2*		*SRV-TECH-OPER-4.2*	✓	*Chapter 10*
SRV-CONS-TECH-9	✓	*Global*		*SRV-CONS-TECH-2.4-B*	✓	*Chapter 4,9*

21

System Sensitivity

With the design completed, it is important to assess how sensitive it is to its requirements and inputs. The parameters the design is the most sensitive to are elaborated in this chapter, and the effects that changing these would have is assessed.

21.1. Crew count

First of all, the crew count influences the capsule design. More crew members means a bigger pressurised volume, leading to an increase in the structural mass of the capsule. Increasing the crew count by a factor x will increase the required volume by the same factor. At the end, this will increase the capsule mass by a factor of about $x^{2/3}$. In addition, the power requirements for the capsule will linearly vary with the crew count. The same can be said for the Life Support subsystem. This will thus increase the capsule mass linearly. Using the current mass fraction of the subsystem of the capsule as in Chapter 17, increasing the crew count by a factor x will increase the mass of the capsule by the following factor: $1 + 0.07x + 0.26x^{2/3}$, further increasing the mass of the complete vehicle.

21.2. LMO orbit and Martian base emplacement

If the inclination of the LMO were to be changed, the ascent profile would need to be tweaked, as to include a bigger inclination change. Also, this would lead to a potentially longer mission duration, increasing the Power and Life Support subsystems masses. Also, if the Martian base were to change latitude, it could potentially reduce the propellant mass required, if the new latitude was closer to the equator. However, this is unlikely, as explained in Chapter 15. If the Martian base emplacement was to be at a position were it never aligns with the LMO node, this would add propellant mass, for the vehicle to correct its orbit. Finally, if the LMO station was to have its orbital altitude higher, more propellant would be required. A new analysis as in Chapter 4 would need to be conducted to determine the precise amount. However, this would exponentially increase the propellant mass required for ascent, due to Tsiolkovsky's rocket equation.

21.3. LOC

The LOC requirement imposes a strong need for the abort system, as the goal is for the vehicle to be as reliable as possible. However, if the LOC number was to be lowered to the same value as the LOV, the complete abort system could be removed. This would reduce the capsule mass by a third, reducing the complete vehicle mass considerably. While this may seem reckless, the current LOV numbers computed in Section 18.5 are lower than the LOC requirement. Also, the similar vehicle Starship does not provide any abort mode [134].

21.4. Isp

The I_{sp}, as well as the propellant selection, dictate the performance of the vehicle propulsion. Following Tsiolkovsky's equation, the mass ratio of the vehicle decreases exponentially with the I_{sp} increasing. Consequently if the combustion efficiency used in Chapter 9 is wrong the impact on the vehicle would be severe, hence a margin of $13[s]$ was used to account for wrong estimates.

21.5. Aerodynamic parameters

If the vehicle was to be redesigned to include more aerodynamic feature, its complete drag coefficient could be lowered. With this, the vehicle would have a lower resistance to the atmosphere during ascent, and require linearly less propellant. However, as the Martian atmosphere is thin, and the vehicle already is aerodynamically optimised, this would not reduce to required propellant mass significantly. Also, the lift coefficient of the vehicle is an important parameter during reentry. If it was to increase, the deceleration would be more gradual, reducing the heating, and decreasing the required TPS mass. However, this would decrease the landing precision.

21.6. Static properties

The centre of gravity emplacement of the vehicle dictates the size of its wings to create an aerodynamic moment during reentry. The wing surface, and their mass, would linearly decrease with the centre of gravity getting higher. Finally, if the MMOI of the vehicle was to decrease, the RCS subsystem would need to induce a lower torque. This would thus reduce the required thrust linearly, reducing the RCS propellant mass the same way.

22

Design Development

This Chapter describes the project design and the development logic during and after the DSE, together with the manufacturing plan of the vehicle. It will start by introducing the Project Design and Development Logic diagram which was further developed from the one stated in the Midterm report [2]. After this, the Chapter will discuss Charon's manufacturing plan, followed by the verification and validation procedures of the vehicle. Finally, the project Gantt chart is made, as shown in Figure 22.4.

22.1. Project Design and Development Logic

Figure 22.1 below shows the diagram of the Project Design and Development Logic, elaborated from the Midterm report [2]. Its structure is based on the project development phases described by NASA in [155]. The diagram shows in which order the phases are executed. After the detailed and final design phases the design is frozen, leading to the end of Phase C with the start of the MAI phase (Manufacturing, Assembly and Integration), where production of the first prototype starts. Producing and assembling the first prototype lays the ground to test the quality of the production methods, the production procedure and it will be used to assess the interfaces and to check whether the developed system functions as designed. In case it does not, a further iteration of the design is necessary. If the prototype works as intended, then the production of the final vehicle can start. The main part of the Qualification Phase is the Verification and Validation procedures of the system. These are explained in more detail in 22.3. Part of the system's Validation requires the vehicle to be launched to Mars to be able to make sure that the system is able to autonomously dock to the node and to land at the Martian base. Once the vehicle has been validated both on Earth and during operational conditions, then the Operational Phase of the vehicle can start, which is then followed by the End-Of-Life phase.

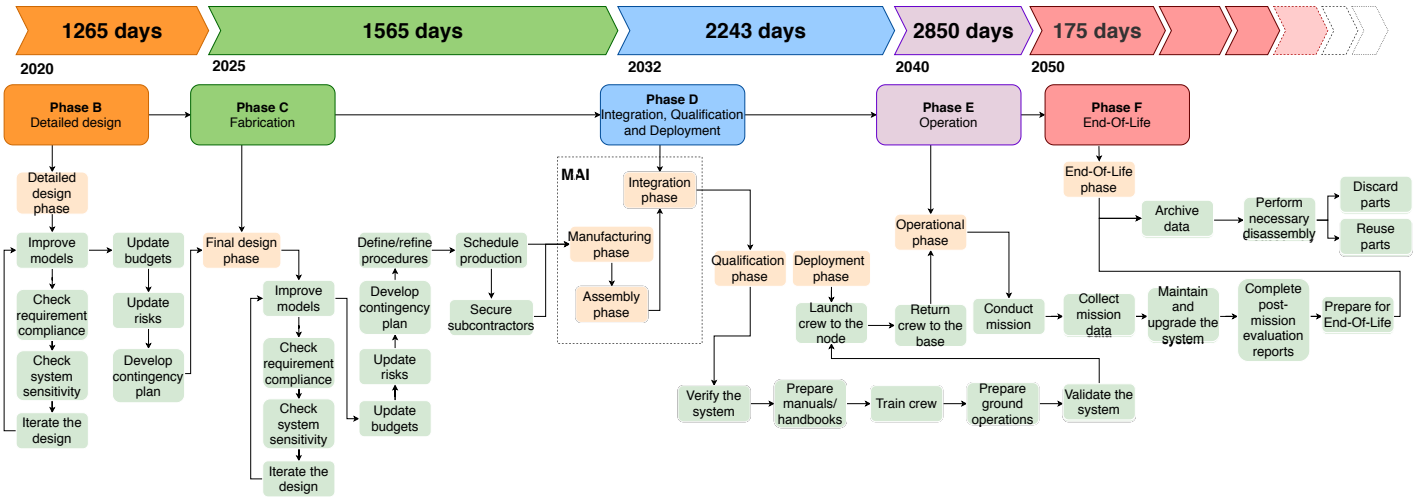

Figure 22.1: Project Design and Development Logic diagram

Furthermore, the organisation for the project after this phase is also presented in the Gantt Chart located in Figure 22.4.

22.2. Manufacturing Plan

One part from the project design and development logic needs more attention, namely the MAI part, hence it was expanded in the Figure 22.2

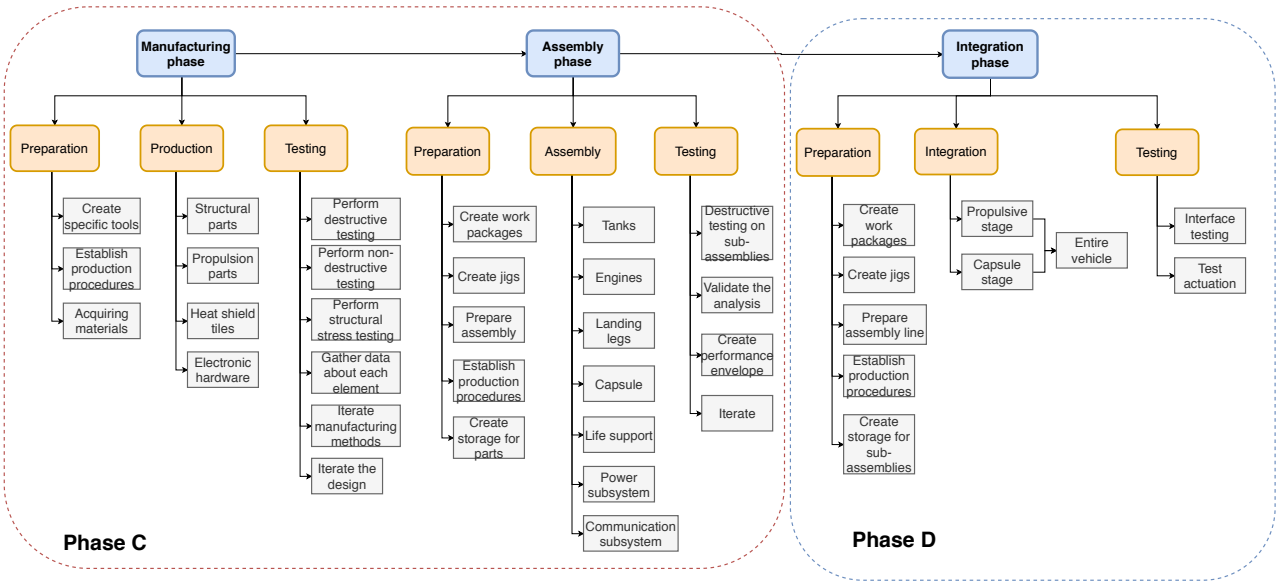

Figure 22.2: Manufacturing, assembly and integration plan diagram

This manufacturing plan is universal for both Airbus and external contractors, as the decision on responsibility will be made later in the project design, taking into account safety, financial aspects but also legacy factors related to long-term contractors of the client. In each of the indicated phases one can distinguish three separate parts like Preparation, production and testing in case of the manufacturing phase for example. Preparation mostly consists of every action that has to be done before any manufacturing can take place. It is mostly related to preparation of tools, moulds or jigs necessary for production but also to the creation of specific guidelines for workers or management. The second part mostly describes everything that is happening during manufacturing, starting from elements going through sub-assembly and finally ending up with the whole integrated system. The last part is about testing, which is performed at the end of each phase. For instance after element manufacturing, materials or components have to be checked and their performance has to be documented. In case of the post-assembly testing, already some qualification tests are performed, which check individual sub-systems. Finally the whole integrated system is tested to see if it can perform the desired goal nominally.

22.3. Verification and Validation Procedures

Figure 22.3 elaborates upon the system verification and validation of Figure 22.1, by identifying the main phases of Verification and Validation throughout the project life cycle. These were found to be: the Development Tests, where smaller parts and material specimen are tested, the Qualification Tests, where a qualification model is used to test the design under ultimate conditions, the Acceptance tests, in which the final flight model is tested under nominal operating conditions, and finally the Pre-launch, in-mission, post-mission tests, where the vehicle is validated under operational conditions during its initial deployment phase. During the Qualification tests the qualification model is discarded after testing, while the Acceptance and Pre-launch tests are performed on the flight model which is then launched to Mars. In addition to identifying the main phases of the system's Verification and Validation, Figure 22.3 also depicts the testing procedures that were established for each testing phase.

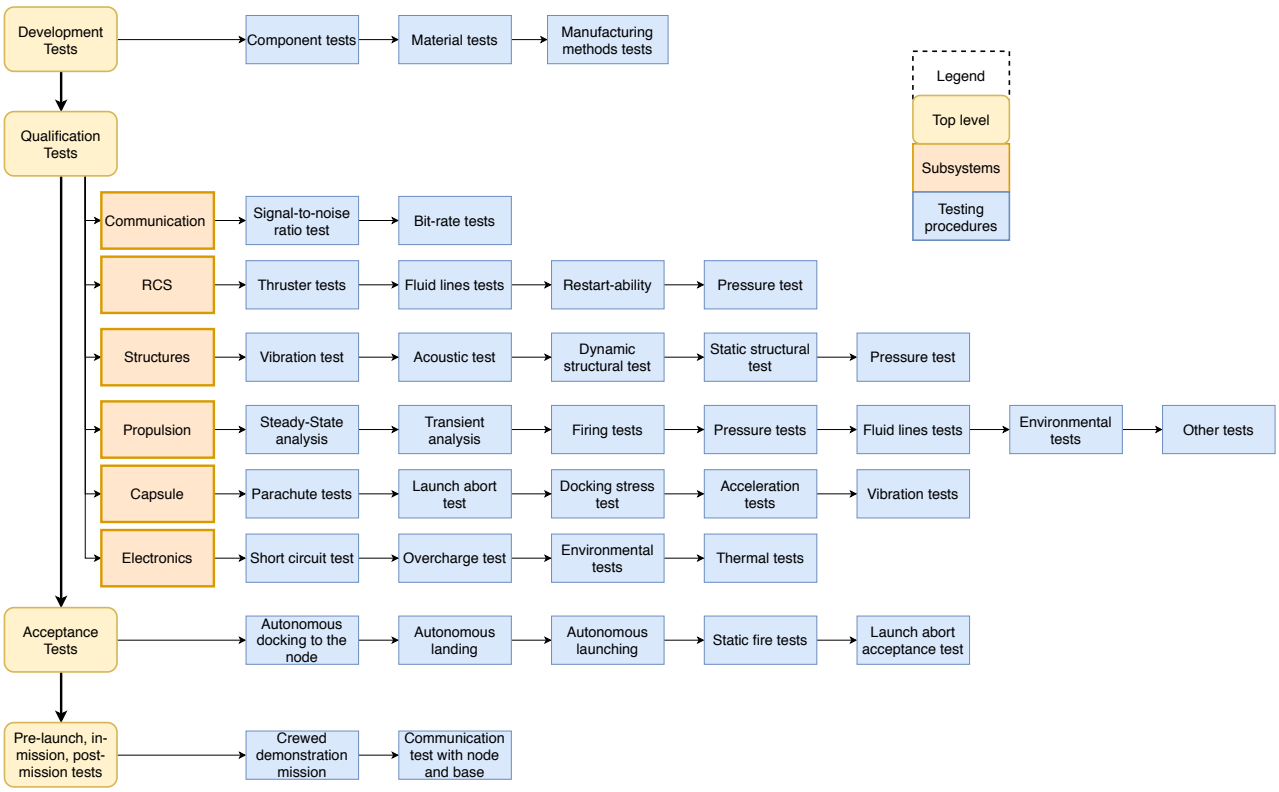

Figure 22.3: Verification and Validation outline

ID	Task Name	Duration	Start	Finish
1	**Charon Development**	**7978 days**	**Mon 7/6/20**	**Wed 2/1/51**
2	**Transition Phase**	**60 days**	**Mon 7/6/20**	**Fri 9/25/20**
3	Prepare team with the client	30 days	Mon 7/6/20	Fri 8/14/20
4	Review the current state off work	30 days	Mon 8/17/20	Fri 9/25/20
5	**Phase B**	**1265 days**	**Sat 9/26/20**	**Thu 7/31/25**
6	**Detailed design phase**	**1178 days**	**Sat 9/26/20**	**Wed 4/2/25**
7	Improve models	917 days	Sat 9/26/20	Sun 3/31/24
8	Check requirements compliance	806 days	Mon 3/1/21	Sun 3/31/24
9	Check system sensitivity	806 days	Mon 3/1/21	Sun 3/31/24
10	Iterate the design	806 days	Mon 3/1/21	Sun 3/31/24
11	Update budgets	88 days	Mon 4/1/24	Wed 7/31/24
12	Update risks	88 days	Mon 4/1/24	Wed 7/31/24
13	Develop contingency plan	175 days	Thu 8/1/24	Wed 4/2/25
14	**Phase C**	**1565 days**	**Fri 8/1/25**	**Thu 7/31/31**
15	**Final design phase**	**697 days**	**Fri 8/1/25**	**Mon 4/3/28**
16	Improve models	543 days	Fri 8/1/25	Tue 8/31/27
17	Check requirements compliance	500 days	Wed 10/1/25	Tue 8/31/27
18	Check system sensitivity	500 days	Wed 10/1/25	Tue 8/31/27
19	Iterate the design	500 days	Wed 10/1/25	Tue 8/31/27
20	Update budgets	88 days	Wed 9/1/27	Fri 12/31/27
21	Update risks	88 days	Wed 9/1/27	Fri 12/31/27
22	Develop contingency plan	66 days	Mon 1/3/28	Mon 4/3/28
23	Define/refine procedures	66 days	Tue 4/4/28	Tue 7/4/28
24	Schedule production	85 days	Wed 7/5/28	Tue 10/31/28
25	Secure subcontractors	67 days	Wed 7/5/28	Thu 10/5/28
26	**Manufacturing Phase**	**413 days**	**Wed 11/1/28**	**Fri 5/31/30**
27	Preparation	109 days	Wed 11/1/28	Sat 3/31/29
28	Production	196 days	Mon 4/2/29	Mon 12/31/29
29	Testing	109 days	Tue 1/1/30	Fri 5/31/30
30	**Assembly Phase**	**413 days**	**Tue 1/1/30**	**Thu 7/31/31**
31	Preparation	109 days	Tue 1/1/30	Fri 5/31/30
32	Assembly	153 days	Sat 6/1/30	Tue 12/31/30
33	Testing	152 days	Wed 1/1/31	Thu 7/31/31
34	**Phase D**	**2243 days**	**Wed 1/1/31**	**Sat 8/6/39**
35	**Integration Phase**	**653 days**	**Wed 1/1/31**	**Fri 7/1/33**
36	Preparation	109 days	Wed 1/1/31	Sat 5/31/31
37	Integration	415 days	Mon 6/2/31	Fri 12/31/32
38	Testing	130 days	Mon 1/3/33	Fri 7/1/33
39	Qualification Phase	651 days	Mon 7/4/33	Mon 12/31/35
40	Verify the system	564 days	Wed 11/2/33	Mon 12/31/35
41	Prepare manuals/handbooks	652 days	Mon 1/1/35	Tue 6/30/37
42	Train crew	1219 days	Wed 3/1/34	Sun 10/31/38
43	Prepare ground operations	2110 days	Wed 1/1/31	Tue 2/1/39
44	Validate the system	370 days	Tue 1/1/36	Sun 5/31/37
45	**Deployment Phase**	**201 days**	**Mon 11/1/38**	**Sat 8/6/39**
46	Transport to Mars	152 days	Mon 11/1/38	Tue 5/31/39
47	Launch crew to the node	44 days	Wed 6/1/39	Sun 7/31/39
48	Return crew to the base	6 days	Mon 8/1/39	Sat 8/6/39
49	**Phase E**	**2850 days**	**Fri 7/1/39**	**Thu 6/2/50**
50	**Operational Phase**	**2717 days**	**Sun 8/7/39**	**Sat 1/1/50**
51	Conduct mission	2607 days	Sun 8/7/39	Sat 7/31/49
52	Collect mission data	2607 days	Sun 8/7/39	Sat 7/31/49
53	Maintain and upgrade the system	2588 days	Thu 9/1/39	Sat 7/31/49
54	Complete post-mission evaluation reports	111 days	Sun 8/1/49	Fri 12/31/49
55	Prepare for End-of-Life	219 days	Sun 8/1/49	Wed 6/1/50
56	**Phase F**	**175 days**	**Thu 6/2/50**	**Wed 2/1/51**
57	**End-of-Life Phase**	**175 days**	**Thu 6/2/50**	**Wed 2/1/51**
58	Archive data	65 days	Thu 6/2/50	Wed 8/31/50
59	Perform necessary disassembly	130 days	Thu 6/2/50	Wed 11/30/50
60	Discard parts	44 days	Thu 12/1/50	Tue 1/31/51
61	Reuse parts	44 days	Thu 12/1/50	Tue 1/31/51

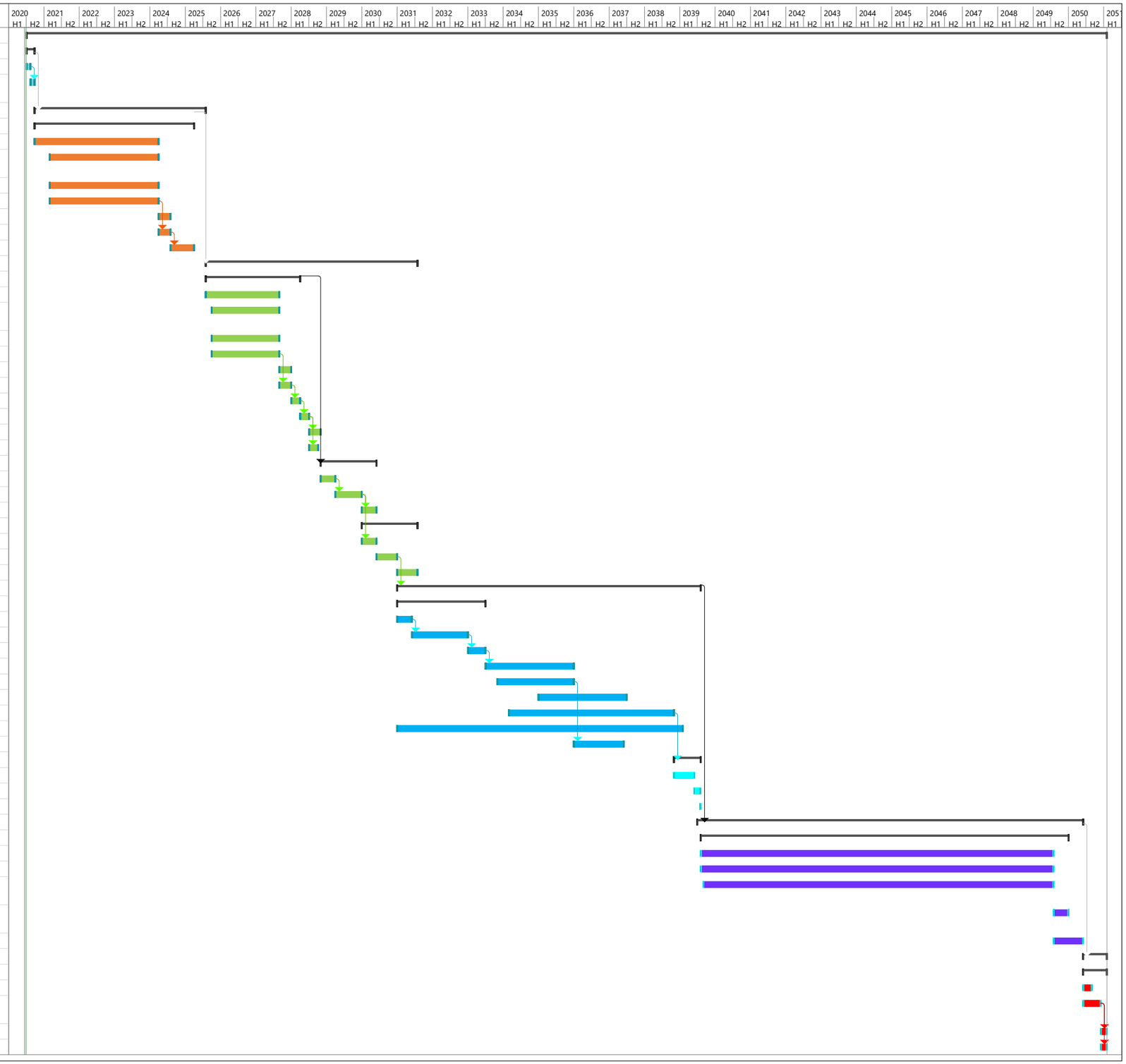

Figure 22.4: Project Gantt Chart

23

Conclusion

The Mars environment and the complexities of manned spaceflight pose great technological challenges for a vehicle such as Charon. The imperative criteria for a manned, reusable, Mars-based rocket have led to a design driven by safety, reliability, and maintainability. As detailed in this report, Charon is an achievable solution to the needs of the mission. LOV, LOC, and LOM risks as estimated are extremely low and satisfy the stakeholder requirements. Technologically, all subsystems of Charon are based on existent components of minimum TRL 4. Thus Charon is feasible on a complexity and technical level. Financially, Charon can be considered an expensive project, given the pre-existing market and similar missions being developed, but its $8 billion price tag over 18 years was deemed reasonable compared to space projects of similar scale, and feasible for Airbus Defence and Space (Chapter 17). As the safety, reliability, and maintainability aspects of the vehicle are the most important, these will be evaluated in more detail.

In ensuring safety, Charon has opted for the use of well-understood and flight-proven technology. Crew life support systems have been designed to create a habitable environment within the capsule for 6 people for 7 sols, with crew capsule power estimations have been validated with Space Shuttle data. Constant communication links with the ground, Charon, and the LMO node ensures the status of the crew is known, and any problems that arise can be handled by more personnel. On the note of reliability, all subsystems have been designed with much redundancy; components are often doubly or triply redundant, while structural materials and dimensions are capable of handling high loads, often at a a factor of 1.5 to the design loads. The propulsion system contains 9 engines, 2 of which are redundant. The capsule contains 4 flight computers, 3 of which can fail. Propellant tanks and landing legs are over-designed for the loads of the vehicles flight.

Ease of maintenance and refurbishment instilled in the design philosophy the idea of modular systems, so that the vehicle could be more readily maintained, especially given the arduous nature of maintenance and refurbishment on Mars. In addition, the consumables of the vehicle will all be producible on Mars, allowing for continued operation without relying on Earth for launch-crucial supplies. Furthermore, non-complex materials and additive manufacturing methods have been chosen such that component refurbishment is as easy and cheap as possible for the colony.

The team concludes that Charon is a reliable vehicle for the given mission purpose, and the program for its development and deployment is technologically and financially feasible. However, the team considers it infeasible that the necessary infrastructure and personnel for operating Charon on Mars will be present by 2040. Development of Mars habitat, mining, and manufacturing technologies is possible to complete by this time, however deployment of this equipment to Mars is likely to be too costly to do within the given time frame of two decades until 2040. Although, this was not the focus of the teams design, and so further research is warranted to form stronger conclusions about Charon's operability.

With this report, the team has completed concept and technology development and the preliminary design of Charon. This places the project in the middle of Phase B. Still to be done in this phase is the completion of the technology, delivered as mock-ups, specification and interface documents, test results, and prototypes. Chapter 24: Recommendations presents the future outlook on the conclusion of Phase B and further considerations that should be investigated.

24

Recommendations

The design process of the Charon vehicle has illustrated the need for very sophisticated existing Martian infrastructure. This extends both to the Martian orbital node, as well as the Mars base as shown in Chapter 15. As Charon is designed to operate between these two mission elements, it is important that the same level of detail is achieved in the design of these nodes in order to verify the mission envelope proposed in this report. For the Martian base specifically, a detailed design of the power plant and the refurbishment infrastructure for Charon are essential to be performed before the detailed design of Charon can be completed. This would also include a detailed cost estimate of the construction of the Martian base and the support infrastructure for Charon.

The next step in Phase B of the design process of the vehicle itself would be a detailed analysis of the refurbishment process, based on the preliminary work performed in Chapter 15, as this is expected to drive component design. This analysis would be performed on a subsystem level with emphasis on the long term degradation of the component in a Martian environment and the possibilities of inspection and in-situ manufacture. This detailed analysis would be the basis for fully verifying requirements **SRV-TECH-MAIN-1** to **SRV-TECH-MAIN-3**, extending to verification of requirement **SRV-CONS-TECH-2.8**, related to the debris impact sensitivity of the vehicle. A more detailed structural design of the components of each subsystem would necessarily include numerical analysis of the sandwich structure used for the skirts, as well as FEA performed on the tank interfaces, landing legs and the capsule. In addition, the corrosion and wear on the tanks and feed system components are necessary to analyse, in conjunction with a detailed study of the manufacturing of certain metal alloys on Mars. The latest information about vehicle dimensions and mass distributions can be used to construct a dynamic stability model of the vehicle. Optimisation of the reentry trajectory for even better deceleration in conjunction with CFD for a better estimate of aerodynamic heating, including modelling of chemical reactions within the gas flow, would also be recommended in this phase of the design.

24.1. Outlook

The desired time frame given for the deployment of Charon is likely unrealistic. The vehicle itself is technically feasible at the current moment. However, the required supporting infrastructure is unlikely to be ready at that time. The actual time frame is highly dependent on the speed of development of human exploration of Mars.

Charon in its current configuration is designed around human transport. Given the capabilities of the vehicle and the modularity of the capsule design, it is recommended to investigate a capsule design capable of cargo-only missions, to and from the orbital node. This could extend the function of Charon to dedicated resupply mission for the Mars base, without being limited by the requirements for a human rated mission.

A possible area of investigation could be the use of Charon for other interplanetary missions. The nature of the requirements for the design of Charon means that the vehicle in its current form is designed specifically for operations in a Martian environment. Simply using the vehicle in an environment it is not designed for would likely be very inefficient compared to designing a dedicated vehicle. Due to the modular nature of design it might, however, be possible to adapt elements of the design to better suit other environments. Specifically, a vehicle to carry humans between a geostationary transfer orbit and the lunar surface. Such a mission profile would require significant redesign to the engines, vehicle structure and propulsion system to account for the lack of an atmosphere.

Bibliography

[1] D.Apostolidis et al. Charon MARS SRV Baseline Report V1.0, TU Delft, 2020.

[2] D.Apostolidis et al. Charon MARS SRV Midterm Report, TU Delft, 2020.

[3] InnovFin Advisory. The future of the European space sector, How to leverage Europe's technological leadership and boost investments for space ventures, 2019.

[4] Bryce Space and Technology LLC. Global Space Industry Dynamics, 2016.

[5] D.R. Komar, R. Moses. Hercules Single-Stage Reusable Vehicle supporting a Safe, Affordable, and Sustainable Human Lunar & Mars Campaign. Technical report.

[6] C.J. Cerimele et al. A Rigid Mid-Lift-to-Drag Ratio Approach to Human Mars Entry, Descent, and Landing. In *AIAA SciTech 2017 Conference*, 2017.

[7] T.Cichan, K. Timmons, K. Coderre, W. D. Pratt. Mars Base Camp. Technical report, Lockheed Martin Corporation, 2017.

[8] K.F. Wakker. *Fundamentals of Astrodynamics*. Delft University of Technology, 2015.

[9] H.Wittenberg, B.A.C. Ambrosius, M.C. Naeije, E.Mooij. *AE4-870A: Rocket Motion*. Delft, Netherlands, 2014.

[10] J. A. Mulder et. al. *Flight Dynamics Lecture Notes*. TU Delft, 2013.

[11] B.T.C. Zandbergen. *AE1222-II Aerospace Design & Systems Engineering Elements I - Part: Spacecraft (bus) Design and Sizing*. 2020.

[12] A. Cervone, B.T.C. Zandbergen. *AE2230-II: Propulsion & Power Rocket Propulsion*. Delft University of Technology, 2017.

[13] A.W.Wilhite,. ANALYSIS OF SEPARATION OF THE SPACE SHUTTLE ORBITER FROM A LARGE TRANSPORT AIRPLANE. Technical report, 1977, NASA TM X-3492.

[14] B.T.C. Zandbergen. *AE1222-II: Aerospace Design & Systems Engineering Elements I Part: Launch Vehicle Design and Sizing*. Delft University of Technology, 2017.

[15] M. Binder, T. Tomsik, J.P. Veres. RL10A-3-3A Rocket Engine Modeling Project. Technical report, 1997.

[16] D.E. Smith, W.L. Sjogren, G.L. Tyler, G. Balmino, F.G. Lemoine, A.S Konopliv. The gravity field of Mars: results from Mars Global Surveyor. *Science*, 286:94–97, 1999.

[17] M.A. Sharaf, H.H. Selim. Final state predictions for J2 gravity perturbed motion of the Earth's artificial satellites using Bispherical coordinates. *NRIAG Journal of Astronomy and Geophysics*, 2013.

[18] P. Withers, M.D. Smith. Atmospheric entry profiles from the Mars Exploration Rovers Spirit and Opportunity. *Icarus*, 185, 2006.

[19] E. Mooij. *AE4870B Re-entry Systems*. TU Delft, 2016.

[20] J.A. Fay, F.R. Riddell. Theory of Stagnation Point Heat Transfer in Dissociated Air. *Journal of the Aeronautical Sciences*, 25:73–122, 1958.

[21] J.D. Anderson. *Fundamentals of aerodynamics*. Mcgraw-Hill Publishing Co., 5th edition, 2011.

[22] B.R. Hollis. Blunt-Body Entry Vehicle Aerothermodynamics: Transition and Turbulence on the CEV and MSL Configurations. *AIAA*, 2012.

[23] M.J. Michael, C.Y. Tang, K.T. Edquist, B.R. Hollis, P. Krasa, C.A. Campbell. A Review of Aerothermal Modeling for Mars Entry Missions. *AIAA*, 2010.

[24] A. M. Waas H. Ng. Wei, P. P. Friedmann. Thermomechanical Analysis of a Thermal Protection System with Defects and Heat Shorts. Technical report, Department of Aerospace Engineering University of Michigan Ann Arbor, 2006.

[25] W. J. Larson, J. R. Wertz. *Space Mission Analysis and Design*. Kluwer Academic Publishers, 2005.

[26] M. I. Skolnik. Theoretical Accuracy of Radar Measurements's. *IRE Transactions on Aeronautical and Navigational Electronicss*, 1960.

[27] H. F. Yang, Z. Wang, H. Fu, Y. Zhang. Integrated navigation for Mars final approach based on Doppler radar and X-ray pulsars with atomic clock error. *Acta Astronautica*, 2019.

[28] Analog Devices. Tactical Grade, Six Degrees of Freedom Inertial Sensor. Technical report, 2019, ADIS 16490.

[29] P.J. Hargrave. A tutorial introduction to Kalman filtering. IEEE, 1989.

[30] Mars Entry Navigation from EKF Processing of Beacon Data. Technical report, NASA Langley Research Center, 2000.

[31] W. Fehse. *Automated Rendezvous and Docking of Spacecraft*. Cambridge University Press, 2003.

[32] J. R. Wertz, R. Bell. Autonomous Rendezvous and Docking Technologies -Status and Prospects. 2003.

[33] E.P. Blackburn et al. Spacecraft Magnetictorque. Technical report, 1969.

[34] L.N. Zhuzgov, S.S. Dolginov. The magnetic field and the magnetosphere of the planet Mars. Technical report, 1991.

[35] SRE-PA & D-TEC. Margin philosophy for science assessment studies, ESA, 2012.

[36] F. Grafwallner . Hydrogen Peroxide (HP) Potential for Space Applications. Technical report.

[37] Ariane Group. 1N, 20N, 400N and heritage thruster. Technical report.

[38] V. Chaudhary, S. Sharma. An overview of ordered mesoporous material. Technical report, Indian Institute of Technology, 2016.

[39] NASA. Closing the Loop: Recycling Water and Air in Space. Technical report, National Science Standards, 2012.

[40] D.King, M.Decker. Gas Cylinders. Technical report, StatPearls, 2020.

[41] J.Broyan. Waste Collector System Technology Comparisons for Constellation Applications. Technical report, NASA Johnson Space Center, 2007.

[42] R.Rendtorff, M.Kashgarian. Stool patterns of healthy adult males. Technical report, University of Tennessee, 1967.

[43] M.Anderson et al. NASA Environmental Control and Life Support Technology Development and Maturation for Exploration. Technical report, 46th International Conference on Environmental Systems, 2016.

[44] Ruag. Thermal Insulation Products. Technical report, Space Thermal Insulation Products, 2015.

[45] M. Sowa. Space Radiation Environment and Human Exploration. Technical report, NASA Ames Research Center, 2017.

[46] K.L.Farrow et al. Operating Characteristics of the Apollo LM Descent Engine with Helium Ingestion and Propellant Depletion in a Simulated Space Environment, Rocket Test Facility Arnold Engineering Development Center, 1967.

[47] Alexander Ponomarenko. Rocket propulsion analysis.

[48] M. Su, B. Young. Mechanical properties of high strength aluminium alloy at elevated temperatures. 2017.

[49] G.J. Butterworth, C.B.A. Fort. A survey of the properties of copper alloys for use as fusion reactor materials. 1992.

[50] M. Martinez-Sanchez. Lecture notes in rocket propulsion, 2005.

[51] L. Denies. Regenerative cooling analysis of oxygen/methane rocket engines. 2015.

[52] Betti et al. Numerical Study of Film Coolingin Oxygen/Methane Thrust Chambers. *4th European conference for aeronautics and space sciences*, 2011.

[53] Arnold et al. Influence Parameters on Film Cooling Effectiveness in a High Pressure Subscale Combustion Chamber. *American Institute of Aeronautics and Astronautics*, 2012.

[54] M. Siuko et al. Water hydraylic actuators for ITER maintenance devices. 2003.

[55] R. Newlands, M. Heywood, A. Lee . Rocket vehicle loads and airframe design. Technical report.

[56] W.A.R. Wildvank. Launch Vehicle Structural Mass Prediction Model, 2018. Master Thesis, Delft University of Technology.

[57] L. M. Calle. Corrosion on Mars: Effect of the Mars Environment on Spacecraft. Technical report, NASA/Technical Publication, 2019.

[58] Aero Metal Alliance. Aluminium Alloy -QQ-A-250/4 '0', 2013. Materials, Datasheet.

[59] H.Zheng, X.Zeng, J.Zhang, H.Sun. The Application of Carbon Fiber Composites in Cryotank. *IntechOpen*, 2018.

[60] B.Mohammadi, M.Rohanifar, D.Salimi-Majd, A.Farrokhabadi. Micromechanical prediction of damage due to transverse ply cracking under fatigue loading in composite laminates. *Journal of Reinforced Plastics and Composites*, 2017.

[61] H. Zheng, X. Zeng,J. Zhang, H. Sun. The Application of Carbon Fiber Composites in Cryotank. *Solidification*, 2018.

[62] J. J. Wijker . *Spacecraft Structures*. Springer, 2010.

[63] P.M. Sforza. *Manned spacecraft design principles*. Elsevier, 2016.

[64] R.Rose. *Man-systems integration standards*. National Aeronautics and Space Administration, 1995.

[65] G. E. Musgrave, A. M. Larsen, T. Sgobba. *Safety design for space systems*. Elsevier India, 2012.

[66] J. T. Somers, D. Gohmert, J. W. Brinkley. Application of the Brinkley Dynamic Response Criterion to Spacecraft Transient Dynamic Events. Technical report, March 2017.

[67] E.H. Baker, C.D. Babcock, R. F. Crawford,J. B. Glassco, A. Kaplan, M.H. Kural, J. Mayers, J. P. Peterson. Buckling of Thin-Walled Truncated Cones. Technical report, September 1968.

[68] V. S. Syromyatnikov. Docking System of Androgynous and Peripheral Type. 1972.

[69] W. Gerstenmaier, A. Kransnov, T. Reiter et al. International Docking System Standard (IDSS) Interface Definition Document (IDD), November 2013.

[70] M. Hardt, J. R. Villa, D. Cocho, P. Urmston, Ó. Gracia. Simulation and Control of an Active Stewart Platform for Docking and Berthing of Space Vehicles. *57th International Astronautical Congress*, 2006.

[71] C.A. Hatfield. ISS - Enabling Exploration through Docking Standards, 2005.

[72] J.R. Burke, J. Phenix. Final Report on a Study of Automated Rendezvous and Docking for ATS-V Despin. Technical report, Space Division North American Rockwell, 1971. SD 71-286.

[73] S.S. Kessler, T. Matuszewski, H. McManus. The Effect of Cryocycling on the Mechanical properties of IM7/977-2. Technical report, Technology laboratory for advanced composites , Massachusetts Institute of Technology.

[74] R. Schmidt, S. Lee, L. Cooke. 3-D Woven Pi Preform Joints: An Enabling Technology For Large Composite Structure. 2008.

[75] C. Rans, J. Melkert. AE2135-I, 2018. Structural Analysis, Lecture Notes.

[76] H. Ullah. Buckling of thin-walled cylindrical shells under axial compression. *International Journal for Numerical Methods in Engineering*, 79(11).

[77] E.F.Bruhn, R. J. H.Bollard. *Analysis and design of flight vehicle structures*. Jacobs Pub., 1973.

[78] C. Winnefeld, T.Kadyk, B.Bensmann, U.Krewer, R.Hanke-Rauschenbach. Modelling and Designing Cryogenic Hydrogen Tanks for Future Aircraft Applications. *Energies*, 11(1):105, 2018.

[79] T.Kramer, E.Brogren, B.Siegel . Evaluation of propellant tank insulation concepts for low-thrust chemical propulsion. Technical report.

[80] B.W. Tew. Preliminary Design of Tubular Composite Structures Using Netting Theory and Composite Degradation Factors. *Journal of Pressure Vessel Technology*, 117(4):390–394, 1995.

[81] K. Li, J. Zheng, S. Liu, H. Ge, G. Sun, Z. Zhang, C. Gu, P. Xu. Buckling behavior of large-scale thin-walled ellipsoidal head under internal pressure. *Thin-Walled Structures*, 141:260–274, 2019.

[82] J. M. Robert. Buckling Of Circular Cylindrical Shells

With Multiple Orthotropic Layers And Eccentric Stiffeners. Jan 1967.

[83] Buckling of Thin-walled circular cylinders . Technical report, 1968. NASA Space Vehicle design criteria, Structures.

[84] J. P. Peterson. Buckling of stiffened cylinders in axial compression and bending - A review of test data. Technical report, NASA/Technical Note, 1969.

[85] W. F. Rogers. Apollo experience report - Lunar module landing gear subsystem. Technical report, NASA/Technical Note, 1972.

[86] J.E. Akin. Impact Load Factors for static analysis. Lecture Notes, Rice University.

[87] B.S. Thompson. Impact, 2005. ME 471 Engineering Design II, Michigan State University.

[88] P.R. Prokopius M. Warshay. The Fuel Cell in Space: Yesterday, Today and Tomorrow. Technical report, 1989.

[89] J. Dumoulin. *NSTS 1988 News Reference Manual*. Kennedy Space Center, NASA, 1988.

[90] I. Jakupca. Fuel Cell Research and Development for Earth and Space Applications. 2018.

[91] F. Zegler. Development Status of an Integrated Propulsion and Power System for Long Duration Cryogenic Spaceflight. Technical report, 2012.

[92] F. Zegler. Integrated Vehicle Fluids: A Combined Propulsion & Power System for Long Duration Spaceflight. 2012.

[93] K.A. Burke. Fuel Cells for Space Science Applications. Technical report, 2003.

[94] J.J. Minnehan, J.W. Pratt. Practical Application Limits of Fuel Cells and Batteries for Zero Emission Vessels . Technical report, Sandia National Laboratories, 2017.

[95] TERMA. *Power Distribution Unit*, v2 edition, January 2012.

[96] L.B. Johnson. STS-68 Space Shuttle Mission Report. Technical report, NASA, 2015.

[97] NASA Office of Inspector General. Conformal and Spectrally Agile Ultra Wideband Phased Array Antenna for Communication and Sensing. Technical report, NASA Glenn Research Center, 2015.

[98] Harris Corporation. *Cavity-Backed Helix Antenna*, 2010.

[99] L3Harris. *T-740 S-BAND LAUNCH VEHICLE TRANSMITTER*, March 2020.

[100] C. Ho, N. Golshan, A. Kliore. *Radio Wave Propagation Handbook for Communication on and Around Mars*. Jet Propulsion Laboratory, 2002.

[101] C. Ho, S. Slobin, M.Sue, E. Njoku. Mars Background Noise Temperatures Received by Spacecraft Antennas. Technical report, Jet Propulsion Laboratory, 2002.

[102] L3Harris Technologies Inc. *Phoenix Flight Computer*, 2020.

[103] Cobham Gaisler AB. *GR740 Quad Core LEON4 SPARC V8 Processor, Preliminary Data Sheet and User's Manual*, v2.3 edition, May 2019.

[104] J.F.Hanaway, R.W.Moorehead. Space shuttle avionics system. Technical report, 1989.

[105] O. Olofinboba, R. DeMers, M.C. Dorneich, C. Hamblin,J. Wise . A Systematic Tool for Deriving Crew Console Layouts . *Proceedings of the Human Factors and Ergonomics Society Annual Meeting*, 2008.

[106] M.C. Dorneich, C. Hamblin, R. DeMers, O. Olofinboba. A Task-Based Reach-Zone Analysis of the Orion Crew Exploration Vehicle Controls. *IEEE Systems, Man, & Cybernetics Conference*, 2011.

[107] N.A. Townsend. Apollo experience report - Launch escape propulsion system. Technical report, NASA, 1973.

[108] T.Scogin, M.Lacerda, J.Marshall. Orion Capsule Launch Abort System Analysis, 2016. Digital Design and Manufacturing Assignment, Georgia Institute of Technology.

[109] K.V. Kumar, W.T. Norfleet. Issues on Human Acceleration Tolerance After Long-Duration Space Flights, NASA, 1992. NASA/TM-104753.

[110] NASA Space Vehicle Design Criteria. Deployable Aerodynamic Deceleration Systems. Technical report, 1971.

[111] T.W. Knacke. *Parachute Recovery Systems: Design Manual*. US Navy, 1991.

[112] K. Stein, R. Benney. Aerodynamic interactions involving multiple parachute canopies. Technical report, 2020.

[113] M.L. Zwicker, R.J. Sinclair. Pack Density Limitations of Hybrid Parachutes. Technical report, 2013.

[114] S. Do, O. Weck. A personal airbag system for the Orion Crew Exploration Vehicle. Technical report, 2012.

[115] L. Wan, R. Wendner, Roman,G. Cusatis. A novel material for in situ construction on Mars: experiments and numerical simulations. *Construction and Building Materials*, 120:222–231, 2016.

[116] W.J.Larson, L.K.Prank. *Human Spaceflight: Mission Analysis and Design*. The McGraw-Hill Companies, Inc., 2000.

[117] National Aeronautics and Space Administration. Space exploration vehicle concept. Technical report, NASA.

[118] G. Mann. Design, Construction and Test Operations Of An Analog Pressurised Planetary Exploration Vehicle. *Science and Technology Series*, 111, 2006.

[119] G. Sanders. Mars Water Mining for Future Human Exploration. Technical report.

[120] S. Hoffman, A. Andrews, K. Watts. "Mining" Water Ice on Mars, an Assessment of ISRU Options in Support of Future Human Missions. Technical report.

[121] A.C. Muscatello, E. Santiago-Maldonado. Mars In Situ Resource Utilization Technology Evaluation. Technical report.

[122] A. C. Muscatello, E. Santiago-Maldonado. Evaluation of Mars CO2 Capture and Gas Separation Technologies. Technical report.

[123] C. Popa, F. Carrozzo, G. DiAchille, S. Silvestro, F. Esposito, V. Mennella. Evidences for Copper Minerals in Shalbatana Valley, Mars. 2014.

[124] T. Encrenaz, T.K. Greathouse, F. Lefevre, S.K. Atreya. Hydrogen peroxide on Mars: Observations, interpretation and future plans. 04 2011.

[125] J. A. Hurowitz, N. J. Tosca, S. M. McLennan, M.A.A. Schoonen. Production of hydrogen peroxide in Martian and lunar soils. *Earth and Planetary Science Letters*, 255(1):41–52, 2007.

[126] F. Baerdemaeker, M. Simek, C. Leys. Efficiency of hydrogen peroxide production by AC capillary discharge in water solution. *Journal of Physics D: Applied Physics*, 40, 2007.

[127] S. Kumar, V. Himabindu. Hydrogen production by PEM water electrolysis – A review. *Materials Science for Energy Technologies*, 2(3):442 – 454, 2019.

[128] J. Appelbaum, D.J. Flood. Solar Radiation on Mars. Technical report, NASA, 1989.

[129] C.L. Whitmarsh, C.L. Whitmarsh Jr., P.T. Kerwin . A 1-Megawatt Reactor Design for Brayton-Cycle Space Power Application. Technical report, 1969.

[130] J. Taylor et al. Igneous and Aqueous Processes On Mars: Evidence From Measurements Of K and Th By the Mars Odyssey Gamma Ray Spectrometer. Technical report.

[131] P. Morgan. Geothermal Energy on Mars. *Mars: Prospective Energy and Material Resources*, pages 331–349, 01 2009.

[132] M.J. Fogg. The utility of geothermal energy on Mars. *Journal of the British Interplanetary Society*, 50:187, January 1997.

[133] D. Preclik, R. Strunz, G. Hagemann, G. Langel. Reusability aspects for space transportation rocket engines: Programmatic status and outlook. *CEAS Space Journal*, 1:71–82, 2011.

[134] SpaceX. Starship Users Guide, Revision 1.0, Mars 2020.

[135] Marshall Space Flight Center. Nasa pcec.

[136] NASA Executive Cost Analysis Steering Group. *NASA Cost Estimating Handbook*. NASA, 2015.

[137] W.J.Brown et al. Safety Standards for Oxygen and Oxygen Systems . Technical report, 1996.

[138] B. Nufer. Hypergolic Propellants: The Handling Hazards and Lessons Learned from use. Technical report, 2010.

[139] S.Beliczey, H.Schulz. The probability of leakage in piping systems of pressurized water reactors on the basis of fracture mechanics and operating experience. *Nuclear Engineering and Design*, 1987.

[140] S.A. Motiwala, D. L. Mathias, C. J. Mattenberger. Conceptual Launch Vehicle and Spacecract Design for Risk Assessment . Technical report, 2014.

[141] L. Burgazzi, B. Giannone, F. Zambardi. Reliability Prediction Method of Hydraulic System by Fuzzy Theory. *IFAC Proceedings Volumes*, 46:457–462, 2013.

[142] M.E. Pate-Cornell, P.S. Fishbeck. Safety of the Thermal Protection System of the Space Shuttle Orbiter: Quantitative Analysis and Organisational Factors. Technical report, 1990.

[143] L. Burgazzi, B. Giannone, F. Zambardi. Unavailability assesment of IFMIF target system. *Safety and Reliability: Proceedings of ESREL 2003, European Safety and Reliability Conference 2003, 15-18 June 2003, Maastricht, the Netherlands*, 2003.

[144] F.J.G. Carazas, G.F.M. De Souza. *Thermal Power Plant Performance Analysis*. Springer, 2012.

[145] D.C. Pytanowski. Rocket-Engine Control-System Reliability-Enhancement Analysis. *Annual Reliability and Maintainability. Symposium. 1999 Proceedings*, 1999.

[146] F. Polizzi. Reliability Considerations For Communication Satellites. 1968.

[147] S.Y. Kim, J.Castet, J. H. Saleh. Spacecraft electrical power subsystem: Failure behavior, reliability, and multi-state failure analyses. *Reliability Engineering & System Safety*, 98:55–65, 2012.

[148] A. Ahmad . Reliability & Failure Rate. Technical report.

[149] E. Fasanella. Multi-Terrain Earth Landing Systems Applicable for Manned Space Capsules. *Journal of Aerospace Engineering - J AEROSP ENG*, 22, 07 2009.

[150] L. Witte. *Touchdown Dynamics and the Probability of Terrain Related Failure of Planetary Landing Systems*. Universität Bremen, 2015.

[151] NASA SMA. Space Launch Report: SpaceX Falcon 9 v1.2. 2018.

[152] J.L. Hyde, M.D. Bjorkman, K.D. Hoffman, E. L. Christiansen, D. M. Lear, T. G. Prior. Micrometeoroid and Orbital Debris Threat Assessment: Mars Sample Return Earth Entry Vehicle. Technical report, 2011.

[153] Y. Zhang, J. Wang, Y. Zeng, J. Zhang. Calculating method of MTBF for integrated circuit. *Journal of Physics Conference Series*, 2018.

[154] NASA. NASA Exploration Systems Architecture Study, 2005.

[155] S.R.Hirshorn. *Systems Engineering Handbook*. NASA, Washington, DC, 2007. NASA SP-2016-6105 Rev2.